

# Advances

## in Clinical and Experimental Medicine

MONTHLY ISSN 1899-5276 (PRINT) ISSN 2451-2680 (ONLINE)

[www.advances.umed.wroc.pl](http://www.advances.umed.wroc.pl)

2020, Vol. 29, No. 9 (September)

Impact Factor (IF) – 1.514  
Ministry of Science and Higher Education – 40 pts.  
Index Copernicus (ICV) – 155.19 pts.



WROCLAW  
MEDICAL UNIVERSITY

Advances  
in Clinical and Experimental  
Medicine



# Advances in Clinical and Experimental Medicine

ISSN 1899-5276 (PRINT)

ISSN 2451-2680 (ONLINE)

www.advances.umed.wroc.pl

**MONTHLY 2020**  
**Vol. 29, No. 9**  
**(September)**

Advances in Clinical and Experimental Medicine is a peer-reviewed open access journal published by Wrocław Medical University. Its abbreviated title is Adv Clin Exp Med. Journal publishes original papers and reviews encompassing all aspects of medicine, including molecular biology, biochemistry, genetics, biotechnology, and other areas. It is published monthly, one volume per year.

---

## Editorial Office

ul. Marcinkowskiego 2–6  
50-368 Wrocław, Poland  
Tel.: +48 71 784 11 36  
E-mail: redakcja@umed.wroc.pl

## Publisher

Wrocław Medical University  
Wybrzeże L. Pasteura 1  
50-367 Wrocław, Poland

© Copyright by Wrocław Medical University,  
Wrocław 2020

Online edition is the original version of the journal

---

## Editor-in-Chief

Maciej Bagłaj

## Vice-Editor-in-Chief

Dorota Frydecka

---

## Editorial Board

Piotr Dziągpiel  
Marian Klinger  
Halina Milnerowicz  
Jerzy Mozrzymas

---

## Thematic Editors

Marzenna Bartoszewicz (microbiology)  
Marzena Dominiak (dentistry)  
Paweł Domosławski (surgery)  
Maria Ejma (neurology)  
Jacek Gajek (cardiology)  
Mariusz Kuształ  
(nephrology and transplantology)  
Rafał Matkowski (oncology)  
Ewa Milnerowicz-Nabzdyk (gynecology)  
Katarzyna Neubauer (gastroenterology)  
Marcin Ruciński (basic sciences)  
Robert Śmigiel (pediatrics)  
Paweł Tabakow (experimental medicine)  
Anna Wiela-Hojeńska  
(pharmaceutical sciences)  
Dariusz Wołowicz (internal medicine)

---

## International Advisory Board

Reinhard Berner (Germany)  
Vladimir Bobek (Czech Republic)  
Marcin Czyz (UK)  
Buddhadeb Dawn (USA)  
Kishore Kumar Jella (USA)

---

## Secretary

Katarzyna Neubauer

Piotr Ponikowski  
Marek Sąsiadek  
Leszek Szenborn  
Jacek Szepietowski

---

## Statistical Editors

Dorota Diakowska  
Leszek Noga  
Lesław Rusiecki

## Technical Editorship

Paulina Kunicka  
Marek Misiak

## English Language Copy Editors

Eric Hilton  
Sherill Howard Pociecha  
Jason Schock  
Marcin Tereszewski

---

Pavel Kopel (Czech Republic)  
Tomasz B. Owczarek (USA)  
Ivan Rychlík (Czech Republic)  
Anton Sculean (Switzerland)  
Andriy B. Zimenkovsky (Ukraine)

## Editorial Policy

Advances in Clinical and Experimental Medicine (Adv Clin Exp Med) is an independent multidisciplinary forum for exchange of scientific and clinical information, publishing original research and news encompassing all aspects of medicine, including molecular biology, biochemistry, genetics, biotechnology and other areas. During the review process, the Editorial Board conforms to the "Uniform Requirements for Manuscripts Submitted to Biomedical Journals: Writing and Editing for Biomedical Publication" approved by the International Committee of Medical Journal Editors ([www.ICMJE.org/](http://www.ICMJE.org/)). The journal publishes (in English only) original papers and reviews. Short works considered original, novel and significant are given priority. Experimental studies must include a statement that the experimental protocol and informed consent procedure were in compliance with the Helsinki Convention and were approved by an ethics committee.

For all subscription-related queries please contact our Editorial Office:  
[redakcja@umed.wroc.pl](mailto:redakcja@umed.wroc.pl)

For more information visit the journal's website:  
[www.advances.umed.wroc.pl](http://www.advances.umed.wroc.pl)

Pursuant to the ordinance No. 134/XV R/2017 of the Rector of Wrocław Medical University (as of December 28, 2017) from January 1, 2018 authors are required to pay a fee amounting to 700 euros for each manuscript accepted for publication in the journal Advances in Clinical and Experimental Medicine.

„Podniesienie poziomu naukowego i poziomu umiędzynarodowienia wydawanych czasopism naukowych oraz upowszechniania informacji o wynikach badań naukowych lub prac rozwojowych – zadanie finansowane w ramach umowy 784/p-DUN/2017 ze środków Ministra Nauki i Szkolnictwa Wyższego przeznaczonych na działalność upowszechniającą naukę”.



Indexed in: MEDLINE, Science Citation Index Expanded, Journal Citation Reports/Science Edition, Scopus, EMBASE/Excerpta Medica, Ulrich's™ International Periodicals Directory, Index Copernicus

Typographic design: Monika Kołęda, Piotr Gil  
DTP: Wydawnictwo UMW  
Cover: Monika Kołęda  
Printing and binding: EXDRUK

## Contents

### Original papers

- 1021 Jędrzej Wierzbicki, Maciej Nowacki, Marta Chrzanowska, Rafał Matkowski, Marcin Ziętek, Katarzyna Nowacka, Adam Maciejczyk, Edyta Pawlak-Adamska  
**Additive manufacturing technologies enabling rapid and interventional production of protective face shields and masks during the COVID-19 pandemic**
- 1029 Sebastian Krupa, Paweł Reichert  
**Clinical and functional evaluation of primary anterior crucial ligament reconstruction by using allograft**
- 1039 Agnieszka Chodkowska, Alicja Bieńkowska, Żaneta Słyk, Joanna Giebułtowicz, Maciej Małecki  
**Anticancer activity of topical ointments with histone deacetylase inhibitor, trichostatin A**
- 1051 Ewa Żurawska-Płaksej, Wiktor Kuliczkowski, Bożena Karolko, Magdalena Cielecka-Prynda, Jakub Dębski, Konrad Kaaz, Andrzej Mysiak, Tomasz Wróbel, Maria Podolak-Dawidziak, Lidia Usnarska-Zubkiewicz  
**Platelet polyphosphate level is elevated in patients with chronic primary thrombocytopenia: A preliminary study**
- 1057 Abdullah Arpacı, Serap Yalın, Hasret Ecevit, Ulku Comelekoglu, Turkan Mete  
**Enzyme activity and genetic polymorphisms in patients with type II diabetes mellitus**
- 1065 Michał Nowicki, Anna Zawiasa-Bryszewska, Małgorzata Taczykowska, Piotr Białasiewicz, Dariusz Nowak  
**The pattern of overnight changes in novel markers of acute kidney injury in patients with obstructive sleep apnea**
- 1073 Ying Shi, Xinghua Wang, Yingyan Qiao, Xueping Bai, Qinxiu Wang, Chenggong Lei  
**The dynamic enhanced characterization with low mechanical index gray-scale harmonic imaging inflammatory pseudotumor of liver compared with hepatic VX2 tumor and normal liver**
- 1083 Kinga Musiał, Danuta Zwolińska  
**Monocyte chemoattractant protein-1, macrophage colony stimulating factor, survivin, and tissue inhibitor of matrix metalloproteinases-2 in analysis of damage and repair related to pediatric chronic kidney injury**
- 1091 Mücahid Yılmaz, Hidayet Kayançığec, Nevzat Gözel, Mehmet Nail Bilen, Ertuğrul Kurtoğlu, Özlem Seçen, Pınar Öner, Suat Demirkıran, Ökkeş Uku, Yusuf Çekici, Orkun Eroglu, Fikret Keleş  
**Spotlights on some electrocardiographic paradigms: How should we evaluate normal reference values of Tp–Te interval, Tp–Te dispersion and Tp–Te/QT ratio?**
- 1101 Beata Nowak, Błażej Poźniak, Jarosław Popłoński, Łukasz Bobak, Agnieszka Matuszewska, Joanna Kwiatkowska, Wojciech Dziewiszek, Ewa Huszcza, Adam Szeląg  
**Pharmacokinetics of xanthohumol in rats of both sexes after oral and intravenous administration of pure xanthohumol and prenylflavonoid extract**
- 1111 Michał Biały, Agnieszka Szust, Piotr Napadłek, Maciej Dobrzyński, Włodzimierz Więckiewicz  
**The three-point bending test of fiber-reinforced composite root canal posts**

### Multicenter study

- 1117 Wojciech Walas, Zenon Halaba, Agata Kubiacyk, Andrzej Piotrowski, Julita Latka-Grot, Tomasz Szczapa, Monika Romul, Iwona Maroszyńska, Ewelina Malinowska, Magdalena Rutkowska, Michał Skrzypek, Robert Śmigiel  
**Skin conductance measurement for the assessment of analgosedation adequacy in infants treated with mechanical ventilation: A multicenter pilot study**

### Reviews

- 1123 Zhigang Cheng, Ping Liang  
**Advances in ultrasound-guided thermal ablation for symptomatic benign thyroid nodules**



# Additive manufacturing technologies enabling rapid and interventional production of protective face shields and masks during the COVID-19 pandemic

Jędrzej Wierzbicki<sup>1,A–D</sup>, Maciej Nowacki<sup>1,A,D–F</sup>, Marta Chrzanowska<sup>1,B–D</sup>, Rafał Matkowski<sup>2,3,E,F</sup>, Marcin Ziętek<sup>2,3,E</sup>, Katarzyna Nowacka<sup>4,E</sup>, Adam Maciejczyk<sup>2,3,E,F</sup>, Edyta Pawlak-Adamska<sup>5,E,F</sup>

<sup>1</sup> The Minimally Invasive and Experimental Surgery Unit, Chair and Department of Surgical Oncology, Ludwik Rydygier's Collegium Medicum in Bydgoszcz, Nicolaus Copernicus University in Toruń, Poland

<sup>2</sup> Department of Oncology, Wrocław Medical University, Poland

<sup>3</sup> Wrocław Comprehensive Cancer Center, Wrocław, Poland

<sup>4</sup> Chair of Cosmetology and Aesthetic Dermatology, Ludwik Rydygier's Collegium Medicum in Bydgoszcz, Nicolaus Copernicus University in Toruń, Poland

<sup>5</sup> Laboratory of Immunopathology, Department of Experimental Therapy, Hirsfeld Institute of Immunology and Experimental Therapy, Polish Academy of Sciences, Wrocław, Poland

A – research concept and design; B – collection and/or assembly of data; C – data analysis and interpretation;

D – writing the article; E – critical revision of the article; F – final approval of the article

Advances in Clinical and Experimental Medicine, ISSN 1899–5276 (print), ISSN 2451–2680 (online)

*Adv Clin Exp Med.* 2020;29(9):1021–1028

## Address for correspondence

Maciej Nowacki

E-mail: maciej.s.nowacki@gmail.com

## Funding sources

None declared

## Conflict of interest

None declared

Received on May 12, 2020

Reviewed on May 28, 2020

Accepted on August 11, 2020

Published online on October 1, 2020

## Cite as

Wierzbicki J, Nowacki M, Chrzanowska M, et al.

Additive manufacturing technologies enabling rapid and interventional production of protective face shields and masks during the COVID-19 pandemic. *Adv Clin Exp Med.* 2020;29(9):1021–1028. doi:10.17219/acem/126296

## DOI

10.17219/acem/126296

## Copyright

© 2020 by Wrocław Medical University

This is an article distributed under the terms of the Creative Commons Attribution 3.0 Unported (CC BY 3.0) (<https://creativecommons.org/licenses/by/3.0/>)

## Abstract

**Background.** Severe acute respiratory syndrome coronavirus 2 (SARS-CoV-2) is transmitted through respiratory droplets and contact routes, hence the demand for personal protective equipment (PPE) has increased during the outbreak of coronavirus disease 2019 (COVID-19). Among the most noticeable shortages was the lack of face shields. The urgent demand for PPE induced interdisciplinary cooperation to overcome the shortages, and additive manufacturing proved to be ideal for the crisis situation.

**Objectives.** To investigate the possibilities of implementing additive manufacturing technologies in the interventional fabrication of protective face shields for medical staff.

**Material and methods.** An Ender 3 Pro 3D printer was used to print headbands and Cura 4.4 was chosen as the slicing software. Open source face shield designs were downloaded as standard tessellation language (STL) files and compared. Only models with scientific support were taken under consideration.

**Results.** The mean time for producing the headbands tested ranged from 59 min to almost 3 h, depending on the design. After setting up our low budget printer and choosing the Prusa RC 3 protective face shield as the main product, we were able to fabricate about 30 face shields per week at a cost of about €1 each. During 4 weeks, 126 face shields were produced and delivered to various hospital wards, which substantially eased the shortages.

**Conclusions.** Additive manufacturing enables immediate responses to needs in emergency situations, and allows for mass production of personal protective equipment in a short time due the rapid exchange of data among printer users. Despite the unregulated legal situation and insufficient scientific evidence, such protective equipment has been approved by clinicians and is currently used by medical personnel around the world.

**Key words:** personal protective equipment, additive manufacturing, 3-dimensional printing, COVID-19, face shield

Historically, each pandemic has provoked many unexpected changes in both national and international health systems.<sup>1,2</sup> This is due to the fact that the course of a pandemic is always unexpected, often characterized by a turbulent course and social panic.<sup>3</sup> From the first well-documented pandemics like the plague or Spanish influenza to recent well-known and widely studied epidemics like Middle East Respiratory Syndrome (MERS) and Severe Acute Respiratory Syndrome (SARS), it is clear that international efforts to contain a given pathogen should always be multidisciplinary and multistage.<sup>4–6</sup> The first medical doctors, researchers and people combating with a new and unknown disease have very quickly noticed that apart from the search for the biological causes of a pandemic or the search for a remedy in the form of an active drug or vaccine, another important aspect is to quickly introduce preventive methods and tools that minimize the number of infected persons.<sup>7,8</sup> The current coronavirus disease 2019 (COVID-19) outbreak, which was initially a regional problem, is now an emerging global challenge involving health care, governments and international institutions.

## Classification of the novel coronavirus

The virus causing COVID-19 was tentatively named by the World Health Organization (WHO) as “2019 novel coronavirus” (2019-nCoV). However, the Coronaviridae Study Group of the International Committee on Taxonomy of Viruses classified 2019-nCoV and renamed it “severe acute respiratory syndrome coronavirus 2” (SARS-CoV-2) on the basis of scientific evidence.<sup>9</sup>

SARS-CoV-2, like MERS-CoV and SARS-CoV, belongs to the Coronaviridae family<sup>9</sup>, and causes similar symptoms in humans, including fever, dyspnea, cough or gastrointestinal manifestations, often leading to pneumonia or severe acute respiratory illness.<sup>10–12</sup> The original place from which COVID-19 derived is the city of Wuhan in Hubei Province, China, from where it spread worldwide.<sup>13</sup> The origin of the virus is still unknown and controversial. Most papers suggest that the probable explanation is that SARS-CoV-2 is a  $\beta$ -coronavirus with a genome very similar to bat coronavirus, which progressed into human-to-human transmission through a seafood market zoonotic infection.<sup>14,15</sup>

## Infectivity and uniqueness of SARS-CoV-2

The first clinical reports raised concerns due to the high mortality and transmissibility of SARS-CoV-2.<sup>16,17</sup> Subsequent reviews showed that the infection demonstrates an exponential model of growth, doubling in just over 6 days.<sup>13</sup> Moreover, information about the virus being spread by people with no signs of the disease appeared which indicated that preventing SARS-CoV-2 transmission could be very challenging.<sup>18,19</sup> Other factors involved

in the exceptional virulence of the virus are its viability in aerosols and durability on various surfaces, like SARS-CoV-1. Studies have shown that SARS-CoV-2 remains stable for up to 72 h on plastic and stainless steel, whereas in aerosols it remains viable for 3 h.<sup>20</sup> Further research found that the virus may be transferred through airflows and settle on protective personal equipment (PPE) as well as on objects in the closest environment of infected people.<sup>21</sup> Therefore, global prevalence of the pathogen has become inevitable.

All of the above has made the virus an unusual opponent. As a result of insufficient effectiveness of the fight to contain it, on March 11, 2020, the WHO announced that we are currently dealing with a pandemic.

## Additive manufacturing versus the pandemic

The international struggle against COVID-19 requires the use of similar resources, which rapidly leads to their depletion. Shortages of PPE on the front lines raised deep concerns due to the effects on pandemic development and patient care.<sup>22</sup>

In response to the growing demand for PPE for health-care workers, there have been grassroots initiatives, industrial efforts and scientists using different approaches to produce medical equipment. Especially during the first phase of the pandemic, additive manufacturing (AM) was perfectly suited to the mass production of PPE.<sup>23</sup> Additive manufacturing techniques, commonly known as 3-dimensional printing, have made appreciable progress since their implementation in the 1980s. Their complementary advantages, such as the ease of use, low costs and a wide range of materials allow for rapid adaptation to immediate needs.<sup>24,25</sup> Moreover, their flexibility means they can be used in many different branches of science and industry.<sup>26,27</sup> The most common 3D printers use fused deposition modeling (FDM) technology, where the nozzle releases a heated filament onto a moving platform and, layer by layer, recreates a previously designed shape.<sup>28</sup>

During the COVID-19 pandemic, the adaptability of AM has become particularly apparent. The online community was able to share ideas for 3D-printed devices (Fig. 1) from the very first days of the pandemic.<sup>24,29</sup> Open-source websites made it possible for hobbyists and specialists to meet, and peer-to-peer comments allowed for quick data exchange.<sup>30</sup> The aim of this paper was to review and analyze the current additive manufacturing technologies enabling rapid interventional production of protective face shields for medical staff during the SARS-CoV-2 pandemic.

## Material and methods

In order to choose the most optimal solutions, it was necessary to establish an action plan. The following steps were defined by our team: identification of possible problems;

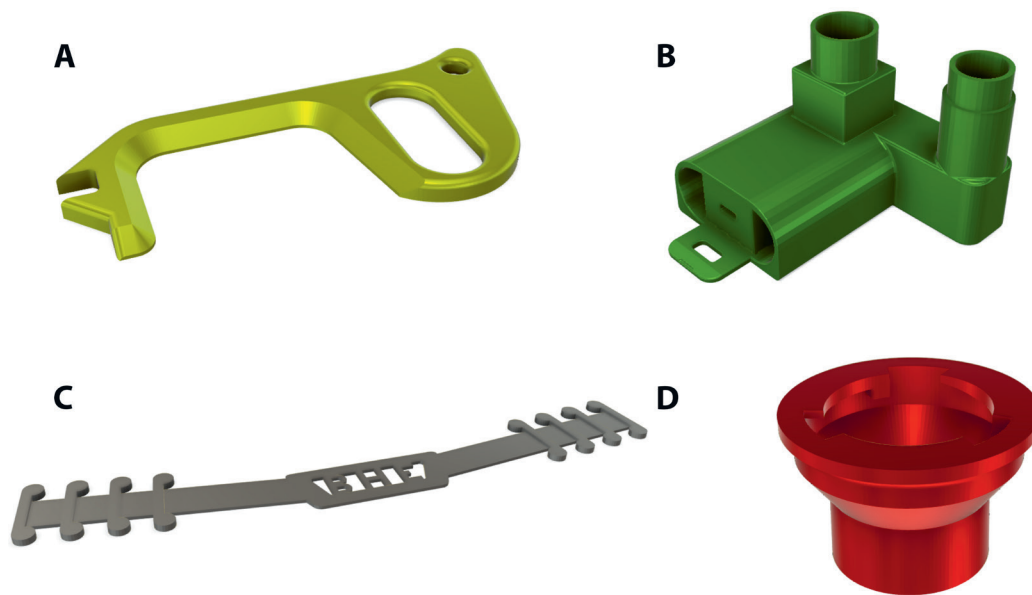


**Fig. 1.** Available designs for COVID-19-related devices  
 A – contactless door opener; B – adapter valve for converting a snorkeling mask into an oxygen mask; C – mask extender to reduce pain from wearing a mask; D – Secura mask connector to a DAR filter.

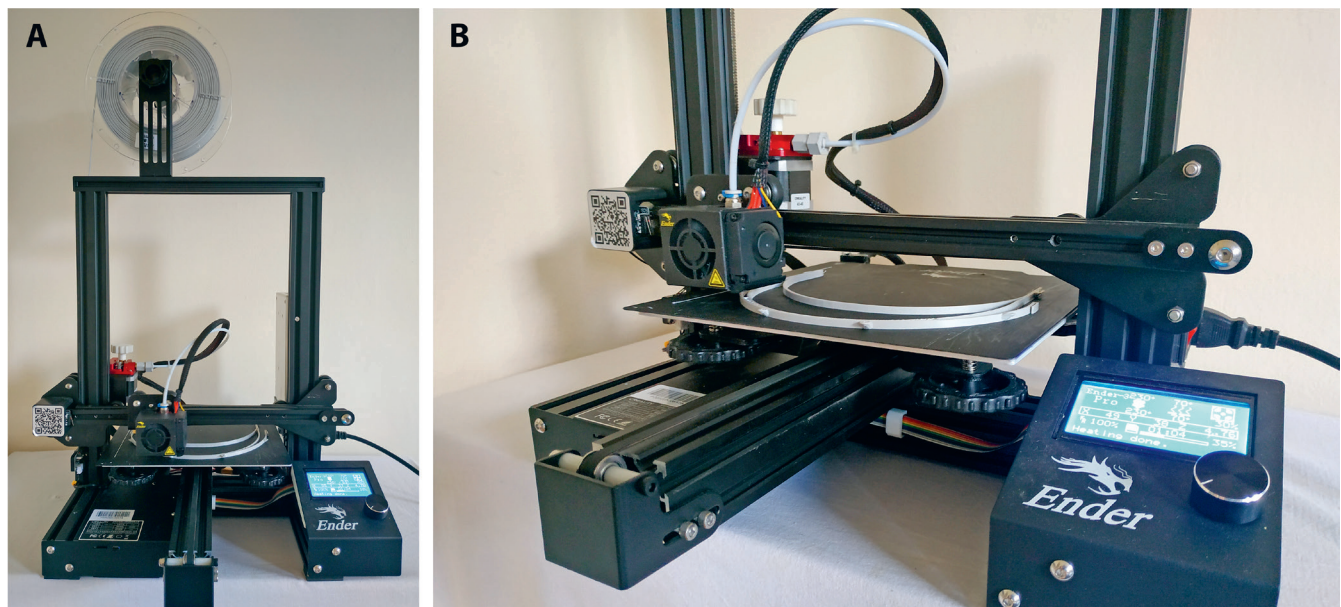


**Fig. 2.** Ender 3 Pro Creality  
 A – overall view of the printer; B – layer-by-layer process of face shield production.

test of available face shield designs; fabrication of a prototype series; assessment of usage in clinical conditions; “mass” production and extensive evaluation under real conditions. In the last days of March we intensively tested different designs of visors and assessed our capacity.

Face shields as standard tessellation language (STL) files were downloaded from the official web pages of the inventors. A low-budget 3D printer capable of producing accurate models<sup>31</sup>, a stock version of Ender 3 Pro (Creality 3D Technology Co. Ltd, Shenzhen, China) (Fig. 2) was used for production, and Cura 4.4 freeware (Ultimaker, Utrecht, the Netherlands) was chosen for the slicing process. For prototyping, testing various available models and

ultimately printing the first series, polylactic acid (PLA) was used due to availability and ease of use. After the test series we changed the filament to glycol-modified polyethylene terephthalate (PETG) due to its higher temperature resistance, durability and proven safety.<sup>32</sup>

We have decided to describe only our experience using PETG. Despite the fact that PETG is a recommended material for face shield manufacturing, its use is controversial. To the best of our knowledge, there have been no comparative studies about PETG sterilization methods and usage protocols in this kind of situation.

We had to adjust some of our printing settings in Cura. As a result of durability tests, the height of a layer was

set to 0.28 mm with 20% infill. A 0.4 mm nozzle was used and the temperature was maintained at 230°C, with a bed temperature of 70°C. After the test series and having established a satisfactory ratio of quality to speed, the printing speed was set at 60 mm/s. The most problematic issues were the retraction distance and retraction speed; in the end these were set to 4 mm and 25 mm/s, respectively. Incorrect retraction would cause so-called oozing, affecting the surface smoothness and the overall appearance.<sup>33</sup> All of the face shields delivered to the medical departments were printed at the given settings.

## Results

### A multitude of face shield designs

We followed the developments and experiences of other groups and finally decided to implement AM techniques for the production of face shields, a shortage of which had been officially reported in our region. In our review during the tests, we took into consideration available designs of visors with scientific support. All of the designs presented in Table 1, apart from the so-called peaked headband, which is popular in Poland, have undergone review in a clinical setting by the National Institutes of Health (NIH; Bethesda, USA). The general assumption of all the designs is the same: A 3D-printed framework is combined with elastic rubber and a transparent visor.<sup>34</sup> It is worth pointing out that all of the resources necessary to produce a face shield can be obtained online without leaving home.

Simplicity of production and significant support from many institutions, laboratories and clinicians in our region were our main reasons for choosing the Prusa RC 3 protective face shield (Prusa Research, Prague, Czech Republic; <https://www.prusaprinters.org/prints/25857-protective-face-shield-rc1>) (Fig. 3). Moreover, the design was developed and analyzed in accordance with the Czech Ministry of Health guidelines. It is noteworthy that the assembly time for this design is about 30 s.

The use of buttonhole rubber (0.6–1.2 mm wide, polyester, purchased by the meter), commonly available in sewing goods stores, means that it is possible to adjust the face shields regardless of head circumference.

For the face covering, different materials may be used depending on accessibility. It is possible to use 0.2–0.7 mm PET foil formed in sheets or available in A4 format. The stiffness of this material increases with thickness; however, the thicker it is, the more difficult it is to process, especially without a laser plotter. We mainly used document-binding covers (A4, 0.2 mm). Thicker foils were harder to obtain and significantly more expensive, due to mass production of face shields in our region. The foil sheets were perforated with a standard office hole puncher and clamped into designated pins.



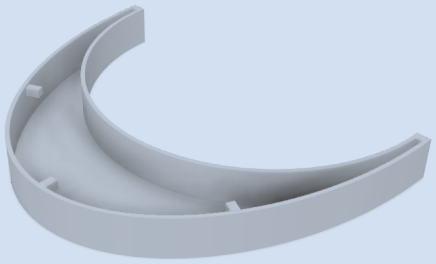
Fig. 3. Prusa RC 3 protective face shield

Due to the urgent demand for PPE, the US Food and Drug Administration allows production of 3D-printed visors outside of the normal mode if they are printed in accordance with instructions.<sup>35</sup> There are various regulations in different regions of the world and it is essential to follow the appropriate authority guidelines. Despite controversies, these visors are accepted and used by medical staff all over the world and are constantly tested by specialists and clinicians. There is a lack of robust evidence in this area, but it is encouraging that the first scientific reports on the use of 3D-printed face shields have appeared.<sup>36</sup>

### Financial aspects

Printers that allow continuous operation and provide relatively high quality are available in the €200–300 price range. The approximate price of 1 kg of average quality PETG filament is about €18, but the cost of each face shield depends on the printing quality and reliability.<sup>37</sup> In our case it was possible to fabricate an average of 28 face shields from 1 kg of PETG, resulting in a cost of €0.62 per item. It is difficult to assess the cost of electricity needed to print a mask, but in our experience it is approx. €0.05 for 2 h of printing. The estimated prices of a single foil and 20 cm of elastic rubber is €0.07 and €0.30, respectively. Summarizing, in our case the cost of producing 1 reusable face shield was €1.04, which was significantly lower than in other groups.<sup>38</sup> This calculation takes into account the price increases that followed the increased demand for the materials.

**Table 1.** Comparison of available face shields produced using Fused Deposition Modeling (FDM)

Project name	Scheme	Printing time (at our settings)	Filament usage [g]	Estimated cost [€]
Prusa RC 3 protective face shield (A)		2 h 12 min	34	0.61
3DVerkstan face shield [B]		59 min	13	0.23
IC3D Budmen face shield [C]		2 h	28	0.50
DTM v3.1 face shield [D]		2 h 52 min	54	0.97
Peaked headband DDS2 [E]		2 h 49 min	47	0.85

Details were estimated based on our settings of the Cura 4.4 slicer; A – Prusa Research, Prague, Czech Republic; <https://www.prusaprinters.org/prints/25857-protective-face-shield-rc1>. Accessed April 26, 2020; B – 3DVerkstan, Stockholm, Sweden; <https://3dverkstan.se/protective-visor/>. Accessed April 26, 2020; C – IC3D Industries, Columbus, USA; <https://3dprint.nih.gov/discover/3dpx-013309/> Accessed April 26, 2020; D – Prusa Research; <https://3dprint.nih.gov/discover/3dpx-013359>. Accessed April 26, 2020; E – #Drukarzedlaszpitali (grassroot initiative), Poland; <https://www.drukarzedlaszpitali.pl/Pliki/>. Accessed April 26, 2020.

## Current knowledge and controversy

Due to the mode of transmission of SARS-CoV-2<sup>14</sup> the 3D printing community is focused on the fabrication of devices to protect the respiratory tract. An unprecedented need for PPE elicited a major cooperative initiative at an international level.<sup>39</sup> However, mass production of protective gear outside of the standard certification system raises controversy, and minimum requirements for self-produced PPE should be developed to ensure the safety of medical personnel.<sup>40</sup>

The use of face shields is not standardized; it depends on different departments' specific protocols and on the availability of PPE. According to Prusa Research recommendations, currently the only safe way to use the face shield is single-use. To our knowledge, paramedics who received our shields have used them that way. Nevertheless, they were well equipped with protective gear due to the fact that they were on the front line. The situation was entirely different in the case of departments potentially less exposed to the novel coronavirus, where multiple uses of equipment, disinfection and replacement of foils and rubber were taken into consideration.<sup>34</sup> Therefore, it was necessary to develop methods for cleaning the face shields so that they could be reused without the risk of infection.

There is a wide range of possible sterilization methods, which are mainly based on 3 factors: gases, temperature and chemical reagents.<sup>41</sup> However, certain characteristics of AM-produced items have implications for disinfection. The primary limitations of sterilizing 3D-printed medical devices are their porous structure and microscopic crevices created during the layer-by-layer process, where pathogens may theoretically withstand disinfection conditions.<sup>42</sup> Another obstacle is the high temperature used in sterilization processes. In the case of synthetic polymers, high temperatures may damage various widely used filaments and cause losses of structural integrity.<sup>43</sup> This partially explains why PETG is the most widely recommended material despite insufficient evidence. In cooperation with leading Czech laboratories and hospitals, Prusa Research performed a series of tests, and as a result they selected recommended methods of sterilization, which are

**Table 2.** Verified methods of sterilizing the Prusa RC 3 protective face shield

Method	Conditions
Hot air dryer	65°C (149°F), 60 min
WHO handrub disinfection	75% IPA, 5 min
Isopropanol (IPA)	96%, 5 min
Isopropanol (IPA)	75%, 5 min
Sodium hypochlorite (household bleach)	min. 0.01% of hypochlorite (e.g., SAVO 1:10), 2 min+
UV-C	radiation, 30 W, wavelength below 280 nm, 15 min
Ethanol	70–80% max, 5 min
Hydrogen peroxide	25%, 5 min

presented in Table 2. These sanitizing practices are in line with the guidelines available on the GetUsPPE web platform for physicians and medical researchers in the USA.<sup>44</sup> Further studies are necessary to determine if these procedures are effective enough to prevent infection.

Subsequent reports and our experience confirm that PPE produced quickly and at low cost should be used by medical staff even if they are not as effective as certified equipment.<sup>36,38</sup> Apart from psychological comfort, simple face shields work as a physical barrier against airborne droplets. The indisputable advantage of face shields is that they protect not only the nose and mouth (surgical masks), or the eyes (protective goggles), but the whole face.<sup>39</sup> Furthermore, 3D-printed visors are lightweight and have sufficient space for goggles, a mask or a N95 respirator.<sup>36</sup>

## Discussion

A pandemic is a difficult period for all the governments of the world. It is necessary not only to introduce optimal restrictions and appropriate financial management, but also to properly distribute protective gear for all services, especially for healthcare workers most exposed to infection.<sup>36</sup> However, it is hard to provide PPE to medical services when its worldwide production cannot keep up with its utilization, which raises various issues.

In the United Kingdom, members of the British Medical Association (BMA) reported that PPE was distributed in small quantities, did not protect medical personnel well enough or in some cases did not reach National Health Service (NHS) staff at all.<sup>45</sup> Reports received from nurses also confirmed a total lack of protection against the coronavirus.<sup>46</sup> A survey carried out by the BMA revealed that more than 40% of the general practitioners (GPs) asked were affected by a lack of fluid-repellent facemasks. Moreover, more than 55% of surveyed hospital doctors reported that they felt only slightly secured against SARS-CoV-2, and 1/3 of them felt unprotected. Among GPs these values were almost 50–50.<sup>47</sup>

Information related to concerns about the lack of protective equipment has also emerged from all around the world. In Australia, recently devastated by the massive bushfires, GPs reported a shortage of face masks as people wore them to protect from harmful smoke.<sup>48</sup> In the USA, the shortage of protective measures included not only PPE for medical personnel, such as masks, gloves, gowns and face shields, but also ventilators for patients.<sup>49</sup> The rapid mobilization of AM printers enabled the production of face shields as well as other protective items on a mass scale. Furthermore, more efficient and personalized N95 masks, ventilator valves and even medications have been designed.<sup>23,36</sup> Concerns about ventilator shortages have been partially alleviated thanks to a variety of free projects.<sup>49</sup>

Rapid implementation of AM techniques was important for another reason. As a result of deficiencies in PPE and

increased contact with infected people, the problem of COVID-19 infection strongly limited medical personnel's ability to work. In the Netherlands, a quick two-day study on health-care workers at 9 hospitals revealed that 4.1% of the staff that presenting slight signs of respiratory infection tested positive for SARS-CoV-2.<sup>50</sup> In China, in turn, on February 24<sup>th</sup>, 2020, the National Health Commission of the People's Republic of China stated that among medical staff, 2055 persons were infected with COVID-19, of whom 22 died.<sup>51</sup> For those who are in the front lines of the fight against the pandemic, PPE is an essential element of everyday life. NHS doctors stated that "health-care workers on the front line without PPE is the equivalent of going to war without armor and protection".<sup>46</sup> Protective gear not only plays a role in building mental comfort and a sense of safety, but also protects wearers from infection and limits transmission.<sup>52</sup> Additive manufacturing is particularly promising in the production of PPE due to a fact that the barrier against transmission of the virus can be not only physical, but also biological, through the use of antimicrobial polymers.<sup>29</sup>

When a pandemic breaks out, medical personnel struggle with rapidly growing numbers of patients, time pressure and information chaos. Consequently, they have to deal with a greater workload, longer working hours and an increased mental burden.<sup>52</sup> In these conditions, medical staff has to cope with variety of sensations from fear and anger, through stress, anxiety and a sense of isolation, to depressive symptoms and/or insomnia.<sup>53</sup> Mental health among medical workers is quite a serious issue, because it results in overall well-being, which leads to grounded self-confidence. In turn, self-efficacy increases their work performance thus their effectiveness in treating patients.<sup>54</sup> Among the most important factors that relate to mental health is a sense of safety, and PPE is a relevant medium to support feeling secure during a pandemic.

## Conclusions

The special role of PPE cannot be overlooked. Apart from preventing the spread of the novel coronavirus, PPE enables medical personnel to treat dramatically ill patients. Furthermore, COVID-19-related shortages of protective gear significantly affect the mental health of medical workers. In accordance with the antique maxim "prevention is better than a cure", emphasis should be placed on ensuring safety and appropriate working conditions for those who are directly exposed to the novel coronavirus and who can limit the ongoing pandemic.

During the COVID-19 pandemic it has been encouraging to see novel approaches to solving problems through global cooperation using open sources and free sharing. A 3D printer alone is definitely not the most efficient tool for mass production; however, the large number of users means that currently there are thousands of 3D-printed face shields in use in many sectors of public health and

there is still a great demand for them. Face shields produced by specialists, companies, hospitals and hobbyists may to some measure reduce the disruptions in supply chains observed around the world. We hope that the data we have presented may reduce the deficit of PPE for medical staff and save valuable time for those who implement these techniques.

## ORCID iDs

Jędrzej Wierzbicki  <https://orcid.org/0000-0001-9959-8855>  
 Maciej Nowacki  <https://orcid.org/0000-0001-8424-7198>  
 Marta Chrzanowska  <https://orcid.org/0000-0002-1371-3371>  
 Rafał Matkowski  <https://orcid.org/0000-0002-1705-5097>  
 Marcin Ziętek  <https://orcid.org/0000-0002-7890-3483>  
 Katarzyna Nowacka  <https://orcid.org/0000-0001-8529-5976>  
 Adam Maciejczyk  <https://orcid.org/0000-0002-7047-0433>  
 Edyta Pawlak-Adamska  <https://orcid.org/0000-0002-0386-7940>

## References

- Mossad SB. Influenza update 2018–2019: 100 years after the great pandemic. *Cleve Clin J Med*. 2018;85(11):861–869. doi:10.3949/ccjm.85a.18095
- Indini A, Aschele C, Cavanna L, et al. Reorganization of medical oncology departments during the novel coronavirus disease-19 pandemic: A nationwide Italian survey. *Eur J Cancer*. 2020;6(132):17–23. doi:10.1016/j.ejca.2020.03.024
- Jakovljevic M, Bjedov S, Jaksic N, et al. COVID-19 pandemia and public and global mental health from the perspective of global health security. *Psychiatr Danub*. 2020;32(1):6–14. doi:10.24869/psyd.2020.6
- Gully PR. Pandemics, regional outbreaks, and sudden-onset disasters. *Health Manage Forum*. 2020;33(4):164–169. doi:10.1177/0840470420901532
- Nickol ME, Kindrachuk J. A year of terror and a century of reflection: Perspectives on the great influenza pandemic of 1918–1919. *BMC Infect Dis*. 2019;6;19(1):117. doi:10.1186/s12879-019-3750-8
- Bramanti B, Dean KR, Walløe L, Chr Stenseth N. The third plague pandemic in Europe. *Proc Biol Sci*. 2019;286(1901):20182429. doi:10.1098/rspb.2018.2429
- Graham BS, Sullivan NJ. Emerging viral diseases from a vaccinology perspective: Preparing for the next pandemic. *Nat Immunol*. 2018;19(1):20–28. doi:10.1038/s41590-017-0007-9
- Morse SS, Mazet JA, Woolhouse M, et al. Prediction and prevention of the next pandemic zoonosis. *Lancet*. 2012;380(9857):1956–1965. doi:10.1016/S0140-6736(12)61684-5
- Coronaviridae Study Group of the International Committee on Taxonomy of Viruses. The species severe acute respiratory syndrome-related coronavirus: Classifying 2019-nCoV and naming it SARS-CoV-2. *Nat Microbiol*. 2020;5(4):536–544. doi:10.1038/s41564-020-0695-z
- Zhang JJ, Dong X, Cao YY et al. Clinical characteristics of 140 patients infected with SARS-CoV-2 in Wuhan, China. *Allergy*. 2020;75(7):1730–1741. doi:10.1111/all.14238
- Nassar MS, Bakhrebah MA, Meo SA, et al. Middle East Respiratory Syndrome Coronavirus (MERS-CoV) infection: epidemiology, pathogenesis and clinical characteristics. *Eur Rev Med Pharmacol Sci*. 2018;22(15):4956–4961. doi:10.26355/eurev\_201808\_15635.
- Po-Ren H, Cheng-Hsiang H, Shiou-Hwei Y, et al. Microbiologic characteristics, serologic responses, and clinical manifestations in severe acute respiratory syndrome, Taiwan. *Emerg Infect Dis*. 2003;9(9):1163–1167. doi:10.3201/eid0909.030367
- Lai CC, Shih TP, Ko WC, et al. Severe acute respiratory syndrome coronavirus 2 (SARS-CoV-2) and coronavirus disease-2019 (COVID-19): The epidemic and the challenges. *Int J Antimicrob Agents*. 2020;55(3):105924. doi:10.1016/j.ijantimicag.2020.105924
- Zhou P, Yang X, Wang X, et al. A pneumonia outbreak associated with a new coronavirus of probable bat origin. *Nature*. 2020;579:270–273. doi:10.1038/s41586-020-2012-7
- Guo YR, Cao QD, Hong ZS, et al. The origin, transmission and clinical therapies on coronavirus disease 2019 (COVID-19) outbreak – an update on the status. *Mil Med Res*. 2020;13;7(1):11. doi:10.1186/s40779-020-00240-0

16. Huang C, Wang Y, Li X, et al. Clinical features of patients infected with 2019 novel coronavirus in Wuhan, China. *Lancet*. 2020;15(395):497–506. doi:10.1016/S0140-6736(20)30183-5
17. Yang X, Yu Y, Xu J, et al. Clinical course and outcomes of critically ill patients with SARS-CoV-2 pneumonia in Wuhan, China: A single-centered, retrospective, observational study. *Lancet Respir Med*. 2020;8:475–481. doi:10.1016/S2213-2600(20)30079-5
18. Bai Y, Yao L, Wei T, et al. Presumed asymptomatic carrier transmission of COVID-19. *JAMA*. 2020;323(14):1406–1407. doi:10.1001/jama.2020.2565
19. Hu Z, Song C, Xu C, et al. Clinical characteristics of 24 asymptomatic infections with COVID-19 screened among close contacts in Nanjing, China. *Sci China Life Sci*. 2020;63:706–711. doi:10.1007/s11427-020-1661-4
20. van Doremalen N, Bushmaker T, Morris DH, et al. Aerosol and surface stability of SARS-CoV-2 as compared with SARS-CoV-1. *N Engl J Med*. 2020;382(16):1564–1567. doi:10.1056/NEJMc2004973
21. Ong SWX, Tan YK, Chia PY, et al. Air, surface environmental, and personal protective equipment contamination by severe acute respiratory syndrome coronavirus 2 (SARS-CoV-2) from a symptomatic patient. *JAMA*. 2020;323(16):1610–1612. doi:10.1001/jama.2020.3227
22. Ranney ML, Griffith V, Jha AK. Critical supply shortages: The need for ventilators and personal protective equipment during the Covid-19 pandemic. *N Engl J Med*. 2020;30;382(18):e41. doi:10.1056/NEJMp2006141
23. Tino R, Moore R, Antoline S, et al. COVID-19 and the role of 3D printing in medicine. *3D Print Med*. 2020;6(1):11. Published on April 27, 2020 doi:10.1186/s41205-020-00064-7
24. Liaw CY, Guvendiren M. Current and emerging applications of 3D printing in medicine. *Biofabrication*. 2017;9(2):024102. doi:10.1088/1758-5090/aa7279
25. Tappa K, Jammalamadaka U. Novel biomaterials used in medical 3D printing techniques. *J Funct Biomater*. 2018;9(1):17. doi:10.3390/jfb9010017
26. Ventola CL. Medical applications for 3D printing: Current and projected uses. *Pharmacy and Therapeutics*. 2014;39(10):704–711. <https://www.ncbi.nlm.nih.gov/pmc/articles/PMC4189697/>
27. Mikołajewska E, Macko M, Mikołajewski D, et al. Medical and military applications of 3D printing. *Scientific Journal of the Military University of Land Forces*. 2016;1:128–141. doi:10.5604/17318157.1201744
28. Konta A, García-Piña M, Serrano D. Personalised 3D-printed medicines: Which techniques and polymers are more successful? *Bio-engineering*. 2017;4(4):79.
29. Zuniga JM, Cortes A. The role of additive manufacturing and antimicrobial polymers in the COVID-19 pandemic [published online ahead of print, on April 30, 2020]. *Expert Rev Med Devices*. 2020;1–5. doi:10.3390/bioengineering4040079
30. Zastrow M. Open science takes on the coronavirus pandemic. *Nature*. 2020;581(7806):109–110. doi:10.1038/d41586-020-01246-3
31. Herrmann KH, Gärtner C, Güllmar D, et al. 3D printing of MRI compatible components: why every MRI research group should have a low-budget 3D printer. *Med Eng Phys*. 2014;36(10):1373–1380. doi:10.1016/j.medengphy.2014.06.008
32. Oth O, Dauchot C, Orellana M, Glineur R. How to sterilize 3D-printed objects for surgical use? An evaluation of the volumetric deformation of 3D-printed genioplasty guide in PLA and PETG after sterilization by low-temperature hydrogen peroxide gas plasma. *Open Dent J*. 2019;13:410–417. doi:10.2174/1874210601913010410
33. Stabile L, Scungio M, Buonanno G, Arpino F, Ficco G. Airborne particle emission of a commercial 3D printer: The effect of filament material and printing temperature. *Indoor Air*. 2016;27(2):398–408. doi:10.1111/ina.12310
34. Sapoval M, Gaultier AL, Del Giudice C, et al. 3D-printed face protective shield in interventional radiology: Evaluation of an immediate solution in the era of COVID-19 pandemic [published online ahead of print, on April 18, 2020]. *Diagn Interv Imaging*. 2020;S2211-5684(20)30097-8. doi:10.1016/j.diii.2020.04.004
35. U.S. Food and Drug Administration. Center for Devices and Radiological Health. Enforcement Policy for Face Masks and Respirators During the Coronavirus Disease (COVID-19) Public Health Emergency (Revised). 2020. <https://www.fda.gov/regulatory-information/search-fda-guidance-documents/enforcement-policy-face-masks-and-respirators-during-coronavirus-disease-covid-19-public-health>. Accessed April 25, 2020.
36. Wesemann C, Pieralli S, Fretwurst T, et al. 3-D printed protective equipment during COVID-19 pandemic. *Materials (Basel)*. 2020;24;13(8). doi:10.3390/ma13081997
37. Gregor A, Filová E, Novák M, et al. Designing of PLA scaffolds for bone tissue replacement fabricated by ordinary commercial 3D printer. *J Biol Eng*. 2017;11(31). doi:10.1186/s13036-017-0074-3
38. Amin D, Nguyen N, Roser SM, Abramowicz S. 3D printing of face shields during COVID-19 pandemic: A technical note [published online ahead of print, on May 1, 2020]. *J Oral Maxillofac Surg*. 2020. doi:10.1016/j.joms.2020.04.040
39. Ishack S, Lipner SR. Applications of 3D printing technology to address COVID-19 related supply shortages [published online ahead of print, on April 21, 2020]. *Am J Med*. 2020;S0002-9343(20)30332-6. doi:10.1016/j.amjmed.2020.04.002
40. Pecchia L, Piaggio D, Maccaro A, Formisano C, Iadanza E. The inadequacy of regulatory frameworks in time of crisis and in low-resource settings: Personal protective equipment and COVID-19 [published online ahead of print, on May 2, 2020]. *Health Technol (Berl)*. 2020;1–9. doi:10.1007/s12553-020-00429-2
41. Tipnis NP, Burgess DJ. Sterilization of implantable polymer-based medical devices: A review. *Int J Pharm*. 2018;544(2):455–460. doi:10.1016/j.ijpharm.2017.12.003
42. Kim E, Shin Y-J and Ahn S-H. The effects of moisture and temperature on the mechanical properties of additive manufacturing components: Fused deposition modeling. *Rapid Prototyp J*. 2016;22:887–894. doi:10.1108/RPJ-08-2015-0095
43. Rogers WJ. Sterilization Techniques for Polymers. In: Lerouge S and Simmons A. *Sterilization of Biomaterials and Medical Devices*. 1st ed. Cambridge, United Kingdom: Elsevier Science & Technology; 2012: 151–211. doi:10.1533/9780857096265.151
44. Gondli S, Beckman AL, Deveau N, et al. Personal protective equipment needs in the USA during the COVID-19 pandemic. *Lancet*. 2020;395(10237):e90–e91. doi:10.1016/S0140-6736(20)31038-2
45. Newman M. Covid-19: Doctors' leaders warn that staff could quit and may die over lack of protective equipment. *BMJ*. 2020;368:m1257. Published on March 26, 2020 doi:10.1136/bmj.m1257
46. Nelson R. Lack of protective gear disrupts oncology care. *Lancet Oncol*. 2020;21(5):631–632. doi:10.1016/S1470-2045(20)30223-0
47. Rimmer A. Covid-19: Doctors still do not have proper PPE. *BMJ*. 2020;369:m1423. doi:10.1136/bmj.m1423
48. Mahase E. Novel coronavirus: Australian GPs raise concerns about shortage of face masks. *BMJ*. 2020;368:m477. doi:10.1136/bmj.m477
49. Ranney ML, Griffith V, Jha AK. Critical supply shortages – the need for ventilators and personal protective equipment during the covid-19 pandemic. *N Engl J Med*. 2020;30;382(18):e41. doi:10.1056/NEJMp2006141
50. Reusken CB, Buiting A, Bleeker-Rovers C, et al. Rapid assessment of regional SARS-CoV-2 community transmission through a convenience sample of healthcare workers, the Netherlands, March 2020. *Euro Surveill*. 2020;25(12):2000334. doi:10.2807/1560-7917
51. Wang J, Zhou M, Liu F. Reasons for healthcare workers becoming infected with novel coronavirus disease 2019 (COVID-19) in China. *J Hosp Infect*. 2020;6:S0195-6701(20)30101-8. doi:10.1016/j.jhin.2020.03.002
52. Cai H, Tu B, Ma J, et al. Psychological Impact and coping strategies of frontline medical staff in Hunan between January and March 2020 during the outbreak of coronavirus disease 2019 (COVID-19) in Hubei, China. *Med Sci Monit*. 2020;15;26:e924171. doi:10.12659/MSM.924171
53. Kang L, Li Y, Hu S, et al. The mental health of medical workers in Wuhan, China dealing with the 2019 novel coronavirus. *Lancet Psychiatry*. 2020;7(3):e14. doi:10.1016/S2215-0366(20)30047-X
54. Xiao H, Zhang Y, Kong D, et al. The effects of social support on sleep quality of medical staff treating patients with coronavirus disease 2019 (COVID-19) in January and February 2020 in China. *Med Sci Monit*. 2020;26:e923549. doi:10.12659/MSM.923549

# Clinical and functional evaluation of primary anterior cruciate ligament reconstruction by using allograft

Sebastian Krupa<sup>1,A–F</sup>, Paweł Reichert<sup>2,A,C,E,F</sup>

<sup>1</sup> Trauma and Orthopedics Department, eMKaMED Medical Center, Wrocław, Poland

<sup>2</sup> Department of Sports Medicine, Wrocław Medical University, Poland

A – research concept and design; B – collection and/or assembly of data; C – data analysis and interpretation; D – writing the article; E – critical revision of the article; F – final approval of the article

Advances in Clinical and Experimental Medicine, ISSN 1899–5276 (print), ISSN 2451–2680 (online)

*Adv Clin Exp Med.* 2020;29(9):1029–1037

## Address for correspondence

Paweł Reichert

E-mail: pawelreichert74@gmail.com

## Funding sources

None declared

## Conflict of interest

None declared

Received on May 18, 2020

Reviewed on May 26, 2020

Accepted on June 30, 2020

Published online on September 1, 2020

## Abstract

**Background.** The reconstruction of the anterior cruciate ligament (ACL) of the knee joint is the gold standard in complete ACL rupture treatment. One of the central discussion topics is choice of graft.

**Objectives.** To assess the outcome of treatment after primary ACL reconstruction using allograft.

**Material and methods.** The study was a retrospective cohort study. Out of 372 male patients who had undergone primary unilateral intra-articular ACL reconstruction using strict inclusion and exclusion criteria, 61 patients who qualified for the study took part. Group I was made up of 31 patients with allograft, while Group II consisted of 30 patients involved with autograft. The Lachman test, Pivot–Shift test, Lysholm Knee Scoring scale, and 2000 International Knee Documentation Committee (IKDC) were used to evaluate the results. Follow-up time was 18 months.

**Results.** The knee joint regained anterior stability in subjective and objective assessments in all the patients in both groups. The subjective results were the following: in Group I,  $96.6 \pm 3.08$  points on the Lysholm scale and  $94.79 \pm 6.53$  points on the IKDC 2000 scale, while in Group II,  $98.00 \pm 1.9$  points on the Lysholm scale and  $94.81 \pm 5.6$  points on the IKDC 2000 scale. The group comparison of the results of the IKDC 2000 and Lysholm Scale obtained postoperatively showed no statistically significant differences between the 2 groups.

**Conclusions.** Primary ACL reconstruction using an allograft is an effective procedure to counteract instability of the anterior knee joint. Comparative analysis of the results of primary ACL reconstruction in the treatment of anterior knee instability using autograft or allograft gives grounds for the possibility of individual selection of graft depending on what the patient's expectations are.

**Key words:** anterior cruciate ligament, allograft, autograft, ACL reconstruction, knee arthroscopy

## Cite as

Krupa S, Reichert P. Clinical and functional evaluation of primary anterior cruciate ligament reconstruction by using allograft. *Adv Clin Exp Med.* 2020;29(9):1029–1037. doi:10.17219/acem/124883

## DOI

10.17219/acem/124883

## Copyright

© 2020 by Wrocław Medical University

This is an article distributed under the terms of the Creative Commons Attribution 3.0 Unported (CC BY 3.0) (<https://creativecommons.org/licenses/by/3.0/>)

## Background

The anterior cruciate ligament (ACL) of the knee joint plays a complex and integral role in stabilizing the knee joint, and resisting anterior displacement and excessive rotation of the tibia relative to the femur.<sup>1</sup> Reconstruction of the ACL of the knee joint<sup>2</sup> followed by a postoperative physiotherapeutic procedure<sup>3</sup> is the standard ACL injury treatment for individuals wishing to return to high-level sports activities. There is no gold-standard treatment option; however, for ACL reconstruction, and when choosing the technique, the surgeon's experience and numerous patient-specific factors, as well as cost and efficacy, are taken into account.<sup>4,5</sup> Available graft options include autografts and allografts, but synthetic ligaments can also be used. The autograft choices are the patellar, hamstring and quadriceps tendons, where allografts include the quadriceps, patellar, Achilles, hamstring, anterior, and posterior tibialis tendons, and the fascia lata.<sup>5</sup> The advantages of allografts include active complications, reduced morbidity rate at the harvest site, a more rapid postoperative recovery, lower incidence of postoperative arthrofibrosis, and lower postoperative pain.<sup>4,6</sup> At the same time, the use of allografts may come with higher rates of rupture, limited availability, delayed healing, and ligamentization in comparison to autografts, as well as the prospect of disease transmission and high price.<sup>7-9</sup> The synthetic materials used in ACL reconstruction are utilized to improve the strength and stability of the graft immediately after the reconstruction, reduce donor site incidence of disease and diminish the potential for disease transmission.<sup>1-3</sup> Differences in the above factors also determine the differences in moving forward with postoperative and rehabilitation proceedings. This is applicable to the time to relieve the operated limb, the necessity and duration of using an orthosis device, the degree of limitation of mobility in the orthosis device, the duration of each stage of both supervised and unattended rehabilitation, and the time to return to work, sport and other physical activities.<sup>2,3</sup>

The objective of this study was to analyze the results of treatment after primary ACL reconstruction using allograft.

## Material and methods

The study had a retrospective design. The assessment was performed in patients who had undergone ACL reconstruction at the eMKaMED Medical Center in Wrocław, Poland. The study was carried out at the Center of Rehabilitation and Medical Education according to the ethical guidelines and principles of the Declaration of Helsinki. All the participants in the present study were informed of its intent and what its approach was. The study was approved by the Bioethics Committee of the Wrocław Medical University and written informed consent forms were

signed by all of the participants prior to commencement of the study.

Patients were separated into 2 research groups. The 1<sup>st</sup> group consisted of patients operated on using the allograft, the 2<sup>nd</sup> group included patients operated on using the autograft. Of the 372 primary ACL reconstruction procedures performed in this period, on 55 patients an allograft procedure was implemented, which represents 14.8% of all patients. A total of 299 patients were operated on with autografts, representing 80.4%. Eighteen patients (4.8%) were operated on using synthetic ligaments.

From the group of patients who underwent primary ACL reconstruction using autografts and allografts, patients were deemed eligible for the study based on the following criteria:

**Inclusion criteria:** knee instability confirmed with clinical examination; age 20–50 years; magnetic resonance imaging (MRI) confirmed the complete ACL rupture; no history of previous injuries to the operated limb; 1 stage surgery performed 6–9 weeks after initial injury; surgery performed by the same surgical team using the same method and the same rehabilitation program.

**Exclusion criteria:** patients operated on immediately after the injury; injuries involving multiple ligaments; accompanying injuries of menisci and cartilage surfaces requiring surgery during surgery.

Thirty-six patients operated on with allograft met these criteria. During the study, 4 patients stopped reporting for follow-up examinations, and 1 patient after returning to physical exertion about 14 months after ACL reconstruction surgery suffered another injury with graft rupture. Ultimately, Group I consisted of 31 patients undergoing ACL reconstruction using an allograft, including 23 men and 8 women. The average age was 37.8 years. The left knee joint was operated on in 18 cases, the right knee joint in 13 cases.

From patients who met the above criteria and were undergoing ACL reconstruction using hamstrings, a control group was selected that was demographically and statistically similar to the research group. One patient did not report for the final follow-up examination 18 months after the surgery due to being abroad.

Group II of patients with hamstrings operated on consisted of 30 patients, including 23 men and 7 women. The average age was 30.4 years. Left knee joint was operated on in 14 cases, right knee joint in 16 cases.

## Surgical procedures

The arthroscopic procedure for reconstruction of the ACL was employed for all grafts. After ACL rupture was confirmed (Fig. 1), the autograft was dissected (Fig. 2,3) and drawn out (Fig. 4) or an allograft was prepared (Fig. 5).

The outside-in technique employing the transtibial technique was utilized for reconstruction. The tibial tunnel



Fig. 1. Arthroscopic image. Right knee joint. View of complete rupture of the distal stump of anterior cruciate ligament



Fig. 4. Cleaned hamstring tendons

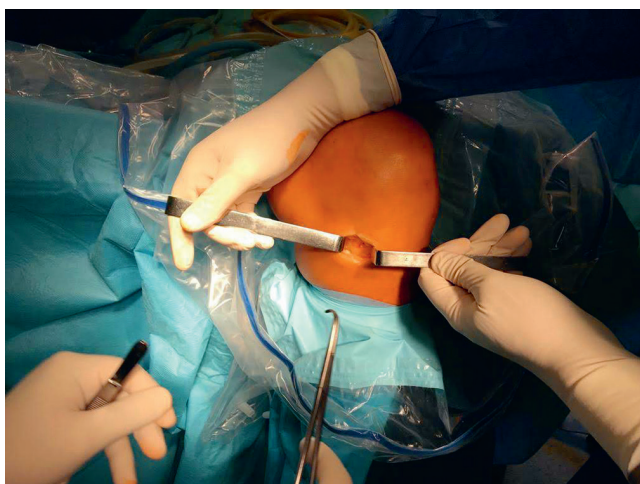


Fig. 2. Intraoperative picture. Left knee joint. Hamstring tendon preparations

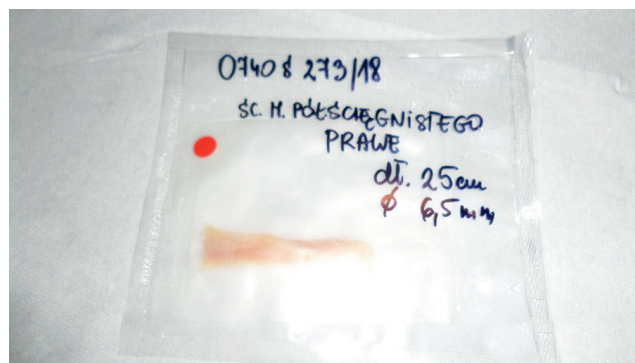


Fig. 5. Freezer allograft from Achilles tendon



Fig. 3. Intraoperative picture. Left knee joint. Isolated tendon, cut off from distal insertion

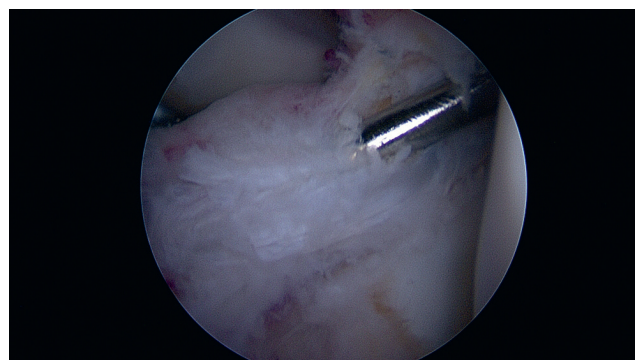


Fig. 6. Arthroscopic image. Left knee joint. K-wire coming out of the tibial footprint

guide pin was placed at the center of the ACL footprint using an ACL guide set at about 65° to the tibial plateau on the sagittal plane (Fig. 6). Then, the guide pin was then over-reamed with a drill. In the next step, a guide pin was drilled from the isometric point across the femur and out the lateral thigh. The autograft/allograft was inserted

through the tunnels and fixed on the femoral side with an interference screw and tensioned (Fig. 7,8). Fixation on the tibial side was performed using an interference screw at 20° of flexion with a posterior drawer force applied to the tibia.

### Choosing the type of transplant by the patient

After qualifying the patient for surgical treatment based on the above criteria and their consent to this method of treatment, the choice of graft was discussed with the patient. The final decision with regard to the graft was made by the patient after the operating physician presented

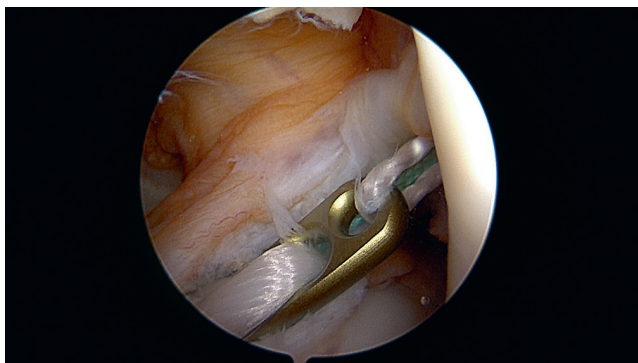


Fig. 7. Arthroscopic image. Left knee joint. View of the Endobutton and loop pull graft into the femoral canal

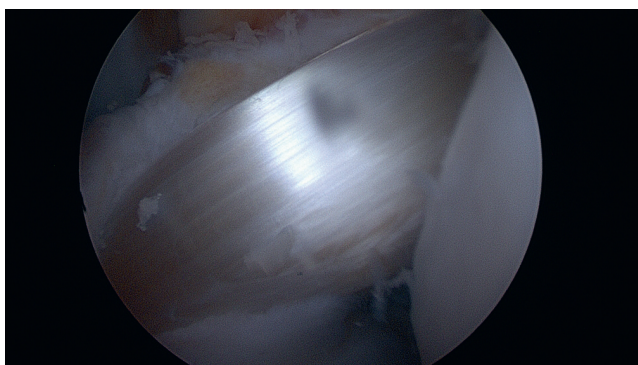


Fig. 8. Arthroscopic image. Left knee joint. View of fixed allograft

the available options along with their advantages and disadvantages. The graft was attached using a Smith–Nephew Endobutton (Smith & Nephew, Warsaw, USA) on the femoral and the Biomet ComposiTCP30 (Zimmer Biomet, Warsaw, USA) interference screw was placed in the tibia.

## Evaluation methods

The first limb evaluated was a non-traumatic limb in order to assess its range of motion and stability, and to familiarize the patient with the examination technique.

Postoperative control examination took place on days 7, 14 and 28 after surgery. Stitches were removed during examination (in the case of reconstruction using the allograft usually on day 7, in the case of autografts on day 14). Stress relief and the use of orthosis were recommended for a period of 3 weeks, increasing the range of flexion in the orthosis in a 30°–60°–90° schedule every 7 days. The active range of motion (ROM) of the knee was measured bilaterally using a standard goniometer.<sup>10</sup> Anterior knee stability was evaluated manually using the Lachman test and anterior drawer test, in accordance with the ligament examination section of the 2000 International Knee Documentation Committee (IKDC).<sup>11</sup> The inter-limb difference in anterior tibial dislocation obtained from the Lachman test and anterior drawer test was rated as normal (0; 0–2 mm), nearly normal (1+; 3–5 mm), abnormal (2+; 6–10 mm), or severely abnormal (3+; >10 mm).<sup>11</sup> Anterolateral rotational knee

stability was assessed manually with the Pivot–Shift test. The Pivot–Shift test was considered negative when, according to the ligament examination section of the 2000 IKDC, the anterolateral rotational dislocation of the tibia relative to the femur was equal in both lower limbs and positive when the difference between the limbs was rated as + (glide), ++ (clunk) or +++ (gross).

## Statistical analysis

Statistical analysis was performed using the TIBCO Statistica™ program (TIBCO Software Inc., Palo Alto, USA) and Microsoft Office Excel 365 Personal (Microsoft Corporation, Redmond, USA).

In the case of the characteristics of the tested material and analysis of the so-called feelings of “giving-way”, Lachman test, anterior drawer and Pivot–Shift test results, and in the analysis of postoperative complications, the number of patients (n) who obtained a given result in particular examined groups were determined. The percentage of the study group in which patients who obtained a given result was calculated through a comparison of the results between the study groups.

The arithmetic mean ( $\bar{x}$ ) and  $\pm$  standard deviation (SD) were calculated for the following parameters tested: active range of extension and flexion in the operated and non-operated limb [°], total number of points obtained on the Lysholm scale in the operated limb (n points) and total number of points obtained in the IKDC 2000 (n points). The Shapiro–Wilk test was performed to examine the normality of the distribution of the analyzed parameters. In the comparison of the values of the active range of extension and flexion obtained in the operated and non-operated limb, a parametric t-test was used for dependent groups. In comparison, within the same group, of the values of the active range of extension and flexion in the operated and non-operated limb scale obtained at particular intervals, a one-way analysis of variance (ANOVA) variance analysis was used followed by Tukey’s post hoc test. To compare the examined groups, the values of the active range of extension and flexion in the operated and non-operated limb, the number of points obtained on the Lysholm scale in the operated limb and the number of points obtained in the IKDC 2000 at the same intervals parametric t-test for independent groups was used.

## Results

### Clinical evaluation results

Comparison of clinical tests in individual groups confirming clinical status before surgery is shown in Fig. 9. The results of knee “giving way”, the Lachman test, anterior drawer test, and Pivot–Shift test were negative in all cases after operation, meaning the knee was stable in both groups

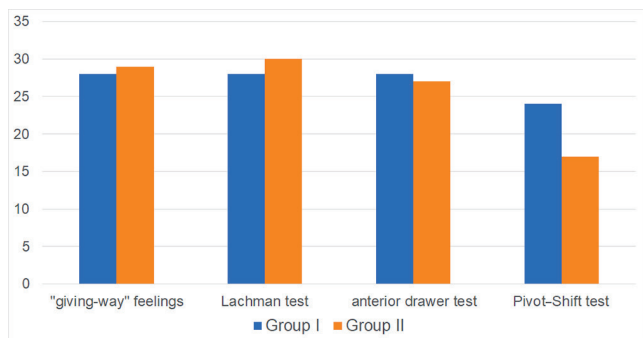


Fig. 9. Comparison of the results of “giving-way”, Lachman test, anterior drawer test, and Pivot-Shift test in Group I and II before surgery index

in all cases. Statistically significant results were found in all tests comparing preoperative examination with examinations after 3, 6 and 18 months after surgery. No statistically significant differences were found when comparing results in an intergroup of 3, 6 and 18 months after reconstruction and in intergroups in identical study periods.

In Group I, the ROM of active knee extension before ACL reconstruction was statistically significantly lower ( $p = 0.005$ ) in the operated limb ( $x = 1.61 \pm 3.00^\circ$ ) compared to the non-operated limb ( $x = 0.00 \pm 0.00^\circ$ ). In the comparison of the obtained active extension range values in the operated limb in Group I, it was noted that there was a statistically significant difference in subsequent measurements ( $p \leq 0.001$ ) (Table 1).

In Group I, before surgery, the ROM of the active knee flexion in the operated limb ( $x = 113.23 \pm 8.32^\circ$ ) was statistically significantly smaller ( $p = 0.001$ ) than in the non-operated limb ( $x = 134.19 \pm 3.19^\circ$ ) as well as at 3 ( $p \leq 0.001$ ) and 6 ( $p \leq 0.001$ ) months after reconstruction. Also, the ROM in the 18<sup>th</sup> month after reconstruction was statistically significantly lower ( $p = 0.031$ ) than in the non-operated limb.

However, such a small difference in obtained values should not be regarded as being of clinical significance (Table 1).

In Group II before ACL reconstruction, the ROM of active extension in the operated limb ( $x = 2.07 \pm 3.08^\circ$ ) was statistically significantly lower ( $p \leq 0.001$ ) than in the non-operated limb ( $x = 0.00 \pm 0.00^\circ$ ). In the studies, ROM was comparable to the non-operated limb within 3, 6 and 18 months after surgery (Table 1).

In Group II before ACL reconstruction, the ROM of active flexion in the operated limb ( $x = 111.33 \pm 10.82^\circ$ ) was statistically significantly lower ( $p \leq 0.001$ ) than in the non-operated limb ( $x = 132.83 \pm 2.84^\circ$ ); similarly, within 3 and 6 months after the operation, there were no statistically significant differences ( $p = 0.129$ ) only after 18 months (Table 1).

The range of active extension movement in the operated limb in Group I statistically significantly increased in the 3<sup>rd</sup> month from the reconstruction of the ACL compared to the result obtained before the surgery ( $p \leq 0.001$ ). Between 3 and 6 months after surgery, the range of extension movement did not change statistically ( $p = 0.998$ ). There were no statistically significant differences between 6 and 18 months after surgery ( $p = 1.000$ ) (Table 2).

The ROM of active flexion in the operated limb in Group I demonstrated a statistically significant increase in the 3<sup>rd</sup> month after reconstruction of the ACL, compared to the result obtained before the surgery ( $p \leq 0.001$ ), and similarly, between 3 and 6 months ( $p \leq 0.001$ ) and between 6 and 18 months ( $p = 0.012$ ) (Table 2).

The ROM of active extension in the operated limb in Group II was statistically significantly larger ( $p = 0.003$ ) within 3 months after ACL reconstruction compared to the ROM before reconstruction. There were no significant changes in the operated limb from 3 months to 18 months after surgery (Table 2).

Table 1. Comparative analysis values of the measurement of the active flexion and extension in the operated and non-operated limb in Group I and II before reconstruction of the ACL and 3, 6 and 18 months after surgery

Variable	Group I			Group II		
	operated limb	non-operated limb	p-value	operated limb	non-operated limb	p-value
Extension [°]						
Before surgery	1.61 ±3.00	0.00 ±0.00	0.005	2.07 ±3.08	0.00 ±0.00	≤0.001
3 months after surgery	0.45 ±1.31	0.00 ±0.00	0.065	0.40 ±1.30	0.00 ±0.00	0.103
6 months after surgery	0.06 ±0.36	0.00 ±0.00	0.325	0.33 ±1.27	0.00 ±0.00	0.161
18 months after surgery	0.00 ±0.00	0.00 ±0.00	1.000	0.00 ±0.00	0.00 ±0.00	0.161
p-value	≤0.001	1.000	–	≤0.001	1.000	–
Flexion [°]						
Before surgery	113.23 ±8.32	134.19 ±3.19	≤0.001	111.33 ±10.82	132.83 ±2.84	≤0.001
3 months after surgery	121.94 ±10.46	134.19 ±3.19	≤0.001	114.50 ±16.10	132.83 ±2.84	≤0.001
6 months after surgery	128.55 ±5.80	134.19 ±3.19	≤0.001	126.00 ±7.36	132.83 ±2.84	≤0.001
18 months after surgery	133.23 ±4.75	134.19 ±3.19	0.031	131.67 ±5.62	132.83 ±2.84	0.129
p-value	≤0.001	1.000	–	≤0.001	1.000	–

Values expressed as the arithmetic mean and ±SD.

**Table 2.** Statistical significance analysis results of the measurement of the active flexion and extension in the operated limb in Group I and II at particular time intervals

Variable	Before surgery		3 months after surgery		6 months after surgery		18 months after surgery	
	Group I	Group II	Group I	Group II	Group I	Group II	Group I	Group II
Extension								
Before surgery	–	–	≤0.001	0.003	≤0.001	0.002	≤0.001	≤0.001
3 months after surgery	≤0.001	0.003	–	–	0.998	0.999	1.000	0.941
6 months after surgery	≤0.001	0.002	0.998	0.999	–	–	0.998	0.974
18 months after surgery	≤0.001	≤0.001	1.000	0.941	0.998	0.974	–	–
Flexion								
Before surgery	–	–	≤0.001	0.665	≤0.001	≤0.001	≤0.001	≤0.001
3 months after surgery	≤0.001	0.665	–	–	≤0.001	≤0.001	≤0.001	≤0.001
6 months after surgery	≤0.001	≤0.001	≤0.001	≤0.001	–	–	0.012	0.179
18 months after surgery	≤0.001	≤0.001	≤0.001	≤0.001	0.012	0.179	–	–

Values expressed as p (level of statistical significance).

**Table 3.** The value of anterior tibial translation in the operated limb in individual study groups between measurements and comparison between study groups

Anterior tibial translation [mm]			
Variable	Group I	Group II	p-value
Before surgery	7.30 ±2.57	7.67 ±2.55	0.571
3 months after surgery	1.81 ±0.70	1.65 ±0.70	0.009
6 months after surgery	1.83 ±0.66	1.58 ±0.65	0.020
18 months after surgery	1.79 ±0.72	1.66 ±0.74	0.021
p-value	≤0.001	≤0.001	–

Values expressed as the arithmetic mean and ±SD.

**Table 4.** The results of the comparative analysis of the value of the anterior tibial shift relative to the thigh in the operated limb in Group I and II between individual measurements

Anterior tibial translation [mm]								
Variable	before surgery		3 months after surgery		6 months after surgery		18 months after surgery	
	Group I	Group II	Group I	Group II	Group I	Group II	Group I	Group II
Before surgery	–	–	≤0.001	≤0.001	≤0.001	≤0.001	≤0.001	≤0.001
3 months after surgery	≤0.001	≤0.001	–	–	1.000	1.000	1.000	1.000
6 months after surgery	≤0.001	≤0.001	1.000	1.000	–	–	1.000	1.000
18 months after surgery	≤0.001	≤0.001	1.000	1.000	1.000	1.000	–	–

A comparison ROM of flexion in the operated limb in Group II showed a statistically significant difference in the measurements taken ( $p \leq 0.001$ ) (Table 2).

In Group I, the tibial translation in the operated limb was  $x = 7.30 \pm 2.57$  mm. After the ACL reconstruction, the translation statistically significantly decreased and amounted to  $x = 1.81 \pm 0.70$  mm when measured 3 months after the ACL reconstruction. In the following months, the anterior displacement of the tibia relative to the thigh was comparable at 6 and 18 months (Table 3).

In Group II, the anterior displacement in the operated limb was  $x = 7.67 \pm 2.55$  mm. After the ACL reconstruction, displacement statistically significantly decreased  $1.65 \pm 0.70$  mm when measured 3 months after the ACL

reconstruction. In the following months, the anterior displacement was comparable at 6 months and at 18 months after reconstruction.

By comparing the results of the tibial translation, statistical significance was demonstrated between surgical and postoperative treatment, while no statistical differences were found when comparing studies in a given research period both in Group I and II (Tables 3 and 4).

## Functional assessment results

Within 18 months of the reconstruction of the ACL, the average total number of points obtained on the Lysholm Group I scale was  $96.97 \pm 3.04$  points. In Group II, patients

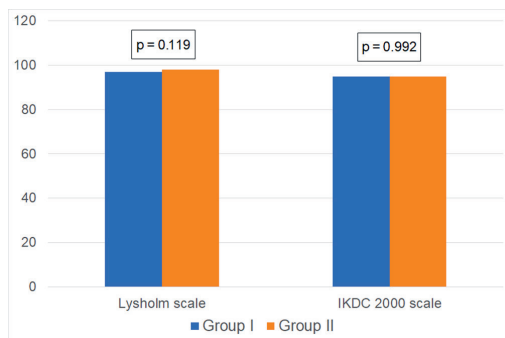


Fig. 10. Comparative analysis of the total number of points on the Lysholm scale and on the IKDC 2000 scale obtained in Group I and Group II

obtained an average of  $98.00 \pm 1.91$  points in the same period since surgery (Fig. 10). A comparative analysis of the results of the functional assessment based on the Lysholm scale did not show statistically significant differences ( $p = 0.119$ ).

Within 18 months of the reconstruction of the ACL, the average total number of points on the IKDC 2000 scale obtained in Group I was  $94.79 \pm 6.54$  points. In Group II, patients obtained an average of  $94.81 \pm 5.63$  points in the same period since surgery (Fig. 10). A comparative analysis of the results of the functional assessment did not show statistically significant differences between the examined groups ( $p = 0.992$ ).

## Discussion

Knee injuries are one of the most common injuries experienced during physical activity, resulting in the need for surgical treatment and a prolonged interruption in the ability to play sports.<sup>3,4</sup>

Statistics and numbers demonstrate the scale of the problem. In the USA alone, the number of cruciate ligament injuries is estimated to be at 250,000 per year, and the cost of diagnosis, treatment and rehabilitation is \$3 trillion.<sup>12,13</sup> No data could be found regarding the number of reconstructions of the ACL in Poland.

Many reports show different views of the researchers regarding the right time for surgical treatment, selection and method of graft attachment, method of bone canal preparation, or postoperative rehabilitation.<sup>10,11,14–22</sup>

The choice of surgical technique and method of graft attachment is usually the responsibility of the surgeon, depending on their preferences and previous experience.<sup>23</sup>

The choice of graft used as a transplant for reconstruction of the ACL also largely depends on the patient's choice and expectations. However, it should be taken into account that according to statistical studies, 74% of patients choose the transplant depending on the doctor's recommendation.<sup>24</sup>

Autograft effects described by other researchers<sup>25</sup> and also observed among patients at the medical center

in Wrocław, mainly related to their data collection, sparked the search for an alternative to a transplant autograft. The number of reports regarding the use of allografts in orthopedics is increasing. Up to 5 million allografts were performed in the USA in the last decade.<sup>25,26</sup>

The Achilles tendon and posterior (TP) and anterior (TA) tendons were used for an allograft. However, a small group of patients and a short observation period did not permit a comparison of their treatment results within the research group. Results published by other researchers show comparable results of treatment using allogeneic Achilles, ST, TA, and TP allografts. They also emphasize the fact that this gives greater freedom in the size of allograft.<sup>27</sup>

The average age of patients in the allograft group was 37.8 years, and 30.4 years in the autograft group. This is in line with the observations of other authors that the allograft is more often chosen by patients over 35 years of age who no longer compete in sports.<sup>28</sup> A more recent meta-analysis by Kaeding et al. observed the increase in the average age of patients operated on using the allograft, starting at 30 years of age during the years 2002–2003 to almost 40 years of age during the years 2008–2009, which, however, also significantly correlated with the decrease in graft bursts – from 11.7% during the years 2002–2003 to 3.7% during the years 2008–2009.<sup>29</sup>

The team at the medical center prepared the tibial canal with the outside-in technique, and the femoral canal was drilled with the transtibial technique. The treatment results in both groups show that it is a repeatable and effective surgical technique. This is in line with the observations of other researchers, showing comparatively good treatment results with this method with the technique of drilling through an additional medial portal.<sup>30–32</sup> However, other authors have indicated better treatment results in patients whose femoral canal was drilled through the medial portal.<sup>33</sup> Despite the use of the same surgical technique and the use of the same fixation methods, the average time of surgery in both groups was different. These data show that the selection of the graft for reconstruction had a direct impact on surgery duration. This difference is due to the need to take graft when using autografts. This coincides with the observations of other authors.<sup>16,25,34</sup> Based on the studies of Ericson et al. and Balasch et al.,<sup>35,36</sup> a Rolimeter was used for the quantitative study of anterior tibial displacement. In our opinion, this examination does not affect the choice of surgical technique, method of attachment or type of graft. It is useful in assessing postoperative improvement in knee stability. It can also be helpful in assessing the patient after re-injury to the knee after ACL reconstruction. The increase in tibial anterior translation after injury compared to the results of post-reconstruction control tests may be evidence of graft damage, which is difficult to assess with MRI.

In both groups, the range of active extension and flexion of the preoperative limb was similar and statistically

different from the range of the non-operated limb. In both groups, during control tests after 3, 6 and 18 months, statistically significant improvement in the ROM was observed, both in terms of extension and flexion. In the group of allografts and autografts in a study after 18 months, there was a smaller range of flexion of the operated to non-operated limb, but it was not clinically significant.

Analysis of the knee joint stability assessment using Lachman, front drawer, Pivot–Shift, and Rolimeter tests showed that proper knee joint stability was obtained in both groups. There was no difference in the results obtained between the 2 groups. Similar observations in their meta-analyses were described by Bottoni et al. and Jia et al.<sup>37,38</sup>

Subjective assessment of knee function in patients from both groups was made using the Lysholm scale and IKDC 2000. Comparative analysis did not show significant differences between the results of patients operated on using allografts and the results of patients operated on using autografts. Good subjective postoperative results were shown.

Our method was limited by the lack of biomechanical tests and a short observation period. In the future, our research requires a longer period of observation and analysis of possible issues of re-tearing of the graft and weakening of the flexor strength of the operated limb after primary reconstruction of ACL using hamstrings.

Today, many studies are underway to highlight genetic predisposition to cruciate ligament injuries. The ACL “suture” techniques require further research and more material. Research on the use of scaffolds, stem cells, platelet rich plasma, and xenografts are also setting new trends. All these current trends in the development of ACL surgery will allow for a more personalized method of surgical treatment, which will probably be presented to the patient as the choice of “à la carte” method of treatment.

## Conclusions

Primary ACL reconstruction using an allograft is an effective method to treat instability of the anterior knee joint. Comparative analysis of the results of primary ACL reconstruction in the treatment of anterior knee instability using autograft and allograft justifies the possibility of individual selection of the graft depending on the patient's expectations.

### ORCID iDs

Sebastian Krupa  <https://orcid.org/0000-0002-3952-8123>

Paweł Reichert  <https://orcid.org/0000-0002-0271-4950>

### References

- Ekstrand J. A 94% return to elite level football after ACL surgery: A proof of possibilities with optimal caretaking or a sign of knee abuse? *Knee Surg Sports Traumatol Arthrosc.* 2011;19(1):1–2. doi:10.1007/s00167-010-1300-4
- Czamara A, Królikowska A, Szuba Ł, Widuchowski W, Kentel M. Single- vs double-bundle anterior cruciate ligament reconstruction: A new aspect of knee assessment during activities involving dynamic knee rotation. *J Strength Cond Res.* 2015;29(2):489–499. doi:10.1519/JSC.0000000000000638
- Królikowska A, Sikorski Ł, Czamara A, Reichert P. Effects of postoperative physiotherapy supervision duration on clinical outcome, speed, and agility in males 8 months after anterior cruciate ligament reconstruction. *Med Sci Monit.* 2018;24:6823–6831. doi:10.12659/MSM.912162
- Cohen SB, Sekiya JK. Allograft safety in anterior cruciate ligament reconstruction. *Clin Sports Med.* 2007;26(4):597–605.
- West RV, Harner CD. Graft selection in anterior cruciate ligament reconstruction. *J Am Acad Orthop Surg.* 2005;13(3):197–207.
- Zeng C, Gao SG, Li H, et al. Autograft versus allograft in anterior cruciate ligament reconstruction: A meta-analysis of randomized controlled trials and systematic review of overlapping systematic reviews. *Arthroscopy.* 2016;32(1):153–163.e18. doi:10.1016/j.arthro.2015.07.027
- Samuelsson K, Andersson D, Ahldén M, Fu FH, Musahl V, Karlsson J. Trends in surgeon preferences on anterior cruciate ligament reconstructive techniques. *Clin Sports Med.* 2013;32(1):111–126. doi:10.1016/j.csm.2012.08.011
- Czamara A, Markowska I, Królikowska A, Szopa A, Domagalska-Szopa M. Kinematics of rotation in joints of the lower limbs and pelvis during gait: Early results-SB ACLR approach versus DB ACLR approach. *Biomed Res Int.* 2015;2015:707168. doi:10.1155/2015/707168
- Królikowska A, Czamara A, Kentel M. Does gracilis tendon harvest during ACL reconstruction with a hamstring autograft affect torque of muscles responsible for shin rotation? *Med Sci Monit.* 2015;21:2084–2093. doi:10.12659/MSM.893930
- Królikowska A, Czamara A, Szuba Ł, Reichert P. The effect of longer versus shorter duration of supervised physiotherapy after ACL reconstruction on the vertical jump landing limb symmetry. *Biomed Res Int.* 2018;4:7519467
- Magarian EM, Fleming BC, Harrison SL, Mastrangelo AN, Badger GJ, Murray MM. Delay of 2 or 6 weeks adversely affects the functional outcome of augmented primary repair of the porcine anterior cruciate ligament. *Am J Sports Med.* 2010;38(12):2528–2534. doi:10.1177/0363546510377416
- Griffin LY, Albohm MJ, Arendt EA, et al. Understanding and preventing noncontact anterior cruciate ligament injuries: A review of the Hunt Valley II meeting, January 2005. *Am J Sports Med.* 2006;34(9):1512–1532.
- Brophy RH, Wright RW, Matava MJ. Cost analysis of converting from single-bundle to double-bundle anterior cruciate ligament reconstruction. *Am J Sports Med.* 2009;37(4):683–687. doi:10.1177/0363546508328121
- Bieri KS, Scholz SM, Kohl S, Aghayev E, Staub LP. Dynamic intraligamentary stabilization versus conventional ACL reconstruction: A matched study on return to work. *Injury.* 2017;48(6):1243–1248. doi:10.1016/j.injury.2017.03.004
- Larsson S, Struglics A, Lohmander LS, Frobell R. Surgical reconstruction of ruptured anterior cruciate ligament prolongs trauma-induced increase of inflammatory cytokines in synovial fluid: An exploratory analysis in the KANON trial. *Osteoarthritis Cartilage.* 2017;25(9):1443–1451. doi:10.1016/j.joca.2017.05.009
- Brown MJ, Carter T. ACL Allograft: Advantages and when to use. *Sports Med Arthrosc Rev.* 2018;26(2):75–78. doi:10.1097/JSA.0000000000000194
- Chen H, Chen B, Tie K, Fu Z, Chen L. Single-bundle versus double-bundle autologous anterior cruciate ligament reconstruction: A meta-analysis of randomized controlled trials at 5-year minimum follow-up. *J Orthop Surg Res.* 2018;13(1):50. doi:10.1186/s13018-018-0753-x
- Speziali A, Delcogliano M, Tei M, et al. Fixation techniques for the anterior cruciate ligament reconstruction: Early follow-up: A systematic review of level I and II therapeutic studies. *Musculoskelet Surg.* 2014;98(3):179–187. doi:10.1007/s12306-014-0338-8
- Debieux P, Franciozi CE, Lenza M, et al. Bioabsorbable versus metallic interference screws for graft fixation in anterior cruciate ligament reconstruction. *Cochrane Database Syst Rev.* 2016;7:CD009772. doi:10.1002/14651858.CD009772.pub2

20. Jiang H, Ma G, Li Q, Hu Y, Li J, Tang X. Cortical button versus cross-pin femoral fixation for hamstring anterior cruciate ligament reconstruction: A meta-analysis of randomized controlled trials. *Am J Sports Med.* 2018;46(9):2277–2284. doi:10.1177/0363546517717672
21. Sarzaeem MM, Najafi F, Razi M, Najafi MA. ACL reconstruction using bone-patella tendon-bone autograft: Press-fit technique vs interference screw fixation. *Arch Orthop Trauma Surg.* 2014;134(7):955–962. doi:10.1007/s00402-014-1999-3
22. Królikowska A, Sikorski L, Czamara A, Reichert P. Are the knee extensor and flexor muscles isokinetic parameters affected by the duration of postoperative physiotherapy supervision in patients eight months after ACL reconstruction with the use of semitendinosus and gracilis tendons autograft? *Acta Bioengi Biomech.* 2018;20(3):89–100.
23. Anderson MJ, Browning WM III, Urband CE, Kluczynski MA, Bisson LJ. A systematic summary of systematic reviews on the topic of the anterior cruciate ligament. *Orthop J Sports Med.* 2016;4(3):2325967116634074. doi:10.1177/2325967116634074
24. Cohen SB, Yucha DT, Ciccotti MC, Goldstein DT, Ciccotti MA, Ciccotti MG. Factors affecting patient selection of graft type in anterior cruciate ligament reconstruction. *Arthroscopy.* 2009;25(9):1006–1010. doi:10.1016/j.arthro.2009.02.010
25. Giedraitis A, Arnoczky SP, Bedi A. Allografts in soft tissue reconstructive procedures: Important considerations. *Sports Health.* 2014;6(3):256–264. doi:10.1177/1941738113503442
26. de Girolamo L, Ragni E, Cucchiari M, van Bergen CJA, Hunziker EB, Chubinskaya S. Cells, soluble factors and matrix harmonically play the concert of allograft integration. *Knee Surg Sports Traumatol Arthrosc.* 2019;27(6):1717–1725. doi:10.1007/s00167-018-5182-1
27. Palmer JE, Russell JP, Grieshaber J, et al. A biomechanical comparison of allograft tendons for ligament reconstruction. *Am J Sports Med.* 2017;45(3):701–707. doi:10.1177/0363546516671944
28. Kaeding CC, Aros B, Pedroza A, et al. Allograft versus autograft anterior cruciate ligament reconstruction: Predictors of failure from a MOON prospective longitudinal cohort. *Sports Health.* 2011;3(1):73–81.
29. Kaeding CC, Pedroza AD, Reinke EK, et al. Change in anterior cruciate ligament graft choice and outcomes over time. *Arthroscopy.* 2017;33(11):2007–2014. doi:10.1016/j.arthro.2017.06.019
30. Robin BN, Jani SS, Marvil SC, Reid JB, Schillhammer CK, Lubowitz JH. Advantages and disadvantages of transtibial, anteromedial portal, and outside-in femoral tunnel drilling in single-bundle anterior cruciate ligament reconstruction: A systematic review. *Arthroscopy.* 2015;31(7):1412–1417. doi:10.1016/j.arthro.2015.01.018
31. Rezaeadeh S, Etehad H, Vosoughi AR. Outcome of arthroscopic single-bundle anterior cruciate ligament reconstruction: Anteromedial portal technique versus transtibial drilling technique. *Musculoskelet Surg.* 2016;100(1):37–41. doi:10.1007/s12306-015-0392-x
32. Musahl V. A modified transtibial technique was similar to an anteromedial portal technique for anterior cruciate ligament reconstruction. *J Bone Joint Surg Am.* 2015;97(16):1373. doi:10.2106/JBJS.9716.ebo102
33. Chen H, Tie K, Qi Y, Li B, Chen B, Chen L. Anteromedial versus transtibial technique in single-bundle autologous hamstring ACL reconstruction: A meta-analysis of prospective randomized controlled trials. *J Orthop Surg Res.* 2017;12(1):167. doi:10.1186/s13018-017-0671-3
34. Kim YK, Ahn JH, Yoo JD. A comparative study of clinical outcomes and second-look arthroscopic findings between remnant-preserving tibialis tendon allograft and hamstring tendon autograft in anterior cruciate ligament reconstruction: Matched-pair design. *Clin Orthop Surg.* 2017;9(4):424–431. doi:10.4055/cios.2017.9.4.424
35. Ericsson D, Östenberg AH, Andersson E, Alricsson M. Test-retest reliability of repeated knee laxity measurements in the acute phase following a knee trauma using a Rolimeter. *J Exerc Rehabil.* 2017;13(5):550–558. doi:10.12965/jer.1735104.552
36. Balasch H, Schiller M, Friebel H, Hoffmann F. Evaluation of anterior knee joint instability with the Rolimeter: A test in comparison with manual assessment and measuring with the KT-1000 arthrometer. *Knee Surg Sports Traumatol Arthrosc.* 1999;7(4):204–208.
37. Bottoni CR, Smith EL, Shaha J, et al. Autograft versus allograft anterior cruciate ligament reconstruction: A prospective, randomized clinical study with a minimum 10-year follow-up. *Am J Sports Med.* 2015;43(10):2501–2509. doi:10.1177/0363546515596406
38. Jia Y, Sun P. Comparison of clinical outcome of autograft and allograft reconstruction for anterior cruciate ligament tears. *Chin Med J (Engl).* 2015;128(23):3163–3166. doi:10.4103/0366-6999.170265



# Anticancer activity of topical ointments with histone deacetylase inhibitor, trichostatin A

Agnieszka Chodkowska<sup>1,A–F</sup>, Alicja Bieńkowska<sup>1,C–E</sup>, Żaneta Słyk<sup>1,B</sup>, Joanna Giebułtowicz<sup>2,B,D</sup>, Maciej Małecki<sup>1,A,C,E,F</sup>

<sup>1</sup> Department of Applied Pharmacy, Faculty of Pharmacy, Medical University of Warsaw, Poland

<sup>2</sup> Department of Bioanalysis and Drugs Analysis, Faculty of Pharmacy, Medical University of Warsaw, Poland

A – research concept and design; B – collection and/or assembly of data; C – data analysis and interpretation; D – writing the article; E – critical revision of the article; F – final approval of the article

Advances in Clinical and Experimental Medicine, ISSN 1899–5276 (print), ISSN 2451–2680 (online)

*Adv Clin Exp Med.* 2020;29(9):1039–1049

## Address for correspondence

Agnieszka Chodkowska

E-mail: [agnieszka.chodkowska@wum.edu.pl](mailto:agnieszka.chodkowska@wum.edu.pl)

## Funding sources

This work was partially supported by the National Centre for Research and Development grant (grant No. Strategmed1/233264/4/NCBR/2014, MentorEYE).

## Conflict of interest

None declared

Received on February 21, 2020

Reviewed on May 25, 2020

Accepted on June 22, 2020

Published online on September 7, 2020

## Abstract

**Background.** Trichostatin A (TSA), being a strong specific histone deacetylase (HDAC) inhibitor, may lead to the inhibition of growth, differentiation and/or apoptosis of cells in a number of tumors. Semisolid drug formulations for topical release of anticancer agents may be an alternative strategy or a supplement of the systemic therapy.

**Objectives.** To prepare semisolid formulations with TSA to be used directly on the skin and to assess the anticancer effect *in vivo* on a mouse model with L1 neoplastic tumors.

**Material and methods.** Twenty-four formulations were prepared in the form of semisolid systems containing TSA as the active ingredient. Then, an *in vitro* study was performed concerning the release of the active substance from the prepared formulations. Four formulations were selected for *in vivo* studies: oil-in-water cream, hydrogel, w/o emulsion ointment on the absorptive hydrophobic medium, and o/w emulsion gel. The tumor size and mouse body weight were measured during the experiment. The tumors and healthy skin of the mice were assessed regarding the skin barrier function with the Corneometer and Tewameter probes.

**Results.** The semisolid formulation with TSA applied on the skin reduced the growth of neoplastic tumors as compared with the control group. This is especially pronounced in the case of w/o emulsion ointment and o/w emulsion gel. The Corneometer shows that neoplastic tumor growth and formulations on the skin have no effect on the skin condition in comparison with the mouse skin without tumor. The measurement performed with the Tewameter has revealed impaired skin barrier function of neoplastic tumors.

**Conclusions.** Semisolid formulations with TSA fit well in the mainstream of research into topical medicines applied directly on neoplastic tumors, which may support and supplement current oncological treatment.

**Key words:** trichostatin A, anticancer topical formulations, ointments, skin cream, cancer applied pharmacy

## Cite as

Chodkowska A, Bieńkowska A, Słyk Ż, Giebułtowicz J, Małecki M. Anticancer activity of topical ointments with histone deacetylase inhibitor, trichostatin A. *Adv Clin Exp Med.* 2020;29(9):1039–1049. doi:10.17219/acem/124439

## DOI

10.17219/acem/124439

## Copyright

© 2020 by Wrocław Medical University

This is an article distributed under the terms of the Creative Commons Attribution 3.0 Unported (CC BY 3.0) (<https://creativecommons.org/licenses/by/3.0/>)

## Introduction

Cancer is one of the main causes of death in the world. In developed countries, it is the 2<sup>nd</sup> cause of death, after cardiovascular diseases. The number of new cases of cancer and cancer-related deaths in the world is increasing every year. According to Globocan, in 2018, the incidence of cancer was 18.1 million, causing the death of 9.6 million people worldwide. It is estimated that in 2040, the number of new cases of cancer will be 29.5 million.<sup>1</sup> On the basis of the Polish National Cancer Registry, 164,875 of new cases of cancer and 99,644 cancer-related deaths were reported in Poland in 2017. The cancer morbidity rate in Poland has increased by 185,630 cases in 2018 and 113,388 deaths in 2018, according to Globocan.<sup>1,2</sup> Strong emphasis is placed on early detection of neoplastic diseases combined with adequate treatment. For the last 20 years, anticancer therapy has been undergoing transformation from traditional cytotoxic drugs to a molecular targeted therapy.<sup>3,4</sup> Currently, anticancer therapy is primarily based on the use of alkylating agents, antimetabolites, plant alkaloids, and anticancer antibiotics. Recently, there has been much discussion regarding the possibility of using epigenetic inhibitors. It has been shown that epigenetic regulation of gene expression is an essential mechanism which, if disturbed, leads to the development of cancer. The mechanisms of epigenetic control involve changes in the expression of genes key to carcinogenesis. Histone deacetylase inhibitors (HDIs) are considered to be used as new generation anticancer drugs, which induce increased histone acetylation.<sup>5,6</sup> Trichostatin A (TSA) inhibits histone deacetylase (HDAC). The inhibitory activity involves chelation of zinc (II) ion by the hydroxamic acid group in TSA in the HDAC active site.<sup>7</sup> Trichostatin A was first described as an antifungal antibiotic in 1976.<sup>8</sup> It shows the activity of a non-competitive, reversible inhibitor of HDAC activity at low nanomoles concentrations.<sup>9</sup> There are reports indicating that TSA, being a strong specific HDAC inhibitor, may lead to the inhibition of growth, differentiation and/or apoptosis of cells in a number of tumors.<sup>10–14</sup> Recently, it has been shown that TSA inhibits angiogenesis by reducing the expression of oxidase 4 (Nox4), which is inhibited by p300-histone acetyltransferase ((p300-HAT)-dependent pathway). This mechanism may be used to reduce angiogenesis in relation to diabetic retinopathy, neoplastic changes and developmental anomalies.<sup>15</sup> The studies also suggest that TSA may have a therapeutic effect on cancerous cells in combination with radiotherapy, chemotherapy or hormone therapy.<sup>16–19</sup> Regarding the pharmaceutical form used in oncology, injection forms are currently predominant. New forms of oncological drugs include subcutaneous implants (Zoladex, Leuprostin) or intracranial implants with carmustine (e.g., Gliadel). The cytostatic agent 5-fluorouracil is used in dermatology in the form

of liquid for papillae (Verrumal) and as ointment (Efu-dix) in the treatment of actinic and solar keratosis, basal cell carcinoma, Bowen's disease, and precancerous skin conditions. Transdermal administration is necessary to ensure prolonged release of medicines and maintain the local effect.<sup>20,21</sup> The present paper focuses on semisolid formulations with TSA. The aim of the studies was to develop TSA formulations to be used topically, and to assess the anticancer activity of the obtained preparations in vivo.

## Material and methods

### Development of the formula and preparation of semisolid formulations with TSA

Adequate media were selected for the initial studies, and 24 formulations were developed. Pharmacopoeial ingredients, compound ready-made media available for a pharmaceutical formulation and new polymer-based media were selected. The compositions of all formulations are presented in Table 1. The following formulations were prepared: w/o emulsions, o/w emulsions, hydrogels, and o/w emulsion gel. The obtained formulations were examined organoleptically during and after their preparation. They were assessed with regard to appearance, consistency and spreading. Semisolid formulations containing ready-made pharmacopoeial media used in the experiment (forming w/o emulsions – No. 1, 2, 8, and 10) and industrial ones (o/w emulsions – No. 3 and 24) were prepared with the use of the mixing system – Cito Unguator<sup>®</sup> e/s (Eprus, Bielsko-Biala, Poland). Formulations in the form of o/w emulsions No. 6, 7, 9, and 19 were prepared by melting the ingredients of the oil phase in the water bath<sup>22</sup> (LaboPLAY Type W 410; LaboPLAY, Bytom, Poland) and emulating water with the ingredients dissolved therein, then mixing with the use of the mixing system (Cito Unguator<sup>®</sup> e/s). Formulations in the form of o/w emulsions (No. 4 and 5), gels (No. 11–18, 20, 22, and 23) and o/w emulsion gel (No. 21) containing gelling, concentrating and stabilizing agents were prepared using standard methods<sup>23–25</sup> and mixing with the use of the mixing system (Cito Unguator<sup>®</sup> e/s). Directly before the study, the TSA solution was added to the prepared media. 0.01% formulations with TSA were prepared for in vitro studies. The TSA (Trichostatin A – Sigma-Aldrich cat. No. T8552; Sigma-Aldrich, St. Louis, USA) solution was prepared by dissolution of 1 mg of TSA in 0.5 mL dimethyl sulfoxide (DMSO) (Sigma-Aldrich). From the obtained solution, 50 µL was collected; then, 500 µL of phosphate-buffered saline (PBS; Gibco, Waltham, USA) was added. One hundred microliters of thus prepared solution contained 18.18 µg of TSA (in DMSO+PBS).

## In vitro study of TSA release from the prepared formulations

The studies on release involved semisolid formulations with TSA prepared in accordance with the composition specified in Table 1. The compositions of 24 formulations containing TSA were developed and a study of the active substance release from the prepared formulations was conducted. Eighteen formulations containing TSA were selected, in which the released TSA was quantified. The formulations with no detected released TSA were rejected from further studies. Then, the formulations were tested for release in order to select semisolid TSA formulations for in vivo studies on a murine model. In order to study the prepared formulations, a method of TSA release in vitro was developed. The studies were conducted with the use of 24-well plates with polyethylene terephthalate (PET) membrane inserts with a diameter of 6.5 mm; the pores were 8  $\mu\text{m}$  (BD BioCoat Matrigel Invasion Chambers; Becton Dickinson Biosciences, San Jose, USA). The inserts were filled with 200 mg of TSA formulation (0.01%), and then the wells were filled with 300  $\mu\text{L}$  of acceptor liquid (Aqua pro injectione; Polpharma, Starogard Gdański, Poland) (Fig. 1).

The study was conducted for 6 h in an incubator (POL-EKO Aparatura, Wodzisław Śląski, Poland) at 37°C. After 6 h, the samples were collected and measured spectrophotometrically with UV-VIS (Quawell Q 5000,  $\lambda = 264 \text{ nm}$ ; Quawell, San Jose, USA) and with liquid chromatography combined with mass spectrometry (LC-MS/MS). Instrumental analysis was performed using Agilent 1260 Infinity (Agilent Technologies, Santa Clara, USA) equipped with a degasser, autosampler and binary pump, coupled to a Hybrid Triple Quadrupole/Linear Ion trap mass spectrometer (QTRAP<sup>®</sup> 4000; AB SCIEX, Framingham, USA). The curtain gas, ion source gas 1, ion source gas 2, and collision gas (all high purity nitrogen) were set at 240 kPa, 410 kPa, 275 kPa, and “medium” instrument units, respectively. The ion spray voltage and source temperature were 5500 V and 600°C, respectively. Chromatographic separation was achieved with a Kinetex RP-18 column (100 mm, 4.6 mm,

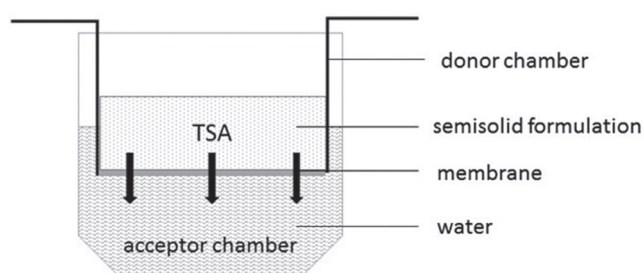


Fig. 1. Membrane model for TSA release. The insert was filled with 200 mg of TSA formulation, then 300  $\mu\text{L}$  of the acceptor liquid – Aqua pro injectione – was added to the well. After  $t = 6 \text{ h}$ , a sample was collected and measured with UV-VIS and LCMS/MS

particle size 2.6  $\mu\text{m}$ ) supplied by Phenomenex (Torrance, USA). The column was maintained at 40°C at a flow rate of 0.5 mL/min. The mobile phases consisted HPLC-grade water with 0.2% formic acid as eluent A and acetonitrile with 0.2% formic acid as eluent B. The gradient B was as follows: 0 min 30%; 0.5 min 30%; 3 min 95%; and 7 min 95%. A total of 10  $\mu\text{L}$  of samples were diluted with 50% acetonitrile and mixed with M344 (internal standard; Santa Cruz Biotechnology, Santa Cruz, USA) to a final concentration of 0.1  $\mu\text{g}/\text{mL}$  in 200  $\mu\text{L}$  of solution. The volume of injection was 5  $\mu\text{L}$ . The target compounds were analyzed in multiple reaction monitoring (MRM) mode, monitoring 2 transitions between the precursor ion and the most abundant ions for each compound was 303->148 (quantitative transition) and 303->120 (qualitative transition) for TSA, and 308->148 (quantitative transition) and 308->120 (qualitative transition) for M344. The compound parameters for quantitative transitions viz. declustering potential (DP), collision energy (CE), entrance potential (EP), and collision exit potential (CXP) were 66, 33, 10, and 10 V, respectively, for TSA, and 61, 25, 10, and 14 V, respectively, for M344.

The results of TSA release marked UV-VIS and LC-MS/MS are presented in Fig. 2.

## Examination of anticancer activity of semisolid TSA formulations in vivo in Balb/c mice with L1 tumor

On the basis of TSA release results, organoleptic assessment and an assessment of the characteristics of the L1 tumor, the following 4 formulations were selected for in vivo studies: 5, 10, 18, and 21. The studies were conducted on laboratory Balb/c mice with the approval of the Bioethics Committee of the Medical University of Warsaw, Poland (approval No. 160/2016). The sites on the mouse back, in the neck area, were shaved before starting the experiments. The females of Balb/c mice (weight: 18–25 g) were administered subcutaneously (s.c.) with cancer cells of murine sarcoma L1  $3 \times 10^5/0.1 \text{ mL}$  PBS per mouse.<sup>26</sup> The cells were obtained from standard in vitro culture of L1 line. Then, when tumors with a diameter of 1–10 mm appeared, the mice were divided into adequate groups ( $n = 3$ ) and the tests were initiated. To perform the tests, TSA was dissolved in DMSO, and PBS was added to achieve 100  $\mu\text{g}$  TSA in 100  $\mu\text{L}$  DMSO + PBS (1 mg TSA + 200  $\mu\text{L}$  DMSO + 800  $\mu\text{L}$  PBS).<sup>27</sup> The TSA solution was administered as intratumor injection and into the semisolid formulations. The active substance (TSA) was introduced to the semisolid formulations immediately before use. Four groups of mice were treated with the selected TSA formulations No. 5, 10, 18, and 21 at a dose of 100  $\mu\text{g}$  TSA/200 mg formulation/mouse/day (divided into 2 doses, three-hour interval) for 5 consecutive days. The mice on which the formulation was applied

**Table 1.** Compositions of the design semisolid formulations: No. 1, 2, 8, and 10 – emulsions w/o; No. 3–7, 9, 19, and 24 – emulsions o/w; No. 11–18, 20, 22, and 23 – gels; No. 21 – o/w emulsion gel. Trichostatin A was introduced ex tempore at a dose of 0.01% for in vitro release and at a dose of 0.05% for in vivo animal tests

Composition	Formulation No.											
	1	2	3	4	5	6	7	8	9	10	11	12
Unguentum Cholesteroli (Pharma-Cosmetic)	50%											
Euceryna (Fagron) Unguentum Eucerini I		50%										
Lekobaza (Pharma-Cosmetic)			50%									
Vaselinum hydrophylicum (Pharma-Cosmetic)								50%				
Methocel® 90HG (Sigma-Aldrich)				0.5%	0.25%							
Paulister-SG Glyceryl Stearate (Paulika)				10%	10%	12%			2.5%			
Isopropyl Myristate (Paulika)				10%	10%							
Karinol-CS Cetearyl Alcohol (Paulika)						2.25%						
Karinol-C Cetyl Alcohol (Paulika)							5%		5%			
Stearic acid (WarChem)							13%		5%			
Cera alba (Pharma-Cosmetic)									2.5%			
Vaselinum album (Aflofarm)									10%	12.5%		
Lanolinum anhydricum (Pharma-Cosmetic)										37.5%		
Carboxymethylcellulose sodium (Sigma-Aldrich)											2%	2%
Sodium dodecyl sulfate (Sigma-Aldrich)							5%					
Triethanolamine (POCH)									2.5%			
Glycerolum 85% (Pharma-Cosmetic)											10%	
Propylene Glycol (WarChem)												10%
Trichostatin A (Sigma-Aldrich) – in vitro	0.01%	0.01%	0.01%	0.01%	0.01%	0.01%	0.01%	0.01%	0.01%	0.01%	0.01%	0.01%
Trichostatin A (Sigma-Aldrich) – in vivo	0.05%	0.05%	0.05%	0.05%	0.05%	0.05%	0.05%	0.05%	0.05%	0.05%	0.05%	0.05%
Aqua pro injectione (Polpharma)	q.s.	q.s.	q.s.	q.s.	q.s.	q.s.	q.s.	q.s.	q.s.	q.s.	q.s.	q.s.

topically were kept separately and observed for 1 h until the formulation was absorbed. The control groups were treated in the same way with semisolid formulations No. 5, 10, 18, and 21 without TSA. Two groups of mice received TSA intratumor injection (100 µg TSA/100 µL DMSO+PBS (C3)) and solvent intratumor injection (100 µL DMSO+PBS (C2)). The injections were given once daily, on the 1<sup>st</sup>, 3<sup>rd</sup> and 5<sup>th</sup> day of the study. Also, a separate control group was formed, including mice not treated with the formulations (C1). Every day throughout the study all the mice were weighed and the tumors were measured with a caliper (Topex). The tumors were

measured in 2 dimensions, perpendicularly. The tumor volume ( $v$ ) was calculated using the formula, where ( $x \leq y$ )<sup>28,29</sup>:

$$v = x^2 \times y \times (\pi/6).$$

Examination of skin moisture and transepidermal water loss (TEWL) was performed with the probes Corneometer® CM 825 and Tewameter® TM 300.<sup>30,31</sup>

On the 1<sup>st</sup> and 8<sup>th</sup> day of the experiment, the skin on tumors and the healthy skin of mice were assessed with the Multi Probe Adapter (MPA) Systems measuring device and with the probes Corneometer® CM 825

**Table 1.** Compositions of the design semisolid formulations: No. 1, 2, 8, and 10 – emulsions w/o; No. 3–7, 9, 19, and 24 – emulsions o/w; No. 11–18, 20, 22, and 23 – gels; No. 21 – o/w emulsion gel. Trichostatin A was introduced ex tempore at a dose of 0.01% for in vitro release and at a dose of 0.05% for in vivo animal tests – cont.

Composition	Formulation No.												
	13	14	15	16	17	18	19	20	21	22	23	24	
Stearic acid (WarChem)							12.5%						
Karinol-CS Cetyl Alcohol (Paulika)							5%						
Methocel® 90HG (Sigma-Aldrich)	3%	3%											
Carbopol® Ultrez 10 (Lubrizol) Carbomer			1%	1%	1%	1%							
Sepineo P 600 (Seppic)								4%	3%				
Sepineo D.E.R.M. (Seppic)										1.5%	1.5%		
PentraVan® (Fagron) oil-in-water emulsion base												50%	
Glycerol Glycerolum 85% (Pharma-Cosmetic)	10%		10%		10%								
Propylene Glycol (WarChem)		10%		10%		10%						10%	
Triethanolamine (POCH)			0.8%	0.8%									
10% NaOH Sodium hydroxide (Chempur)					2.5%	2.5%							
Sodium dodecyl sulfate (Sigma-Aldrich)							2.5%						
Oleum Amygdalae dulcium (Profarm)									20%				
Trichostatin A (Sigma-Aldrich) – in vitro	0.01%	0.01%	0.01%	0.01%	0.01%	0.01%	0.01%	0.01%	0.01%	0.01%	0.01%	0.01%	
Trichostatin A (Sigma-Aldrich) – in vivo	0.05%	0.05%	0.05%	0.05%	0.05%	0.05%	0.05%	0.05%	0.05%	0.05%	0.05%	0.05%	
Aqua pro injectione (Polpharma)	q.s.	q.s.	q.s.	q.s.	q.s.	q.s.	q.s.	q.s.	q.s.	q.s.	q.s.	q.s.	

Methocel® 90HG – hydroxypropylmethylcellulose; Sepineo P 600 – acrylamide/sodium acryloyldimethyl taurate copolymer/isohexadecane and polysorbate 80; Sepineo D.E.R.M. – hydroxyethyl acrylate/sodium acryloyldimethyl taurate copolymer; q.s. – quantum satis (just far enough).

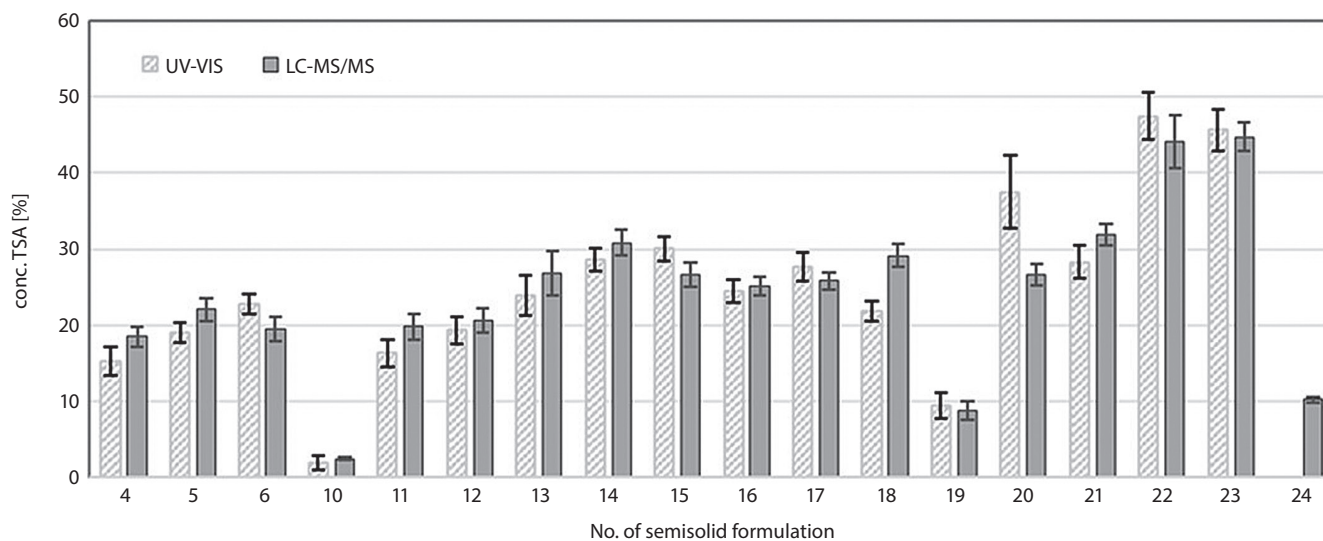


**Fig. 2.** Amount of TSA% released from semisolid formulations after 6 h (n = 7)

and Tewameter<sup>®</sup> TM 300 (Courage+Khazaka Electronic GmbH, Cologne, Germany). The skin on neoplastic tumors and healthy skin surrounding the tumor were assessed. Hair was removed from the skin the day before the measurements. Then, the mice were euthanized, and the tumors and skin were collected for further studies.

The measurement of skin humidity with the Corneometer probe is based on a recognized international volumetric method. It provides confirmed and well-confirmed measurements of skin hydration.<sup>32,33</sup> The Tewameter probe was used to assess TEWL without impairing the skin microenvironment. The Tewameter probe measures the density gradient of the water evaporation from the skin indirectly by the sensors of temperature and relative humidity, with the use of open chamber diffusion technique. The measurement of the water evaporation from the skin is the basic parameter in the assessment of the epidermal barrier function.<sup>34</sup>

## Statistical evaluation

The studies were performed in accordance with the protocol approved by the Bioethics Committee of the Medical University of Warsaw (approval No. 160/2016). The results are presented in the form of mean and standard deviation (SD). Statistical significance ( $p < 0.05$ ) of differences between the groups was analyzed with the use of one-way analysis of variance (ANOVA). The post hoc Tukey's test was used. Statistical significance was assessed with the use of GraphPad Prism v. 7 software (GraphPad Software, San Diego, USA). Statistically significant differences are marked with asterisks (\*  $p < 0.05$ ; \*\*  $p < 0.01$ ; \*\*\*  $p < 0.001$ ).

## Results

### Preparation of semisolid formulations

Semisolid formulations were developed with the use of ingredients available on the market. Ready-made media and pharmacopoeial ingredients used in the field of pharmacy were selected: Unguentum cholesteroli, Unguentum eucerini, Vaselineum hydrophylicum, Vaselineum album, Lanolinum; industrial media: Lekobaza, Pentravan; gelling, concentrating and stabilizing substances: Carboxymethylcellulose sodium, Carbomer, Hydroxypropylmethylcellulose, Sepineo P600, and Sepineo D.E.R.M. Organoleptic analysis was performed during and after preparation. The formulations were assessed with regard to appearance, consistency and spreading. Twenty-four formulations were obtained: No. 1, 2, 8, and 10 – w/o emulsions; No. 3, 4, 5, 6, 7, 9, 19, and 24 – o/w emulsions; No. 11–18, 20, 22, and 23 – gels; and No. 21 – o/w emulsion gel (Table 1). The obtained formulations were homogeneous, had adequate consistency and spread well.

### Assessment of TSA release from semisolid formulations

A test of TSA release from the obtained formulations was conducted. For this purpose, a method of in vitro TSA release was developed. The samples were measured spectrophotometrically with UV-VIS and with LC-MS/MS. The measurements performed with these 2 methods were comparable for most of the formulations (Fig. 2). The formulations No. 1, 2, 3, 8, and 9 were rejected, since there was no TSA release as measured using LC-MS/MS and there were difficulties with the UV-VIS measurement. Eighteen semisolid formulations were selected, and the release tests were performed again. On the basis of the release tests, the following formulations were selected for in vivo studies: No. 5 – o/w emulsion with a concentrating and stabilizing substance (hydroxypropylmethylcellulose)<sup>35</sup>; No. 18 – hydrogel with propylene glycol, which increases skin penetration of the formulation and prolongs its stability<sup>36</sup>; and No. 21 – o/w emulsion gel based on polymers and almond oil.<sup>24,25</sup> The w/o emulsion ointment on the absorptive hydrophobic medium No. 10 was qualified for in vivo studies due to its occlusive properties, which could increase skin penetration by TSA.

### Assessment of anticancer activity of semisolid TSA formulations in vivo in Balb/c mice

Everyday throughout the study (8 days) the mice were weighed and the tumor size was measured. No significant change in the mouse body weight was observed during the study. Rubbing the semisolid formulations with TSA in the tumors and intratumor TSA injections had no effect on the body weight of the mice. The tumors were measured in all the mice with a caliper for 8 days. The results are summarized in Table 2. It shows that the tumors treated with TSA formulations grow more slowly than the tumors treated with non-TSA formulations. The growth of tumors treated with TSA formulations was lower than in the corresponding control groups. Control tumors which were not treated with TSA formulations showed a regular growth. The tumors treated with TSA grew slowly, and their growth was inhibited.

### Assessment of skin hydration and TEWL with the probes Corneometer<sup>®</sup> CM 825 and Tewameter<sup>®</sup> TM 300

A study with the Corneometer<sup>®</sup> CM 825 and Tewameter<sup>®</sup> TM 300 probes was conducted on the 1<sup>st</sup> day of the experiment, before testing the mice and on the last day, prior to autopsy.<sup>36</sup> The skin on neoplastic tumors and the healthy skin surrounding the tumor were assessed. Hair was removed from the skin the day before the measurements. The measurement of skin humidity is based

**Table 2.** Assessment of anticancer activity of semisolid TSA formulations in Balb/c mice with L1 tumor. Measurement of tumor volume v [mm<sup>3</sup>]

Formulation	Day 1	Day 2	Day 3	Day 4	Day 5	Day 6	Day 7	Day 8
C1	41.6	41.6	78	131.04	203.84	229.32	520	692.12
C1	41.6	41.6	91	168.48	229.32	366.08	366.08	463.32
C1	18.72	49.92	131.04	421.2	421.2	572	572	692.12
C2	421.2	421.2	624	817.96	817.96	880.88	943.8	943.8
C2	112.32	112.32	178.36	266.24	266.24	299.52	299.52	421.2
C2	65	65	149.76	272.636	203.84	299.52	421.2	624
C3	463.32	399.36	399.36	547.56	547.56	631.8	780	780
C3	229.32	421.2	332.8	463.32	299.52	463.32	505.44	505.44
C3	299.52	299.52	203.84	266.24	379.08	421.2	421.2	421.2
5	78	78	78	131.04	203.84	366.08	366.08	463.32
5	78	112.32	131.04	203.84	266.24	299.52	299.52	332.8
5	65	65	65	112.32	178.36	266.24	266.24	299.52
5+TSA	149.76	203.84	203.84	203.84	203.84	203.84	421.2	421.2
5+TSA	0.52	0.52	0.52	0.52	0.52	0.52	0.52	0.52
5+TSA	14.04	14.04	18.72	18.72	18.72	18.72	41.6	41.6
18	254.8	366.08	463.32	463.32	624	676	676	817.96
18	299.52	299.52	332.8	421.2	421.2	572	624	676
18	149.76	203.84	254.8	254.8	280.28	366.08	505.44	624
18+TSA	6.24	6.24	18.72	18.72	18.72	18.72	18.72	41.6
18+TSA	112.32	112.32	78	78	78	78	78	91
18+TSA	203.84	203.84	203.84	203.84	254.8	254.8	254.8	254.8
10	6.24	6.24	18.72	28.08	49.92	149.76	299.52	332.8
10	41.6	149.76	168.48	168.48	187.2	254.8	280.28	331.24
10	1.04	18.72	65	131.04	131.04	149.76	168.48	187.2
10+TSA	78	131.04	229.32	229.32	229.32	254.8	254.8	280.28
10+TSA	131.04	131.04	266.24	266.24	299.52	332.8	332.8	399.36
10+TSA	131.04	178.36	299.52	299.52	299.52	421.2	421.2	572
21	6.24	41.6	58.24	104	149.76	229.32	332.8	463.32
21	0.52	1.04	4.16	6.24	14.04	78	78	149.76
21	4.16	4.16	14.04	65	112.32	149.76	254.8	366.08
21+TSA	6.24	14.04	4.16	14.04	41.6	91	91	104
21+TSA	18.72	18.72	18.72	41.6	41.6	78	78	104
21+TSA	4.16	4.16	4.16	4.16	4.16	4.16	18.72	78

C1 – control group; C2 – control group – intratumor injection (DMSO+PBS); C3 – control group – intratumor injection with TSA; 5 – formulation No. 5; 5+TSA – formulation No. 5 with TSA; 18 – formulation No. 18; 18+TSA – formulation No. 18 with TSA; 10 – formulation No. 10; 10+TSA – formulation No. 10 with TSA; 21 – formulation No. 21; 21+TSA – formulation No. 21 with TSA.

on a recognized international volumetric method, which provides confirmed and well-confirmed measurements of skin hydration.<sup>32,33</sup> The findings of the Corneometer are presented in contract units. The higher the values, the drier and less moisturized skin. The effect of the tumor and its growth, and the effect of intratumor injection and TSA on skin moisturizing were not confirmed. As presented in Fig. 3, the measurement of skin moisture with Corneometer showed that the tumor growth and treatment with TSA and non-TSA formulations had no effect on the skin condition. The Tewameter probe was used to assess TEWL without impairing the skin microenvironment.

The Tewameter probe is based on the open-chamber diffusion technique (sensors of temperature and relative humidity), where the gradient of the water evaporation from the skin is measured according to Fick's law and is expressed as evaporation coefficient in g/h/m<sup>2</sup>. The Tewameter probe is a reliable tool to measure water evaporation from the skin.<sup>34</sup> The higher the result, the greater water loss and worse skin condition. The skin on the tumor shows similar humidity to the skin near the tumor that has not been treated with formulations. Figure 4 shows that the epidermal barrier function of neoplastic tumors has been reduced. The measurement with the Tewameter

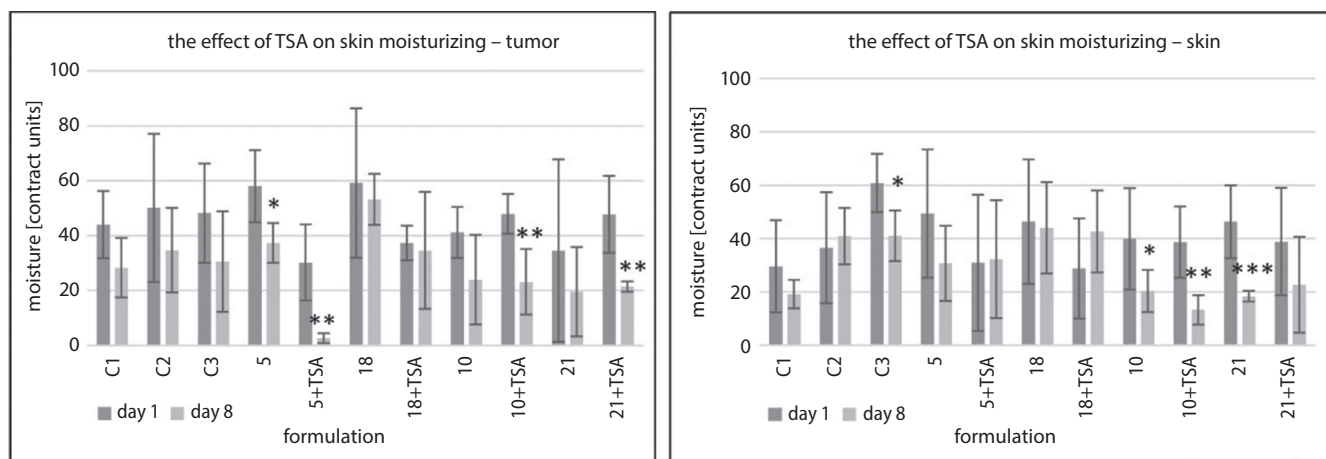


Fig. 3. Assessment of anticancer activity of semisolid TSA formulations in Balb/c mice with L1 tumor. Assessment of skin moisture. Measurement with the Corneometer probe (n = 10)

C1 – control group; C2 – control group – intratumor injection (DMSO+PBS); C3 – control group – intratumor injection with TSA; 5 – formulation No. 5; 5+TSA – formulation No. 5 with TSA; 18 – formulation No. 18; 18+TSA – formulation No. 18 with TSA; 10 – formulation No. 10; 10+TSA – formulation No. 10 with TSA; 21 – formulation No. 21; 21+TSA – formulation No. 21 with TSA. Statistically significant differences are marked with an asterisk (\* p < 0.05; \*\* p < 0.01; \*\*\* p < 0.001).

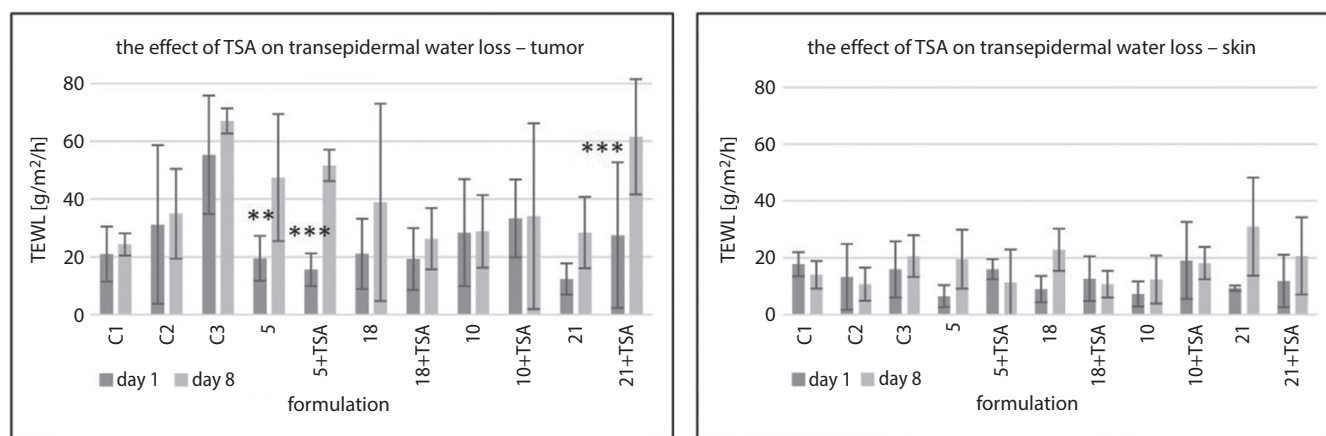


Fig. 4. Assessment of anticancer activity of semisolid TSA formulations in Balb/c mice with L1 tumor. Assessment of transepidermal water loss (TEWL). Measurement with the Tewameter probe (n = 5) with standard deviation (SD) of 0.2

C1 – control group; C2 – control group – intratumor injection (DMSO+PBS); C3 – control group – intratumor injection with TSA; 5 – formulation No. 5; 5+TSA – formulation No. 5 with TSA; 18 – formulation No. 18; 18+TSA – formulation No. 18 with TSA; 10 – formulation No. 10; 10+TSA – formulation No. 10 with TSA; 21 – formulation No. 21; 21+TSA – formulation No. 21 with TSA. Statistically significant differences are marked with an asterisk (\*\* p < 0.01; \*\*\* p < 0.001).

probe indicates that the water loss through tumor skin is higher in comparison with the skin on the areas not treated with the formulations.

## Discussion

Currently, the experimental research in the field of innovative anticancer drugs are focused on the search for new active substances and are significantly associated with the development of effective carriers and strategies for drug transfer. Recently, research has also been performed on new drug forms for known active substances in order to extend the therapeutic indications of registered medicines. This study is part of the current research

on medicines.<sup>37–39</sup> The aim of the experiment was to obtain a preparation with antitumor activity for external use. The excipients used in the pharmaceutical formulation were selected, as well as new multiphase substrates with liposomes or based on polymers. A semi-solid formulation with a histone deacetylase inhibitor, TSA, was prepared. The antitumor activity of the preparation was evaluated in a model of transplantable L1 tumor in Balb/c laboratory mice. The available sources of scientific research are reporting that much research has been conducted in the field of histone deacetylase (HDAC) inhibition over the past decade.<sup>40–42</sup> The HDAC inhibitors (HDACi) have high anticancer potential. The HDACi (e.g., vorinostat, panobinostat, belinostat) approved by the Federal Drug Administration (FDA) are used for treatment of various types

of cancer.<sup>42</sup> Many HDACi (e.g., entinostat) are in clinical research phase.<sup>42,43</sup> The HDACi present anti-tumor activity through various mechanisms, i.e., cell cycle arrest, induction of apoptosis and autophagy in transformed cells, and inhibition of angiogenesis.<sup>42,44</sup> The growing interest of HDACi because of their effectiveness in cancer therapy encourages the search and research of other substances that belong to this group.<sup>40</sup> It has been confirmed that TSA is a reversible HDAC inhibitor and affects cancer cells by activating apoptotic pathways and arresting the cell cycle. Induction of apoptosis occurs through external (death receptor) or internal (mitochondrial) pathways; both of them lead to caspase activation and cell death induction.<sup>16,44</sup> In the study by Ma et al., TSA has been shown to have antiproliferative activity on cells of the esophageal squamous cell carcinoma line by inducing cell cycle arrest and apoptosis.<sup>45</sup> It seems that TSA can be considered as an anticancer active substance to use in the preparation of semi-solid formulations for external application in cancer. Studies show that known anticancer substances, e.g., vismodegib, imiquimod, 5-fluorouracil, methotrexate, or gabapentin, applied topically are helpful in the treatment of cancer.<sup>46–52</sup> In one of the first studies which proposed a local application of vismodegib, developed by Caliceni et al., nanoformulation in the treatment of basal-cell cancer was obtained. Vismodegib was incorporated into liposomes to provide a local nanodrug delivery system that may be useful in reducing systemic distribution and, as a consequence, side effects, while simultaneously penetrating the stratum corneum.<sup>46</sup> Kubicki et al. reported complete remission of primary cutaneous anaplastic large cell lymphoma after topical application of imiquimod.<sup>47</sup> Another study showed that 5% imiquimod for topical use is an acceptable treatment option for patients with malignant melanoma who prefer local treatment over surgery or radiation therapy.<sup>48</sup> A mouse model study found that methotrexate encapsulated in liposomes administered topically may be a new, less toxic treatment opportunity for human psoriasis.<sup>49</sup> On the other hand, a study by Shahid et al. showed that gabapentin can also be used topically, but not as an antitumor substance, but to treat neuropathic pain. The study demonstrated that both local and systemic administration of gabapentin to rats weakens peripheral neuropathy caused by chemotherapy. Topical use of gabapentin may be an auxiliary or alternative way of treating neuropathic pain when administration of systemic drugs threatens the patient's life due to side effects.<sup>50</sup> In the study by Kanaya et al., patients with ocular surface squamous neoplasia after local tumor resection were locally treated with interferon  $\alpha$ -2b. Topical administration of interferon  $\alpha$ -2b contributed to inhibiting tumor recurrence and improving the patients' quality of vision.<sup>51</sup> Another study showed that topically applied interferon  $\alpha$ -2b in the form of eye drops is an effective and safe treatment for conjunctival papilloma. Three months after the start of treatment with interferon  $\alpha$ -2b, complete regression of the lesion was

achieved.<sup>52</sup> In the treatment of cancer, combination therapy is extremely important. This approach of treatment takes advantage of the fact that anticancer substances can more effectively inhibit tumor growth in combination with radiation and/or another anticancer substances, which suggests a promising strategy in the treatment of skin metastases. Topical application of imiquimod cream simultaneously with radiation therapy significantly reduced the growth of a breast cancer tumor in a mouse model, compared to using these therapies separately. Moreover, administration of cyclophosphamide prior to imiquimod and radiation therapy potentiates the therapeutic effect, suggesting that this combination is a very promising strategy for metastases of breast cancer to the skin.<sup>53</sup>

In the current study, it was important to choose the right formulation to achieve proper TSA release. It is known that skin permeability is increased due to the presence of water, which causes swelling of keratin and increases intercellular spaces. Semi-solid preparations that form an occlusive layer on the skin also increase the hydration of the stratum corneum and the absorption of drugs through the skin.<sup>54</sup> Therefore, semi-solid preparations were selected for in vivo studies that released TSA well and those with occlusive properties: the o/w emulsion with a thickening and stabilizing substance (hydroxypropylmethylcellulose), the w/o emulsion on an absorbent-hydrophobic medium, the hydrogel with propylene glycol (which increases the penetration of the formulation through the skin and prolongs the stability of the preparation), and the o/w emulsion gel based on polymers and almond oil was used. As Fig. 5 shows, it was observed that the growth of tumors treated with TSA preparations was lower than the growth in the control groups (without TSA). Anticancer activity of topical preparations was also noticed in other works on HDAC inhibitors. In the study

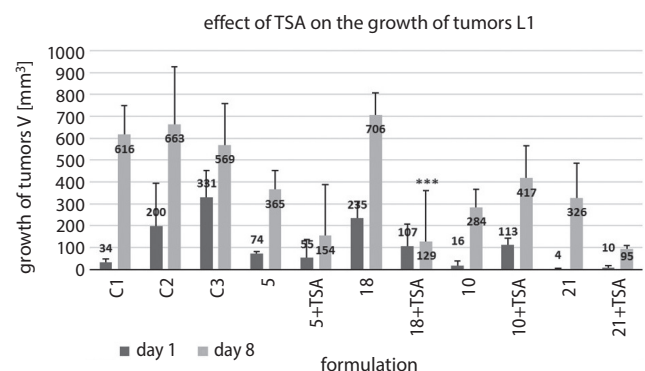


Fig. 5. Assessment of anticancer activity of semisolid TSA formulations in Balb/c mice with L1 tumor

C1 – control group; C2 – control group – intratumor injection (DMSO+PBS); C3 – control group – intratumor injection with TSA; 5 – formulation No. 5; 5+TSA – formulation No. 5 with TSA; 18 – formulation No. 18; 18+TSA – formulation No. 18 with TSA; 10 – formulation No. 10; 10+TSA – formulation No. 10 with TSA; 21 – formulation No. 21; 21+TSA – formulation No. 21 with TSA. Statistically significant differences are marked with an asterisk (\*\*\*)  $p < 0.001$ .

performed by Dai et al., a hydrogel with vorinostat was used on rats.<sup>55</sup> The purpose of this study was to develop a new formulation with vorinostat that would be effective in the early stages of cutaneous T cell lymphoma and free of serious side effects. As a result, topical administration with a much lower dose showed a higher area under the curve (AUC) (cumulative amount of vorinostat retention through the skin) than oral administration, and the hydrogel achieved sustained permeation of vorinostat in the skin for 24 h in vivo. This indicated that higher relative bioavailability of vorinostat from the hydrogel was achieved compared to oral route. Researchers found that a hydrogel can deliver vorinostat to local skin more effectively and without adverse effects than oral administration. A study performed by Dai et al. confirms that the topical application of the preparation to the skin achieves higher availability of the active substance and additionally reduces the adverse effects of the treatment.<sup>55</sup> These results encourage the search for new substances that can be used in the same way, but there is also a need to suggest new/appropriate formulations for topical application. Another study used entinostat (MS-275), which at a concentration of 2 mg/kg significantly slowed the growth of squamous cell carcinoma of the skin in a hairless SKH-1 mouse model. MS-275 was cell-permeable as a topical preparation and induced changes in histone acetylation in mouse tumor tissue. It was also effective in inhibiting the proliferation of patient-derived squamous cell carcinoma lines and was especially effective towards cells isolated from regional metastases in an immunocompromised individual.<sup>43</sup>

## Conclusions

In summary, the performed research indicates that tumor growth may be limited through external administration of active substances with histone deacetylase inhibitory activity. This study provides useful information for planning future clinical protocols in oncology. The formulations for topical use with TSA can be considered as future preparations supporting the treatment of patients with cancer. It is also worth noting that the non-invasive, external route of application of prescription semi-solid formulations allows the patient to use the medicinal preparation outside the clinic. According to the results of the performed research on external applications, we recommend o/w emulsion pharmaceutical formulations based on hydroxypropylmethylcellulose and SEPINEO P600/almond oil.

### ORCID iDs

Agnieszka Chodkowska  <https://orcid.org/0000-0002-8920-1057>  
 Alicja Bieńkowska  <https://orcid.org/0000-0002-7675-0428>  
 Żaneta Słyk  <https://orcid.org/0000-0002-1178-7908>  
 Joanna Giebułtowicz  <https://orcid.org/0000-0002-2567-4453>  
 Maciej Małecki  <https://orcid.org/0000-0002-7078-4918>

## References

1. International Agency for Research on Cancer. <https://gco.iarc.fr/tomorrow/home>. Accessed August 24, 2020.
2. Krajowy Rejestr Nowotworów. <http://onkologia.org.pl/nawotwory-zlosliwe-ogolem-2/>. Accessed August 24, 2020.
3. Chessum N, Jones K, Pasqua E, Tucker M. Recent advances in cancer therapeutics. *Prog Med Chem*. 2015;54:1–63. doi:10.1016/bs.pmch.2014.11.002
4. Collins I, Workman P. New approaches to molecular cancer therapeutics. *Nat Chem Biol*. 2006;2(12):689–700.
5. Grabarska A, Dmoszyńska-Graniczka M, Nowosadzka E, Stepulak A. Histone deacetylase inhibitors: Molecular mechanisms of actions and clinical applications. *Postepy Hig Med Dosw (Online)*. 2013;67:722–735.
6. Smith LT, Otterson GA, Plass C. Unraveling the epigenetic code of cancer for therapy. *Trends Genet*. 2007;23(9):449–456.
7. Kudo K, Ozaki T, Shin-ya K, Nishiyama M, Kuzuyama T. Biosynthetic origin of the hydroxamic acid moiety of trichostatin A: Identification of unprecedented enzymatic machinery involved in hydroxylamine transfer. *J Am Chem Soc*. 2017;139(20):6799–6802. doi:10.1021/jacs.7b02071
8. Tsuji N, Kobayashi M, Nagashima K, Wakisaka Y, Koizumi K. A new antifungal antibiotic, trichostatin. *J Antibiot (Tokyo)*. 1976;29(1):1–6. doi.org/10.7164/antibiotics.29.1
9. Yoshida M, Horinouchi S, Beppu T. Trichostatin A and trapoxin: Novel chemical probes for the role of histone acetylation in chromatin structure and function. *Bioessays*. 1995;17(5):423–430. doi:10.1002/bies.950170510
10. Kim SH, Kang HJ, Na H, Li MO. Trichostatin A enhances acetylation as well as protein stability of ERalpha through induction of p300 protein. *Breast Cancer Res*. 2010;12(2):R22. doi:10.1186/bcr2562
11. Sharma P, Kumar S, Kundu GC. Transcriptional regulation of human osteopontin promoter by histone deacetylase inhibitor, trichostatin A in cervical cancer cells. *Mol Cancer*. 2010;9:178. doi:10.1186/1476-4598-9-178
12. Cheng DD, Yang QC, Zhang ZC, Yang CX, Liu YW. Antitumor activity of histone deacetylase inhibitor trichostatin A in osteosarcoma cells. *Asian Pac J Cancer Prev*. 2012;13(4):1395–1399. doi:10.7314/apjcp.2012.13.4.1395
13. Park H, Lee YJ, Kim TH, et al. Effects of trichostatin A, a histone deacetylase inhibitor, on the regulation of apoptosis in H-ras-transformed breast epithelial cells. *Int J Mol Med*. 2008;22(5):605–611.
14. Geng Y, Liu J, Xie Y, et al. Trichostatin A promotes GLI1 degradation and P21 expression in multiple myeloma cells. *Cancer Manag Res*. 2018;10:2905–2914. doi:10.2147/CMAR.S167330
15. Hakami NY, Disting GJ, Peshavariya HM. Trichostatin A, a histone deacetylase inhibitor suppresses NADPH oxidase 4-derived redox signaling and angiogenesis. *J Cell Mol Med*. 2016;20(10):1932–1944. doi:10.1111/jcmm.12885
16. Hajji N, Wallenborg K, Vlachos P, Nyman U, Hermanson O, Joseph B. Combinatorial action of the HDAC inhibitor trichostatin A and etoposide induces caspase-mediated AIF-dependent apoptotic cell death in non-small cell lung carcinoma cells. *Oncogene*. 2008;27(22):3134–3144.
17. Wu J, Hu CP, Gu QH, Li YP, Song M. Trichostatin A sensitizes cisplatin-resistant A549 cells to apoptosis by up-regulating death-associated protein kinase. *Acta Pharmacol Sin*. 2010;31(1):93–101. doi:10.1038/aps.2009.183
18. Zhang XF, Yan Q, Shen W, Gurunathan S. Trichostatin A enhances the apoptotic potential of palladium nanoparticles in human cervical cancer cells. *Int J Mol Sci*. 2016;17(8):1354. doi:10.3390/ijms17081354
19. Suraweera A, O'Byrne KJ, Richard DJ. Combination therapy with histone deacetylase inhibitors (HDACi) for the treatment of cancer: Achieving the full therapeutic potential of HDACi. *Front Oncol*. 2018;8:92. doi:10.3389/fonc.2018.0009
20. Ghiciuc CM, Strat AL, Ochiuz L, et al. Inhibition of bcl-2 and cox-2 protein expression after local application of a new carmustine-loaded clinoptilolite-based delivery system in a chemically induced skin cancer model in mice. *Molecules*. 2017;22(11):2014. doi:10.3390/molecules22112014

21. Shakeel F, Haq N, Al-Dhfyar A, Alanazi FK, Alsarra IA. Chemoprevention of skin cancer using low HLB surfactant nanoemulsion of 5-fluorouracil: A preliminary study. *Drug Deliv*. 2015;22(4):573–580. doi:10.3109/10717544.2013.868557
22. *Pharmacopoea Polonica Editio XI*. Vol. I. Warszawa, Poland: Polskie Towarzystwo Farmaceutyczne; 2017:122.
23. Sznitowska M. *Farmacja stosowana. Technologia postaci leku*. Warszawa, Poland: PZWL; 2017;369–442, 883–930.
24. Seppic SA. <https://www.seppic.com/en/technologies/polymerization>. Accessed August 24, 2020.
25. Bonacucina G, Cespi M, Palmieri GF. Characterization and stability of emulsion gels based on acrylamide/sodium acryloyldimethyl taurate copolymer. *AAPS PharmSciTech*. 2009;10(2):368–375. doi:10.1208/s12249-009-9218-1
26. Janik P, Szaniawska B. Search for an influence of natural immunity on the lung colony assay of a syngeneic transplanted murine tumour. *Br J Cancer*. 1978;37(6):1083–1085. doi:10.1038/bjc.1978.157
27. Vigushin DM, Ali S, Pace PE, et al. Trichostatin A is a histone deacetylase inhibitor with potent antitumor activity against breast cancer in vivo. *Clin Cancer Res*. 2001;7(4):971–976.
28. Ali NS, Akudugu JM, Howell RH. A preliminary study on treatment of human breast cancer xenografts with a cocktail of paclitaxel, doxorubicin, and 1311-anti-epithelial cell adhesion molecule (9C4). *World J Nucl Med*. 2019;18(1):18–24. doi:10.4103/wjnm.WJNM\_9\_18
29. Tomayko MM, Reynolds CP. Determination of subcutaneous tumor size in athymic (nude) mice. *Cancer Chemother Pharmacol*. 1989;24(3):148–154. doi:10.1007/bf00300234
30. <https://www.courage-khazaka.de/en/scientific-products/all-products/16-wissenschaftliche-produkte/alle-produkte/183-corneometer-e>. Accessed August 24, 2020.
31. <https://www.courage-khazaka.de/en/scientific-products/all-products/16-wissenschaftliche-produkte/alle-produkte/257-tewameter-hex-e>. Accessed August 24, 2020.
32. Lodén M, Hagforsen E, Lindberg M. The presence of body hair influences the measurement of skin hydration with the Corneometer. *Acta Derm Venereol*. 1995;75(6):449–450. doi:10.2340/0001555575449450
33. Wakeman MP. An open-label forearm-controlled pilot study to assess the effect of a proprietary emollient formulation on objective parameters of skin function of eczema-prone individuals over 14 days. *Clin Cosmet Investig Dermatol*. 2017;10:275–283. doi:10.2147/CCID.S135841
34. De Paepe K, Houben E, Adam R, Wiesemann F, Rogiers V. Validation of the VapoMeter, a closed unventilated chamber system to assess transepidermal water loss vs the open chamber Tewameter. *Skin Res Technol*. 2005;11(1):61–69. doi:10.1111/j.1600-0846.2005.00101.x
35. Lunter DJ, Daniels R. New film forming emulsions containing Eudragit® NE and/or RS 30D for sustained dermal delivery of nonivamide. *Eur J Pharm Biopharm*. 2012;82(2):291–298.
36. Dyja R, Jankowski A. The effect of additives on release and in vitro skin retention of flavonoids from emulsion and gel semisolid formulations. *Int J Cosmet Sci*. 2017;39(4):442–449. doi:10.1111/ics.12395
37. Sarkar R, Banerjee S, Amin SA, Adhikari N, Jha T. Histone deacetylase 3 (HDAC3) inhibitors as anticancer agents: A review. *Eur J Med Chem*. 2020;192:112171. doi:10.1016/j.ejmech.2020.112171
38. Pucci C, Martinelli C, Ciofani G. Innovative approaches for cancer treatment: Current perspectives and new challenges. *Ecancermedicalscience*. 2019;13:961. doi:10.3332/ecancer.2019.961
39. Stoff JA. Selected office-based anticancer treatment strategies. *J Oncol*. 2019;2019:7462513. doi:10.1155/2019/7462513
40. Zhang H, Shang YP, Chen HY, Li J. Histone deacetylases function as novel potential therapeutic targets for cancer. *Hepatol Res*. 2017;47(2):149–159. doi:10.1111/hepr.12757
41. Schizas D, Mastoraki A, Naar L, et al. Concept of histone deacetylases in cancer: Reflections on esophageal carcinogenesis and treatment. *World J Gastroenterol*. 2018;24(41):4635–4642. doi:10.3748/wjg.v24.i41.4635
42. Singh AK, Bishayee A, Pandey AK. Targeting histone deacetylases with natural and synthetic agents: An emerging anticancer strategy. *Nutrients*. 2018;10(6):731. pii: E731. doi:10.3390/nu10060731
43. Kalin JH, Eroglu A, Liu H, et al. Investigation into the use of histone deacetylase inhibitor MS-275 as a topical agent for the prevention and treatment of cutaneous squamous cell carcinoma in an SKH-1 hairless mouse model. *PLoS One*. 2019;14(3):e0213095. doi:10.1371/journal.pone.0213095
44. Sanaei M, Kavooosi F. Histone deacetylases and histone deacetylase inhibitors: Molecular mechanisms of action in various cancers. *Adv Biomed Res*. 2019;8:63. doi:10.4103/abr.abr\_142\_19
45. Ma J, Guo X, Zhang S, et al. Trichostatin A, a histone deacetylase inhibitor, suppresses proliferation and promotes apoptosis of esophageal squamous cell lines. *Mol Med Rep*. 2015;11(6):4525–4531. doi:10.3892/mmr.2015.3268
46. Calienni MN, Febres-Molina C, Llovera RE, et al. Nanoformulation for potential topical delivery of Vismodegib in skin cancer treatment. *Int J Pharm*. 2019;565:108–122. doi:10.1016/j.ijpharm.2019.05.002
47. Kubicki SL, Park KE, Aung PP, Duvic M. Complete resolution of primary cutaneous anaplastic large cell lymphoma with topical imiquimod. *J Drugs Dermatol*. 2019;18(5):460–462.
48. Tio DCKS, van Montfrans C, Ruijter CGH, Hoekzema R, Bekkenk MW. Effectiveness of 5% topical imiquimod for lentigo maligna treatment. *Acta Derm Venereol*. 2019;99(10):884–888. doi:10.2340/00015555-3241
49. Bahramizadeh M, Bahramizadeh M, Kiafar B, et al. Development, characterization and evaluation of topical methotrexate-entrapped deformable liposome on imiquimod-induced psoriasis in a mouse model. *Int J Pharm*. 2019;569:118623. doi:10.1016/j.ijpharm.2019.118623
50. Shahid M, Subhan F, Ahmad N, Sewell RDE. Efficacy of a topical gabapentin gel in a cisplatin paradigm of chemotherapy-induced peripheral neuropathy. *BMC Pharmacol Toxicol*. 2019;20(1):51. doi:10.1186/s40360-019-0329-3
51. Kanaya R, Kase S, Ishijima K, Ishida S. Usefulness of topical interferon alpha-2b eye drop as an adjunctive therapy following surgical resection in ocular surface squamous neoplasia. *In Vivo*. 2019;33(6):2211–2215. doi:10.21873/invivo.11724
52. Bolek B, Wylęgała A, Teper S, Kokot J, Wylęgała E. Treatment of conjunctival papilloma with topical interferon alpha-2b: Case report. *Medicine (Baltimore)*. 2020;99(7):e19181. doi:10.1097/MD.00000000000019181
53. Dewan MZ, Vanpouille-Box C, Kawashima N, et al. Synergy of topical toll-like receptor 7 agonist with radiation and low-dose cyclophosphamide in a mouse model of cutaneous breast cancer. *Clin Cancer Res*. 2012;18(24):6668–6678. doi:10.1158/1078-0432.CCR-12-0984
54. Sznitowska M, Kaliszan R. *Biofarmacja*. Wrocław, Poland: Elsevier Urban & Partner; 2014:221–234.
55. Dai W, Wang C, Yu C, et al. Preparation of a mixed-matrix hydrogel of vorinostat for topical administration on the rats as experimental model. *Eur J Pharm Sci*. 2015;78:255–263. doi:10.1016/j.ejps.2015.07.019



# Platelet polyphosphate level is elevated in patients with chronic primary thrombocytopenia: A preliminary study

Ewa Żurawska-Plaksej<sup>1,A,C-F</sup>, Wiktor Kuliczkowski<sup>2,A,C,D,F</sup>, Bożena Karolko<sup>2,B,C,F</sup>, Magdalena Cielecka-Prynda<sup>2,B,E,F</sup>, Jakub Dębski<sup>2,B,C,F</sup>, Konrad Kaaz<sup>2,B,E,F</sup>, Andrzej Mysiak<sup>2,A,E,F</sup>, Tomasz Wróbel<sup>3,B,E,F</sup>, Maria Podolak-Dawidziak<sup>3,C-F</sup>, Lidia Usnarska-Zubkiewicz<sup>1,A,E,F</sup>

<sup>1</sup> Department of Pharmaceutical Biochemistry, Wrocław Medical University, Poland

<sup>2</sup> Department and Clinic of Cardiology, Wrocław Medical University, Poland

<sup>3</sup> Department of Hematology, Blood Neoplasms and Bone Marrow Transplantation, Wrocław Medical University, Poland

A – research concept and design; B – collection and/or assembly of data; C – data analysis and interpretation;

D – writing the article; E – critical revision of the article; F – final approval of the article

Advances in Clinical and Experimental Medicine, ISSN 1899–5276 (print), ISSN 2451–2680 (online)

*Adv Clin Exp Med.* 2020;29(9):1051–1056

## Address for correspondence

Ewa Żurawska-Plaksej

E-mail: ewa.zurawska-plaksej@umed.wroc.pl

## Funding sources

Internal grant of Wrocław Medical University, Poland, No. ST C. 14.16.077.

## Conflict of interest

None declared

Received on February 16, 2020

Reviewed on May 4, 2020

Accepted on July 16, 2020

Published online on September 18, 2020

## Abstract

**Background.** Platelets are key players in hemostasis. These blood cells contain different types of granules. Recently, there has been a growing interest in the role of inorganic polyphosphate (polyP) structures stored in dense granules of platelets and secreted during platelet activation.

**Objectives.** To measure platelet polyP levels in patients with thrombocytopenia and thrombocytopenia, and to examine the relationship of this indicator with platelet aggregation.

**Material and methods.** The study included 36 patients with hematological disorders (26 with primary chronic thrombocytopenia and 10 with essential thrombocythemia (ET)) and 40 healthy subjects. Platelet reactivity was measured using whole blood impedance aggregometry. The polyP levels were isolated from lysed platelets, which were obtained from citrated platelet-rich plasma. The procedure included inactivating endogenous phosphatases, removing phosphate units derived from DNA and proteins, and finally hydrolyzing them into monophosphate units. A colorimetric assay using malachite green and ammonium molybdate was performed in order to quantify polyP levels.

**Results.** The polyP concentrations were significantly higher in the patients with thrombocytopenia than in the patients with thrombocythemia or the controls. The polyP level was not correlated with the level of aggregation.

**Conclusions.** The higher polyP levels observed in the patients with low platelet counts may indicate the existence of a compensatory mechanism that prevents excessive bleeding in such patients. Our study provides evidence of an essential role of polyP in platelet function and the coagulation process.

**Key words:** coagulation, platelets, thrombocytopenia, essential thrombocythemia, platelet polyphosphate

## Cite as

Żurawska-Plaksej E, Kuliczkowski W, Karolko B, et al.

Platelet polyphosphate level is elevated in patients with chronic primary thrombocytopenia: A preliminary study.

*Adv Clin Exp Med.* 2020;29(9):1051–1056.

doi:10.17219/acem/125430

## DOI

10.17219/acem/125430

## Copyright

© 2020 by Wrocław Medical University

This is an article distributed under the terms of the Creative Commons Attribution 3.0 Unported (CC BY 3.0)

(<https://creativecommons.org/licenses/by/3.0/>)

## Introduction

Platelets are small, highly specialized anucleate blood cells that participate in primary hemostasis, forming a platelet plug at sites of vascular injury to prevent blood loss. Platelets become activated in response to various stimuli, triggering the release of their granular contents into the surrounding environment. Platelets contain  $\alpha$ -granules, dense granules and lysosomes. Platelet dense granules contain a unique pool of molecules (e.g., serotonin [5-HT], nucleotides and polyphosphate (polyP) that can also provide a sensitive measurement of platelet activity. Platelet polyP is a highly anionic, linear strand of inorganic orthophosphate residues connected by high-energy phosphoanhydride bonds; it is found in all living organisms.<sup>1</sup> Platelet-derived polyP composed of about 60–100 phosphate monomers in length accelerates factor V activation, opposes the anticoagulant action of tissue factor pathway inhibitor (TFPI), modulates fibrin clot structure and promotes factor XI activation.<sup>2</sup> Due to its highly anionic nature, polyP lends itself to being a natural activator of the contact system. Activation of the contact system accelerates thrombin generation. The net effect is increased fibrin formation and platelet activation, resulting in faster clot formation. The polyP is incorporated into the forming clot, thereby modifying the structure of the resulting fibrin network and its susceptibility to degradation by certain plasminogen activators.<sup>3</sup> Studies in mice and human plasma also revealed that polyP can serve as the long sought-after FXII-activating surface on activated platelets to link primary and secondary hemostasis.<sup>4</sup> Patients with polyP deficiency (Hermansky–Pudlak syndrome) have defective platelet-driven FXII activation and clotting.<sup>5</sup> On the other hand, the circulating von Willebrand factor (VWF) isolated from human platelets and plasma was shown to contain tightly bound polyP, which can enhance VWF ristocetin cofactor activity without affecting the bonding of VWF to collagen or VWF multimerization.<sup>6</sup>

Apart from many animal and *in vitro* studies, the data on polyP in humans is still not wholly understood. Starting from the basics, there are no data on the relationship between platelet polyP level and platelet count or between platelet polyP level and its reactivity.

The aim of this study was to measure platelet polyP levels in patients with thrombocytopenia and thrombocytosis, and to correlate it to platelet aggregation.

## Material and methods

### Patients

Patient recruitment was carried out as part of the project entitled “Assessment of the Efficacy and Safety of Antiplatelet Therapy in Patients with Multiple Myeloma and Essential Thrombocythemia Cancer

Undergoing Invasive Diagnostic and Therapeutic Procedures” (internal grant of Wrocław Medical University, Poland, No. STC.140.16.077). The study involved 36 patients with hematological disorders: 26 with primary chronic thrombocytopenia and 10 with essential thrombocythemia (ET) attending the outpatient clinic at the Department of Hematology, Blood Neoplasms and Bone Marrow Transplantation in Wrocław, Poland. Forty healthy adults with no history of thrombosis or bleeding events served as controls. Neither the patients nor the controls were treated with antiplatelet drugs. The patients with thrombocythemia had been treated with hydroxycarbamide or aspirin in the past, but they were not actively being treated during the study. The study was approved by the Bioethics Committee of Wrocław Medical University in accordance with the Declaration of Helsinki of 1975, as revised in 2000. All patients and controls provided written informed consent for the study. The characteristics of the patients and controls are presented in Table 1.

The normal platelet count in adults ranges between  $150.0 \times 10^9/L$  and  $450.0 \times 10^9/L$ . Thrombocytopenia was defined as a platelet count of less than  $150 \times 10^9/L$ , while thrombocytosis was defined as a platelet count of more than  $450 \times 10^9/L$ . Blood for polyP level and platelet aggregation was drawn the morning after at least 6 h of overnight fasting from the antecubital vein with a 21G needle.

### Platelet aggregation

Platelet reactivity was measured with whole blood impedance aggregometry (Multiplate analyzer; Roche Diagnostics, Basel, Switzerland). According to the manufacturer's instruction, impedance aggregometry does not require platelet count adjustments in the test probe before starting aggregation. Aggregation agonists included arachidonic acid (AA) at a target concentration of 0.5 mM, adenosine diphosphate (ADP) at a target concentration of 6.4  $\mu M$  and thrombin receptor agonist peptide (TRAP) at a target concentration of 32  $\mu M$ . The reagents were provided by the manufacturer of the aggregometer. Aggregation was assessed within 2 h of blood sampling with hirudin as an anticoagulant; the results were described by the area under the aggregation curve (AUC). Each aggregation measurement was performed twice, and the mean value was calculated. In the case of a 10% difference between the 2 measurements, the result was rejected and aggregation was repeated.

### Platelet polyP

A non-enzymatic assay to quantify platelet-derived polyP in cell lysates from patients was developed from various methods described for measuring polyP in biological samples.<sup>7–9</sup> After collecting blood into sodium citrate tubes (Vacutainer; Becton Dickinson, Franklin Lakes, USA), 9:1 (blood-to-citrate ratio) prostaglandin I<sub>2</sub> (PGI<sub>2</sub>;

**Table 1.** Patient characteristics, results of platelet aggregometry measurements and level of platelet-derived polyphosphate in the study groups

Variable	Thrombocytopenia (n = 26)	Essential thrombocytopenia (n = 10)	Controls (n = 40)	Statistical significance from post hoc tests
	(1)	(2)	(3)	
Age [years], mean $\pm$ SD	68 $\pm$ 10	56 $\pm$ 22	61 $\pm$ 9	(1) vs (2) p < 0.0001 (1) vs (3) p < 0.0001
Gender (men/women)	14/12	5/5	19/21	NS
PLT [ $\times 10^9$ /L], mean $\pm$ SD	73 $\pm$ 34	686 $\pm$ 230	176 $\pm$ 75	(1) vs (2) vs (3) p < 0.001
MPV [fL], mean $\pm$ SD	9.7 $\pm$ 1.3	9.1 $\pm$ 0.89	9.4 $\pm$ 1.1	NS
Hb [g/dL], median (IQR)	10.4 (9.1–12.6)	13.3 (12.3–13.4)	13.0 (11.5–14.1)	(1) vs (2) p < 0.0001 (1) vs (3) p < 0.0001
Ht [%], median (IQR)	34.0 (28.5–39.2)	41.2 (38.2–44.6)	40.8 (36.4–42.5)	(1) vs (2) p < 0.0001 (1) vs (3) p < 0.0001
RBC [ $\times 10^{12}$ /L], mean $\pm$ SD	3.6 $\pm$ 0.8	4.5 $\pm$ 0.7	4.1 $\pm$ 0.7	(1) vs (2) p < 0.0001 (1) vs (3) p < 0.0001
WBC [ $\times 10^9$ /L], median (IQR)	5.3 (3.2–7.1)	9.0 (7.3–9.7)	6.4 (5.3–7.9)	(2) vs (1) p < 0.0001 (2) vs (3) p < 0.0001
AA-induced aggregation [AUC], mean $\pm$ SD	33.7 $\pm$ 28.5	74.7 $\pm$ 46.6	34.8 $\pm$ 30.9	(2) vs (1) p < 0.001 (2) vs (3) p < 0.001
ADP-induced aggregation (AUC), mean $\pm$ SD	43.1 $\pm$ 27.7	107.2 $\pm$ 40.8	51.4 $\pm$ 26.3	(2) vs (1) p < 0.001 (2) vs (3) p < 0.001
TRAP-induced aggregation [AUC], mean $\pm$ SD	60.9 $\pm$ 28.9	117.7 $\pm$ 17.4	86.8 $\pm$ 28.2	(2) vs (1) p < 0.001 (2) vs (3) p < 0.001
PolyP [nmol per $10^8$ platelets], median (IQR)	1.62 (1.24)	1.29 (0.22)	1.12 (0.92)	(1) vs (3) p = 0.007 (1) vs (2) p = 0.006
Arterial hypertension	12	5	–	NS
Diabetes	1	1	–	NS
Ischemic heart diseases	0	1	–	NS
Kidney insufficiency	1	1	–	NS
Gout	0	1	–	NS

PLT – platelets; MPV – mean platelet volume; Hb – hemoglobin; Ht – hematocrit; RBC – red blood cells; WBC – white blood cells; AA – arachidonic acid; ADP – adenosine 5'-diphosphate; TRAP – thrombin receptor agonist peptide-6; AUC – area under curve; SD – standard deviation; IQR – interquartile range.

Cayman Chemicals, Ann Arbor, USA) was carefully added to a final concentration of 5  $\mu$ M in order to prevent platelet activation. A platelet fraction was obtained through the standard procedure. In brief, blood was centrifuged at 200  $\times$  g for 20 min at room temperature without braking. The resulting platelet-rich plasma (PRP) was transferred into a new plastic tube, supplemented with PGI<sub>2</sub> (final concentration of 1  $\mu$ M) and centrifuged at 900  $\times$  g for 10 min (room temperature, no braking). The platelet pellet was washed in HEPES buffer (20 mM HEPES, 140 mM NaCl and 1  $\mu$ M PGI<sub>2</sub>) by centrifugation for 10 min (800  $\times$  g, room temperature, no braking). To measure the total platelet-derived polyP, the cells were lysed with 1 mL of HEPES buffer supplemented with 1% NP40 (Sigma-Aldrich, St. Louis, USA), a 1:100 protease inhibitor cocktail (Thermo Fisher, Waltham, USA), and 1 mM sodium orthovanadate; they were then counted in a complete blood count (CBC) hematological analyzer (Shenzhen Mindry Bio-Medical Electronic Co., Shenzhen, China) and frozen at  $-80^{\circ}$ C. Before measurement, the samples were subjected to a triple freeze–thaw cycle and diluted to 3  $\times 10^8$  cells/mL. The total

protein concentration was measured with a Pierce™ BCA Protein Assay Kit (Thermo Fisher). Next, sulfuric acid (0.3 M) and sodium chloride (3.5 M) was added to the lysates in order to extract membrane-bound polyP. The mixtures were incubated for 30 min at 4°C, neutralized with 2 M NaOH, sonicated (60 s) and homogenized. To remove nucleic acids, the lysates were incubated with 50  $\mu$ g/mL Benzonase® (Sigma-Aldrich) in the presence of 3.5 mM manganese (II) chloride as an activator for 30 min at 37°C. Then, 750  $\mu$ g/mL of proteinase K (Sigma-Aldrich) was added to discard protein impurities (1 h incubation at 37°C). Subsequently, the samples were centrifuged for 10 min at 17,600  $\times$  g in a microcentrifuge and the supernatants were used in the next stages of the isolation procedure. After the addition of NaI (final concentration of 4.5 M) as a chaotropic agent, the mixtures were loaded onto silica spin columns (Qiagen, Hilden, Germany), washed twice with an elution buffer (with 50% ethanol) according to the manufacturer's protocol and the polyP was finally eluted with 10 mM Tris (pH 7.4). The phosphate polymers were hydrolyzed with 1 M HCl (1 h of incubation at 96°C).

The concentration of orthophosphate units was measured using a colorimetric phosphate assay kit (Abcam, Cambridge, UK). The assay involves a formulation of malachite green and ammonium molybdate which forms a chromogenic complex at a maximum absorption band of 650 nm. The polyP levels were expressed in nmol per  $10^8$  platelets.

## Statistical analysis

The statistical analysis was performed in STATISTICA v. 13.1 (StatSoft Poland, Kraków, Poland). The data is presented as means  $\pm$  standard deviation (SD) for normal distributions and as medians with interquartile ranges (IQR) in non-normal distributions. The normality of distribution and homogeneity of variance were checked with the Lilliefors test and Levene's test, respectively. In normally distributed data, multiple comparisons were performed with the analysis of variance (ANOVA) method followed by the least significant differences (LSD) post hoc test; in data without normal distribution, the Kruskal–Wallis test was followed by the Dunn test. Bonferroni adjustment was used for multiple comparisons with a resulting  $p < 0.01$  as the cut-off threshold for statistical significance.

## Results

In patients with ET, the platelet aggregation level was significantly higher than in those with thrombocytopenia or the controls (Table 1). We observed the highest mean polyP concentration in patients with thrombocytopenia (Fig. 1). The level of polyP did not correlate with platelet aggregation in either group. There was a weak, but significant negative correlation between polyP concentration and platelet count (Fig. 2). However, this was observed only in the total population, not in subgroups. Patients with thrombocytopenia differed significantly in age from the ET and control groups, but neither the level of aggregation or the concentration of polyP correlated with age.

## Discussion

Platelet-derived polyP has been proposed as an important player in the coagulation network at the level of FXII FV and fibrin clot formation.<sup>10,11</sup> Recent findings have yielded new insights into the undiscovered regulatory pathways of coagulation reactions and have created new therapeutic possibilities. In this study, we showed for the first time that platelet-derived polyP levels are significantly elevated in patients with a low platelet count in comparison to those with normal platelet counts or thrombocytosis. These patients also had the lowest levels of aggregation, but this result was not significantly different from the control subjects. We could not find any

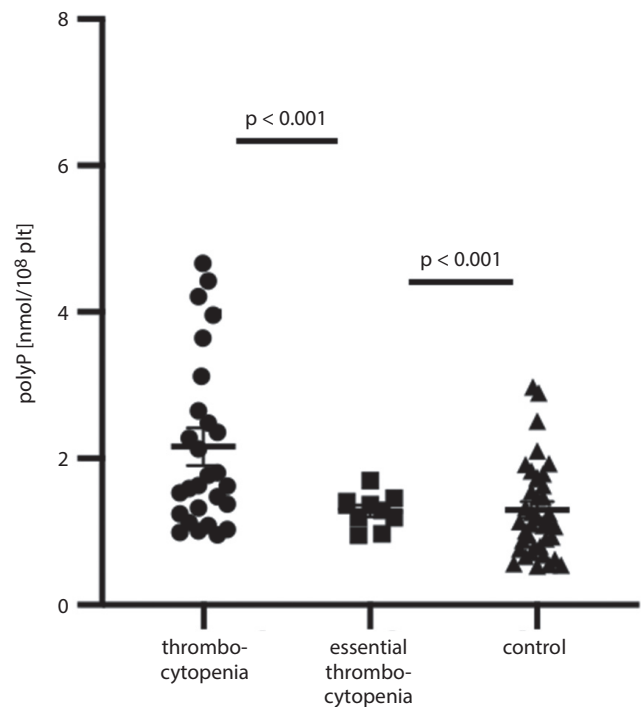


Fig. 1. Platelet-derived polyP level in patients with different platelet count

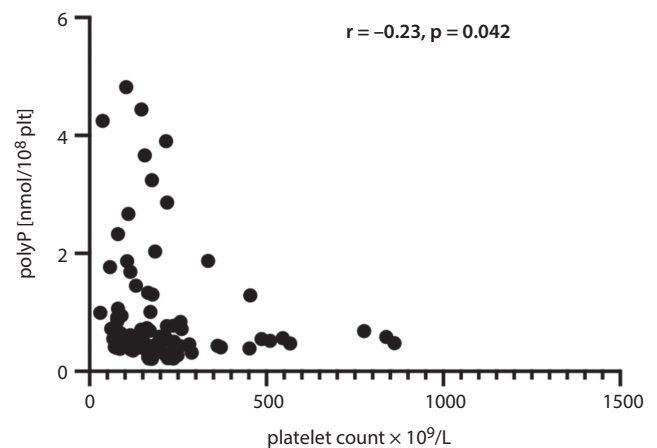


Fig. 2. Correlation plot of polyP concentration and platelet count

correlation between polyP concentration and aggregation level in the study groups, which may at first glance suggest that polyP does not directly influence the platelet aggregation pathway. This is in accordance with evidence provided by Whyte et al.<sup>12</sup> that polyP downregulates fibrinolysis by generating fibrin clots with a specific structure, which results in reduced binding of tPA and plasminogen to fibrin, as proposed previously.<sup>13</sup> The authors showed that the fibrin network formed in the presence of polyP was heterogeneous and more resistant to degradation by fibrinolytic proteases. Any changes to the structure or mechanical properties of a fibrin clot are not detectable using aggregometry. Among the study population, we observed the highest aggregation levels in patients with ET. Since it has been confirmed that thrombin formation is higher in thrombocytosis than in healthy subjects,<sup>14</sup>

this supports the hypothesis that platelet-derived polyP enhances coagulation by amplifying thrombin generation at different steps, e.g., by activating procoagulant factors and cofactors (e.g., FVa or FXIa) or by neutralizing anticoagulants (e.g., TFPI).<sup>15,16</sup> A growing body of data suggests that changes in lipid composition are necessary but not sufficient enough to account for platelet surface regulation of thrombin generation.<sup>17</sup> Our results add to the existing data which show a decrease in platelet polyP content in patients with dense granule storage pool disease.<sup>18</sup> In our study, platelets from thrombocytopenic patients had significantly elevated polyP content (Fig. 1).

There is still the question about the role of the higher polyP levels in thrombocytopenia. It could be regarded as a compensatory mechanism, where fewer platelets are more packed with polyP and can presumably exert to some extent its clot-forming action, like in patients with normal platelet counts. Interestingly, we observed a negative correlation between polyP concentration and platelet count, but only in the entire study population, which may somehow confirm this hypothesis (Fig. 2). It was previously demonstrated that when intracellular polyP gets released, it may induce responses through P2Y signaling; indeed, long-chain polyP induces thrombosis via FXII activation, but also leads to platelet activation and consumptive coagulopathy.<sup>5</sup> This polyP action could in turn explain why some patients with low platelet counts do not present with bleeding; however, that issue remains to be elucidated.<sup>19</sup> Importantly, in this study the subjects had a comparable mean platelet volume (MPV) between the groups, reflecting the average platelet size (Table 1). Since some forms of thrombocytopenia are characterized by abnormal platelet size, and patients with an elevated platelet volume may have less bleeding episodes than patients with the same platelet count of normal-sized platelets, we can exclude the influence of platelet size on both polyP concentration and aggregation. Recent advances in research on the mechanism of coagulation indicate that the role of platelet-derived polyP can be much more diverse, and this class of molecules appears to be a promising target in drug development.

## Study limitations

This is a preliminary study exploring new field of platelet pathophysiology. The small study population, especially in the ET group, resulted from our inclusion criteria, which made recruitment difficult. We looked for subjects who had not been treated with any concomitant antiplatelet drugs. Moreover, the age of the patients with thrombocytopenia was significantly different from the other study groups, so it cannot be excluded that the observed results are age-dependent. We are aware that the data presented herein are underpowered for drawing firm conclusions, and should be considered only as an idea to generate and foster future research.

## Conclusions

Platelet-derived polyP levels were elevated in patients with chronic primary thrombocytopenia in comparison with those with ET and healthy subjects. The polyP level did not correlate with platelet reactivity as measured with aggregation in any of the study groups. The increased levels of polyP observed in patients with low platelet counts may indicate the existence of a compensatory mechanism that prevents excessive bleeding in those patients. Our study provides evidence of an essential role of polyP in platelet function and the coagulation process.

## ORCID iDs

Ewa Żurawska-Plaksej  <https://orcid.org/0000-0001-8566-3943>  
 Wiktor Kuliczowski  <https://orcid.org/0000-0001-6284-0820>  
 Bożena Karolko  <https://orcid.org/0000-0001-6253-1817>  
 Magdalena Cielecka-Prynda  <https://orcid.org/0000-0003-3779-6658>  
 Jakub Dębski  <https://orcid.org/0000-0002-2944-0929>  
 Konrad Kaaz  <https://orcid.org/0000-0001-5227-0027>  
 Andrzej Mysiak  <https://orcid.org/0000-0002-4728-2565>  
 Tomasz Wróbel  <https://orcid.org/0000-0002-6612-3535>  
 Maria Podolak-Dawidziak  <https://orcid.org/0000-0003-3987-3100>  
 Lidia Usnarska-Zubkiewicz  <https://orcid.org/0000-0002-5893-1989>

## References

- Travers RJ, Smith SA, Morrissey JH. Polyphosphate, platelets, and coagulation. *Int J Lab Hematol*. 2015;37(1):31–35.
- Morrissey JH, Smith SA. Polyphosphate as modulator of hemostasis, thrombosis, and inflammation. *J Thromb Haemost*. 2015;13(Suppl 1):S92–S97.
- Mutch NJ. Polyphosphate as a haemostatic modulator. *Biochem Soc Trans*. 2016;44(1):18–24.
- Morrissey JH. Contributions of platelet polyphosphate to hemostasis and thrombosis. In: Saba HI, Roberts HR, eds. *Hemostasis and Thrombosis*. Oxford, UK: Wiley Blackwell UK; 2014:2360–2453.
- Mailer RKW, Hänel L, Allende M, Renné T. Polyphosphate as a target for interference with inflammation and thrombosis. *Front Med (Lausanne)*. 2019;6:1–10.
- Montilla M, Hernandez-Ruiz L, Garcia-Cozar FJ, Alvarez-Laderas I, Rodríguez-Martorell J, Ruiz FA. Polyphosphate binds to human von Willebrand factor in vivo and modulates its interaction with glycoprotein Ib. *J Thromb Haemost*. 2012;10(11):2315–2323.
- Nickel KF, Ronquist G, Langer F, et al. The polyphosphate-factor XII pathway drives coagulation in prostate cancer-associated thrombosis. *Blood*. 2015;126(11):1379–1389.
- Verhoef JJF, Barendrecht AD, Nickel KF, et al. Polyphosphate nanoparticles on the platelet surface trigger contact system activation. *Blood*. 2017;129(12):1707–1717.
- Schlagenhauf A, Pohl S, Haidl H, Leschnik B, Gallistl S, Muntean W. Non-enzymatic quantification of polyphosphate levels in platelet lysates and releasates. *J Pharm Biomed Anal*. 2016;131:1–5.
- Smith SA, Morrissey JH. Polyphosphate enhances fibrin clot structure. *Blood*. 2008;112(7):2810–2816.
- Mitchell JL, Lionikiene AS, Georgiev G, et al. Polyphosphate colocalizes with factor XII on platelet-bound fibrin and augments its plasminogen activator activity. *Blood*. 2016;128(24):2834–2845.
- Whyte CS, Chernysh IN, Domingues MM, et al. Polyphosphate delays fibrin polymerisation and alters the mechanical properties of the fibrin network. *Thromb Haemost*. 2016;116(5):897–903.
- Mutch NJ, Engel R, Uitte de Willige S, Philippou H, Ariëns RAS. Polyphosphate modifies the fibrin network and down-regulates fibrinolysis by attenuating binding of tPA and plasminogen to fibrin. *Blood*. 2010;115(19):3980–3988.
- Duchemin J, Ugo V, Ianotto J-C, Lecucq L, Mercier B, Abgrall J-F. Increased circulating procoagulant activity and thrombin generation in patients with myeloproliferative neoplasms. *Thromb Res*. 2010;126(3):238–242.

15. Choi SH, Smith SA, Morrissey JH. Polyphosphate is a cofactor for the activation of factor XI by thrombin. *Blood*. 2011;118(26):6963–6970.
16. Wood JP, Petersen HH, Yu B, Wu X, Hilden I, Mast AE. TFPIa interacts with FVa and FXa to inhibit prothrombinase during the initiation of coagulation. *Blood Adv*. 2017;1(27):2692–2702.
17. Monroe DM, Hoffman M, Robert HR. Platelets and thrombin generation. *Atherosc Thromb Vasc Biol*. 2002;22(9):1381–1389.
18. Hernández-Ruiz L, Sáez-Benito A, Pujol-Moix N, Rodríguez-Martorell J, Ruiz FA. Platelet inorganic polyphosphate decreases in patients with delta storage pool disease. *J Thromb Haemost*. 2009;7(2):361–363.
19. Melazzini F, Zaninetti C, Balduini CL. Bleeding is not the main clinical issue in many patients with inherited thrombocytopaenias. *Haemophilia*. 2017;23(5):673–681.

# Enzyme activity and genetic polymorphisms in patients with type II diabetes mellitus

Abdullah Arpacı<sup>1,A–F</sup>, Serap Yalın<sup>2,C</sup>, Hasret Ecevit<sup>3,D–F</sup>, Ulku Comelekoglu<sup>4,A,E</sup>, Turkan Mete<sup>5,A,B</sup>

<sup>1</sup> Department of Biochemistry, Medical Faculty, Hatay Mustafa Kemal University, Turkey

<sup>2</sup> Department of Biochemistry, Pharmacy Faculty, Mersin University, Turkey

<sup>3</sup> Department of Medical Biology, Medical Faculty, Hatay Mustafa Kemal University, Turkey

<sup>4</sup> Department of Biophysics, Medical Faculty, Mersin University, Turkey

<sup>5</sup> Department of Gastroenterology, Samsun Training and Research Hospital, Turkey

A – research concept and design; B – collection and/or assembly of data; C – data analysis and interpretation;

D – writing the article; E – critical revision of the article; F – final approval of the article

Advances in Clinical and Experimental Medicine, ISSN 1899–5276 (print), ISSN 2451–2680 (online)

*Adv Clin Exp Med.* 2020;29(9):1057–1063

## Address for correspondence

Abdullah Arpacı

E-mail: arpacı57@gmail.com

## Funding sources

This study was supported with a grant from Scientific Research Projects Commission of Adiyaman University, Turkey (grant No. TIPFBAP 2010/0001).

## Conflict of interest

None declared

Received on March 18, 2020

Reviewed on May 19, 2020

Accepted on July 14, 2020

Published online on September 14, 2020

## Abstract

**Background.** Diabetes mellitus (DM) has become more and more common and has a high morbidity and mortality rate worldwide. It is a multifactorial chronic disease affected by both genetic and environmental factors.

**Objectives.** To evaluate the association between antioxidant enzyme activities and their genetic variations and the level of malondialdehyde (MDA) in type II diabetes patients living in the Adiyaman province in the southeast part of Turkey.

**Material and methods.** One hundred patients diagnosed with type II DM (T2DM) and 100 healthy controls were included in the study. Malondialdehyde levels and antioxidant enzyme activities were measured spectrophotometrically. DNA isolation was performed and genotyping was carried out using polymerase chain reaction–restriction fragment length polymorphism (PCR–RFLP).

**Results.** Our results revealed no significant differences in genotype distributions and allele frequencies of all polymorphisms between groups ( $p > 0.05$ ). Significantly elevated MDA levels and a significant reduction in catalase (CAT) and paraoxonase (PON) enzyme activities were observed in patients compared to the control group in terms of study groups and genetic variations ( $p < 0.05$ ). Moreover, CAT activity was reduced in TT genotype in terms of CAT –262 C/T polymorphism in patients ( $p < 0.05$ ). Paraoxonase activity was observed to be lower in MM genotype in both groups ( $p < 0.05$ ).

**Conclusions.** CAT –262 C/T polymorphism may be one of the factors that lead to severe clinical situation in DM. Our results suggest that TT genotype may be more prone to lipid peroxidation.

**Key words:** diabetes mellitus, oxidative stress, cat, malondialdehyde, paraoxonase

## Cite as

Arpacı A, Yalın S, Ecevit H, Comelekoglu U, Mete T. Enzyme activity and genetic polymorphisms in patients with type II diabetes mellitus. *Adv Clin Exp Med.* 2020;29(9):1057–1063. doi:10.17219/acem/125397

## DOI

10.17219/acem/125397

## Copyright

© 2020 by Wrocław Medical University

This is an article distributed under the terms of the Creative Commons Attribution 3.0 Unported (CC BY 3.0) (<https://creativecommons.org/licenses/by/3.0/>)

## Introduction

Diabetes mellitus (DM) has become more and more common and has a high morbidity and mortality rate worldwide. It is a multifactorial chronic disease affected by both genetic and environmental factors.<sup>1,2</sup> Type II DM (T2DM) account for 90% of the DM cases. The reduction of insulin secretion or development of insulin resistance results in the impairment of macromolecule metabolisms, such as proteins, carbohydrates and lipids.<sup>3,4</sup> The pharmaceutical development of insulin revolutionized the treatment of DM, but T2DM is still the most common disease globally with chronic complications.<sup>4,5</sup>

The complications of DM can be expressed with 4 major mechanisms, including the production of reactive oxygen species (ROS), which is triggered by hyperglycemia, polyol pathway, the formation of advanced glycosylation end products (AGE), activation of protein kinase C, and hexamine pathway.<sup>6</sup> Several factors, such as environmental factors, genetic risk factors, obesity, and oxidative stress, may all be associated with the development of T2DM. The oxidant/antioxidant balance in the organism shifts towards oxidation with a potential which results in the development of organopathies, such as cardiomyopathies, neuropathies and retinopathies.<sup>6,7</sup> The excessive level of free radicals and ROS may result in several cellular injuries. In such cases, the antioxidant system may be insufficient to defend the cell against free-radical structures. The major components of the antioxidant system are enzymatic antioxidants, such as superoxide dismutase (SOD), catalase (CAT), paraoxonase 1 (PON1), and glutathione peroxidase (GPx).<sup>7,8</sup>

Our study aims to examine the association between CAT -262 cysteine (C)/threonine (T) and PON1 55 leucine (L)/methionine (M) genetic polymorphisms, CAT and PON1 antioxidant enzyme activities, and the level of oxidative damage marker malondialdehyde (MDA) in T2DM.

## Material and methods

### Sample collection

This study included a total of 200 individuals consisting of 100 healthy controls without any disorders (including DM) in their medical histories and 100 patients diagnosed with T2DM who were admitted to the Internal Clinic at Adiyaman University Training and Research Hospital, Turkey. The confirmation by Adiyaman University Ethic Committee (approval No. 2011/02-1) and a written consent from each subject have been provided after participants were properly informed. All experiments were performed according to the Declaration of Helsinki.

## Biochemical analyzes

Fasting venous blood samples were collected into EDTA tubes and centrifuged at 3000 rpm for 10 min. After centrifugation, the plasma portion was separated and stored at  $-20^{\circ}\text{C}$  until the analyses were performed. The enzymatic activities of CAT and PON1, and the level of MDA, the end product of lipid peroxidation, as an indicator of oxidative stress, were measured. Malondialdehyde forms a pink colored complex as a result of its incubation with thiobarbituric acid at a pH of 3.5 and  $95^{\circ}\text{C}$  in aerobic conditions. Based on this principle, the amount of MDA was determined with spectrophotometric measurement of this complex at 532 nm.<sup>9</sup> The CAT enzyme activity was determined using spectrophotometric measurement of the substrate molecule hydrogen peroxide ( $\text{H}_2\text{O}_2$ ) absorbance; it decreased over time as a result of its interaction with catalase at 240 nm.<sup>10</sup>

The PON1 activity was determined in alignment with the technique developed by Eckerson et al., which is based on monitoring the production of p-nitrophenol by the enzymatic hydrolysis of PON1 at 412 nm. A 100 mM Tris-HCl at pH 8, containing 2 mM  $\text{CaCl}_2$  and 4 mM paraoxon was used as a buffer to measure its activity.<sup>11</sup>

## Molecular analyses

For the molecular analysis, leukocytes were separated from whole blood samples and DNA isolation was performed according to the method described by Poncz et al.<sup>12</sup> Genotype determination was carried out using the polymerase chain reaction-restriction fragment length polymorphism (PCR-RFLP) technique.

The most commonly studied PON1 55 L/M polymorphism was determined using the PCR-RFLP method. The PCR amplification samples were digested with *Nla* III restriction endonuclease. Digestion products were separated on 2% agarose gel and visualized with ultraviolet light after ethidium bromide staining. Alleles of leucine and methionine for the PON1 55 position were assigned based on the presence of a 172 bp (undigested) fragment and 106 bp and 66 bp (digested) fragments, respectively.<sup>13,14</sup> CAT -262 C/T polymorphism was similarly determined using PCR-RFLP method. The PCR amplification samples were digested with *Sma*I restriction endonuclease. Then, the digested products were separated on an agarose gel and visualized with ultraviolet light after ethidium bromide staining. The alleles of CAT -262 C/T polymorphism, threonine and cysteine were assigned based on the presence of a 340 bp (undigested) fragment and 185 bp and 155 bp (digested) fragments, respectively.<sup>15</sup>

The statistical analyses were performed using MedCalc v. 12.3 software (MedCalc, Ostend, Belgium). The Shapiro-Wilk test was used to determine whether all parameters were normally distributed. Abnormally distributed data are presented as median (min-max) and

mean ± standard deviation (SD), and group comparisons were conducted using the Mann–Whitney U test. The  $\chi^2$  and Fisher’s tests were used to evaluate the differences between the groups in terms of the genotype distribution and allele frequencies. Statistical significance for all analyses was set at a p-value <0.05.

## Results

### Biochemical analysis

In the current study, descriptive statistic data of biochemical analyses of study groups were given in Table 1. Malondialdehyde levels were found to be significantly higher in the diabetic group compared to the control (p < 0.0001). A significant reduction in plasma CAT and PON1 enzyme activities was observed in the diabetic group (p < 0.0001). Descriptive statistic data of biochemical analyses were displayed in Table 2.

### Molecular analysis

There was no statistically significant difference between the diabetic and control groups with respect to genetic distribution and allele frequencies of CAT -262 C/T and PON1 55 L/M polymorphisms (p > 0.05). The genotype distributions and allele frequencies of the CAT -262 C/T and PON1 55 L/M polymorphisms between diabetic and control groups were displayed in Table 3.

In PON1 55 L/M polymorphism, the activity of the PON1 enzyme was lower for carriers of the MM allele, both in diabetic and control group compared to LL and LM genotypes (p = 0.0001) (Table 4A). In all genotypes, the MDA

Table 1. Descriptive statistic data of biochemical analyses

Parameter	T2DM group mean ±SD	Control group mean ±SD	p-value
HbA1c [%]	8.92 ±2.56	–	–
Insulin [mLU/L]	10.65 ±15.16	–	–
FBG [mmol/L]	10.95 ±5.62	5.15 ±0.40	<0.0001***
CHO [mg/dL]	208.6 ±45.95	180.2 ±41.79	0.0003***
TG [mg/dL]	185.1 ±108.8	115.9 ±63.25	<0.0001***
HDL-CHO [mg/dL]	40.36 ±9.7	42.59 ±10.46	0.236
LDL-CHO [ng/dL]	131.5 ±34.92	113.9 ±33.75	0.0038**
Age	56.75 ±10.86	36.65 ±14.67	<0.0001***
HOMA-IR	5.91 ±11.55	–	–
HOMA-β	36.14 ±33.82	–	–

Mann–Whitney U test; \*p < 0.05; \*\*p < 0.01; \*\*\* p < 0.001; T2DM – type 2 diabetes mellitus; HbA1c – glyated hemoglobin; FBG – fasting blood glucose; CHO – cholesterol; TG – triglycerides; HDL-CHO – high-density lipoprotein cholesterol; LDL-CHO – low-density lipoprotein cholesterol; HOMA-IR – homeostatic model assessment for insulin resistance; HOMA-β – homeostatic model assessment for β-cell function.

Table 2. Descriptive statistic data of biochemical analyses

Variable	T2DM group (n = 100)	Control group (n = 100)	p-value
	median (min–max)	median (min–max)	
MDA [nmol/L]	13.56 (4.25–43.31)	7.06 (1.36–10.76)	0.0001***
CAT [U/L]	19.50 (6.03–54.91)	47.16 (9.87–89.25)	0.0001***
PON [U/L]	21.42 (3.05–39.28)	43.35 (13.47–98.14)	0.0001***

Mann–Whitney U test; \*p < 0.05; \*\*p < 0.01; \*\*\* p < 0.001; T2DM – type 2 diabetes mellitus; MDA – malondialdehyde; CAT – catalase; PON – para-oxonase.

Table 3. The genotype distributions and allele frequencies of the CAT -262 C/T and PON55 L/M polymorphisms between diabetic patients and control group

Genotype	Control group (n = 100)		T2DM group (n = 100)		$\chi^2$ test p-value	Interval OR (95% CI)	OR p-value
	n	%	n	%			
CAT							
TT	35	35	29	29	0.522	1	reference
CT	52	52	60	60		1.393 (0.75–2.58)	0.292
CC	13	13	11	11		1.021 (0.39–2.62)	0.965
Allele frequency					0.904		
T	122	61	118	59		–	–
C	78	39	82	41	1.087 (0.73–1.62)	0.683	
PON55							
LL	50	50	47	47	0.878	–	–
LM	38	38	39	39		1.092 (0.60–1.99)	0.774
MM	12	12	14	14		1.241 (0.52–2.96)	0.626
Allele frequency					0.669		
L	138	69	133	66.5		–	–
M	62	31	67	33.5	1.212 (0.74–1.71)	0.593	

$\chi^2$  test; \*p < 0.05; \*\*p < 0.01; \*\*\* p < 0.001; T2DM – type 2 diabetes mellitus; CAT – catalase; OR – odds ratio; 95% CI – 95% confidence interval.

**Table 4.** Genotype comparison in terms of PON 55 L/M polymorphism (A) and CAT -262 C/T polymorphism (B)

Parameters	A. PON 55 L/M polymorphism			B. CAT -262 C/T polymorphism		
	genotype	T2DM group (n = 100)	control group (n = 100)	genotype	T2DM group (n = 100)	control group (n = 100)
		p-value	p-value		p-value	p-value
MDA [nmol/L]	LL-LM	0.122	0.736	CC-CT	0.962	0.780
	LL-MM	0.204	0.428	CC-TT	0.743	0.702
	LM-MM	0.944	0.407	CT-TT	0.602	0.931
CAT [U/L]	LL-LM	0.609	0.950	CC-CT	0.259	0.857
	LL-MM	0.237	1.000	CC-TT	0.492	0.618
	LM-MM	0.408	1.000	CT-TT	0.017*	0.348
PON [U/L]	LL-LM	0.184	0.646	CC-CT	0.195	0.522
	LL-MM	0.0001***	0.0001***	CC-TT	0.116	0.359
	LM-MM	0.0001***	0.0001***	CT-TT	0.546	0.634

Mann-Whitney U test; \* $p < 0.05$ ; \*\* $p < 0.01$ ; \*\*\* $p < 0.001$ ; T2DM – type 2 diabetes mellitus; MDA – malondialdehyde; CAT – catalase; PON – paraoxonase.

level was observed to be significantly higher ( $p = 0.0001$  for LL and LM genotypes,  $p = 0.002$  for MM genotype, respectively), while CAT ( $p = 0.0001$  for LL and LM genotypes,  $p = 0.001$  for MM genotype, respectively) and PON1 ( $p = 0.0001$  for all genotypes) enzyme activities were observed to be significantly lower in patient group compared to control (Fig. 1).

No significant differences were observed regarding CAT -262 C/T polymorphism between genotypes in the control group ( $p > 0.05$ ). However, CAT activity was seen to be significantly lower in TT genotype compared to CT genotype in the T2DM group ( $p = 0.017$ ) (Table 4B). Moreover, in all genotypes, MDA level was observed to be significantly higher ( $p = 0.001$  for CC genotype,  $p = 0.0001$  for CT and TT genotypes, respectively), whereas CAT ( $p = 0.004$  for CC genotype,  $p = 0.0001$  for CT and TT genotypes, respectively) and PON1 ( $p = 0.001$  for CC genotype,  $p = 0.0001$  for CT and TT genotypes, respectively) enzyme activities were observed to be significantly lower in the T2DM compared to the control group (Fig. 2).

## Discussion

Diabetes mellitus has a very high incidence of 10.9% in countries of the Middle East and North Africa, including Turkey as well. The incidence in Turkey is reported to be 14.85% and it constitutes a major health problem.<sup>16</sup> According to the report by International Diabetes Federation (IDF) from 2015, there are 415 million diabetic patients in the world and it is estimated that this figure will reach 642 million in 2040.<sup>17</sup> Diabetes is an oxidative stress state, in which free radicals are increased and/or antioxidant mechanisms are inhibited. The production of free radicals increases as a result of protein glycation and glucose autoxidation.<sup>6</sup> Oxidative stress causes bodily complications such as nephropathy, cardiovascular diseases and neuropathy, all of which decrease the quality of life.<sup>9</sup>

Although the genetic predisposition is recognized in DM, the information on the specific genetic defects is limited.<sup>6</sup> Therefore, we aimed to examine the oxidative stress state in T2DM by evaluating antioxidant enzyme activities and its association with their polymorphisms in our geographical region. There are 2 reasons why we carry out our study in the southeast region of our country. The population living in this region does not have the habit of eating a Mediterranean type diet and has of a different ethnic structure compared to some other regions of our country.

Malondialdehyde has been studied as a lipid oxidation indicator. We have found significantly high levels of MDA in diabetic patients compared to the control group, similarly to the previous studies, confirming the presence of severe oxidative stress in our patients.<sup>18,19</sup> Likewise, the enzyme activities of CAT and PON1 were found to be significantly reduced in diabetic patients compared to the control group. Our enzymatic activity results are consistent with most recent studies.<sup>20,21</sup> Unlike our study, Sozmen et al. and Memisogullari et al. reported increased CAT enzyme activity in diabetic patients.<sup>22,23</sup> The impact of environmental factors (climate, air pollution, nutrition, lifestyle, etc.) and genetic background on DM development is indisputable. For example, Sozmen et al. carried out their study in a different region of Turkey in terms of eating habits (where the Mediterranean-type eating habit is preferred) and ethnicity, compared to our study (Adiyaman region). This may be the reason for the different results we have achieved regarding CAT enzyme activity. Therefore, the role of antioxidant defense mechanism in diabetic patients is controversial and requires further research, in which genetic background may be at least partly elucidated. Our study results may suggest that oxidative stress has developed in our patients and the antioxidant mechanism has become insufficient.

The issue of the effect of antioxidant enzyme polymorphisms on DM is unclear and controversial. Flekac et al. studied genetic polymorphisms of SOD and CAT

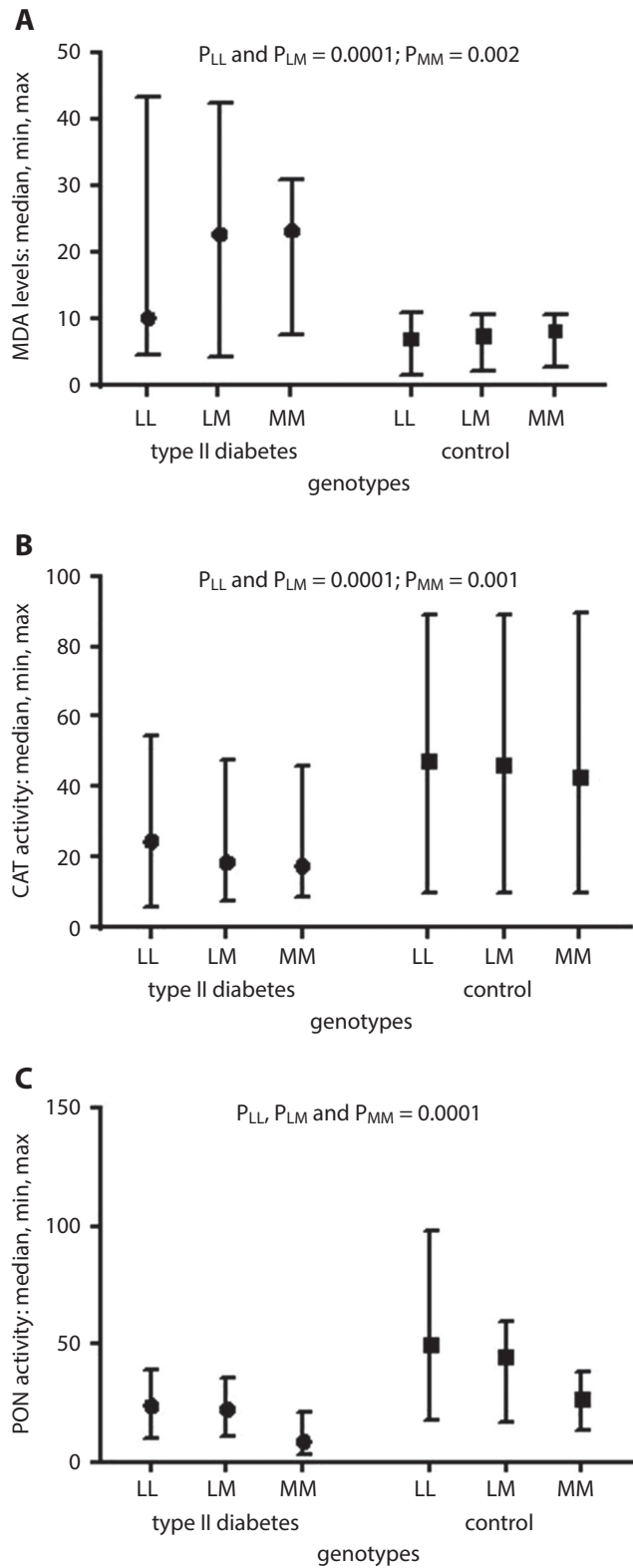


Fig. 1. PON 55 L/M polymorphism genotype comparison in terms of MDA level (A), and CAT (B), PON (C) enzyme activities between controls (circle) and patients (square) with T2DM

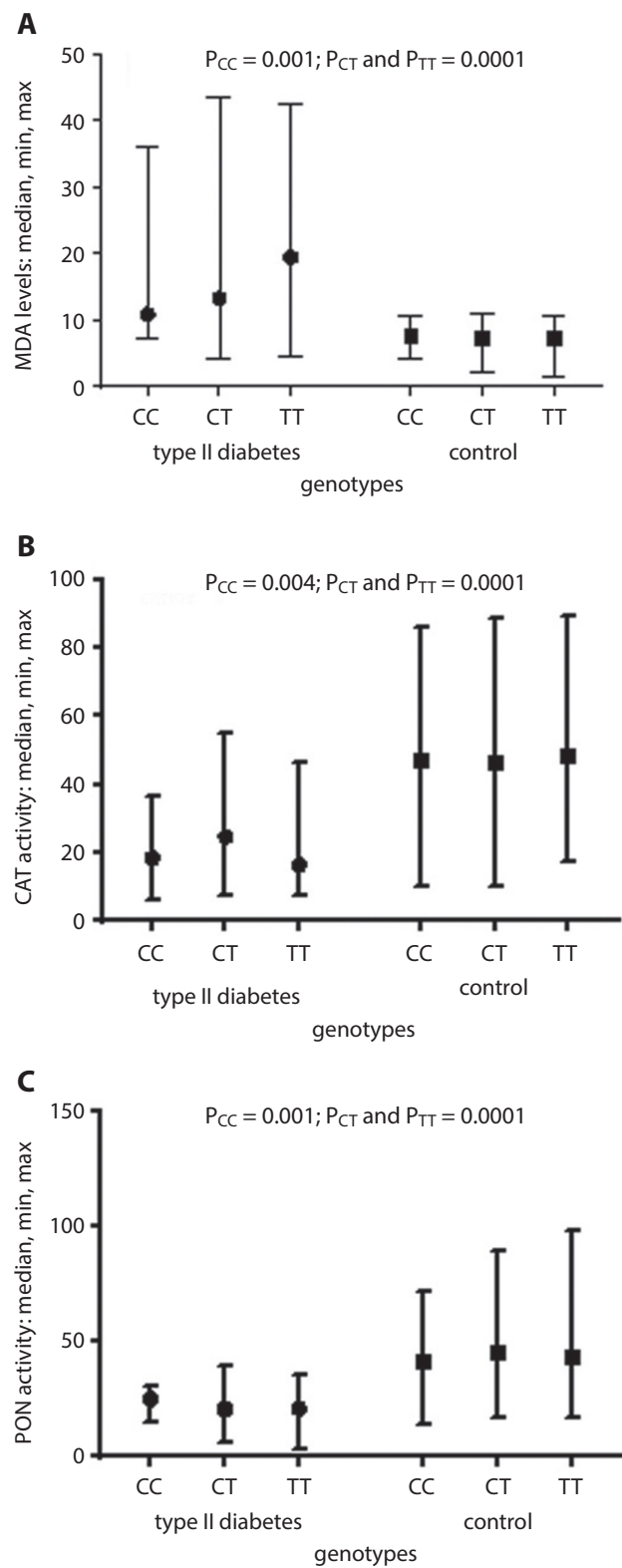


Fig. 2. CAT -262 C/T polymorphism genotype comparison in terms of MDA level (A) and CAT (B), PON (C) enzyme activities between controls (circle) and patients (square) with T2DM

in patients with DM, concluding that the superoxide dismutase (SOD) activity was higher in the CC and AA genotypes compared to the TT and CC genotypes of SOD Ala-9Val and SOD +35 A/C polymorphisms, respectively

( $p < 0.05$ ). Moreover, they found significant differences regarding allele frequencies of SOD Ala-9Val polymorphism between control and diabetic groups. T allele expression level was observed to be significantly higher, whereas

C allele expression was significantly lower in the diabetic group compared to the control ( $p < 0.05$ ). However, they did not observe any association with CAT polymorphism.<sup>24</sup> Kasznicki et al. did not observe any significant change in CAT and SOD enzyme activities between T2DM patients and controls as well as any association between their polymorphisms (CAT -262 C/T and SOD +35 A/C) and activity of these polymorphisms.<sup>20</sup> In our study, CAT activity was found to be significantly lower in TT genotype, which is in line with previous study performed by Flekac et al. compared to CT genotype in diabetic group, which suggests a significant association. CAT -262 C/T polymorphism may be at least partly responsible for the reduction of CAT enzyme activity which mediates oxidative stress state and leads to severe clinic situation in DM (secondary effect of DM developing over time such as frequent urination, fatigue, tiredness, blurred vision, frequent infections, itching and dryness of the skin, loss of weight, micro- and macrovascular damage which reduce quality of life over time). Moreover, in all genotypes of all polymorphisms examined in our study, CAT activity was observed to be significantly lower in the diabetic group when compared to the control. Any significant difference was not observed in terms of genetic distribution and allele frequencies of CAT -262 C/T between the diabetic and the control group. Tarnai et al. observed an elevation in the catalase enzyme activity in CT+TT genotype of C111T polymorphism in patients with T2DM.<sup>25</sup> Therefore, the relation between DM and polymorphisms of CAT and SOD is considered controversial because of previous studies with different results. There are studies in which the relationship between polymorphisms and enzyme activity has been shown,<sup>25,26</sup> as well as studies in which such relationship was not found.<sup>27,28</sup>

Gupta et al. studied serum PON1 activity and its different polymorphisms in T2DM patients in an ethnic population in northwestern India. They found significant reductions in the enzyme activity compared to the control group, similarly to our findings. Moreover, PON enzyme activity was reported to be significantly lower in all genotypes of diabetic patients compared to control group in terms of both PON1 192 Q/R and PON1 55 L/M polymorphisms. In addition, the enzyme activity was found to be highest in the RR genotype, whereas it was the lowest in the QQ genotype in both diabetic patients and controls.<sup>29</sup> Gupta et al. observed a higher enzyme activity in LL genotype compared to the LM genotype in the control group. However, they did not find a significant difference in the diabetic group.<sup>29</sup> Altuner et al. studied PON1 polymorphisms in the middle geographical region of Turkey (in Ankara). They reported reduced activities of PON1 in QQ and QR genotypes compared to RR genotype in terms of PON1 192 Q/R polymorphism both in control and diabetic groups. Similarly, they reported higher PON1 enzyme activity in LL genotype compared to MM in terms of PON1 55 L/M polymorphism in both diabetic and control groups, which

is in line with our results. They did not report any significant difference between the control and diabetic groups in terms of genotype distributions and allele frequencies.<sup>30</sup>

In our study, PON1 enzyme activity was observed to be lower in MM genotype compared to LL genotype in terms of PON1 55 L/M polymorphism in both the T2DM and the control groups, which was in line with a previous study carried out in Turkey by Altuner et al.<sup>30</sup> In addition, we observed significantly lower PON1 enzyme activity in all genotypes in the T2DM group compared to the controls, which was in line a study performed by Gupta et al., whereas Altuner et al. did not report any significant difference between the groups in terms of genotype distributions and allele frequencies.<sup>29,30</sup> As can be seen, there are similarities and differences between our study results and previous studies. This can be explained by the fact that different studies were performed in regions with different environmental conditions (climate, air pollution, nutrition, lifestyle, etc.) and in study populations with different genetic backgrounds and ethnicities. However, when the current studies are evaluated, PON1 55 L/M polymorphism does not seem to have a significant effect on the development of T2DM.

## Conclusions

In this study, we concluded that there was a significant state of oxidative stress in diabetic patients. In addition, CAT enzyme activity was observed to be lower in TT genotype within the diabetic group, which suggests an association between CAT -262 C/T polymorphism and T2DM. Therefore, genetic testing in T2DM may be useful in the future to determine the relationship between genetic and environmental factors in development of the disease and its complications as well as the genetic predisposition, which requires further studies to confirm.

## ORCID iDs

Abdullah Arpaci  <https://orcid.org/0000-0002-6077-8258>  
 Serap Yalin  <https://orcid.org/0000-0002-1286-2172>  
 Hasret Ecevit  <https://orcid.org/0000-0002-4444-475X>  
 Ulku Comelekoglu  <https://orcid.org/0000-0001-8060-6333>  
 Turkan Mete  <https://orcid.org/0000-0002-4159-1965>

## References

1. Gray SP, Jandeleit-Dahm K. The pathobiology of diabetic vascular complications: Cardiovascular and kidney disease. *J Mol Med (Berl)*. 2014;92(5):441–452.
2. Banerjee M, Vats P. Reactive metabolites and antioxidant gene polymorphisms in Type 2 diabetes mellitus. *Redox Biol*. 2014;2:170–177.
3. Ahmed FN, Naqvi FN, Shafiq F. Lipid peroxidation and serum antioxidant enzymes in patients with type 2 diabetes mellitus. *Ann NY Acad Sci*. 2006;1084:481–489.
4. International Diabetes Federation. International Diabetes Federation Diabetes Atlas. 8<sup>th</sup> ed. International Diabetes Federation; 2017. <https://www.idf.org/e-library/epidemiology-research/diabetes-atlas/134-idf-diabetes-atlas-8th-edition.html>. Chapter 1:18.
5. Bednarek E, Sitkowski J, Bocian W, et al. Structure and pharmaceutical formulation development of a new long-acting recombinant human insulin analog studied by NMR and MS. *J Pharm Biomed Anal*. 2017;135:126–132.

6. Tabatabaei-Malazy O, Khodaeian M, Bitarafan F, Larijani B, Amoli MM. Polymorphisms of antioxidant genes as a target for diabetes management. *Int J Mol Cell Med*. 2017;6(3):135–147.
7. Van Dam PS, Van Asbeck BS, Erkelens DW, Marx JJ, Gispen WH, Bravenboer B. The role of oxidative stress in neuropathy and other diabetic complications. *Diabetes Metab Rev*. 1995;11(3):181–192.
8. Bullon P, Newman HN, Battino M. Obesity, diabetes mellitus, atherosclerosis and chronic periodontitis: A shared pathology via oxidative stress and mitochondrial dysfunction? *Periodontol 2000*. 2014;64(1):139–153.
9. Yagi K. Simple procedure for specific assay of lipid hydroperoxides in serum or plasma. *Methods Mol Biol*. 1998;108:107–110.
10. Aebi H. Catalase in vitro. *Methods Enzymol*. 1984;105:121–126.
11. Eckerson HW, Wyte CM, La Du BN. The human serum paraoxonase/arylesterase polymorphism. *Am J Hum Genet*. 1983;35(6):1126–1138.
12. Poncz M, Solowiejczyk D, Harpel B, Mory Y, Schwartz E, Surrey S. Construction of human gene libraries from small amounts of peripheral blood: Analysis of beta-like globin genes. *Hemoglobin*. 1982;6(1):27–36.
13. Lakshmy R, Ahmad D, Abraham RA, et al. Paraoxonase gene Q192R & L55M polymorphisms in Indians with acute myocardial infarction & association with oxidized low density lipoprotein. *Indian J Med Res*. 2010;131:522–529.
14. Humbert R, Adler DA, Disteche CM, Hassett C, Omiecinski CJ, Furlong CE. The molecular basis of the human serum paraoxonase activity polymorphism. *Nat Genet*. 1993;3(1):73–76.
15. Goulas A, Fidani L, Kotsis A, et al. An association study of a functional catalase gene polymorphism, -262C→T, and patients with Alzheimer's disease. *Neurosci Lett*. 2002;330(2):210–213.
16. Kharroubi AT, Darwish HM. Diabetes mellitus: The epidemic of the century. *World J Diabetes*. 2015;6(6):850–867.
17. Ogurtsova K, da Rocha Fernandes JD, Huang Y, et al. IDF Diabetes Atlas: Global estimates for the prevalence of diabetes for 2015 and 2040. *Diabetes Res Clin Pract*. 2017;128:40–50.
18. Banerjee J, Mishra N, Damle G, et al. Beyond LDL-c: The importance of serum oxidized LDL in predicting risk for type 2 diabetes in the middle-aged Asian Indians. *Diabetes Metab Syndr*. 2019;13(1):206–213.
19. Ghazizadeh Z, Khaloo P, Alemi H, et al. Definition of an oxidative stress status by combined assessment of malondialdehyde and oxidized-LDL: A study in patients with type 2 diabetes and control. *Meta Gene*. 2019;19:91–97.
20. Kasznicki J, Sliwinska A, Kosmalski M, et al. Genetic polymorphisms (Pro197Leu of Gpx1, +35A/C of SOD1, -262C/T of CAT), the level of antioxidant proteins (GPx1, SOD1, CAT) and the risk of distal symmetric polyneuropathy in Polish patients with type 2 diabetes mellitus. *Adv Med Sci*. 2016;61(1):123–129.
21. Tartan Z, Orhan G, Kasikcioglu H, et al. The role of paraoxonase (PON) enzyme in the extent and severity of the coronary artery disease in type-2 diabetic patients. *Heart Vessels*. 2007;22(3):158–164.
22. Sozmen EY, Sozmen B, Delen Y, Onat T. Catalase/superoxide dismutase (SOD) and catalase/paraoxonase (PON) ratios may implicate poor glycemic control. *Arch Med Res*. 2001;32(4):283–287.
23. Memisogullari R, Taysi S, Bakan E, Capoglu I. Antioxidant status and lipid peroxidation in type II diabetes mellitus. *Cell Biochem Funct*. 2003;21(3):291–296.
24. Flekac M, Skrha J, Hilgertova J, Lacinova Z, Jarolimkova M. Gene polymorphisms of superoxide dismutases and catalase in diabetes mellitus. *BMC Med Genet*. 2008;9:30.
25. Tarnai I, Csordas M, Sukei E, Shemirani AH, Káplár M, Góth L. Effect of C111T polymorphism in exon 9 of the catalase gene on blood catalase activity in different types of diabetes mellitus. *Free Radic Res*. 2007;41(7):806–811.
26. Houldsworth A, Hodgkinson A, Demaine A, et al. Catalase polymorphism may influence the pathogenesis of diabetes mellitus. *J Endocrinol Diabetes*. 2016;3(6):1–7.
27. dos Santos KG, Canani LH, Gross JL, et al. The catalase -262C/T promoter polymorphism and diabetic complications in Caucasians with type 2 diabetes. *Dis Markers*. 2006;22(5–6):355–359.
28. Pask R, Cooper JD, Walker NM, et al. No evidence for a major effect of two common polymorphisms of the catalase gene in type 1 diabetes susceptibility. *Diabetes Metab Res Rev*. 2006;22(5):356–360.
29. Gupta N, Binukumar BK, Singh S, et al. Serum paraoxonase-1 (PON1) activities (PONase/AREase) and polymorphisms in patients with type 2 diabetes mellitus in a North-West Indian population. *Gene*. 2011;487(1):88–95.
30. Altuner D, Ates I, Suzen SH, Koc GV, Aral Y, Karakaya A. The relationship of PON1 QR 192 and LM 55 polymorphisms with serum paraoxonase activities of Turkish diabetic patients. *Toxicol Ind Health*. 2011;27(10):873–878.



# The pattern of overnight changes in novel markers of acute kidney injury in patients with obstructive sleep apnea

Michał Nowicki<sup>1,A–F</sup>, Anna Zawiasa-Bryszewska<sup>1,A–D</sup>, Małgorzata Taczykowska<sup>1,B</sup>, Piotr Białasiewicz<sup>2,A–C,E</sup>, Dariusz Nowak<sup>2,A,C,E,F</sup>

<sup>1</sup> Department of Nephrology, Hypertension and Kidney Transplantation, Medical University of Lodz, Poland

<sup>2</sup> Chair of Physiology, Medical University of Lodz, Poland

A – research concept and design; B – collection and/or assembly of data; C – data analysis and interpretation;

D – writing the article; E – critical revision of the article; F – final approval of the article

Advances in Clinical and Experimental Medicine, ISSN 1899–5276 (print), ISSN 2451–2680 (online)

*Adv Clin Exp Med.* 2020;29(9):1065–1072

## Address for correspondence

Michał Nowicki

E-mail: nefro@wp.pl

## Funding sources

The study was funded with a research grant No. N N402 5593 40 from the National Science Centre in Poland.

## Conflict of interest

None declared

## Acknowledgements

The study has been registered in the National Library of Medicine (NLM) ClinicalTrials.gov database (identifier NCT00947479).

Received on May 17, 2019

Reviewed on August 24, 2019

Accepted on June 2, 2020

Published online on September 7, 2020

## Cite as

Nowicki M, Zawiasa-Bryszewska A, Taczykowska M, Białasiewicz P, Nowak D. The pattern of overnight changes in novel markers of acute kidney injury in patients with obstructive sleep apnea. *Adv Clin Exp Med.* 2020;29(9):1065–1072. doi:10.17219/acem/123356

## DOI

10.17219/acem/123356

## Copyright

© 2020 by Wrocław Medical University

This is an article distributed under the terms of the Creative Commons Attribution 3.0 Unported (CC BY 3.0) (<https://creativecommons.org/licenses/by/3.0/>)

## Abstract

**Background.** Obstructive sleep apnea (OSA) may predispose patients to acute kidney injury (AKI) and chronic kidney disease (CKD).

**Objectives.** We postulated that apneic episodes during sleep in patients with OSA may result in episodes of subclinical AKI that may be detected by the use of novel sensitive serum and urine markers. The treatment of OSA may protect against renal injury.

**Material and methods.** The study involved 86 men who had positive screening test results for OSA and estimated glomerular filtration rates (eGFR) calculated with the Chronic Kidney Disease Epidemiology Collaboration (CKD-EPI) equation  $>60$  mL/min/1.73 m<sup>2</sup>. All the patients underwent overnight polysomnography (the diagnostic night). The patients were divided into 2 groups: 45 patients with mild OSA and 41 patients with moderate-to-severe OSA. Those in the latter group were qualified for 6–8 weeks of continuous positive airway pressure (CPAP) treatment. Blood pressure, serum creatinine, high sensitivity C-reactive protein (hsCRP), urine creatinine, AKI markers cystatin C and neutrophil gelatinase-associated lipocalin (NGAL), kidney injury molecule 1 (KIM-1), liver-type fatty acid-binding protein, and endothelium marker intercellular adhesion molecule-1 (ICAM-1) were assessed in both groups before and after polysomnography. The same parameters were also measured in the patients with moderate-to-severe OSA after CPAP therapy.

**Results.** Kidney injury molecule 1 and urine NGAL significantly increased after the diagnostic night in the whole group and in mild OSA patients ( $p = 0.04$  and  $p = 0.001$ , respectively). Serum ICAM-1 significantly decreased after the diagnostic night only in mild OSA patients ( $p = 0.03$ ). Urine cystatin C increased after 6–8 weeks of CPAP treatment in the moderate-to-severe OSA group (0.003). Serum ICAM-1 decreased after the CPAP treatment ( $p = 0.02$ ). The CPAP therapy led also to a decrease in mean and diastolic ( $p = 0.005$ ) blood pressure.

**Conclusions.** The pattern of overnight changes in serum and urine AKI markers after apneic episodes during sleep may suggest an increased risk of subclinical AKI in patients with OSA. The CPAP therapy is not protective against AKI, but may reduce some of its risk factors, including high blood pressure and endothelial damage.

**Key words:** biomarkers, acute kidney injury, obstructive sleep apnea, NGAL

## Introduction

Obstructive sleep apnea (OSA) is a common and growing clinical problem with many important negative health implications, characterized by recurrent episodes of hypoxia and hypercapnia during sleep, resulting in daytime sleepiness.<sup>1</sup> Hypoxia and hypercapnia induced by OSA may have negative effects resulting from the activation of the sympathetic nervous system, the renin-angiotensin-aldosterone system (RAAS), and increased oxidative stress and free-radical generation.<sup>1–3</sup> The detrimental consequences of hypoxia, which include endothelial dysfunction, systemic inflammation, platelet aggregation, atherosclerosis, and fibrosis, may predispose individuals to cardiovascular events and are likely to induce renal damage.<sup>2,3</sup> As much as half of all patients with chronic kidney (CKD) disease suffer from nocturnal hypoxia, which has been recognized as a potential cause of chronic renal dysfunction and cardiovascular risk.<sup>3</sup> Obstructive sleep apnea has also recently been identified as a strong risk factor for acute kidney injury (AKI) in a large population of critically ill patients.<sup>4</sup>

It has recently been suggested that frequent apneic episodes during sleep may result in repeated renal hypoxia and release of inflammatory mediators, which may cause AKI and eventually contribute to CKD.<sup>2,3</sup> Obstructive sleep apnea has also been associated with glomerular hyperfiltration and the development of focal glomerulosclerosis, and may be an independent predictor of proteinuria, a major risk factor for CKD progression.<sup>5,6</sup> Obstructive sleep apnea may mediate renal damage through several mechanisms, i.e., hypoxemia-induced endothelial dysfunction, accelerated atherosclerosis or altered cardiovascular hemodynamics.<sup>1–3</sup> Therefore, there is a need to better elucidate the possible impact of OSA on the incidence of kidney injury and CKD progression.

The current routine diagnostics of AKI are based mainly on changes in serum creatinine, but these measurements may lack the sensitivity necessary to detect early and acute deterioration in kidney function.<sup>7</sup> Serum creatinine concentration may not change until about 50% of kidney function has already been lost. Furthermore, serum creatinine levels vary widely with age, sex, muscle mass, muscle metabolism, medications, and hydration status.<sup>8</sup> Novel, more specific and sensitive AKI biomarkers are neutrophil gelatinase-associated lipocalin (NGAL), cystatin C, kidney injury molecule 1 (KIM-1), and liver-type fatty acid-binding protein (L-FABP), the concentrations of which in urine or serum rise significantly in patients with AKI and correlate well with the severity of kidney injury.<sup>7,8</sup>

The treatment of OSA with continuous positive airway pressure (CPAP) offers a unique opportunity to alleviate most maladaptive changes in the cardiovascular system. Several clinical and experimental studies have indicated that CPAP may lead to an improvement in endothelial function, decrease free radical release from neutrophils, decrease inflammatory mediators, increase vasodilator

serum levels, and induce a decrease in vasoconstrictor levels in patients with sleep apnea.<sup>9,10</sup> It is likely that CPAP treatment could mitigate renal injury and improve renal outcomes.<sup>11</sup>

The aim of this study was to assess the effect of sleep apnea episodes on the pattern of changes in novel serum and urine markers of AKI and endothelial function in patients with different levels of severity of OSA, and to examine whether CPAP treatment of moderate-to-severe OSA could influence the overnight changes in AKI markers.

## Material and methods

Ninety-nine men aged 40–67 years and having estimated glomerular filtration rate calculated with the Chronic Kidney Disease Epidemiology Collaboration (CKD-EPI) equation ( $eGFR_{CKD-EPI} >60$  mL/min/1.73 m<sup>2</sup>) were referred to the Sleep and Respiratory Disorders Center in Łódź (Poland) after screening for OSA based on the Berlin Questionnaire and Epworth Sleepiness Scale (ESS) for daytime sleepiness assessment. All the patients underwent a diagnostic night: standard nocturnal polysomnography (8 h, from 10:00 pm to 06:00 am) using Sleep Lab (Jaeger Vi-sys Healthcare, Höchberg, Germany), operated by a single technician with long-term experience in polysomnography. All the readings were analyzed and interpreted by a clinical physiologist (P.B.) who was blinded to the endpoints and design of the study.

Sleep and baseline respiratory parameters were defined and scored according to the 2007 American Academy of Sleep Medicine (AASM) criteria.<sup>12</sup> Obstructive sleep apnea was defined as  $\geq 90\%$  cessation of airflow persisting for at least 10 s relative to basal amplitude. Hypopnea was defined as less than or equal to 70% reduction for at least 10 s. The apnea-hypopnea index (AHI) was calculated as the number of OSA events plus the number of obstructive hypopnea events per 1 h of sleep time recorded by the device. The severity of OSA was determined as mild (AHI 5–14/h), moderate (AHI 15–29/h) or severe (AHI  $\geq 30$ /h).

After positive screening tests for OSA, 86 males with apnea-hypopnea indexes  $\geq 15$  episodes/h and  $eGFR_{CKD-EPI} >60$  mL/min/1.73 m<sup>2</sup> were qualified for the study. The demographic and clinical characteristics of the study population are presented in Table 1. The exclusion criteria included proteinuria  $>1.0$  g/24 h/1.73 m<sup>2</sup> body surface; acute and chronic inflammatory conditions including urinary tract infection (UTI), defined as  $>8$  leukocytes in urinary sediment or clinical symptoms of UTI; New York Heart Association (NYHA) heart insufficiency class 3 or 4; uncontrolled diabetes mellitus (glycated hemoglobin (HbA1C)  $>8.5\%$ ); triglyceride and/or total cholesterol concentration  $>300$  mg/dL; chronic therapy with drugs with confirmed nephrotoxicity, excluding sporadic use of non-steroidal anti-inflammatory drugs; use of sympathomimetics; chronic use of sleep

**Table 1.** Clinical characteristics of the whole study population and the subgroups of patients with mild and moderate-to-severe OSA

Variable	All patients	Patients with mild OSA	Patients with moderate-to-severe OSA	p-value (mild vs moderate-to-severe OSA)
Number of patients	86 (100%)	45 (52.3%)	41 (47.7%), including 13 with mild OSA and 28 with severe OSA	
Age [years]	44.6 ±10.6	41.9 ±11.8	47.5 ±8.5	p = 0.01
BMI [kg/m <sup>2</sup> ]	34.5 ±6.0	32.5 ±5.4	36.7 ±6.1	p = 0.02
WHR	1.05 ±0.08	1.02 ±0.08	1.08 ±0.07	p = 0.02
eGFR [mL/min/1.73 m <sup>2</sup> ]	81.2 ±13.8	82.3 ±14.8	79.9 ±13.0	p = 0.03
Blood pressure [mm Hg] systolic	137.6 ±14.9	135.8 ±12.0	139.5 ±17.6	–
diastolic	85.5 ±9.6	84.9 ±9.0	86.1 ±10.4	–
Hypertension and/or use of antihypertensive medication	45 (52.3%)	20 (44.4%)	25 (61%)	–
Diabetes mellitus	11 (12.8%)	4 (8.9%)	7 (17.1%)	–
Coronary artery disease	11 (12.8%)	7 (24.1%)	4 (9.76%)	–
Number of patients with urine protein excretion >0.3 g/L	9 (10.5%)	3 (6.7%)	6 (14.6%)	–
Active smokers	22 (25.6%)	10 (22.2%)	12 (29.3%)	–
Antihypertensive treatment				
ACEI	40 (46.5%)	17 (37.7%)	23 (56.1%)	
ARB	26 (30.2%)	10 (17.2%)	16 (39.0%)	
CCB	9 (10.5%)	3 (10.3%)	6 (14.6%)	
BB	13 (15.1%)	3 (10.3%)	10 (24.4%)	–
α blockers	16 (18.6%)	7 (15.5%)	9 (21.9%)	
loop diuretics	5 (5.8%)	1 (2.2%)	4 (9.8%)	
thiazide diuretics	17 (19.8%)	5 (11.1%)	12 (29.3%)	
AA	2 (2.3%)	1 (2.2%)	1 (2.4%)	
Lipid-lowering therapy	18 (20.9%)	9 (20.0%)	9 (21.9%)	–
AHI (events per 1 h of recorded sleep time)	32.1 ±28.5	11.2 ±12.3	38.3 ±20.7	p = 0.000

OSA – obstructive sleep apnea; BMI – body mass index; WHR – waist-hip ratio; eGFR – estimated glomerular filtration rate; CKD – chronic kidney disease; AHI – apnea-hypopnea index; ACEI – angiotensin-converting enzyme inhibitors; ARB – angiotensin receptor blockers; CCB – calcium channel blockers; BB – beta-adrenergic receptor blockers; AA – aldosterone receptor antagonists.

medications; alcohol abuse; liver disease; or chronic obstructive and restrictive pulmonary diseases. Subjects with uncontrolled arterial hypertension with systolic blood pressure (SBP) >160 mm Hg and diastolic blood pressure (DBP) >100 mm Hg were also excluded.

The research was conducted in accordance with the Declaration of Helsinki, and the study protocol was approved by the ethics committee at the Medical University of Łódź. All the participants signed informed consent prior to their recruitment.

The subjects' blood pressure was measured with an electronic automatic sphygmomanometer (Omron M1 Plus; Omron Healthcare Co. Ltd., Kyoto, Japan) twice, before and after each diagnostic night. For the blood pressure analysis, the values of the mean arterial pressure (MAP) were calculated with the standard formula:  $MAP = [(DBP + 1/3 \cdot (SBP - DBP))]$ . The eGFR was calculated from serum creatinine using the CKD-EPI formula:  $eGFR_{CKD-EPI} = 141 \times \min(S_{Cr}/\kappa, 1)^{\alpha} \times \max(S_{Cr}/\kappa, 1)^{-1.209} \times 0.993^{age}$ .

Forty-one patients diagnosed with moderate-to-severe OSA were qualified for treatment with CPAP (RemStar Plus CPAP Machine; Respiration, Murrysville, USA). They all received 6–8 weeks of nightly CPAP treatment after

appropriate training and a titration period. The CPAP therapy was supervised by one of the authors (P.B.). Compliance with the therapy was checked throughout the treatment, and use of the CPAP device for ≥4 h per night was considered acceptable compliance. The remaining 45 patients with mild OSA did not receive CPAP treatment and were managed conservatively. Figure 1 shows the design of the study and a flowchart of the patients; Table 1 presents the participants' clinical characteristics.

The patients were asked to come to our sleep lab in the evening before their polysomnography (PSG) between 7:00 and 9:00 pm to sign the consent form and to receive detailed instructions about the study protocol, including lab sample collections. At that time, baseline blood and urine samples were taken. The 2<sup>nd</sup> biochemical blood and urine samples were taken in the morning after the diagnostic night, after the completion of all the procedures, at around 7:00–8:00 am. Serum creatinine, total and low-density lipoprotein (LDL) cholesterol, triglycerides, serum high-sensitivity C-reactive protein (hsCRP), and endothelium marker intercellular adhesion molecule-1 (ICAM-1) were measured at baseline in the evening before the diagnostic night and all the measurements were

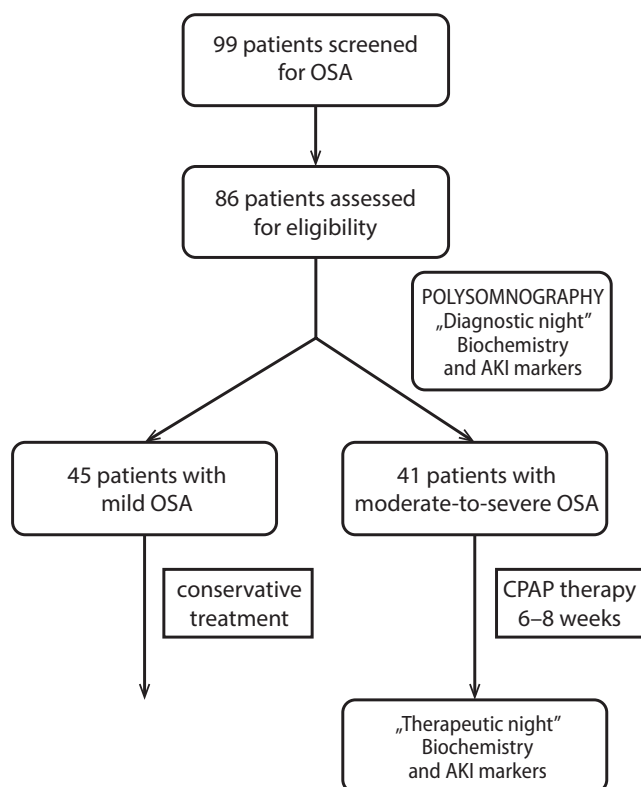


Fig. 1. Flowchart showing the study design

repeated the morning after the diagnostic night. Urine markers including creatinine, cystatin C, NGAL, L-FABP, and KIM-1 were assessed in a sample of urine given before polysomnography protocol was started and in the morning after the polysomnography. The results of the measurements of biomarkers in urine were expressed as ratios per gram of urine creatinine to avoid the differences in the time and volume of urine collection. In the patients with mild-to-moderate OSA qualified for CPAP therapy, the same measurements were repeated in the morning after 6–8 weeks of the therapy. All the patients who were initially qualified completed the study procedures.

Serum and urine samples were stored at  $-70^{\circ}\text{C}$  until analysis. All the measurements were performed in duplicate. The intra- and inter-assay coefficients of variation were below 5% for the biomarkers that were measured. All the laboratory assessments were performed in 1 batch in our university central research lab to minimize analytic variations. Urine cystatin C was measured using an enzyme-linked immunosorbent assay (ELISA) (cystatin C human ELISA kits; BioVendor LLC, Candler, USA). Urinary NGAL was also measured with ELISA kits (Lipocalin-2/NGAL Human ELISA kits; BioVendor LLC). The KIM-1 and L-FABP were assessed with KIM-1 Human ELISA and L-FABP human ELISA kits (R&D Systems Clinical Controls, Inc., Minneapolis, USA). Serum hsCRP and ICAM-1 were measured using hsCRP Human ELISA kits and sICAM-1 Human ELISA kits respectively (both from BioVendor, LLC). Data regarding urine excretion of cystatin C,

NGAL, L-FABP, and KIM-1 were expressed as nanograms per gram of creatinine. Serum and urine creatinine, total cholesterol, HDL- and LDL-cholesterol, triglycerides were measured using standard automated laboratory methods in our university central research lab using an Olympus AU 680 multianalyzer (Olympus Corp., Tokyo, Japan).

The statistical analysis was performed with STATISTICA AXAP software, v. 9.1PL (StatSoft Polska, Kraków, Poland). The results were expressed as mean  $\pm$  standard deviation (SD), and absolute changes of the variables as mean (95% confidence interval (95% CI)). P-values  $<0.05$  were considered significant. The t-test for independent samples was used to test between-group differences. For non-normally distributed variables, the Mann–Whitney rank test was used. For intragroup comparisons, a one-way analysis of variance (ANOVA) was used. Qualitative variables between groups were analyzed using  $\chi^2$  test. Spearman's test was used to analyze the correlations between AHI and urine biomarkers of AKI (NGAL, KIM-1, L-FABP, cystatin C) and serum ICAM-1.

## Results

The patients with moderate-to-severe OSA and mild OSA did not differ with respect to SBP and DBP, MAP, proteinuria, mean plasma glucose level, serum hsCRP, fasting total cholesterol, triglycerides and LDL cholesterol concentration, hemoglobin concentration, or incidence of arterial hypertension. As shown in Table 1, significant differences between the groups were found with respect to age, body mass index (BMI), waist-to-hip ratio (WHR), and eGFR. The patients with moderate-to-severe OSA were significantly older than the patients with mild OSA. Body mass, BMI and WHR were significantly higher in the moderate-to-severe OSA patients than in the mild OSA group. Baseline eGFR was lower in moderate-to-severe OSA patients compared to mild OSA patients.

As shown in Table 2, urine cystatin C was unchanged after the polysomnography night in the whole study group and in both subgroups. Urine cystatin C measured in the first morning sample of urine after 6–8 weeks of CPAP therapy decreased significantly.

Urine L-FABP did not change significantly throughout the study, including after 6–8 weeks of CPAP therapy in the moderate-to-severe OSA subgroup (Table 2). Urine NGAL excretion was significantly higher after the diagnostic night in the whole study group ( $p = 0.04$ ) and in the mild OSA patients ( $p = 0.03$ ) (Table 2). Urine KIM-1 excretion significantly increased after the diagnostic night in patients with mild OSA ( $p = 0.000$ ) and in the whole study group ( $p = 0.001$ ), but not in the patients with more severe OSA. No significant changes of urine KIM-1 were observed after 6–8 weeks of CPAP treatment (Table 2). Serum ICAM-1 significantly decreased after the diagnostic night in the mild OSA group ( $p = 0.02$ ), as well after

**Table 2.** Serum and urine biomarkers of kidney injury, endothelial function and inflammation before and after the diagnostic night with polysomnography in all patients with OSA and in subgroups of patients with mild and moderate-to-severe OSA; the levels of biomarkers after 6–8 weeks of CPAP therapy in moderate-to-severe OSA

Variable	All			Mild OSA			Moderate-to-severe OSA				
	before diagnostic night	after diagnostic night	Δ diagnostic night	before diagnostic night	after diagnostic night	Δ diagnostic night	before diagnostic night	after diagnostic night	Δ diagnostic night	after 6–8 weeks of CPAP therapy	Δ CPAP therapy
Urine cystatin C [ng/g creatinine]	431 ±252	454 ±215	23.1 [–30.1;77.1]	436 ±281	432 ±186	–4.7 [–93.9;84.6]	426 ±221.8	479 ±246	53.6 [–6.2;113.4]	369 ±214*	–110 [–188;–32]
Urine L-FABP [ng/g creatinine]	12.4 ±25.1	9.8 ±8.3	–2.6 [–8.2;2.9]	10.6 ±9.4	9.9 ±8.4	–0.67 [–3.5;2.1]	14.4 ±35.3	9.6 ±8.5	–4.8 [–16.2;6.7]	11.3 ±20.3	1.7 [–4.4;7.7]
Urine NGAL [ng/g creatinine]	46.8 ±62.9	60.8 ±64.7*	14.0 [0.2;28.6]	41.7 ±45.7	59.4 ±67.4†	17.7 [0.3;34.8]	52.4 ±78.4	62.4 ±63.3	10.0 [–14.8;34.8]	105.2 ±199.8	42.8 [–18.4;104.0]
Urine KIM-1 [ng/g creatinine]	4.6 ±4.1	6.8 ±5.1**	2.2 [1.3;3.1]	3.9 ±3.6	7.0 ±5.5††	3.1 [1.9;4.3]	5.5 ±4.6	6.6 ±5.6	1.2 [–0.3;2.6]	6.4 ±5.4	–0.2 [–1.9;1.5]
Serum ICAM-1 [mg/L]	439.9 ±363.0	380.3 ±229	–59.6 [–119;1.2]	466.8 ±446.0	365.8 ±279.0†††	–101 [–194;–8.4]	410.5 ±251.2	396.2 ±164	–14.3 [–89;61]	276.0 ±143**	–120 [–175;–66]
Serum hsCRP [μg/mL]	77.6 ±134.8	93.3 ±192.5	15.7 [–9.9;41.3]	70.0 ±149.7	82.9 ±181.2	13.0 [–22.4;48.3]	86.0 ±119.7	104.7 ±208.0	18.7 [–20.1;57.5]	68.8 ±106.4	–35.8 [–98.3;26.6]
eGFR <sub>CKD-EPI</sub> [mL/min/1.73 m <sup>2</sup> ]	81.2 ±13.8	86.0 ±13.6***	4.8 [2.8;6.8]	82.3 ±14.8	86.6 ±13.5††††	4.3 ±9.0 [1.6;7.0]	79.9 ±13.0	85.3 ±13.9#	5.4 [2.3;8.4]	84.1 ±12.0	–1.2 [–4.7;2.2]

OSA – obstructive sleep apnea; CPAP – continuous positive airway pressure; eGFR – estimated glomerular filtration rate; L-FABP – liver-type fatty acid-binding protein; NGAL – neutrophil gelatinase-associated lipocalin; KIM-1 – kidney injury molecule 1; ICAM-1 – endothelium marker intercellular adhesion molecule-1; hsCRP – high-sensitivity C-reactive protein. Results presented as mean ± standard deviation (SD) or mean (95% confidence interval (95% CI)) for absolute changes (Δ). Significance of the difference after vs before the diagnostic night: 1) all patients: \* p = 0.04; \*\* p = 0.001; \*\*\* p = 0.0001; \*\*\*\* p = 0.00001; † p = 0.03; †† p = 0.002; ††† p = 0.0003; †††† p = 0.00003; 2) moderate-to-severe OSA: † p = 0.003; †† p = 0.0003; ††† p = 0.00003; †††† p = 0.000003.

6–8 weeks of CPAP therapy in the moderate-to-severe OSA group (p = 0.002) (Table 2). Serum hsCRP did not change significantly during the diagnostic night or in the further course of the study (Table 2).

Systolic blood pressure did not change significantly at any time during the study. A significant decrease in DBP was observed after the diagnostic night in both the mild OSA patients (p = 0.005) and the moderate-to-severe OSA patients (p = 0.005). Diastolic blood pressure also decreased significantly after 6–8 weeks of CPAP treatment in the moderate-to-severe OSA group. Similar significant changes were seen in MAP (Table 3).

Before the CPAP treatment, there was a significant positive correlation between AHI and the absolute change in serum ICAM-1 (R = 0.27, p = 0.009) and urine cystatin C (R = 0.27, p = 0.009) in all the subjects. After the 6–8 weeks CPAP intervention, a significant negative correlation between AHI and the absolute change in urine L-FABP concentration (R = –0.35, p = 0.02) was revealed.

## Discussion

The results of our study only partially support the concept that OSA may result in subclinical AKI and that the treatment of OSA with CPAP may reduce the extent of kidney damage and decrease blood pressure. The latter finding is not unexpected, since the treatment of OSA with CPAP resulted in a significant decrease in glomerular pressure and hyperfiltration.<sup>11</sup> Comparable results were presented by Koga et al., who evaluated 27 patients with OSA but without CKD both before and 3 months after CPAP therapy, and found a small but a significant improvement in eGFR.<sup>13</sup> In our study, there was a small but significant overnight increase in eGFR in the patients with mild OSA, and that finding may also indirectly support the concept of hyperfiltration caused by apneic episodes during sleep. In most of the studies that have been carried out so far, the impairment of kidney function in patients with OSA was assessed only with changes in standard markers such as the eGFR, serum creatinine, urinary albumin excretion, or a sodium thiosulphate and para-aminohippurate (PAH) double clearance test.<sup>11,13,14</sup> We were able to identify only 1 very recent publication in which a similar protocol to our study was used, showing elevated serum cystatin C and NGAL in patients with AKI at baseline, and the levels of these markers were positively correlated with OSA severity.<sup>15</sup> Similar relations were not confirmed in our study, and that also applied to other sensitive AKI markers that we measured, including KIM-1 and L-FABP. The choice of AKI biomarkers

**Table 3.** Systolic, diastolic and mean blood pressure in the patients with OSA and in the subgroups of patients with mild and moderate-to-severe OSA

Parameter	All OSA		Mild OSA		Moderate-to-severe OSA			
	before diagnostic night	after diagnostic night	before diagnostic night	after diagnostic night	before diagnostic night	after diagnostic night	before therapeutic night	after therapeutic night
SBP [mm Hg]	137.6 ±14.9	136.5 ±14.7	135.8 ±12.0	135.2 ±12.3	139.5 ±17.6	138.1 ±17.1	137.8 ±14.5	135.8 ±13.0
DBP [mm Hg]	85.5 ±9.6	82.5 ±9.4*	84.9 ±9.0	81.8 ±8.5 <sup>††</sup>	86.1 ±10.4	83.2 ±10.4 <sup>††</sup>	83.8 ±10.6 <sup>#</sup>	81.2 ±9.3 <sup>**</sup>
MAP [mm Hg]	102.8 ±10.6	100.5 ±10.5 <sup>††</sup>	101.8 ±9.1	99.6 ±9.1 <sup>†</sup>	103.9 ±12.2	101.5 ±12.0 <sup>†</sup>	101.7 ±11.4 <sup>##</sup>	100.9 ±10.7

OSA – obstructive sleep apnea; SBP – systolic blood pressure; DBP – diastolic blood pressure; MAP – mean arterial pressure. Significant differences after vs before the diagnostic night: \*  $p = 0.001$ ; \*\*  $p = 0.000$ ; <sup>†</sup>  $p = 0.002$ ; <sup>††</sup>  $p = 0.005$ . Significant differences before therapeutic night No. 1 vs before diagnostic night: <sup>#</sup>  $p = 0.003$ ; <sup>##</sup>  $p = 0.002$ .

in our research included the 4 most validated biomarkers of AKI.<sup>7,8</sup> The biomarkers of AKI could be measured both in the urine and the plasma.<sup>7,8</sup> In our study, in contrast to a study by Chuang et al.,<sup>15</sup> we decided to measure urine markers of AKI, because most data from the literature have confirmed that in contrast to measurements in urine, plasma biomarkers show less specificity for AKI, since they also affected by non-renal factors such as the inflammatory state itself.<sup>7,16</sup>

The time course of the changes in each biomarker after AKI is different.<sup>7,8,16</sup> That important fact was taken into account in our study. We were, however, limited by the timing of the routine diagnostics of OSA and CPAP treatment. Urinary NGAL has been found to increase 15-fold within 2 h and 25-fold 4 h and 6 h after cardiac surgery; urine L-FABP increased 6 h after an injury, and urine cystatin C within 6 h; while urine KIM-1 had 90% sensitivity to detect cardiac surgery-associated AKI when tested 2 h and 6 h after surgery.<sup>7,17–19</sup> However, the complete time course of urinary levels for each urinary biomarker in AKI due to different or multiple renal injuries is unknown.<sup>7</sup> The samples in our study were collected after 8 h overnight PSG, during which potential repeated AKIs caused by episodes of apnea were expected to occur.

McIlroy et al. found that urine NGAL best identified AKI in patients with normal baseline renal function.<sup>20</sup> In that study, among the patients with baseline eGFR  $\geq 60$  mL/min, urinary NGAL was higher in those who developed AKI.<sup>20</sup> Our study population included only patients with eGFR<sub>CKD-EPI</sub>  $\geq 60$  mL/min; thus, the potential effect of OSA on subclinical kidney injury should have been noticeable in assessments of urine NGAL. Urine NGAL increased significantly during the diagnostic night in the whole study population and in the patients with mild OSA. However, in patients with more advanced OSA, no significant changes in urine NGAL were seen during the diagnostic night, and 6–8 weeks of CPAP treatment induced no significant effects on that parameter of kidney injury. We can only speculate that the lack of effect of CPAP on urine NGAL in the patients with more advanced OSA may be

due to the fact that more severe disease may be associated with longer and more intensive ischemic “preconditioning” of the kidneys, making them resistant to subtle insults caused by frequent apneic episodes during the night. The results on the relationship between NGAL as a marker of AKI and the severity of OSA have been conflicting since Cheung et al.<sup>15</sup> reported a relationship between the two, but the authors of another study found that plasma NGAL may not serve as a specific biomarker of OSA in clinical practice, because the kidney injury induced by OSA may only slightly contribute to systemic NGAL secretion; serum NGAL levels appeared to be influenced largely by other factors.<sup>21</sup> We tried to overcome that limitation by measuring urine NGAL instead of serum NGAL, but we were unable to identify any significant association between AHI and the overnight change in NGAL in our patients.

Urinary cystatin C excretion is another biomarker of AKI, since its excretion increases when the reabsorptive capacity of proximal tubular cells is impaired due to AKI.<sup>7</sup> There is little information on the association of OSA with serum or urine cystatin C levels. In our study, urine cystatin C significantly decreased after 6–8 weeks of CPAP treatment, which may suggest that the treatment provides some nephroprotection, but longer observations would be needed to confirm that effect. Most studies to date have investigated serum levels rather than the urine excretion of this biomarker and have been focused on chronic rather than acute effects. Zhang et al. performed a cross-sectional study and showed that serum cystatin C was associated with the severity of OSA in younger men.<sup>22</sup> In another study by Zhang et al., patients with severe OSA were recruited and treated with CPAP for 3 months, and the authors assessed serum cystatin C, creatinine and eGFR after the CPAP treatment. That study demonstrated that CPAP can decrease cystatin C levels in severe OSA patients and may prevent latent renal impairment.<sup>23</sup> Additionally, Kato et al. found that severe OSA was independently associated with increased serum cystatin C concentration.<sup>24</sup> Chuang et al.<sup>15</sup> did not find any significant change of serum cystatin C after 6 months of CPAP treatment.

Most novel biomarkers of AKI, such as urinary KIM-1 and L-FABP, have not yet been extensively investigated. We were unable to identify any studies in which these novel biomarkers have been investigated in patients with OSA.

Serum ICAM-1 has traditionally been linked to endothelial dysfunction associated with vascular injury, which is associated with OSA.<sup>25</sup> In our study, we found that 6–8 weeks of CPAP treatment resulted in a significant decrease in serum ICAM-1 concentration in the patients with moderate-to-severe OSA. In 2 previous studies, serum ICAM-1 was higher in patients with OSA<sup>26,27</sup> and showed a positive correlation with the severity of OSA and in particular with the intensity of nocturnal hypoxemia episodes.<sup>27</sup> In a multiple logistic regression analysis, Ursavaş et al. revealed that OSA was associated with high ICAM-1 levels independently of age, sex, BMI, smoking status, and cardiovascular disease.<sup>28</sup> Ohga et al. measured circulating ICAM-1 levels before and after long-term CPAP therapy in patients with OSA.<sup>29</sup> They reported that 8 months of CPAP treatment was associated with a significant decrease in serum ICAM-1, and that ICAM-1 was significantly related to oxygen desaturation and nasal CPAP therapy. The influence of CPAP treatment on ICAM-1 levels was also studied by Chin et al.<sup>30</sup> They confirmed that CPAP therapy significantly decreased serum ICAM-1 after 3 or 4 days, 1 month, or 6 months of treatment. Our results were concordant with the results of Wang et al., who confirmed that CPAP treatment decreased levels of ICAM-1 in patients with moderate and severe OSA.<sup>31</sup>

Although our study was not designed to analyze the relationship between OSA and systemic inflammation, we measured serum CRP levels but did not find any significant changes in this parameter after the diagnostic night in either group, or after CPAP therapy in the patients with moderate-to-advanced OSA. This result contrasts with most recent findings. The topic has been intensively studied, and a recent meta-analysis reported that patients with OSA develop a systemic inflammation.<sup>32</sup>

We also demonstrated a significant decrease in DBP and MAP after the diagnostic night in both of the study groups, while CPAP treatment favorably influenced only DBP. The data from the literature is ambiguous. Among the patients with OSA and resistant hypertension in the HIPARCO randomized clinical trial, CPAP treatment for 12 weeks resulted in a decrease in 24-hour MAP and DBP, and an improvement in the nocturnal blood pressure pattern.<sup>33</sup> Likewise, Durán-Cantolla et al. reported that CPAP produced a small but statistically significant reduction in blood pressure in patients with systemic hypertension and OSA.<sup>34</sup> On the contrary, Muxfeldt et al. found that CPAP treatment had no significant effect on clinic or ambulatory blood pressure in patients with resistant hypertension and moderate-to-severe OSA.<sup>35</sup>

Our study has several strengths. This is the first study that has comprehensively analyzed most novel specific urine

AKI biomarkers, including NGAL, KIM-1, L-FABP, and cystatin C, in patients with recurrent episodes of hypoxia and hypercapnia during sleep apneic episodes. Recruiting males for the study meant we assembled a homogenous population and avoided significant sex-related differences in several biomarkers, including urinary NGAL, of which women have higher levels.<sup>36</sup> We also avoided age-related differences in urinary NGAL levels and the effect of age-related kidney function decline, since we enrolled only males aged 40–59. We also carefully excluded patients with leukocyturia, systemic inflammation, glucocorticoid therapy, advanced CKD, and proteinuria >1.0 g/24 h/1.73 m<sup>2</sup> body surface, which may have influenced the results of urinary NGAL and cystatin C.

Our study has also several limitations. The issue of the time lag between renal injury and urine sampling may have had a significant impact on the results, since urinary NGAL levels vary greatly depending on their proximity in time to ischemic injury. In studies where NGAL was measured after cardiac bypass surgery, NGAL was elevated for at least 24 h after injury, but appeared to peak at ~6 h after an insult. Therefore, if the injury occurred acutely or a long time after OSA, an increase in urinary NGAL may have been missed. A relatively short duration of CPAP therapy may also be a limitation of the study. Even with the biomarker-aided improvement in risk stratification, we are unable to assess the potential implications of CPAP for clinical management without a prospective randomized trial.

In summary, we found that OSA may cause subclinical AKI, mainly in patients with mild OSA. The CPAP therapy may reduce the extent of the injury, but prospective randomized trials are required to confirm the potential implications of our results for the management of sleep apnea in patients with renal function impairment.

#### ORCID iDs

Michał Nowicki  <https://orcid.org/0000-0002-0823-5440>

Anna Zawiasa-Bryszewska  <https://orcid.org/0000-0002-7964-4268>

Małgorzata Taczykowska  <https://orcid.org/0000-0002-1066-4412>

Piotr Białasiewicz  <https://orcid.org/0000-0002-8338-1747>

Dariusz Nowak  <https://orcid.org/0000-0001-9273-3970>

#### References

- Gonzaga C, Bertolami A, Bertolami M, Amodeo C, Calhoun D. Obstructive sleep apnea, hypertension and cardiovascular diseases. *J Hum Hypertens.* 2015;29(12):705–712.
- Foster GE, Poulin MJ, Hanly PJ. Intermittent hypoxia and vascular function: Implications for obstructive sleep apnoea. *Exp Physiol.* 2007;92(1):51–65.
- Domenech P, Perez T, Saldarini A, Uad P, Musso CG. Kidney-lung pathophysiological crosstalk: Its characteristics and importance. *Int Urol Nephrol.* 2017;49(7):1211–1215.
- Dou L, Lan H, Reynolds DJ, et al. Association between obstructive sleep apnea and acute kidney injury in critically ill patients: A propensity-matched study. *Nephron.* 2017;135(2):137–146.
- Tsioufis C, Thomopoulos C, Dimitriadis K, et al. Association of obstructive sleep apnea with urinary albumin excretion in essential hypertension: A cross-sectional study. *Am J Kidney Dis.* 2008;52(2):285–293.
- Agrawal V, Vanhecke TE, Rai B, Franklin BA, Sangal RB, McCullough PA. Albuminuria and renal function in obese adults evaluated for obstructive sleep apnea. *Nephron Clin Pract.* 2009;113(3):c140–c147.

7. Kashani K, Cheungpasitporn W, Ronco C. Biomarkers of acute kidney injury: The pathway from discovery to clinical adoption. *Clin Chem Lab Med*. 2017;55(8):1074–1089.
8. Vanmassenhove J, Vanholder R, Nagler E, Van Biesen W. Urinary and serum biomarkers for the diagnosis of acute kidney injury: An in-depth review of the literature. *Nephrol Dial Transplant*. 2013;28(2):254–273.
9. Lattimore JL, Wilcox I, Skilton M, Langenfeld M, Celermajer DS. Treatment of obstructive sleep apnoea leads to improved microvascular endothelial function in the systemic circulation. *Thorax*. 2006;61(6):491–495.
10. Pépin JL, Tamisier R, Baguet JP, Lévy P. Arterial health is related to obstructive sleep apnea severity and improves with CPAP treatment. *Sleep Med Rev*. 2013;17(1):3–5.
11. Kinebuchi S, Kazama JJ, Satoh M, et al. Short-term use of continuous positive airway pressure ameliorates glomerular hyperfiltration in patients with obstructive sleep apnoea syndrome. *Clin Sci (Lond)*. 2004;107(3):317–322.
12. Berry RB, Budhiraja R, Gottlieb DJ, et al; American Academy of Sleep Medicine. Rules for scoring respiratory events in sleep: Update of the 2007 AASM Manual for the Scoring of Sleep and Associated Events. Deliberations of the Sleep Apnea Definitions Task Force of the American Academy of Sleep Medicine. *J Clin Sleep Med*. 2012;8(5):597–619.
13. Koga S, Ikeda S, Yasunaga T, Nakata T, Maemura K. Effects of nasal continuous positive airway pressure on the glomerular filtration rate in patients with obstructive sleep apnea syndrome. *Intern Med*. 2013;52(3):345–349.
14. Faulx MD, Storfer-Isser A, Kirchner HL, Jenny NS, Tracy RP, Redline S. Obstructive sleep apnea is associated with increased urinary albumin excretion. *Sleep*. 2007;30(7):923–929.
15. Chuang LP, Lin SW, Lee LA, et al. Elevated serum markers of acute kidney injury in patients with obstructive sleep apnea. *J Clin Sleep Med*. 2019;15(2):207–213.
16. Soto K, Coelho S, Rodrigues B, et al. Cystatin C as a marker of acute kidney injury in the emergency department. *Clin J Am Soc Nephrol*. 2010;5(10):1745–1754.
17. Bennett M, Dent CL, Ma Q, et al. Urine NGAL predicts severity of acute kidney injury after cardiac surgery: A prospective study. *Clin J Am Soc Nephrol*. 2008;3(3):665–673.
18. Huang Y, Don-Wauchope AC. The clinical utility of kidney injury molecule 1 in the prediction, diagnosis and prognosis of acute kidney injury: A systematic review. *Inflamm Allergy Drug Targets*. 2011;10(4):260–271.
19. Shao X, Tian L, Xu W, et al. Diagnostic value of urinary kidney injury molecule 1 for acute kidney injury: A meta-analysis. *PLoS One*. 2014;9(1):e84131.
20. McIlroy DR, Wagener G, Lee HT. Neutrophil gelatinase-associated lipocalin and acute kidney injury after cardiac surgery: The effect of baseline renal function on diagnostic performance. *Clin J Am Soc Nephrol*. 2010;5(2):211–219.
21. Murase K, Mori K, Yoshimura C, et al. Association between plasma neutrophil gelatinase associated lipocalin level and obstructive sleep apnea or nocturnal intermittent hypoxia. *PLoS One*. 2013;8(1):e54184.
22. Zhang XB, Lin QC, Deng CS, Chen GP, Cai ZM, Chen H. Elevated serum cystatin C in severe OSA younger men without complications. *Sleep Breath*. 2013;17(1):235–241.
23. Zhang XB, Jiang XT, Lin QC, Chen X, Zeng HQ. Effect of continuous positive airway pressure on serum cystatin C among obstructive sleep apnea syndrome patients. *Int Urol Nephrol*. 2014;46(10):1997–2002.
24. Kato K, Takata Y, Usui Y, et al. Severe obstructive sleep apnea increases cystatin C in clinically latent renal dysfunction. *Respir Med*. 2011;105(4):643–649.
25. Ohga E, Nagase T, Tomita T, et al. Increased levels of circulating ICAM-1, VCAM-1 and L-selectin in obstructive sleep apnea syndrome. *J Appl Physiol (1985)*. 1999;87(1):10–14.
26. El-Solh AA, Mador MJ, Sikka P, Dhillon RS, Amsterdam D, Grant BJ. Adhesion molecules in patients with coronary artery disease and moderate-to-severe obstructive sleep apnea. *Chest*. 2002;121(5):1541–1547.
27. Zamarron-Sanz C, Ricoy-Galbaldo J, Gude-Sampedro F, Riveiro-Riveiro A. Plasma levels of vascular endothelial markers in obstructive sleep apnea. *Arch Med Res*. 2006;37(4):552–555.
28. Ursavaş A, Karadağ M, Rodoplu E, Yilmaztepe A, Oral HB, Gözü RO. Circulating ICAM-1 and VCAM-1 levels in patients with obstructive sleep apnea syndrome. *Respiration*. 2007;74(5):525–532.
29. Ohga E, Tomita T, Wada H, Yamamoto H, Nagase T, Ouchi Y. Effects of obstructive sleep apnea on circulating ICAM-1, IL-8 and MCP-1. *J Appl Physiol (1985)*. 2003;94(1):179–184.
30. Chin K, Nakamura T, Shimizu K, et al. Effects of nasal continuous positive airway pressure on soluble cell adhesion molecules in patients with obstructive sleep apnea syndrome. *Am J Med*. 2000;109(7):562–567.
31. Wang YN, Yang Y, Luo YQ, Chen LL. Effects of nasal continuous positive airway pressure short-term treatment on C-reactive protein and intercellular adhesion molecule-1 in patients with obstructive sleep apnea-hypopnea syndrome [in Chinese]. *Zhong Nan Da Xue Xue Bao Yi Xue Ban*. 2005;30:666–669.
32. Li K, Wei P, Qin Y, Wei Y. Is C-reactive protein a marker of obstructive sleep apnea? A meta-analysis. *Medicine (Baltimore)*. 2017;96(19):e6850.
33. Martínez-García MA, Capote F, Campos-Rodríguez F, et al. Effect of CPAP on blood pressure in patients with obstructive sleep apnea and resistant hypertension: The HIPARCO randomized clinical trial. *JAMA*. 2013;310(22):2407–2415.
34. Durán-Cantolla J, Aizpuru F, Montserrat JM, et al. Continuous positive airway pressure as treatment for systemic hypertension in people with obstructive sleep apnoea: Randomised controlled trial. *BMJ*. 2010;341:c5991.
35. Muxfeldt ES, Margallo V, Costa LM, et al. Effects of continuous positive airway pressure treatment on clinic and ambulatory blood pressures in patients with obstructive sleep apnea and resistant hypertension: A randomized controlled trial. *Hypertension*. 2015;65(4):736–742.
36. Cullen MR, Murray PT, Fitzgibbon MC. Establishment of a reference interval for urinary neutrophil gelatinase-associated lipocalin. *Ann Clin Biochem*. 2012;49(Pt 2):190–193.

# The dynamic enhanced characterization with low mechanical index gray-scale harmonic imaging inflammatory pseudotumor of liver compared with hepatic VX2 tumor and normal liver

Ying Shi<sup>A-F</sup>, Xinghua Wang<sup>A,E</sup>, Yingyan Qiao<sup>B,C</sup>, Xueping Bai<sup>B,C</sup>, Qinxu Wang<sup>B</sup>, Chenggong Lei<sup>C</sup>

Department of Ultrasound, Second Hospital of Shanxi Medical University, Taiyuan, China

A – research concept and design; B – collection and/or assembly of data; C – data analysis and interpretation; D – writing the article; E – critical revision of the article; F – final approval of the article

Advances in Clinical and Experimental Medicine, ISSN 1899–5276 (print), ISSN 2451–2680 (online)

*Adv Clin Exp Med.* 2020;29(9):1073–1081

## Address for correspondence

Xinghua Wang  
E-mail: wang\_xh1972@sina.com

## Funding sources

This research project was supported by Shanxi Scholarship Council of China (grant No. 2013-058), Nature Science Foundation of Shanxi Province (grant No. 201801D121323) and Doctor Start-up Fund of Shanxi Medical University, Taiyuan, China (grant No. BS201716).

## Conflict of interest

None declared

Received on January 24, 2018  
Reviewed on September 17, 2018  
Accepted on June 27, 2019

Published online on September 4, 2020

## Cite as

Shi Y, Wang X, Qiao Y, Bai X, Wang Q, Lei C. The dynamic enhanced characterization with low mechanical index gray-scale harmonic imaging inflammatory pseudotumor of liver compared with hepatic VX2 tumor and normal liver. *Adv Clin Exp Med.* 2020;29(9):1073–1081. doi:10.17219/acem/110315

## DOI

10.17219/acem/110315

## Copyright

© 2020 by Wrocław Medical University  
This is an article distributed under the terms of the Creative Commons Attribution 3.0 Unported (CC BY 3.0) (<https://creativecommons.org/licenses/by/3.0/>)

## Abstract

**Background.** Inflammatory pseudotumor of the liver (IPTL) is misdiagnosed usually as a malignant tumor based on the imaging findings. Differential diagnosis should be established to avoid hepatic resection. At imaging, IPTL has been misdiagnosed usually as hepatocellular carcinoma (HCC). It is usually found firstly using conventional ultrasonic examination, which cannot give a definitive diagnosis. Because of its atypical clinical presentation and radiological appearance, a presumptive diagnosis of malignancy is frequently made. With the development of ultrasound systems and ultrasound contrast agents (UCA), contrast-enhanced ultrasound is widely used in diagnosing focal lesions of the liver.

**Objectives.** To delineate the hemodynamic features of IPTL compared with hepatic VX2 tumor and normal liver using contrast-enhanced ultrasound.

**Material and methods.** Freund's complete adjuvant (FCA) was injected using a modified method into the desirable portion of the liver in rabbits. Two weeks after the injection, solitary IPTLs were formed (which was proved with pathological examination). Ten rabbits with IPTL, 10 rabbits with VX2 carcinoma and 10 healthy rabbits were studied using contrast-enhanced ultrasound with bolus injection of SonoVue™ through the peripheral vein. Corresponding parameters such as time to enhancement (ET), time to peak intensity (PIT), time to ascent (AT), and time to lighten (LT) were measured with wash-in/wash-out curve.

**Results.** Contrast-enhanced imaging clearly delineated the dynamic enhancement of the lesions and liver parenchyma during the whole phase. Inflammatory pseudotumor of the liver showed the same enhanced features as the liver parenchyma. In VX2 tumors, hyperechoic enhancement in arterial phase and hypoechoic enhancement was observed in the portal and delayed phase compared with the surrounding hepatic parenchyma. The normal liver showed whole of liver parenchyma enhanced in portal phase.

**Conclusions.** The study showed that contrast-enhanced ultrasound provided useful information about perfusion in IPTL and VX2 carcinoma. Contrast-enhanced ultrasound is a useful technique in the differential diagnosis of focal liver lesions if combined with time-intensity curve.

**Key words:** liver, ultrasonography, inflammatory pseudotumor, contrast agent, ultrasonic diagnosis

## Introduction

Inflammatory pseudotumor of the liver (IPTL) is a benign, tumor-like mass, which was first described in 1953 by Pack and Baker.<sup>1</sup> The lesion is characterized by encapsulated proliferating connective tissue admixed with inflammatory cells.<sup>2</sup> Clinical presentation and morphological appearance may vary.<sup>3</sup> It is difficult to arrive at a definitive diagnosis in the absence of a clinical abnormality.<sup>4</sup> Inflammatory pseudotumor of the liver is misdiagnosed usually as a malignant tumor based on the imaging findings.<sup>5–7</sup> The diagnosis in most cases was confirmed during surgery and biopsy.<sup>8</sup> Differential diagnosis should be established to avoid hepatic resection.<sup>9</sup>

At imaging, IPTL has been misdiagnosed usually as hepatocellular carcinoma (HCC). Inflammatory pseudotumor of the liver is usually found with conventional ultrasonic examination, which cannot give the definitive diagnosis. Further examination, such as contrast-enhanced computed tomography (CT) and contrast-enhanced magnetic resonance imaging (MRI), needs to be undertaken. However, sonographic enhancement demonstrates a variable pattern of echogenicity. The lesion has been documented as hypo- or hyperechogenic, with or without mosaic pattern, and with ill-defined or well-circumscribed margins.<sup>4,10</sup> Because of its atypical clinical presentation and radiological appearance, a presumptive diagnosis of malignancy is frequently made.

With the development of ultrasound systems and ultrasound contrast agents (UCA), contrast-enhanced ultrasound is widely used in diagnosing focal lesions of the liver.<sup>11,12</sup> The perfusion of lesions is assessed with gray-scale harmonic imaging at a low mechanical index (MI) level. Dynamic changes of contrast enhancement in the liver tumor are observed using real-time continuous gray-scale imaging. Furthermore, quantitative assessment of circulation in liver is achieved with the time-intensity-curve software, which obtains different curves indicating tissue and vascular uptake, transit times, and wash-out of the contrast agent.<sup>13–17</sup>

Therefore, we performed a pilot study to establish an animal model carrying IPTL in rabbits with Freund's complete adjuvant (FCA) serving for contrast-enhanced ultrasound, and to explore the dynamic enhancement characterization of the IPTL compared with hepatic VX2 tumor, surrounding parenchyma and normal liver. Corresponding parameters such as time to enhancement (ET), time to peak intensity (PIT), time to ascent (AT), and time to lighten (LT) were measured with a time-intensity curve to evaluate the potential usefulness of quantifying perfusions in focal liver lesions.

## Material and methods

### Animal model

Twenty male rabbits, weighing 1.8–2.5 kg (mean body weight: 2.2 kg) with healthy livers, were divided into

3 groups (A, B and C). Group A was the IPTL group (included 10 rabbits), group B the VX2 hepatic tumor group (10 rabbits), and group C the healthy control group (10 rabbits).

### Establishment of hepatic inflammatory pseudotumor modified model

Ten rabbits were anesthetized with Sumianxin (Changchun Argo-Pastoral University, Jilin, China), which does not affect the cardiovascular system, at a dose of 1.5 mg/kg bw. through an intramuscular injection. The rabbits were placed in a supine position after the skin of the abdomen was shaved with 8% sodium sulfide solutions. Using a sterile technique, a small subxyphoid midline incision was made. In the test experiment, FCA (containing tuberculin, steroid, protein, and polysaccharide) was directly injected into the lobe of the liver in 10 rabbits according to the recorded method.<sup>18</sup> However, histopathological examination proved that no focal lesions formed in the place of large size areas with diffuse necrosis. Then, we modified the method and inserted 1 mm<sup>3</sup> of gelfoam into the left and right liver lobes with ophthalmic forceps through laparotomy incisions. Next, FCA was injected slowly into the gelfoam. The incision hole was pressed for 2–3 min after pulling out the syringe so FCA did not flow out from the needle tunnel. The sonographic study was conducted 2 weeks after the implantations.

### Establishment of hepatic VX2 tumor model

Ten rabbits were prepared as IPTL group. A small subxyphoid midline incision was made and about 1 mm<sup>3</sup> of tumor tissue from a carrier rabbit was inserted into the left and right liver with ophthalmic forceps under direct observation. The sonographic study was conducted 2 weeks after the implantation.

The rabbits were sacrificed after the sonographic study, and histopathological examinations were performed. The studies were conducted in compliance with the regulations of the Animal Ethics Committee of Shanxi Medical University, Taiyuan, China.

### Contrast agents and administration

The contrast agent used in the study was SonoVue™ (Bracco SpA, Milan, Italy), which is a lipid-shelled ultrasound contrast agent that contains millions of microbubbles filled with sulphur hexafluoride gas. A white, milky suspension of microbubbles was obtained by adding 5 mL of physiologic saline (0.9% sodium chloride) to the powder (25 mg) with the use of standard clinical aseptic techniques, followed by hand agitation. The injection of SonoVue™ was administered through a 26-gauge catheter placed into a marginal ear vein, followed by 2 mL of saline flush. SonoVue™ at a dose of 0.1 mL/kg bw. was applied.

## Equipment and data analysis

Fundamental gray-scale imaging and contrast-tuned imaging (CnTI) were conducted using a Technos MPX DU8 ultrasonography system (Esaote Biomedical SpA, Genoa, Italy). A broad-band linear array transducer, operating at 8–3 MHz for fundamental imaging and 1.56 MHz for CnTI, was used. The scanning settings for the optimal visualization, including the gain, scanning depth, field of view, and time gain control, were determined from a test experiment in several rabbits and remained unchanged throughout this study. The rabbits were scanned using conventional ultrasound to observe the lesions and normal liver (the left and right liver lobe), recording the location, the size, the features of the echogenicity, and the color flowing characterization before injecting the contrast agent. The probe was fixed during the whole period of contrast-enhanced examination when determining the optimal imaging plane showing the lesions surrounding parenchyma or normal liver each the left and right liver lobe. Then CnTI was triggered with a low MI of 0.106. After each UCA injection, digitized gray-scale images of the liver in situ within 2 min were stored in a continuous loop review and recorded on a built-in hard disk for off-line analysis.

For the analysis of gray-scale parameters, the digitally stored data of the lesions surrounding parenchyma and normal liver, were measured offline with wash-in/wash-out software built into the Technos<sup>MPX</sup> DU8 system. The regions of interest (ROI) of the same shape and size were set in liver lesions surrounding parenchyma and normal liver, each the left and right liver lobe, in approximately the same depth. The ROI were established in the center and/or the enhanced rim of the lesions. Corresponding parameters including time to enhancement (ET), time to peak intensity (PIT), time to ascent (AT), and time to lighten (LT) were measured using a time-intensity curve. The ET was defined as the delay from injection until the first echogenic bubbles of contrast agent could be seen. The PIT was defined as the interval from the beginning of the injection to the peak of the time-intensity curve. The AT was the interval calculated as PIT minus ET. The LT was defined as the interval from the injection to wash-out platform of the time-intensity curve after the enhancement peak.

## Statistical analyses

Data was expressed as means and standard deviations (SD). The ET, PIT, AT, and LT of liver lesions and surrounding parenchyma in IPTL group and VX2 tumor group for each imaging protocol were compared using a paired two-tailed Student's *t*-test. The ET, PIT, AT, and LT for each imaging protocol were compared with a one-way analysis of variance (ANOVA) among IPTL group, VX2 tumor group and the normal liver group, and post hoc tests of pairwise comparison were used for comparisons

between the 3 groups. Differences were considered significant at  $p < 0.05$ . The software used was SPSS v. 11.5 (SPSS Inc., Chicago, USA).

## Results

### Pathology results

#### IPTL group

Twenty lesions were implanted in 10 rabbits and 17 nodules (range: 4.6–13.8 mm) were formed successfully. The incidence rate is 85%. Gross appearance showed white, round and solid nodules with definite capsules (Fig. 1A). Microscopically, the nodule showed marked fibrosis with infiltration of mixed population of inflammatory cells and multinucleate cells (Fig. 1B). The middle zone was proliferated granulomatous tissue and fibrous tissue. Degenerated liver tissue was seen in the center of the nodule. Scattered necrosis, diffused fat and amorphous substance were also present. Obvious inflammatory reaction and fibrous tissue were observed at the periphery of the lesions. More venous vessels than arteries were seen in the peripheral zone of the lesion. Degeneration and necrosis were observable in most of tiny arteries.

#### VX2 tumor group

Twenty lesions were implanted in 10 rabbits and 19 nodules (range: 4.2–15.3 mm) were formed successfully. Gross appearance showed grayish-white, hard and round nodules (Fig. 1C) whose borders were well-circumscribed but not encapsulated. Microscopically, the tumor showed scattered cancer nests infiltrating the liver tissues (Fig. 1D). The tumor nests consisted of large polygonal cells with many mitotic figures. Disorder hepatic cord and dilated small vessels were present around the cancer nests. There were abundant newborn capillaries, in some of which tumor emboli were observed.

#### Healthy control group

Twenty liver lobes (both left and right liver lobe of each 10 healthy rabbits) were collected. Each liver lobe was red and had no nodules (Fig. 1E). Microscopically, the liver lobes had hepatocytes with normal architecture and observable sinusoids (Fig. 1F).

### On-site observation and offline assessment

Low-MI gray-scale imaging clearly delineated the dynamic enhancement of the lesions and parenchyma during the whole phase. The comparison of the on-site enhancement between IPTL VX2 tumors and normal livers is shown in Table 1. The time-intensity curves were analyzed during the phases of acquisition time (wash-in) and release of the contrast agent (wash-out), in addition to the evaluation of the shape of the resulting curve.

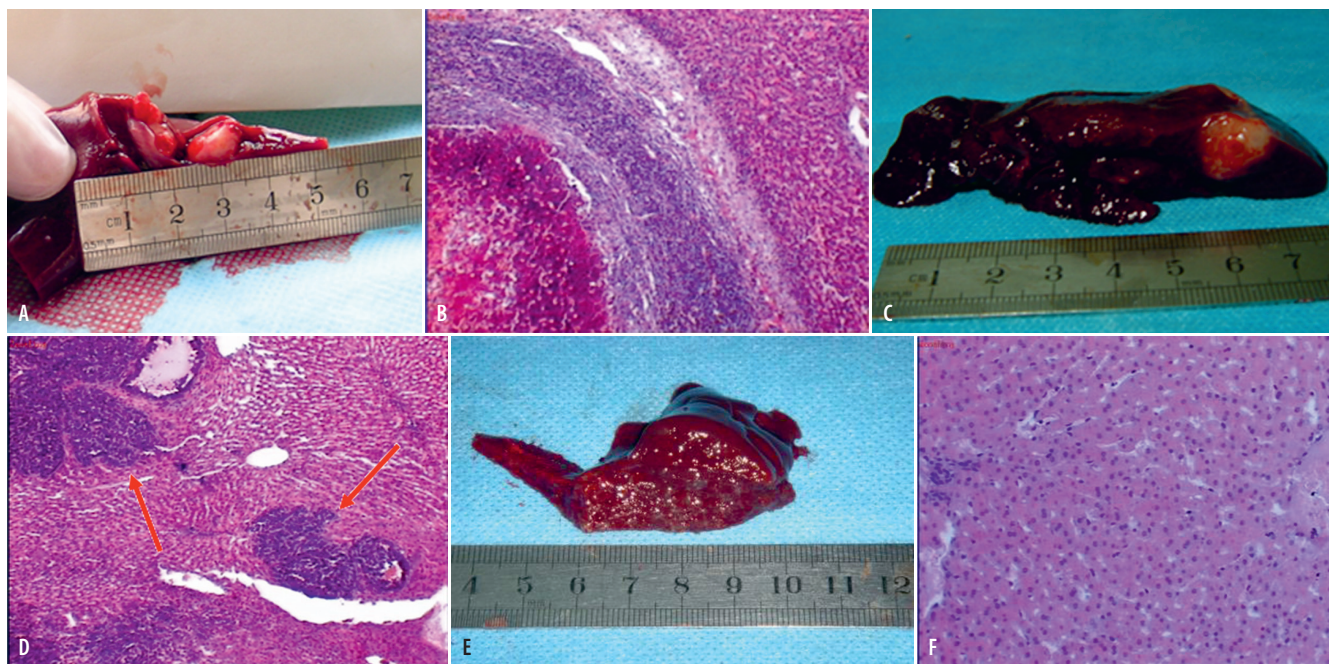


**Fig. 1.** Pathology results. A – IPTL group. Photograph of gross appearance showing white, round and solid nodules with definite capsule. B – IPTL group. Photomicrograph showing marked fibrosis with infiltration of mixed population of inflammatory and multinucleate cells (H&E staining, magnification  $\times 100$ ). C – VX2 tumor group. Photograph of gross appearance showing grayish-white mass well-circumscribed with no definite capsules. D – photomicrograph showing scattered cancer nests infiltrated among the liver tissues (red arrow) (H&E staining, magnification  $\times 100$ ). E – normal liver group. Photograph of gross appearance showed red and homogeneous liver, without nodes. F – normal liver group. Photomicrograph showing normal liver lobe had hepatocytes with normal architecture and observable sinusoids (H&E staining, magnification  $\times 400$ )

**Table 1.** The enhancement in IPTL and VX2 tumors in whole phase

Group	Arterial phase	Portal phase	Delayed phase
IPTL	same as parenchyma	no dark areas	no dark areas
VX2 tumor	marked enhanced	decreased enhancement	marked dark areas
Normal liver	enhanced hepatic artery	enhanced liver parenchyma	delayed liver parenchyma

IPTL – inflammatory pseudotumor of the liver.

**Table 2.** The comparison of ET, PIT, AT, and LT between IPTL and parenchyma

Group	ET [s]	PIT [s]	AT [s]	LT [s]
IPTL	10.46 $\pm$ 2.05	30.35 $\pm$ 9.81	17.93 $\pm$ 8.03	80.59 $\pm$ 25.68
Parenchyma	10.84 $\pm$ 2.46	27.43 $\pm$ 9.27	16.59 $\pm$ 8.73	77.95 $\pm$ 25.68
p-value	0.653	0.199	0.526	0.655

Values are presented as means  $\pm$  standard deviation (SD); IPTL – inflammatory pseudotumor of the liver; ET – time to enhancement; PIT – time to peak intensity; AT – time to ascent; LT – time to lighten.

### IPTL group

Ordinary ultrasound scanning showed iso- or hyperechoic nodules of IPTL (Fig. 2A), which revealed an absence of color flow before the injection of UCA (Fig. 2B). After the injection of UCA, IPTL showed the same enhanced features and dynamic changes as that of liver parenchyma during the whole enhanced phase. The enhancement of all nodules was no greater than that of parenchyma in arterial phase (Fig. 2C). Hypoechoic nodules were not observed in portal phase and delayed phase compared with parenchyma (Fig. 2D). The curves obtained from the IPTL and parenchyma had similar

patterns, showing a regular progressive wash-in and slowly wash-out of the UCA (Fig. 2E,F). The ET, PIT, AT, and LT in IPTL were 10.46  $\pm$  2.05 s, 30.35  $\pm$  9.81 s, 17.93  $\pm$  8.03 s, and 80.59  $\pm$  25.68 s, respectively. The ET, PIT, AT, and LT in parenchyma of IPTL were 10.84  $\pm$  2.46 s, 27.43  $\pm$  9.27 s, 16.59  $\pm$  8.73 s, and 77.95  $\pm$  25.68 s, respectively. There was no significant difference for ET, PIT, AT, and LT between IPTL and parenchyma ( $p > 0.05$ ) (Table 2).

### VX2 tumor group

Ordinary ultrasound scanning revealed that the VX2 tumors showed hypo-, iso- or hyperechoic imaging (Fig. 3A).

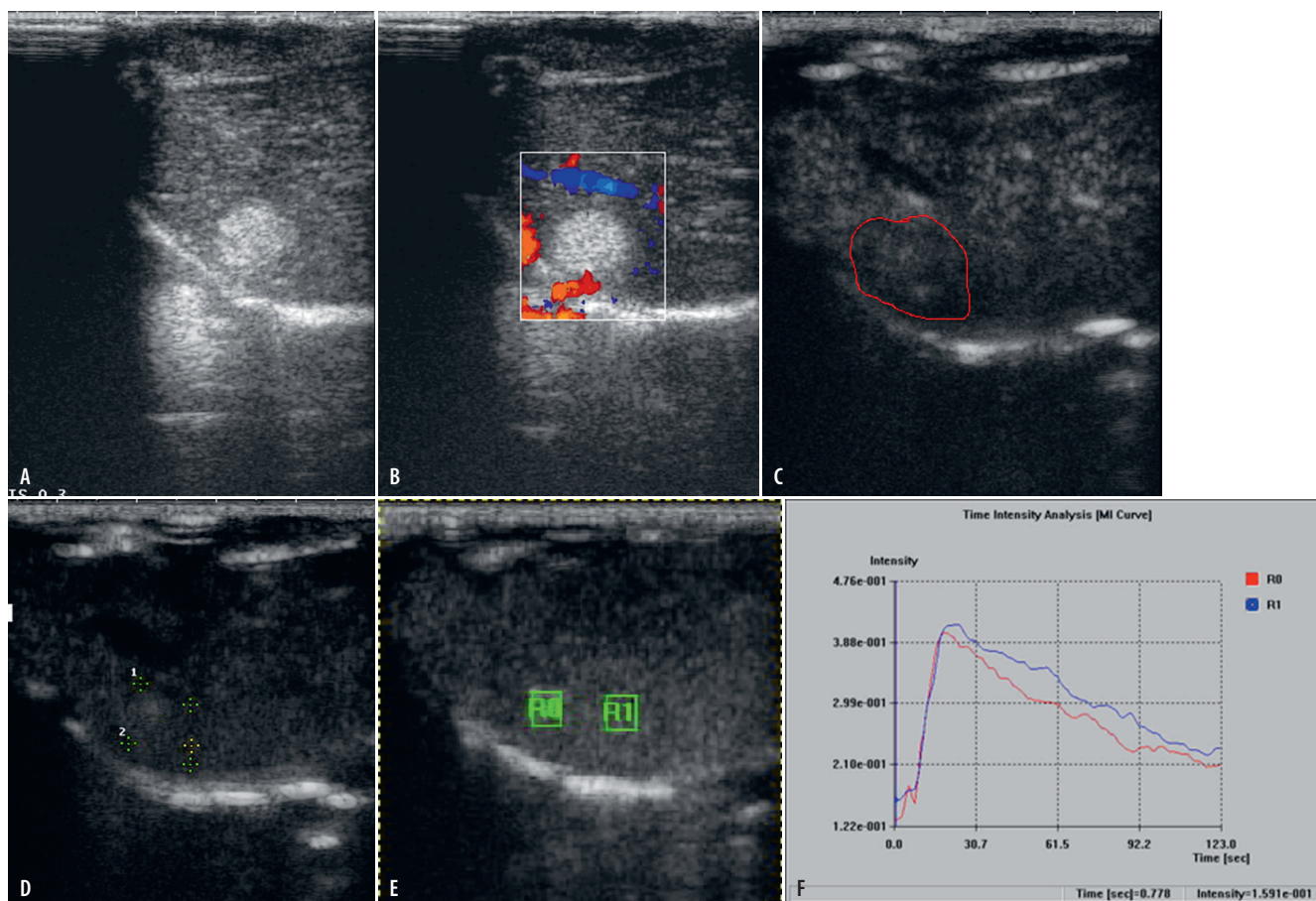


**Fig. 2.** IPTL group. A – hyperechoic nodule in conventional ultrasound imaging; B – no blood flow in color Doppler flow imaging; C – enhancement in the arterial phase, no marked enhanced change compared with the parenchyma (red circle); D – enhanced feature same as the parenchyma in delayed phase; E – the ROI were set in the center of the lesion (R0) and parenchyma (R1) in approximately the same depth; F – the curves obtained from the IPTL and parenchyma had similar patterns and showed a regular progressive wash-in and slowly wash-out of the UCA (red curve – IPTL; blue curve – parenchyma)

Noise signal was seen in 9 tumors (Fig. 3B) and artery signal was observed in 4 tumors. After the UCA injection, the tumors were enhanced markedly in the early arterial phase (Fig. 3C). The features of the enhancement in the early arterial phase showed 3 patterns: enhancement on the rim of the tumors (7 nodules), homogeneous enhancement of the whole tumors (2 nodules) and heterogeneous enhancement of the tumors (4 nodules). The tumors were clearly and easily identified as areas of enhancement because the parenchyma was just slightly enhanced in the early arterial phase. After the arterial phase, the echogenicity of the surrounding liver tissue increased, and the intensity of the tumors decreased gradually before falling off abruptly. The UCA was washed out earlier from tumors than from parenchyma. The tumors were clearly identified as dark areas compared with the enhanced parenchyma in portal (Fig. 3D) and delayed phases.

#### Results obtained in the VX2 tumor and liver parenchyma

The curves obtained from the VX2 tumors had different patterns from those obtained from the surrounding

live parenchyma. The curve obtained in VX2 tumors displayed abruptly rapid wash-in curve and returned much earlier than the parenchyma to the baseline (Fig. 3E,F). The ET, PIT, AT, and LT in VX2 tumor were  $7.59 \pm 1.58$  s,  $22.47 \pm 7.16$  s,  $14.75 \pm 7.37$  s, and  $34.47 \pm 13.15$  s, respectively. The ET, PIT, AT, and LT in parenchyma of VX2-tumor bearing rabbits were  $10.02 \pm 2.74$  s,  $32.53 \pm 12.07$  s,  $22.60 \pm 11.51$  s, and  $81.84 \pm 23.55$  s, respectively. The ET, PIT, AT and LT in VX2 tumors were significantly ( $p < 0.05$ ) shorter than those of the live parenchyma (Table 3).

#### Healthy control group

Ordinary ultrasound scanning revealed that the normal liver lobes showed homogeneous isoechoic imaging (Fig. 4A), which had normal color flow before the injection of UCA (Fig. 4B). After the injection of UCA, the liver lobes showed only hepatic artery enhanced in the arterial phase (Fig. 4C), while later the whole liver parenchyma was enhanced in portal phase (Fig. 4D) and decayed in delayed phase. The curves obtained from the normal liver parenchyma showed a regular progressive wash-in and slow wash-out of the UCA. The ET,

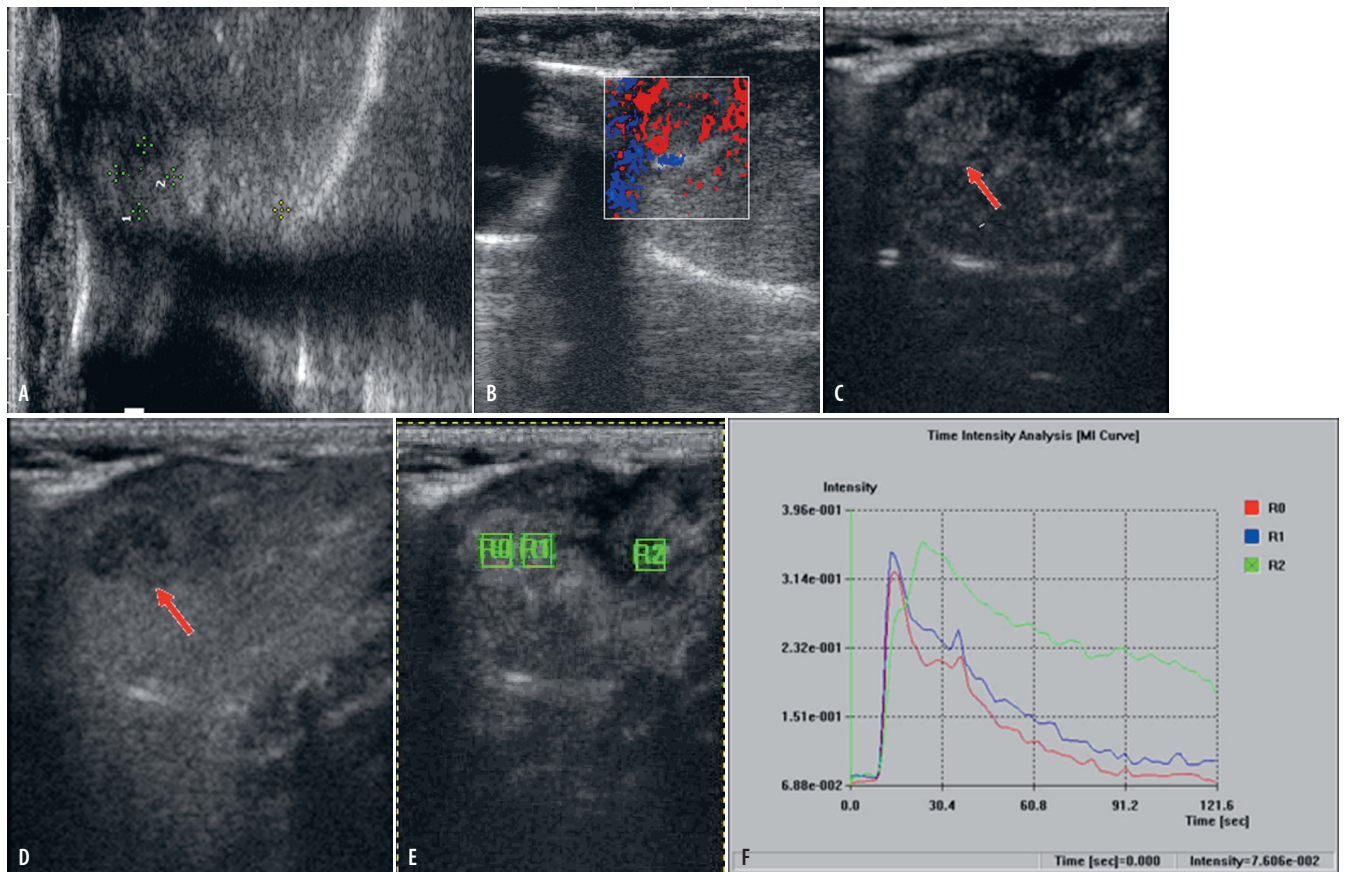


**Fig. 3.** VX2 tumor group. A – hypoechoic nodule with ill-definite in conventional ultrasound imaging; B – no blood flow instead of noise in color Doppler flow imaging; C – marked enhancement (red arrow) in the arterial phase compared with the parenchyma; D – wash-out UCA and dark lesion in portal phase (red arrow); E – the ROI were set in the center of the lesion (R0), the rim of lesion (R1) and parenchyma (R2) in approximately the same depth; F – the curves displayed abruptly rapid wash-in curve and returned much earlier than the parenchyma to the baseline (red curve – the center of VX2 tumor, blue curve – the rim of VX2 tumor, green curve – parenchyma)

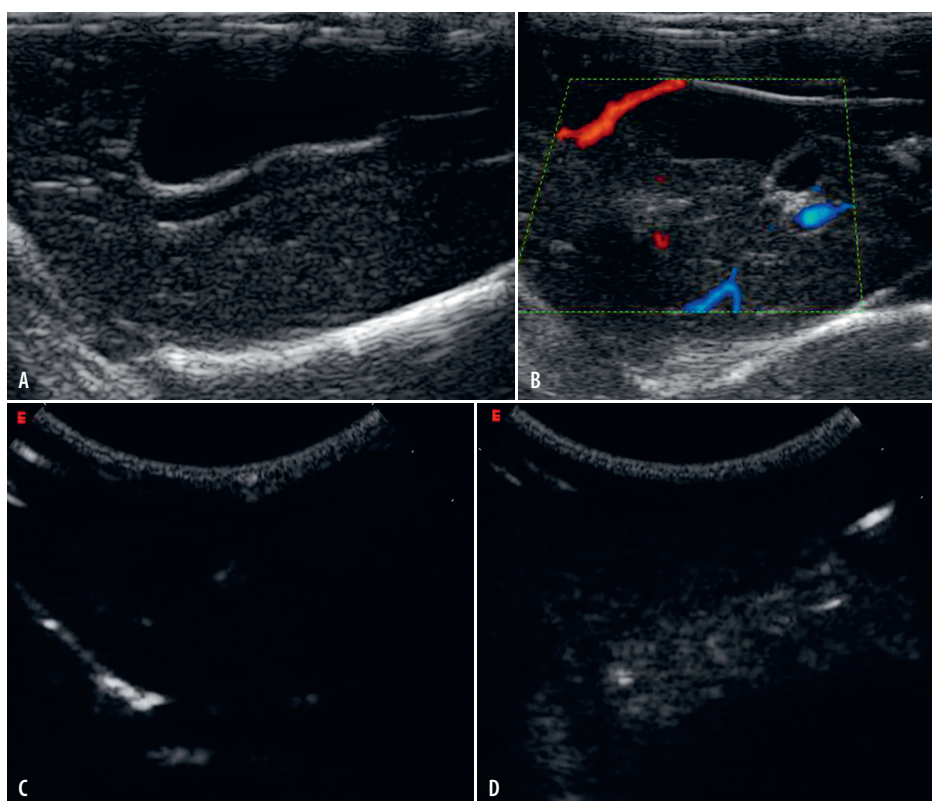


**Fig. 4.** Normal liver group. A – the normal liver lobes showing homogeneous isoechoic imaging; B – normal shape of color flow in color Doppler flow imaging; C – the liver lobes showing only hepatic artery enhanced in the arterial phase; D – whole liver parenchyma enhanced in portal phase

**Table 3.** The comparison of ET, PIT, AT, and LT between VX2 tumors and parenchyma

Group	ET(s)	PIT(s)	AT(s)	LT(s)
VX2	7.59 ±1.58	22.47 ±7.16	14.75 ±7.37	34.47 ±13.15
Parenchyma	10.02 ±2.74	32.53 ±12.07	22.60 ±11.51	81.84 ±23.55
p-value	0.006*	0.009*	0.038*	0.000*

Values are presented as means ± standard deviation (SD); \*  $p < 0.05$ . ET – time to enhancement; PIT – time to peak intensity; AT – time to ascent; LT – time to lighten.

**Table 4.** The comparison of ET, PIT, AT, and LT among IPTL and VX2 tumors and normal liver

Group	ET(s)	PIT(s)	AT(s)	LT(s)
IPTL	10.46 ±2.05 <sup>#</sup>	30.35 ±9.81 <sup>#</sup>	17.93 ±8.03	80.59 ±25.68 <sup>#</sup>
VX2	7.59 ±1.58*	22.47 ±7.06*	14.75 ±7.37	34.47 ±13.15*
Normal liver	10.16 ±1.76 <sup>#</sup>	29.18 ±9.99 <sup>#</sup>	18.30 ±6.67	79.00 ±16.87 <sup>#</sup>

Values are presented as means ± standard deviation (SD); \* value is significantly different from the IPTL group value,  $^{\#} p < 0.05$ ; # value is significantly different from the VX2 tumor group value,  $^{\#} p < 0.05$ . IPTL – inflammatory pseudotumor of the liver; ET – time to enhancement; PIT – time to peak intensity; AT – time to ascent; LT – time to lighten.

PIT, AT, and LT in IPTL in a normal liver parenchyma were 10.16 ±1.76 s, 29.18 ±9.99 s, 18.30 ±6.67 s, and 79.00 ±16.87 s, respectively.

#### Comparison of ET, PIT, AT, and LT among IPTL, VX2 tumors and a normal liver

The ET, PIT and LT in VX2 tumors were significantly shorter than those of IPTL and a normal liver (IPTL and VX2 tumors,  $p$ -value in ET group ( $P_{ET}$ ) = 0.000,  $p$ -value in PIT group ( $P_{PIT}$ ) = 0.011,  $p$ -value in AT group ( $P_{AT}$ ) = 0.984,  $p$ -value in LT group ( $P_{LT}$ ) = 0.000; normal liver and VX2 tumors,  $P_{ET}$  = 0.000,  $P_{PIT}$  = 0.025,  $P_{AT}$  = 0.146,  $P_{LT}$  = 0.000). There was no significant difference for ET, PIT, AT, and LT between IPTL and a normal liver ( $P_{ET}$  = 0.888,  $P_{PIT}$  = 0.658,  $P_{AT}$  = 0.152,  $P_{LT}$  = 0.645) (Table 4).

## Discussion

An ultrasound examination is usually the first line of investigation in the assessment of liver disease because it is non-invasive and widely available. The detection of focal hepatic lesions is relatively straight-forward with sonography, but the differentiation between benign and malignant lesions is usually difficult. There are different blood supply patterns observed for different tumors; therefore, assessment of tumor perfusion and blood supply is very useful to differentiate between benign and malignant focal lesions of the liver. Knowledge of the vascularity of a hepatic mass is essential in determining the nature of the mass. To this end, CT and MRI are performed regularly with contrast agents using different methods of administration and different imaging sequences to optimize vascular information.<sup>19</sup> With the rapid development of contrast-enhanced ultrasound and time-intensity curve quantification software, low-MI gray-scale harmonic imaging has provided an effective technique to identify the focal liver lesions<sup>20–22</sup>

because low-MI continuous harmonic imaging without destroying the contrast bubbles reveals vessels that are not seen when conventional Doppler US modes are used.

Inflammatory pseudotumor of the liver is a relatively benign tumor-like lesion. It was originally described in the lung.<sup>23</sup> The liver is the 2<sup>nd</sup> most common site.<sup>24</sup> The prognosis for IPTL is good and spontaneous regression has been described.<sup>8</sup> The knowledge of IPTL is limited because of the small number of reported cases. With surgery and imaging techniques for advanced cases, more and more IPTL cases were reported.<sup>4,7,9</sup> Inflammatory pseudotumor of the liver is classified into 3 subtypes according to its pathological features: hyalinized sclerosing granuloma, xanthogranuloma and plasma cell granuloma.<sup>6,25</sup> This classification is reflected in a variety of radiological findings that have been reported. Inflammatory pseudotumor of the liver is often misdiagnosed as a malignant tumor based on the imaging findings. Therefore, improving knowledge about IPTL imaging is important to avoid unnecessary invasive therapy. To date, reports about IPTL are mostly clinical cases and there is an absence of reliable animal model for experimental research. There is a report<sup>16</sup> that injecting FCA into the liver can induce IPTL lesions. However, when FCA was injected directly into the lobe of livers of 10 rabbits, histopathological examination proved that no focal lesions formed instead of large size areas with diffuse necrosis. The reason for this is the solution flowed along the parenchyma and it was difficult to form focal nodule in situ. Then, we modified the method and inserted 1 mm<sup>3</sup> of gelfoam first into the left and right liver lobe with ophthalmic forceps through incisions at laparotomy. Because FCA is liquid and easy to flow, the gelfoam can restrict the flow of injected FCA and form nodules. Freund's complete adjuvant contains tuberculin, abundant steroid, protein, and polysaccharide, which can induce damage, degeneration and necrosis of hepatic cells. At the same time, fibrous tissue proliferated because of inflammatory cell

infiltration. The histopathological examination in our experiment proved that the modified method could establish the IPTL animal model successfully, and after implanting of 20 lesions, 17 nodules were formed successfully (85%).

Inflammatory pseudotumor of the liver is a proliferating fibrovascular lesion pathologically characterized by infiltrated chronic inflammatory cells including lymphocytes, histiocytes and plasma cells.<sup>26</sup> The microscopical results in our modified IPTL model revealed proliferated granulomas with marked fibrous tissue infiltrated by a mixed population of inflammatory and multinucleate cells. Degenerated liver tissue was seen in the center of the nodule. Scattered necrosis, diffused fat and amorphous substance were also present. Inflammatory reaction and fibrous tissue were observed at the periphery of the lesions. More venous vessels were seen in arteries in the peripheral zone of the lesion; degeneration and necrosis were seen in most of the tiny arteries. It was proved that the modified IPTL model is a proliferated nodule, which mostly supplied by portal vein, short of hepatic artery supply.

VX2 hepatic tumor is an established malignant model in rabbits.<sup>27</sup> It has the similar blood supply as human malignant tumor which is supplied mainly by artery vessels. The IPTL is supplied mainly by venous vessels same as the normal live parenchyma. The various hemodynamic changes result in a variety of enhancements in their IPTL imaging, normal liver, surrounding parenchyma, and VX2 tumor. The experiment results showed that the IPTL had similar patterns as the normal liver and the surrounding parenchyma because of the same blood supply of venous vessels. No significant difference was observed in ET, PIT, AT, and LT between the IPTL and normal liver and surrounding parenchyma. However, VX2 tumor showed a rapid wash-in/wash-out of enhancement because the supply is mainly by arteries. The ET, PIT and LT in VX2 tumors were observed significantly earlier than those of IPTL. The ET, PIT, AT, and LT in VX2 tumors were observed significantly earlier than those of the normal liver and surrounding parenchyma. This prominent difference of enhancement combined with the time-intensity curve quantification improves the accuracy of diagnosis. Contrast-enhanced sonography improves sensitivity and specificity in discriminating between benign and malignant focal liver lesions compared with baseline sonography.

The enhanced features in our IPTL model differ from that of the clinical report, in which the enhanced IPTL was similar to HCC.<sup>28</sup> The different pathological features might result in a diversity of enhanced imaging. A pilot study about the proliferated nodule short of hepatic artery supply was performed as a part of this study. The pathology of this model might be different than in the reported clinical case, in which inflammatory cell infiltration might be the main feature. Thus, further studies, e.g., related to the different growth stages and different pathology foundations of IPTL, need to be undertaken.

## Conclusions

The study established a modified IPTL model in rabbits. The modified model easily formed solitary and solid lesion in situ, and had the advantages of high incidence rate, short latent period and easiness in duplication. Inflammatory pseudotumor of the liver is mainly supplied by the same vein as normal living tissue, and a small part of blood supply is provided by hepatic artery.

Based on the preliminary data, we believe that the low-MI continuous gray-scale harmonic contrast-enhanced ultrasound and analysis of wash-in/wash-out curves can be useful and reliable in diagnosing liver focal lesions and would be potentially useful in a clinical setting. However, our study is still in its early stages and is based on a small number of cases; therefore, further research needs to be performed.

### ORCID iDs

Ying Shi  <https://orcid.org/0000-0002-5061-7119>  
 Xinghua Wang  <https://orcid.org/0000-0001-9586-5573>  
 Yingyan Qiao  <https://orcid.org/0000-0002-7910-4210>  
 Xueping Bai  <https://orcid.org/0000-0002-2622-178X>  
 Qinxiu Wang  <https://orcid.org/0000-0002-6676-4092>  
 Chenggong Lei  <https://orcid.org/0000-0002-3714-5102>

### References

1. Pack GT, Baker HW. Total right hepatic lobectomy: Report of a case. *Ann Surg.* 1953;138(2):253–258.
2. Nitta T, Kataoka J, Inoue Y, et al. A case of multiple inflammatory hepatic pseudotumor protruding from the liver surface after colonic cancer. *Int J Surg Case Rep.* 2017;37:261–264.
3. Al-Jabri T, Sanjay P, Shaikh I, Woodward A. Inflammatory myofibroblastic pseudotumor of the liver in association with gall stones: A rare case report and brief review. *Diagn Pathol.* 2010;5:53.
4. Yafei Z, Hongwei L, Hong J, Yiming L. Inflammatory pseudotumor of the liver: A case report and literature review. *Intractable Rare Dis Res.* 2015;4(3):155–158.
5. Fukuya T, Honda H, Matsumata T, et al. Diagnosis of inflammatory pseudotumor of the liver: Value of CT. *AJR Am J Roentgenol.* 1994; 163(5):1087–1091.
6. Honmyoa N, Kobayashia T, Tashiroa H, et al. Inflammatory pseudotumor of the liver occurring during the course of hepatitis C virus-related hepatocellular carcinoma treatment: A case report. *Int J Surg Case Rep.* 2016;20:96–100.
7. Gesualdo A, Tamburrano R, Gentile A, Giannini A, Palasciano G, Palmieri VO. A diagnosis of inflammatory pseudotumor of the liver by contrast-enhanced ultrasound and fine-needle biopsy: A case report. *Eur J Case Rep Intern Med.* 2017;4(2):000495.
8. Kawaguchi T, Mochizuki K, Kizu T, et al. Inflammatory pseudotumor of the liver and spleen diagnosed by percutaneous needle biopsy. *World J Gastroenterol.* 2012;18(1):90–95.
9. Yamaguchi J, Sakamoto Y, Sano T, Shimada K, Kosuge T. Spontaneous regression of inflammatory pseudotumor of the liver: Report of three cases. *Surg Today.* 2007;37(6):525–529.
10. Matsuo Y, Sato M, Shibata T, et al. Inflammatory pseudotumor of the liver diagnosed as metastatic liver tumor in a patient with a gastrointestinal stromal tumor of the rectum: Report of a case. *World J Surg Oncol.* 2014;12:140.
11. Leoni S, Serio I, Pecorelli A, Marinelli S, Bolondi L. Contrast-enhanced ultrasound in liver cancer. *Hepatic Oncol.* 2015;2(1):51–62.
12. Durot I, Wilson SR, Willmann JK. Contrast-enhanced ultrasound of malignant liver lesions. *Abdom Radiol (NY).* 2018;43(4):819–847.
13. Derchi LE, Martinoli C, Pretolesi F, Crespi G, Buccicardi D. Quantitative analysis of contrast enhancement. *Eur Radiol.* 1999;9(Suppl 3): S372–376.

14. Marret H, Sauget S, Giraudeau B, et al. Contrast-enhanced sonography helps in discrimination of benign from malignant adnexal masses. *J Ultrasound Med*. 2004;23(12):1629–1639.
15. Kljucsek D, Vidmar D, Urlep D, Dezman R. Dynamic contrast-enhanced ultrasound of the bowel wall with quantitative assessment of Crohn's disease activity in childhood. *Radiol Oncol*. 2016;50(4):347–354.
16. Li J, Dong BW, Yu XL, Li C. Ultrasonographic portography with low mechanical index gray-scale imaging in hepatic VX2 tumor. *Ultrasound Med Biol*. 2006;32(5):641–647.
17. Yang W, Mou S, Xu Y, Du J. Contrast-enhanced ultrasonography for assessment of tubular atrophy/interstitial fibrosis in immunoglobulin A nephropathy: A preliminary clinical study. *Abdom Radiol (NY)*. 2018;43(6):1423–1431.
18. Xu YK, Liu XY, Zhang JN, et al. Experiment study of intravenous hepatosplenography with a new iodized oily emulsion for detection of small liver foci: Preliminary results. *MMJ Bimonthly*. 1998;7:272–273.
19. Caramella T, Novellas S, Fournol M, et al. Imaging of inflammatory pseudotumors of the liver [in French]. *J Radiol*. 2007;88(6):882–888.
20. Lee J, Jeong WK, Lim HK, Kim AY. Focal nodular hyperplasia of the liver: Contrast-enhanced ultrasonographic features with sonazoid. *J Ultrasound Med*. 2018;37(6):1473–1480.
21. Soye JA, Mullan CP, Porter S, Beattie H, Barltrop AH, Nelson WM. The use of contrast-enhanced ultrasound in the characterisation of focal liver lesions. *Ulster Med J*. 2007;76(1):22–25.
22. Bagley JE, Paul DE, Halferty S, DiGiacinto D. The use of contrast-enhanced ultrasonography for the characterisation of focal liver lesions. *Sonography*. 2018;5(3):120–134.
23. Vjjanic GM, Milovanovic D, Aleksandrovic S. Aggressive inflammatory pseudotumor of the abdomen 9 years after therapy for Wilms tumor: A complication, coincidence, or association. *Cancer*. 1992;70(9):2362–2366.
24. Toda K, Yasuda I, Nishigaki Y, et al. Inflammatory pseudotumor of the liver with primary sclerosing cholangitis. *J Gastroenterol*. 2000;35(4):304–309.
25. Miliak K, Madhavan KK, Bellamy C, Garden OJ, Parks RW. Inflammatory pseudotumors of the liver: Experience of a specialist surgical unit. *J Gastroenterol Hepatol*. 2009;24(9):1562–1566.
26. Oto T, Akata D, Besim A. Peritoneal inflammatory myofibroblastic pseudotumor metastatic to the liver: CT findings. *Eur Radiol*. 2000;10(9):1501.
27. Mastuda H, Sugimachi K, Kuwano H, Mori M. Hyperthermia, tissue microcirculation, and temporarily increased thermosensitivity in VX2 carcinoma in rabbit liver. *Cancer Res*. 1989;49(10):2777–2782.
28. Wang Y, Yu XL, Cheng ZG. Contrast-enhanced ultrasonographic features of inflammatory pseudotumor of the liver. *Chin J Med Ultrasound*. 2006;3:31–33.



# Monocyte chemoattractant protein-1, macrophage colony stimulating factor, survivin, and tissue inhibitor of matrix metalloproteinases-2 in analysis of damage and repair related to pediatric chronic kidney injury

Kinga Musiał<sup>A–D,F</sup>, Danuta Zwolińska<sup>C,E,F</sup>

Department and Clinic of Pediatric Nephrology, Wrocław Medical University, Poland

A – research concept and design; B – collection and/or assembly of data; C – data analysis and interpretation; D – writing the article; E – critical revision of the article; F – final approval of the article

Advances in Clinical and Experimental Medicine, ISSN 1899–5276 (print), ISSN 2451–2680 (online)

*Adv Clin Exp Med.* 2020;29(9):1083–1090

## Address for correspondence

Kinga Musiał  
E-mail: kinga\_musial@hotmail.com

## Funding sources

None declared

## Conflict of interest

None declared

Received on March 22, 2020

Reviewed on May 13, 2020

Accepted on June 2, 2020

Published online on September 9, 2020

## Cite as

Musiał K, Zwolińska D. Monocyte chemoattractant protein-1, macrophage colony stimulating factor, survivin, and tissue inhibitor of matrix metalloproteinases-2 in analysis of damage and repair related to pediatric chronic kidney injury.

*Adv Clin Exp Med.* 2020;29(9):1083–1090.

doi:10.17219/acem/123350

## DOI

10.17219/acem/123350

## Copyright

© 2020 by Wrocław Medical University

This is an article distributed under the terms of the Creative Commons Attribution 3.0 Unported (CC BY 3.0) (<https://creativecommons.org/licenses/by/3.0/>)

## Abstract

**Background.** Kidney injury in the course of chronic kidney disease (CKD) is a consequence of aggravated cell migration, inflammation, apoptosis, and fibrosis. However, the sequence of these phenomena, as well as of the reparatory mechanisms, are not fully known. Monocyte chemoattractant protein 1 (MCP-1) and macrophage colony-stimulating factor (MCSF) trigger monocyte migration to the sites of inflammation and their transition into macrophages. Tissue inhibitor of matrix metalloproteinases-2 (TIMP-2) plays a protective role against excessive matrix remodeling, whereas survivin is known for its anti-apoptotic activity.

**Objectives.** To analyze the serum, urine and fractional excretion (FE) values of MCP1, MCSF, TIMP-2, and survivin in children at subsequent stages of CKD being treated conservatively, and to analyze the potential applicability of these markers in the evaluation of CKD-related renal damage and protective mechanisms against it.

**Material and methods.** The study group consisted of 70 children with conservatively treated CKD, stages 1–5, and 12 controls. The serum and urine concentrations of MCP1, MCSF, TIMP-2, and survivin were assessed using enzyme-linked immunosorbent assay (ELISA). The FE of these parameters in the urine was also assessed.

**Results.** The serum values of all parameters were significantly elevated at CKD stage 1 compared to the controls. The urinary concentrations of MCP-1 and MCSF (stages 1–2) rose earlier than TIMP-2 and survivin (stage 4) concentrations. The FE values started increasing at CKD stage 3 (MCP-1) or stage 4 (other parameters).

**Conclusions.** The complex analysis of serum/urinary/FE values of the selected parameters revealed a sequence of multifaceted CKD-related phenomena, when the migration of cells and inflammation were followed by delayed and insufficient anti-fibrotic and anti-apoptotic activity.

**Key words:** apoptosis, chronic kidney disease, fibrosis, inflammation, urinary fractional excretion

## Introduction

Renal interstitial fibrosis is the final step in the progression of chronic kidney disease (CKD), irrespective of its origin, and confirms its irreversibility.<sup>1</sup> It is a consequence of an imbalance between tissue repair and damage.<sup>2</sup> Tubular damage in particular seems to determine the renal outcome.<sup>3</sup> Chronic kidney disease triggers both destructive and protective mechanisms in the kidney, concerning immunocompetent cell activity, inflammation or apoptosis.<sup>2</sup> However, the sequence of interactions between injury and regeneration and pro- and anti-inflammatory/apoptotic/fibrotic stimuli is unknown.

Monocyte chemoattractant protein 1 (MCP-1) and macrophage colony stimulating factor (MCSF) are engaged in the early phase of injury: immunocompetent cell migration to the sites of inflammation. The chemotactic activity of MCP-1 controls migration of monocytes, whereas the MCSF guidance triggers their transition into macrophages in situ.<sup>4</sup> The localization of MCP-1 in renal proximal tubules, as well as its pro-inflammatory and pro-fibrotic activity, have been proven in animal models.<sup>5,6</sup> Studies in children with CKD focused on the *MCP1* gene (MCP-1-2518 A/G polymorphism) in focal segmental glomerulosclerosis and on connections between plasma MCP-1 and lipid metabolism in CKD.<sup>7,8</sup> Our previous study revealed increased serum concentrations of MCP-1 in children with mild stages of CKD compared to those at the advanced stages.<sup>9</sup> However, the role of MCP-1 as a marker of progressive kidney injury in the course of CKD is unknown.

So far, MCSF has been analyzed mainly as a marker of atherosclerosis in adults on chronic hemodialysis.<sup>10,11</sup> Data concerning the role of MCSF in the pathogenesis of CKD-related damage is limited to our preliminary report on elevated serum and urine concentrations in children; this issue not been analyzed in the context of the apoptotic or fibrotic aspects of CKD progression.<sup>9</sup>

Survivin takes part in the regulation of cell division, proliferation and apoptosis.<sup>12</sup> Its ability to inhibit apoptosis was first proven in oncology, but further studies have also revealed anti-apoptotic and protective activity in response to ischemia/reperfusion injury in the course of acute kidney injury.<sup>13,14</sup> Moreover, its location in the apical membrane of proximal tubule cells and internalization by megalin prove that it is reabsorbed from the primary urine.<sup>15</sup> Studies in CKD patients are restricted to our previous reports on elevated survivin concentrations in children with advanced CKD.<sup>16</sup> However, the question of whether survivin shows any protective features against chronic kidney injury remains unknown.

The anti-fibrotic activity of TIMP-2 and its role in the cell cycle regulation have been known for some time, but it was only recently confirmed in vitro to be located in the distal tubule cells.<sup>17</sup> Urinary TIMP-2 is an established marker of acute kidney injury, but its potential role in assessing renal damage in the course of CKD progression is unknown.<sup>18</sup>

Our previous observations have suggested that the fractional excretion (FE) of molecules in the urine may be added value in the analysis of tubular function in children with CKD.<sup>9,19,20</sup>

This study is the first attempt to evaluate inflammatory/fibrotic/apoptotic phenomena using the combined analysis of serum/urinary/FE values of the selected parameters throughout all stages of pediatric CKD. Our aim was to analyze the usefulness of MCP-1, MCSF, survivin, and TIMP-2 in the assessment of CKD-related mechanisms of kidney injury in children, including inflammation, apoptosis and fibrosis, as well as the protective mechanisms against them.

## Material and methods

### Study design and settings

This is a retrospective cross-sectional study, carried out from 2016 to 2018 on 70 children with CKD and 12 controls. The CKD patients were divided into 5 groups according to CKD stage (patient flow is shown in in Fig. 1). Table 1 shows the basic demographic and biochemical data. The control group consisted of children with monosymptomatic nocturnal enuresis and normal kidney function.

The enrollment criteria for CKD children were age between 2 and 18 years and at least three-month follow-up since the diagnosis of CKD. The exclusion criteria consisted of comorbidities (diabetes, malignancy, allergy, systemic disease or primary glomerulopathy, vasculitis, peripheral vascular disease, and obesity), smoking, immunosuppression or corticosteroid therapy, current infection, or antibiotic therapy.

The causative factors for CKD were obstructive uropathy (23 patients), hypo-/dysplastic kidneys (15), reflux nephropathy (14), polycystic kidney disease (4), other genetic disorders (5), acute kidney injury (4), and unknown factors (5). Hypertension was diagnosed according to the criteria of the European Society of Hypertension in children and adolescents.<sup>21</sup>

Informed consent was obtained from the patients and their parents, if necessary. The research project was approved by the Wrocław Medical University (Wrocław, Poland) ethics committee, in accordance with the Declaration of Helsinki.

## Methods

Blood samples were drawn after an overnight fast from the peripheral veins. Samples were clotted for 30 min and centrifuged at room temperature for 10 min; the serum was then stored at  $-80^{\circ}\text{C}$  until assayed. Urine was collected aseptically from the first morning sample, centrifuged at room temperature for 10 min and stored at  $-80^{\circ}\text{C}$  until assayed.

The serum and urine concentrations of MCP-1, MCSF, survivin, and TIMP-2 were evaluated using commercially available enzyme-linked immunosorbent assay (ELISA) kits (MCP-1 – reagent kit DCP00; MCSF – reagent kit DMC00B;

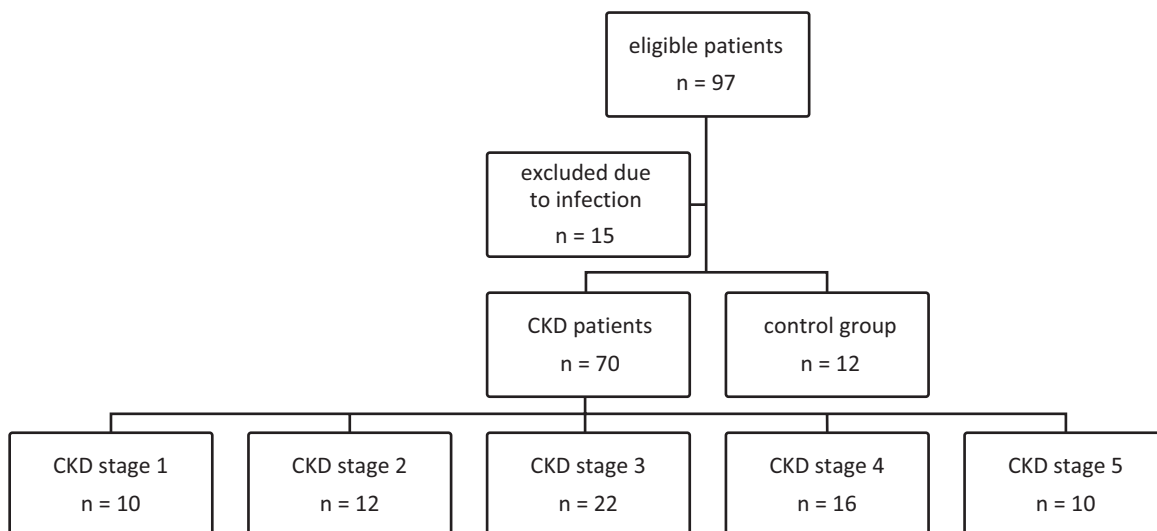


Fig. 1. Patient flow diagram

Table 1. Basic demographic and clinical data

Parameter (median value (lower–upper quartile))	Study groups					
	Control group (n = 12)	CKD 1 (n = 10)	CKD 2 (n = 12)	CKD 3 (n = 22)	CKD 4 (n = 16)	CKD 5 (n = 10)
Gender	6 girls, 6 boys	4 girls, 6 boys	6 girls, 6 boys	7 girls, 15 boys	7 girls, 9 boys	4 girls, 6 boys
Age [years]	10.5 (7.9–14.2)	13.4 (4.1–14.3)	10.1 (8.4–15.4)	9.1 (6.3–12.0)	10.9 (6.8–15.2)	9.2 (2.8–15.2)
eGFR [mL/min/1.73 m <sup>2</sup> ]	115 (94–120)	112 (106–123)	74 <sup>ab</sup> (62–82)	45 <sup>ac</sup> (35–52)	23 <sup>ad</sup> (20–26)	11 <sup>ae</sup> (9–13)
Proteinuria [mg/mg creatinine]	3.0 (0.0–5.1)	4.8 (0.0–108.7)	31.6 <sup>a</sup> (0.0–482.0)	31.7 <sup>a</sup> (0.0–351.5)	79.4 <sup>ad</sup> (10.7–718.4)	197.3 <sup>ae</sup> (54.4–2,119.8)

Mann–Whitney U test: <sup>a</sup>p < 0.001 CKD compared to control group; <sup>b</sup>p < 0.001 CKD stage 2 compared to stage 1; <sup>c</sup>p < 0.001 CKD stage 3 compared to stage 2; <sup>d</sup>p < 0.001 CKD stage 4 compared to stage 3; <sup>e</sup>p < 0.001 CKD stage 5 compared to stage 4. eGFR – estimated glomerular filtration rate; CKD – chronic kidney disease.

survivin – reagent kit DSV00; and TIMP-2 – reagent kit DTM200; all from R&D Systems, Minneapolis, USA). The measurements were performed according to the manufacturer’s instructions, and the results were calculated by reference to standard curves. The intra-assay and inter-assay coefficients of variation (%CV) for the examined parameters did not exceed 8.2% and 9.3%, respectively.

Serum and urine markers were measured with automated routine diagnostic tests: creatinine OSR61204 reagent using Beckman Coulter AU2700 analyzer (Beckman Coulter, Brea, USA) and proteinuria using turbidimetry. Estimated glomerular filtration rate (eGFR) was calculated according to Schwartz’s formula.<sup>22</sup> The urinary concentrations of the selected parameters were normalized for urinary creatinine values. The FE of the parameters was calculated based on the following formula:

$$FE = \frac{([\text{urine parameter concentration}] \times [\text{serum creatinine concentration}])}{([\text{serum parameter concentration}] \times [\text{urine creatinine concentration}])} \times 100\%.$$

## Statistical analysis

The results are expressed as median values and interquartile ranges (IQR). The null hypothesis of normality of distribution of the analyzed variables was rejected using a Shapiro–Wilk test. Thus, the comparisons and correlations between the subgroups were evaluated using non-parametric tests (Kruskal–Wallis test, Mann–Whitney U test and Spearman’s correlation coefficient). The statistically significant correlations in the whole group were then analyzed using linear regression analysis. The linear regression equations were calculated according to the following formula:

$$y = \beta x + a,$$

where y is the dependent variable, β is the regression coefficient, x is the independent variable, and a is a constant). Statistical analysis was performed using the STATISTICA v. 13.0 software package (StatSoft, Inc., Tulsa, USA). A p-value <0.05 was considered significant.

## Results

### Serum MCP-1, MCSF, survivin, and TIMP-2 concentrations

The serum concentrations of all examined parameters were significantly higher in comparison with the controls, even from the earliest stages of CKD (Fig. 2–5). The steep rise in CKD stage 1 was observed in the case of MCP-1, MCSF and TIMP-2, where the concentrations increased more than threefold, whereas those of survivin only by 30% (Fig. 2–5). However, MCSF and survivin values showed a gradual increase along with the progression of CKD (Fig. 3–4), whereas in the case of MCP-1, a short plateau phase appeared between CKD stages 2 and 3 (Fig. 2). The TIMP-2 concentrations rose at CKD stage 1 and then stabilized until stage 4, when they peaked again until stage 5 (Fig. 5).

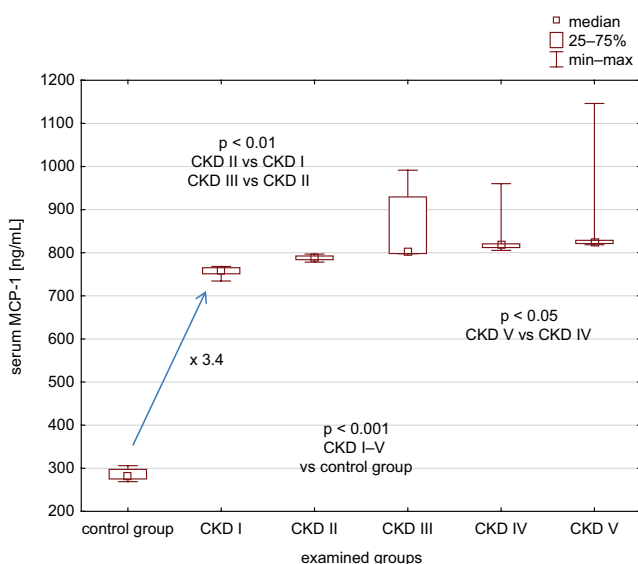


Fig. 2. Serum MCP-1 concentrations in children with CKD and controls

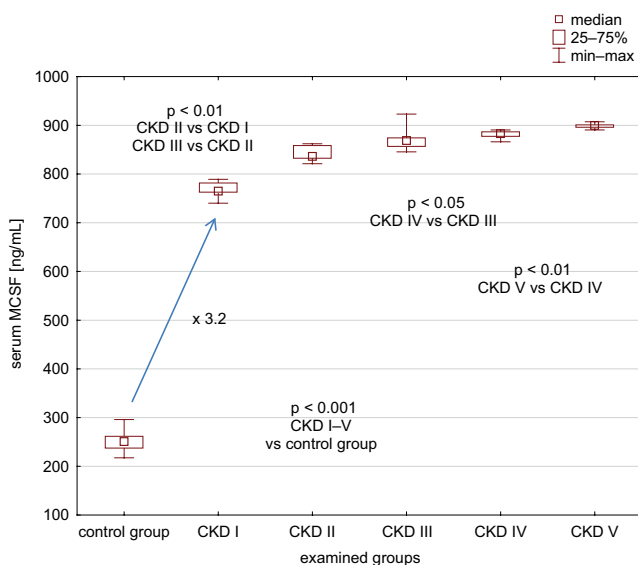


Fig. 3. Serum MCSF concentrations in children with CKD and controls

### Urine MCP-1, MCSF, survivin, and TIMP-2 concentrations

The urinary concentrations of the selected parameters, normalized for creatinine in urine, behaved differently. The MCP-1 values were elevated in comparison with the controls even at CKD stage 1; they rose until stage 2 and then remained stable until stage 5 (Table 2). The MCSF values grew in relation to the control group in CKD stage 2 and also remained unchanged until stage 5 (Table 2). Survivin and TIMP-2 augmentation reached the level of statistical significance no sooner than at stage 4 and remained unchanged in stage 5 (Table 2). All urinary values were significantly higher in CKD stage 2 than in stage 1.

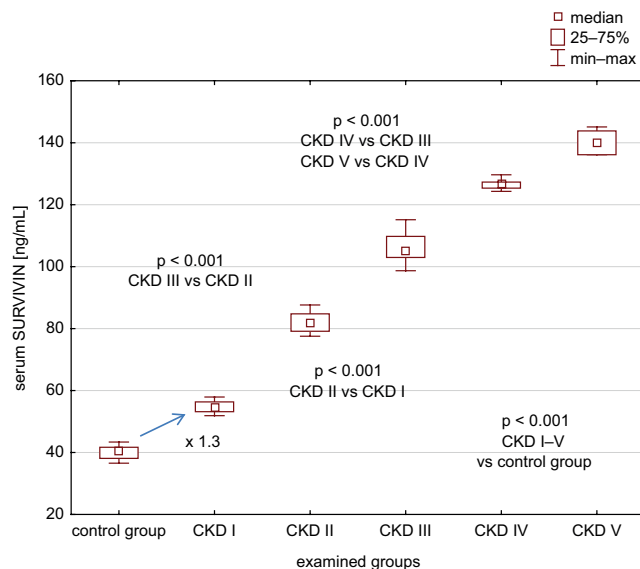


Fig. 4. Serum survivin concentrations in children with CKD and controls

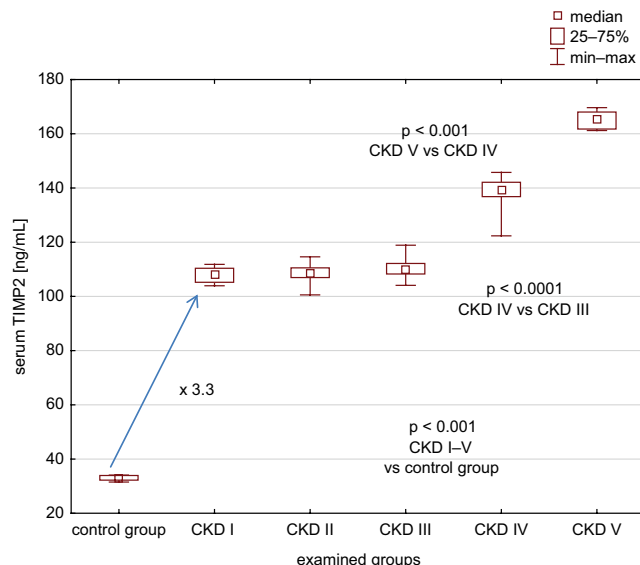


Fig. 5. Serum TIMP-2 concentrations in children with CKD and controls

**Table 2.** Urinary (u) values of the parameters under study

Parameter	Study group	Control group (n = 12)	CKD stage 1 (n = 10)	CKD stage 2 (n = 12)	CKD stage 3 (n = 22)	CKD stage 4 (n = 16)	CKD stage 5 (n = 10)
u MCP-1 [ng/mg creatinine]		2.38 (2.26–2.99)	5.11 <sup>a</sup> (3.58–6.88)	8.43 <sup>a,b</sup> (4.89–11.45)	12.14 <sup>a</sup> (6.51–16.64)	9.73 <sup>a</sup> (7.33–10.42)	11.39 <sup>a</sup> (8.17–12.28)
u MCSF [ng/mg creatinine]		27.65 (26.82–32.08)	41.46 (30.91–59.17)	74.92 <sup>a,b</sup> (40.89–98.87)	96.63 (58.47–142.28)	86.72 <sup>a</sup> (62.43–90.86)	88.92 <sup>a</sup> (64.31–95.98)
u survivin [ng/mg creatinine]		0.55 (0.53–0.63)	0.42 (0.41–0.77)	0.94 <sup>b</sup> (0.49–1.21)	0.95 (0.56–1.07)	1.11 <sup>a</sup> (0.88–1.20)	1.28 <sup>a</sup> (0.60–2.87)
uTIMP-2 [ng/mg creatinine]		0.13 (0.11–0.14)	0.11 (0.10–0.21)	0.24 <sup>b</sup> (0.13–0.31)	0.23 (0.14–0.27)	0.34 <sup>a</sup> (0.27–0.39)	0.44 <sup>a</sup> (0.21–0.99)

Mann–Whitney U test: <sup>a</sup>p < 0.001 CKD compared to control group; <sup>b</sup>p < 0.001 CKD stage 2 compared to stage 1. CKD – chronic kidney disease; MCP-1 – monocyte chemoattractant protein 1; MCSF – macrophage colony-stimulating factor; TIMP-2 – tissue inhibitor of matrix metalloproteinases-2.

### The values of urinary FE of MCP-1, MCSF, survivin, and TIMP-2

The FE values of MCSF, survivin and TIMP-2 were significantly lower than those of the control group at CKD stage 1, whereas the FE values of MCP-1 remained comparable to those in controls (Table 3). In CKD stage 2, none of the FE values differed from those in the control group. Contrarily, the FE of MCP-1 was significantly different than that of the control group at CKD stage 3, whereas the FE of the other parameters reached that threshold at CKD stage 4 (Table 3). The values of FE of survivin were the only ones that continued growing from stage 4 until stage 5 (Table 3).

Of note, the FE of MCSF presented values above 1% in both the controls and in all CKD patients. The FE of MCP-1 and survivin surpassed 1% at CKD stage 2, while the FE values of TIMP-2 did so at stage 4.

### Correlations

Correlation analysis within subgroups revealed no significant results. In the whole group of CKD children, the serum concentrations of the analyzed parameters correlated positively with each other (Table 4), with the exception

of MCP-1 and the values for survivin and TIMP-2. Additionally, serum survivin and TIMP-2 correlated negatively with eGFR and positively with the corresponding urinary values and proteinuria (Table 4). The urinary values of all markers correlated with proteinuria. Survivin and TIMP-2 urine values also correlated negatively with eGFR (Table 4). The FE values of all markers correlated with proteinuria.

However, on linear regression analysis, only serum survivin could predict eGFR ( $R^2 = 0.86$ ;  $p < 0.0000001$ ), whereas FE of survivin ( $R^2 = 0.69$ ;  $p < 0.000001$ ) and FE of TIMP-2 ( $R^2 = 0.73$ ;  $p < 0.000001$ ) were good predictors of proteinuria.

### Discussion

Our study revealed the various patterns of elevated serum and urinary values of MCP-1, MCSF, survivin, and TIMP-2, as well as changes in the urinary FE of these parameters, in pediatric patients with CKD compared to a control group.

While analyzing the dynamics of the observed fluctuations, the elevation of MCP-1 concentration was the earliest (CKD stage 1) and was seen concomitantly in the serum and urine. These results were in agreement with our

**Table 3.** Fractional excretion values of the parameters under study

Parameter	Study group	Control group (n = 12)	CKD stage 1 (n = 10)	CKD stage 2 (n = 12)	CKD stage 3 (n = 22)	CKD stage 4 (n = 16)	CKD stage 5 (n = 10)
FE MCP-1 [%]		0.59 (0.65–0.87)	0.40 (0.36–0.56)	0.69 <sup>b</sup> (0.57–2.07)	2.03 <sup>a</sup> (0.99–3.39)	3.45 <sup>a</sup> (2.10–4.91)	4.42 <sup>a</sup> (4.19–5.54)
FE MCSF [%]		8.09 (6.44–10.67)	3.88 <sup>a</sup> (3.14–4.49)	7.33 <sup>b</sup> (4.83–17.54)	16.33 (9.29–28.19)	28.74 <sup>a</sup> (16.89–40.28)	32.47 <sup>a</sup> (29.90–40.19)
FE survivin [%]		0.96 (0.76–1.20)	0.64 <sup>a</sup> (0.55–0.79)	0.79 (0.67–2.41)	1.14 (0.73–2.95)	2.79 <sup>a,d</sup> (1.67–3.84)	4.26 <sup>a,e</sup> (2.95–14.55)
FE TIMP-2 [%]		0.24 (0.22–0.36)	0.08 <sup>a</sup> (0.08–0.11)	0.16 <sup>b</sup> (0.14–0.48)	0.28 (0.18–0.69)	0.87 <sup>a,d</sup> (0.47–1.02)	1.20 <sup>a</sup> (0.87–4.30)

Mann–Whitney U test: <sup>a</sup>p < 0.001 CKD compared to control group; <sup>b</sup>p < 0.001 CKD stage 2 compared to stage 1; <sup>c</sup>p < 0.001 CKD stage 3 compared to stage 2; <sup>d</sup>p < 0.001 CKD stage 4 compared to stage 3; <sup>e</sup>p < 0.001 CKD stage 5 compared to stage 4. CKD – chronic kidney disease; FE – fractional excretion; MCP-1 – monocyte chemoattractant protein 1; MCSF – macrophage colony-stimulating factor; TIMP-2 – tissue inhibitor of matrix metalloproteinases-2.

Table 4. Significant correlations between parameters

Parameter	u survivin [ng/mg creatinine]	u TIMP-2 [ng/mg creatinine]	eGFR [mL/min/1.73 m <sup>2</sup> ]	Proteinuria [g/dL]
s survivin [ng/mL]	r = 0.40 p = 0.0009	r = 0.47 p = 0.00008	r = -0.91 p = 0.0000001	r = 0.42 p = 0.003
s TIMP-2 [ng/mL]	r = 0.33 p = 0.007	r = 0.42 p = 0.0005	r = -0.77 p = 0.0000001	r = 0.52 p = 0.0002
FE survivin [%]	r = 0.47 p = 0.00007	r = 0.55 p = 0.000002	r = -0.66 p = 0.0000001	r = 0.69 p = 0.0000001
FE TIMP-2 [%]	r = 0.60 p = 0.0000001	r = 0.68 p = 0.0000001	r = -0.76 p = 0.0000001	r = 0.69 p = 0.0000001
eGFR [mL/min/1.73 m <sup>2</sup> ]	r = -0.35 p = 0.005	r = -0.42 p = 0.0005	---	r = -0.46 p = 0.001
Proteinuria [g/dL]	r = 0.56 p = 0.00004	r = 0.61 p = 0.000005	r = -0.46 p = 0.001	---

eGFR – estimated glomerular filtration rate; FE – fractional excretion; MCP-1 – monocyte chemoattractant protein 1; MCSF – macrophage colony-stimulating factor; TIMP-2 – tissue inhibitor of matrix metalloproteinases-2; s – serum; u – urinary.

previous observations differentiating between mild and advanced CKD.<sup>9</sup> Similarly, Vianna et al.<sup>8</sup> described elevated plasma MCP-1 levels in children with CKD.

The MCP-1 is a low-molecular-weight protein, freely filtered through the glomeruli, and its early rise in urine might be a simple consequence of increased serum concentration. However, neither serum nor urinary MCP-1 correlated with eGFR, so together with the location of MCP-1 in the proximal tubules, these facts may suggest that this molecule is secreted in situ into the urine. Another argument for this hypothesis is the correlation between MCP-1 expression and monocyte infiltration in the kidneys.<sup>23</sup> The latter may also explain the plateau phase of MCP-1 urinary values prior to CKD stage 5, when MCP-1-dependent monocyte migration is followed by their MCSF-dependent transition into macrophages.

The clarification of the abovementioned doubts came with the analysis of FE values. First, they had surpassed 1% by CKD stage 2, signaling the commencement of tubular dysfunction. This observation was concordant with our previous results concerning FE.<sup>20</sup> Then, the FE values of MCP-1 were higher compared to the controls at stage 3, confirming the damage of tubular structure. Interestingly, this rise was followed by the plateau phase until stage 5. Thus, the FE rise followed the elevation in urinary MCP-1 and was probably a response to the increased serum concentration and net filtration through the glomeruli. As a consequence, serum concentration remained stable until CKD stage 4. A further increase could not be balanced by the compensatory overactivity of the proximal tubules, already damaged in the course of CKD. Thus, the complex analysis of serum, urinary and FE values of MCP-1 suggested early migratory and inflammatory overactivity aimed at adjusting tubular function to new conditions, until irreversible tubular damage. Correlation of MCP-1 FE with proteinuria would be of added value in the assessment of the early and complex features of tubular damage in the course of CKD.

Not surprisingly, the MCSF serum elevation in CKD stage 2 followed that of MCP-1 in CKD stage 1, likely depicting the transition of monocytes into macrophages that comes after monocyte migration. Likewise, the lack of correlation between eGFR and serum/urinary MCSF could suggest a CKD-triggered systemic and kidney overproduction of MCSF. Moreover, urinary MCSF concentrations (before correction for urine creatinine) were significantly higher than those in the serum of both the controls and the CKD patients, and this finding was specific to MCSF. Thus, MCSF in situ renal production, aggravated by CKD conditions, was a probable explanation.

The FE MCSF values above 1% in both the controls and the children with CKD seemed to confirm the intra-renal source of MCSF production. Moreover, FE values diminished significantly in CKD stage 1, suggesting early functional response of proximal tubules to increased serum MCSF. However, this mechanism turned out insufficient in advanced CKD, when FE became higher than in controls, most likely due to the tubular damage and subsequent aggravated leakage of MCSF with urine. Of note, MCSF FE correlated with proteinuria, making this parameter another useful tool for the analysis of tubular damage in CKD patients. Moreover, the assessment of serum, urinary and MCSF FE, confronted to corresponding serum, urinary and FE values of MCP-1, suggested the sequence of inflammatory and migratory activities during the early stages of CKD.

The early rise of survivin in the serum and its negative correlation with eGFR values could suggest an accumulation of the molecule. Moreover, serum survivin was the only predictor of eGFR. Like MCP-1 and MCSF, it is a protein that freely filters through the glomeruli. However, its serum concentration in CKD stage 1 only increased by 30%, whereas the elevation of the abovementioned chemokines under similar conditions was threefold. Thus, this moderate elevation seemed to be independent of additional triggers, like inflammatory factors, since survivin has shown no correlation with MCP-1.

Further elevation of serum survivin in the course of CKD progression was similar to our previous observations.<sup>19</sup> This gradual and significant rise, stage by stage, was another argument for the molecule accumulation along with eGFR decrease. Surprisingly, it had no influence on urinary survivin, which became elevated compared to the controls no sooner than in CKD stage 4. This late increase of urinary survivin, in accordance with our previous study<sup>16</sup> and together with its correlation with eGFR, could be explained by the filtration of this molecule through the damaged tubules rather than by in situ generation. It suggests a delayed anti-apoptotic reaction in relation to pro-inflammatory MCP-1 and MCSF overactivity.

The FE values of survivin were lower in CKD stage 1, mimicking the MCSF FE behavior and pointing at the probable adjustment of tubular function to the increased survivin content in the serum. However, they crossed the threshold of 1% at CKD stage 2, confirming the early tubular dysfunction. The lack of elevation above the control values before CKD stage 4 is another sign of the inefficient reaction against excessive molecule loss through the urine.

Finally, serum and urinary survivin correlated with proteinuria, and the FE values were able to predict it, suggesting their usefulness in the assessment of structural changes to the renal parenchyma, which are responsible for kidney injury.

An early threefold rise in the serum TIMP-2 levels of children with CKD stage 1 was followed by a plateau phase until CKD stage 3 and a further rise until stage 5. This pattern was specific to only this molecule. The negative correlation between TIMP-2 and eGFR would suggest accumulation, whereas the plateau phase concurring with a decrease in eGFR would suggest concomitant systemic generation. Indeed, TIMP-2 acts in concert with MMP-2 activity, starting early in the course of CKD.<sup>24</sup> Therefore, this elevation could be triggered by MMP-2 overactivity, already perceptible at CKD stage 1.<sup>24</sup>

As is the case with survivin, the early stages of CKD did not demonstrate an increased net content of TIMP-2 in the urine. Thus, there was a probable mechanism protecting against excessive loss of TIMP-2 through the urine and keeping the serum levels in balance until CKD stage 3. The decrease in the FE values of TIMP-2 in CKD stage 1, which were also observed in MCSF and survivin, would suggest the increased tubular reabsorption of TIMP-2. However, presence of the latter in the proximal tubules is negligible. Instead, TIMP-2 expression and secretion is strictly connected with the distal tubules.<sup>17</sup> Thus, could the probable mechanism be absorption in the proximal tubules and secretion by the distal tubules? This hypothesis requires verification in experimental studies.

Irrespective of the background, the process seemed effective until CKD stage 4, when the serum, urinary and FE values of TIMP-2 increased concomitantly, ending the preceding plateau period. The late urinary increase, parallel to that of survivin, could also be the sign of anti-fibrotic

protective reaction, distant in time from pro-inflammatory and migratory triggers.

As in the case of survivin, serum, urinary and FE values of TIMP-2 correlated with proteinuria, adding to their role as markers of tubular damage in pediatric CKD.

In summary, the multifaceted evaluation of serum, urine and FE values of the examined parameters enabled a detailed analysis of CKD-related kidney injury stage by stage, suggesting the sequence of cell migration, inflammation and fibrosis in light of the progressing tubular damage.

Finally, we have to acknowledge the limitations of our study. Due to the lack of comparative data and reference values for the majority of the parameters under study, conclusions must be drawn cautiously. There is also a possibility of potential bias, caused by the relatively small study group and the transverse design. However, both the number of analyzed patients and the study design were adjusted to the overall size of the pediatric population with CKD.

## Conclusions

Serum, urinary and FE values of MCP-1, MCSF, survivin, and TIMP-2 may become a useful tool in the complex assessment of CKD-related kidney injury, covering cell migration, inflammation, apoptosis, and fibrosis. The MCP-1 and MCSF FE values could serve as early markers of migration and inflammation, concomitant with tubular overactivity. The FE values of survivin and TIMP-2 demonstrate the late adjustment of protective anti-apoptotic and anti-fibrotic mechanisms, as they appear once tubular damage is already complete.

## ORCID iDs

Kinga Musiał  <https://orcid.org/0000-0002-9000-7585>

Danuta Zwolińska  <https://orcid.org/0000-0002-6714-3992>

## References

1. Guiteras R, Flaquer M, Cruzado JM. Macrophage in chronic kidney disease. *Clin Kidney J.* 2016;9(6):765–771.
2. Laurent P, Jolivel V, Manicki P, et al. Immune-mediated repair: A matter of plasticity. *Front Immunol.* 2017;8:454. doi:10.3389/fimmu.2017.00454
3. Takaori K, Nakamura J, Yamamoto S, et al. Severity and frequency of proximal tubule injury determines renal prognosis. *J Am Soc Nephrol.* 2016;27(8):2393–2406.
4. Meng XM, Tang PMK, Li J, Lan HY. Macrophage phenotype in kidney injury and repair. *Kidney Dis (Basel).* 2015;1(2):138–146.
5. Ma W, Tao L, Wang X, et al. Sorafenib inhibits renal fibrosis induced by unilateral ureteral obstruction via inhibition of macrophage infiltration. *Cell Physiol Biochem.* 2016;39(5):1837–1849.
6. Lai KN, Leung JCK, Chan LYY, Guo H, Tang SCW. Interaction between proximal tubular cells and infiltrating monocytes/T cells in the proteinuric state. *Kidney Int.* 2007;71(6):526–538.
7. Besbas N, Kalyoncu M, Cil O, Ozgul RK, Bakkaloglu A, Ozaltin F. MCP1 2518 A/G polymorphism affects progression of childhood focal segmental glomerulosclerosis. *Ren Fail.* 2015;37(9):1435–1439.
8. Vianna HR, Soares CM, Silveira KD, et al. Cytokines in chronic kidney disease: Potential link of MCP-1 and dyslipidemia in glomerular diseases. *Pediatr Nephrol.* 2013;28(3):463–469.

9. Musiał K, Bargenda A, Drożdż D, Zwolińska D. New markers of inflammation and tubular damage in children with chronic kidney disease. *Dis Markers*. 2017;2017:9389432.
10. Kihara T, Miyata Y, Furukawa M, et al. Predictive value of serum macrophage colony-stimulating factor for development of aortic calcification in haemodialysis patients: A 6 year longitudinal study. *Nephrol Dial Transplant*. 2005;20(8):1647–1652.
11. Haraguchi K, Kubo M, Saito T, et al. Serum level of macrophage colony-stimulating factor and atherosclerosis in hemodialysis patients. *Nephron Clin Pract*. 2006;102(1):c14–c20.
12. Ambrosini G, Adida C, Altieri DC. A novel anti-apoptosis gene, survivin, expressed in cancer and lymphoma. *Nat Med*. 1997;3(8):917–921.
13. Altieri DC. Survivin, versatile modulation of cell division and apoptosis in cancer. *Oncogene*. 2003;22(53):8581–8589.
14. Chen J, Chen JK, Conway EM, Harris RC. Survivin mediates renal proximal tubule recovery from AKI. *J Am Soc Nephrol*. 2013;24(12):2023–2033.
15. Jobst-Schwan T, Knaup KX, Nielsen R, et al. Renal uptake of the anti-apoptotic protein survivin is mediated by megalin at the apical membrane of the proximal tubule. *Am J Physiol Renal Physiol*. 2013;305(5):F734–F744.
16. Bargenda A, Musiał K, Zwolińska D. Urine survivin, E-cadherin and matrix metalloproteinases as novel biomarkers in children with chronic kidney disease. *Biomarkers*. 2015;20(3):177–182.
17. Emlet DR, Pastor-Soler N, Marciszyn A, et al. Insulin-like growth factor binding protein 7 and tissue inhibitor of metalloproteinases-2: Differential expression and secretion in human kidney tubule cells. *Am J Physiol Renal Physiol*. 2017;312(2):F284–F296.
18. Koyner JL, Shaw AD, Chawla LS, et al. Tissue inhibitor metalloproteinase-2 (TIMP-2) and IGF-binding protein-7 (IGFBP7) levels are associated with adverse long-term outcomes in patients with AKI. *J Am Soc Nephrol*. 2015;26(7):1747–1754.
19. Bargenda A, Musiał K, Zwolińska D. Fractional excretion of survivin, EMMPRIN and MMP-7 in children with chronic kidney disease. *Eur Med J*. 2016;17:675–682.
20. Musiał K, Zwolińska D. Fractional excretion as a new marker of tubular damage in children with chronic kidney disease. *Clin Chim Acta*. 2018;480:99–106.
21. Lurbe E, Cifkova R, Kennedy Cruickshank J, et al; European Society of Hypertension. Management of high blood pressure in children and adolescents: Recommendations of the European Society of Hypertension. *J Hypertens*. 2009;27(9):1719–1742.
22. Schwartz GJ, Muñoz A, Schneider MF, et al. New equations to estimate GFR in children with CKD. *J Am Soc Nephrol*. 2009;20:629–637.
23. Rice JC, Spence JS, Yetman DL, Safirstein RL. Monocyte chemoattractant protein-1 expression correlates with monocyte infiltration in the post-ischemic kidney. *Ren Fail*. 2002;24(6):703–723.
24. Musiał K, Zwolińska D. Novel indicators of fibrosis-related complications in children with chronic kidney disease. *Clin Chim Acta*. 2014;430:15–19.

# Spotlights on some electrocardiographic paradigms: How should we evaluate normal reference values of Tp–Te interval, Tp–Te dispersion and Tp–Te/QT ratio?

Mücahid Yılmaz<sup>1,A,C–F</sup>, Hidayet Kayaççek<sup>2,A–C,E,F</sup>, Nevzat Gözel<sup>3,B,C,E,F</sup>, Mehmet Nail Bilen<sup>1,A,B,E,F</sup>, Ertuğrul Kurtoğlu<sup>4,A,C,E,F</sup>, Özlem Seçen<sup>1,A,B,E,F</sup>, Pınar Öner<sup>5,A,C,E,F</sup>, Suat Demirkıran<sup>2,A,B,E,F</sup>, Ökkeş Uku<sup>1,A–C,E,F</sup>, Yusuf Çekici<sup>6,A,C,E,F</sup>, Orkun Eroglu<sup>7,A,C,E,F</sup>, Fikret Keleş<sup>1,A,B,E,F</sup>

<sup>1</sup> Department of Cardiology, Elazığ Education and Research Hospital, Turkey

<sup>2</sup> Department of Cardiology, Elazığ Medical Park Hospital, Istinie University, Turkey

<sup>3</sup> Department of Internal Medicine, Firat University School of Medicine, Elazığ, Turkey

<sup>4</sup> Department of Cardiology, Malatya Education and Research Hospital, Turkey

<sup>5</sup> Department of Microbiology, Elazığ Education and Research Hospital, Turkey

<sup>6</sup> Department of Cardiology, Dr. Ersin Arslan Education and Research Hospital, Gaziantep, Turkey

<sup>7</sup> Department of Ear, Nose and Throat, Elazığ Education and Research Hospital, Turkey

A – research concept and design; B – collection and/or assembly of data; C – data analysis and interpretation;

D – writing the article; E – critical revision of the article; F – final approval of the article

Advances in Clinical and Experimental Medicine, ISSN 1899–5276 (print), ISSN 2451–2680 (online)

Adv Clin Exp Med. 2020;29(9):1091–1099

## Address for correspondence

Mücahid Yılmaz

E-mail: mucahid.yilmaz@hotmail.com

## Funding sources

None declared

## Conflict of interest

None declared

Received on October 5, 2018

Reviewed on February 19, 2019

Accepted on January 30, 2020

Published online on September 16, 2020

## Cite as

Yılmaz M, Kayaççek H, Gözel N, et al. Spotlights on some electrocardiographic paradigms: How should we evaluate normal reference values of Tp–Te interval, Tp–Te dispersion and Tp–Te/QT ratio? *Adv Clin Exp Med.* 2020;29(9):1091–1099. doi:10.17219/acem/117684

## DOI

10.17219/acem/117684

## Copyright

© 2020 by Wrocław Medical University

This is an article distributed under the terms of the Creative Commons Attribution 3.0 Unported (CC BY 3.0) (<https://creativecommons.org/licenses/by/3.0/>)

## Abstract

**Background.** Experimental and clinical studies evaluating the Tp–Te interval and Tp–Te/QT ratio have reported conflicting data. The overlap between normal Tp–Te/QT ratios ( $0.17 \pm 0.02$ – $0.27 \pm 0.06$  ms) and pathological values ( $0.20 \pm 0.03$ – $0.30 \pm 0.06$  ms) measured in earlier studies has raised questions about this ECG measurement technique.

**Objectives.** To analyze normal values of the Tp–Te interval, Tp–Te dispersion Tp–Te(d) and the Tp–Te/QT ratio based on electrocardiographic (ECG) assessment across sex and age groups in a healthy Turkish population.

**Material and methods.** A total of 1,485 healthy participants (723 men) were enrolled into the study. The age of the participants ranged 17–75 years and they did not have either any cardiovascular/systemic disorders or risk factors for atherosclerosis which were detected with physical examination and laboratory tests. The Tp–Te interval, Tp–Te(d) and Tp–Te/QT ratio were determined from V1–V6 derivations.

**Results.** For the entire study, the median Tp–Te interval was 66.0 (64.0–70.0) ms, the Tp–Te(d) was 15.0 (10.0–20.0) ms, and the Tp–Te/QT ratio was 0.18 (0.17–0.19). The Pearson's correlation test demonstrated that the Tp–Te/QT ratio significantly correlated with older age ( $r = 0.297$ ;  $p < 0.0001$ ), left ventricular (LV) end-diastolic diameter (LVEDD;  $r = 0.481$ ;  $p < 0.0001$ ), body mass index (BMI;  $r = 0.421$ ;  $p < 0.0001$ ), body surface area (BSA;  $r = 0.191$ ;  $p < 0.0001$ ), LV end-diastolic volume (LVEDV;  $r = 0.484$ ;  $p < 0.0001$ ), LVEDV index ( $r = 0.450$ ;  $p < 0.0001$ ), LV mass ( $r = 0.548$ ;  $p < 0.0001$ ), and LV mass index ( $r = 0.539$ ;  $p < 0.0001$ ).

**Conclusions.** The reference values for Tp–Te interval, Tp–Te(d) and Tp–Te/QT ratio are associated with age, BMI, BSA, LVEDV, LVEDV index, LV mass, and LV mass index. These structural elements should be considered when using these ECG parameters for assessing repolarization inhomogeneity. These findings may guide further studies assessing healthy and diseased populations.

**Key words:** Tp–Te interval, Tp–Te/QT ratio, Tp–Te dispersion, LV mass, LV mass index

## Introduction

Myocardial repolarization heterogeneity is considered to be sensitive to malignant ventricular arrhythmias.<sup>1</sup> For many years, non-invasive parameters of malignant ventricular arrhythmias obtained from electrocardiograms (ECG) have been used in cases with cardiovascular disease. These parameters focus mostly on the QT distance.<sup>2,3</sup> Dispersion of QT, which is obtained by subtracting the lowest measured QT duration from the highest measured QT duration, is also widely used in many studies and is associated with the risk of sudden death.<sup>4–6</sup> Actually, QT dispersion is a simple, approximate evaluation of the overall heterogeneity of ventricular repolarization.<sup>7</sup> It is also difficult to determine the normal and abnormal ranges of QT dispersion. The most important reason for this is the wide range of values reported in various studies (10–71 ms).<sup>8,9</sup> Furthermore, the ranges considered as normal and abnormal values were overlapped between studies and some of these values were considered as abnormal. Some authors have reported that the upper limit of QT dispersion in normal healthy individuals is 65 ms, while others have reported that QT dispersion is a simple, approximate measurement of myocardial repolarization abnormalities and that all values proposed as the upper limit in healthy individuals are unreliable; therefore, it is possible that only the abnormal QT dispersion values >100 ms outside the margin of error for the calculations could have clinical importance in demonstrating repolarization abnormality.<sup>10,11</sup> The failure to identify ECG parameters adequately and to reach a consensus on the values has spurred the search for a different assessment method for the repolarization period.<sup>12</sup>

Recent studies have identified the time from the peak of the T wave to the latest point of the T wave (Tp–Te interval) on an ECG and the ratio of this time to the QT interval (Tp–Te/QT) as new electrocardiographic parameters for myocardial repolarization dispersion, and these parameters have been accepted as measurement methods of transmural dispersion of repolarization (TDR) which is accepted as an indicator of ventricular arrhythmias.<sup>13,14</sup> The Tp–Te/QT ratio is not changed by fluctuations in heart rate (HR) and is more reliable for demonstrating predisposition to ventricular arrhythmia than other similar, ECG-derived indices.<sup>15,16</sup> Gupta et al. standardized the normal value of the Tp–Te/QT ratio as  $0.21 \pm 0.03$  based on measurements obtained from the V6 derivation, which reflects the left ventricular (LV) transmural axis best in healthy individuals.<sup>15</sup> However, the overlap of normal Tp–Te/QT ratios ( $0.17 \pm 0.02$ – $0.27 \pm 0.06$ ) and pathological values ( $0.20 \pm 0.03$ – $0.30 \pm 0.06$ ) has raised doubts about this ECG measurement technique.<sup>17–21</sup> To overcome reliability issues that may develop in relation to this measurement technique and to increase its applicability, we believe that the normal values can be standardized in comprehensive studies on healthy individuals with an emphasis on gender, age, body mass index (BMI), body surface area (BSA),

LV volume, LV volume index, LV mass, and LV mass index. In addition, no large-scale study has assessed the Tp–Te indices. For this reason, we aimed to conduct a prospective study to overcome these issues and provide standardized reference values for future studies.

## Material and methods

### Study population

This prospective study recruited 1,485 healthy participants who were admitted to the outpatient clinic of our hospital between June 2016 and January 2018. The age of the subjects who were enrolled into the study ranged from 17 to 75 years; they did not have either any cardiovascular/systemic disorders or risk factors for atherosclerosis which were detected using transthoracic echocardiography (TTE), myocardial perfusion scintigraphy or exercise stress test. The study was carried out in conformity with the Helsinki principles and ethics approval was obtained from the Presidency of T.C. Firat University Ethics Committee, Elazığ, Turkey.

The exclusion criteria were electrolyte imbalances, any drug use that might influence the QT interval (such as anti-arrhythmia agents, probucol, terfenadine, erythromycin, clarithromycin, antidepressant agents, or antipsychotic agents), pregnancy, more than 3 births, being a professional athlete, and having a BMI > 30 kg/m<sup>2</sup>. In addition, the subjects who had a left or right bundle-branch block in ECG were not included in the analysis.

The blood pressure, BMI and BSA parameters were measured and recorded. The subjects who were taking antihypertensive medications, had a systolic blood pressure  $\geq 140$  mm Hg, and/or a diastolic blood pressure  $\geq 90$  mm Hg were considered hypertensive and not included in the analysis.

The BMI and BSA were evaluated according to the following formulas:

$$\text{BMI} = \frac{\text{weight [kg]}}{\text{height}^2 \text{ [m}^2\text{]}}$$

$$\text{BSA (Mosteller formula)} = \sqrt{(\text{height [cm]} \times \text{weight [kg]})/3600}$$

### Electrocardiography

By tuning the voltage value to 10 mm/mV and the paper speed to 50 mm/s, commonly used ECG equipment (CardiofaxV model 9320; Nihon Kohden, Tokyo, Japan) was used to record the 12-derivated ECG. After scanning the whole of the ECG recording, the intervals of the Tp–Te, the QT and the RR were evaluated. The evaluations were done with the help of a computer program which is coded in MATLAB® software (MathWorks, Natick, USA). The computer software code was developed by an engineer and was dependent on the image manipulation algorithms.

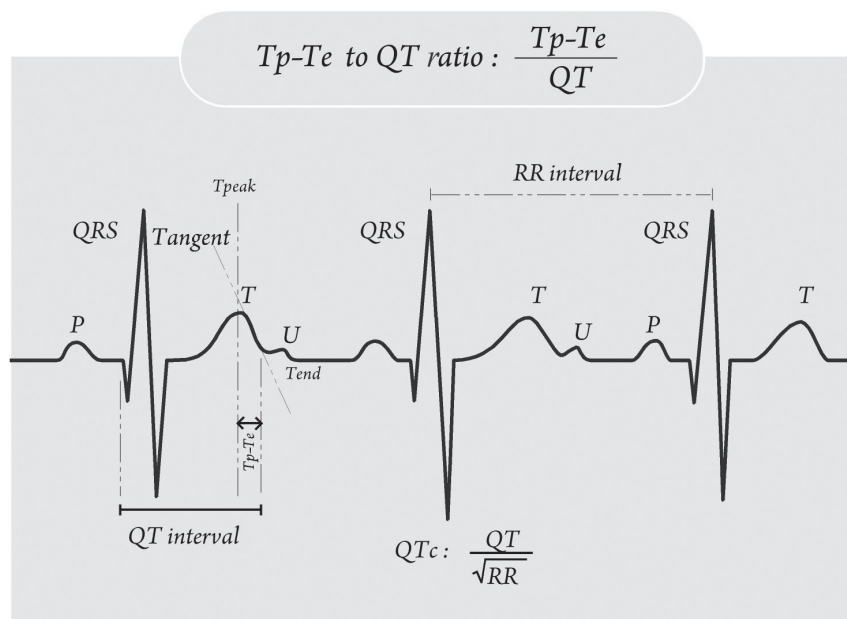


Fig. 1. Bazzett's formula and Tp-Te/QT ratio

the subsequent U wave). When the T wave was followed by a U wave, the lowest point between the T and U waves was determined as the endpoint of the T wave (Fig. 1).<sup>24,25</sup> The T peak was identified as the nadir of the T wave when negative or biphasic T waves were present (Fig. 3).<sup>24</sup>

In case of a notched T wave, the endpoint of the QT distance was identified by utilizing the tangent line defined by the downward part of the 2<sup>nd</sup> notch (Fig. 4). In the calculations, only the T wave amplitudes which were greater than 1.5 mm were included in the measurements. Otherwise they were neglected.<sup>25</sup>

All of the precordial derivations were used for the Tp-Te interval measurement records. The highest values were accepted as the Tp-Te intervals. The Tp-Te (d) values were determined by subtracting the values corresponding to the maximum and minimum Tp-Te intervals. The value of the Tp-Te/QT ratio was determined by dividing Tp-Te to QTmax values.

The QT interval was determined by intersecting the start value of the QRS with the final value of the T wave. This distance was evaluated by taking into account the T wave and the isoelectric line. The intersection of the tangent (drawn from the downward part of the T wave) and the isoelectric line yielded the QT interval.<sup>22</sup> Such measurements were taken from V1–V6 derivations. The QTmax values were recorded by determining the maximum values, and the QTc was determined using Bazett's formula.<sup>23</sup> (Fig. 1). The distance between the highest peak of the T wave and the endpoint of the T wave was identified as the Tp-Te interval (Fig. 2). The endpoint of the T wave was identified as the point of intersection of the tangent line and the isoelectric line (when a U wave was not subsequent to the T wave or if the T wave was not distinct from

### Echocardiography

In order to perform the transthoracic echocardiography, a Vivid 5 ultrasound machine with a 2.5-MHz transducer (GE Medical Systems, Milwaukee, USA) was used. The American Society of Echocardiography suggestions were followed.<sup>26</sup> M-mode echocardiography was used to measure interventricular septal thickness (IVS), posterior wall thickness (PW), and systolic and diastolic

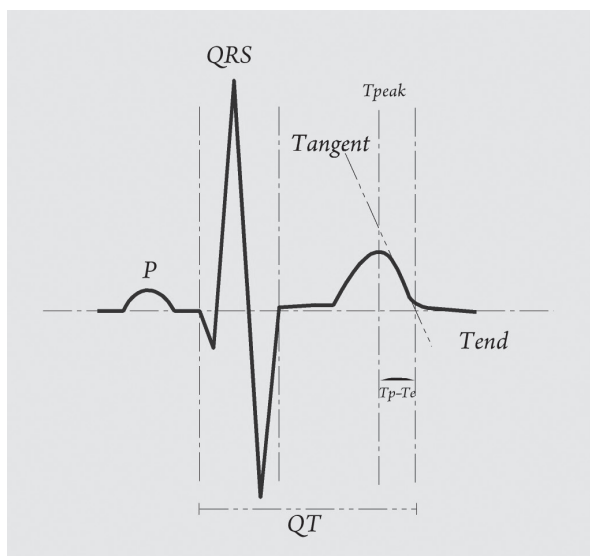


Fig. 2. The schematic presentation of the measurement of the Tp-Te and QT interval

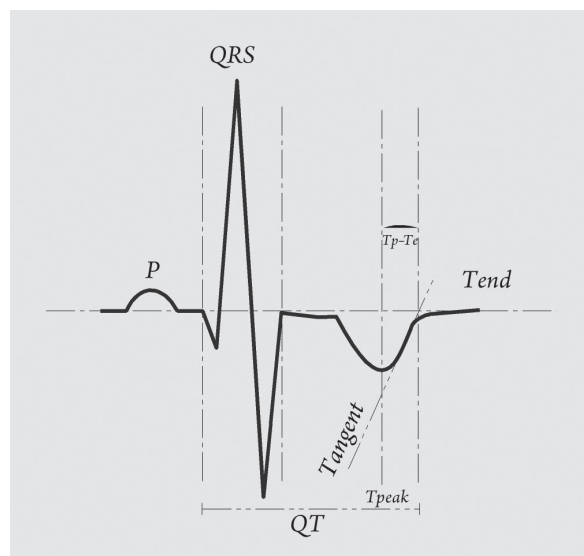


Fig. 3. The schematic presentation of the measurement of the Tp-Te interval in the presence of a negative T wave

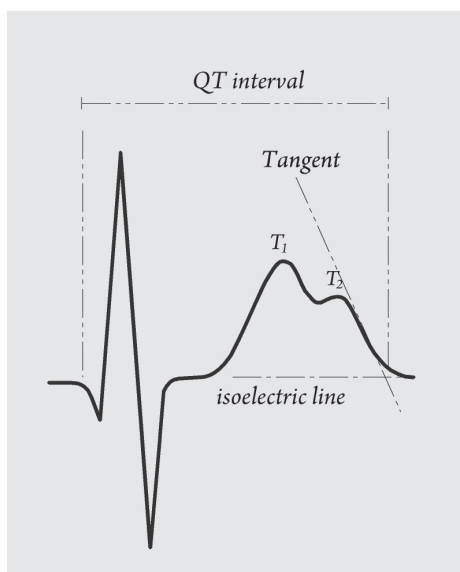


Fig. 4. Maximum slope intercept method in the presence of a notched T wave

diameters of the LV. The method that was utilized to determine the LV mass is Deveureux's formula<sup>27</sup>:

$$\text{LV mass [g]} = 0.8 \times [1.04 \times ((\text{LVEDD} + \text{IVSd} + \text{PWd})^3 - (\text{LVEDD})^3)] + 0.6$$

where LVEDD is the LV end-diastolic diameter.

The LV mass index was computed with the help of this formula<sup>27</sup>:

$$\text{LV mass index [g/m}^2\text{]} = \text{left ventricular mass/BSA}$$

Respectively, LVEDV (LV end-diastolic volume) and LVESV (LV end-systolic volume) values were computed as follows<sup>28</sup>:

$$\text{LVEDV [mL]} = (7/2.4 + \text{LVEDD}) \times \text{LVEDD}^3$$

$$\text{LVESV [mL]} = (7/2.4 + \text{LVESD}) \times \text{LVESD}^3$$

The LVEDV index (LVEDVI) was computed as follows<sup>28</sup>:

$$\text{LVEDVI [mL/m}^2\text{]} = \left( \frac{\text{LVEDV}}{\text{BSA}} \right)$$

LV ejection fraction (EF) and FS (fractional shortening) were determined with the help of the following formulas, respectively<sup>26</sup>:

$$\text{EF (\%)} = \left( \frac{\text{LVEDV} - \text{LVESV}}{\text{LVEDV}} \right) \times 100$$

$$\text{FS (\%)} = \left( \frac{\text{LVEDD} - \text{LVESD}}{\text{LVEDD}} \right) \times 100$$

## Exercise stress test

In order to conduct the stress test, a Cardiosis TEPA Exercise Stress Test device (TEPA Medical and Electronic Products Industry and Trade Company, Ankara, Turkey) was used. Specifically, the tests were done according

to the Bruce or modified Bruce treadmill protocols. Such protocols are known to be non-invasive for functional capacity and exercise tolerance for patients who likely do not have cardiovascular disorders.<sup>29</sup>

## Myocardial perfusion scintigraphy

Myocardial perfusion scintigraphy was carried out utilizing a treadmill according to Bruce or modified Bruce protocols. Sestamibi (MIBI) tagged with 10 mCi of <sup>99m</sup>Tc (Cardio-Spect; Medi-Radiopharma, Budapest, Hungary) was administered intravenously to the subjects when the maximum HR (85–100%) was reached. Gated single-photon emission computed tomography (SPECT) imaging was taken 30 min later. The imaging was carried out using a GE Infinia GP3 gamma monitor system (General Electric Healthcare, Tirat Carmel, Israel) with a low-energy high-resolution (LEHR) collimator. The images were evaluated using Emory Cardiac Toolbox (ECTb) myocardial quantification software (General Electric Healthcare Company).

## Statistical analysis

The statistical evaluation of the results was carried out with the help of SPSS v. 16.0 (SPSS Inc., Chicago, USA) analysis program for Windows. The fit of the continuous variables to a normal distribution was analyzed with the Kolmogorov–Smirnov test. The continuous variables are presented as means with standard deviations (SD) or medians with 25<sup>th</sup>–75<sup>th</sup> percentiles. Aside from the Tp–Te/QTc ratio and BSA [m<sup>2</sup>], none of the continuous variables were distributed normally, and the Kolmogorov–Smirnov test was used to evaluate these variables. A descriptive statistics test was used to evaluate the Tp–Te/QTc ratio and BSA [m<sup>2</sup>]. These values are presented as means ±SD. All other data is presented as medians with 25<sup>th</sup>–75<sup>th</sup> percentiles. Pearson's correlation test was used to perform correlation analyses. A value of  $p < 0.05$  was required for statistical significance.

## Results

Table 1 summarizes the baseline features of the participants. The study involved 1,485 healthy subjects (723 men and 762 women). The age of all participants, male participants and female participants was 42.0 years (30.0–53.5), 41.0 years (30.0–52.0) and 43.5 years (30.0–55.0), respectively. Table 1 also lists the findings for the ventricular repolarization parameters. The median Tp–Te interval was 66.0 ms (64.0–70.0), the Tp–Te/QT ratio was 0.18 (0.17–0.19), the mean Tp–Te/QTc ratio was  $0.16 \pm 0.014$ , and the median Tp–Te(d) was 15.0 ms (10.0–20.0) for all participants.

The results revealed that the Tp–Te/QT ratio significantly correlated with age, PW, IVS, LVEDD, BMI, BSA,

**Table 1.** Clinical characteristics of the study population

Parameters	All participants n = 1,485	Men n = 723	Women n = 762
Age	42.0 (30.0–53.5)	41.0 (30.0–52.0)	43.5 (30.0–55.0)
Tp–Te [ms]	66.0 (64.0–70.0)	66.0 (63.0–70.0)	67.0 (64.0–70.0)
QTmax [ms]	361.0 (353.5–371.0)	360.0 (352.0–370.0)	362.0 (355.0–372.0)
QTc [ms]	398.73 (383.02–417.79)	393.56 (380.0–410.79)	402.77 (387.60–422.62)
Tp–Te/QT ratio	0.18 (0.17–0.19)	0.18 (0.17–0.19)	0.18 (0.18–0.19)
Tp–Te/QTc ratio <sup>#</sup>	0.16 ±0.014	0.17 ±0.015	0.16 ±0.014
Tp–Te(d) [ms]	15.0 (10.0–20.0)	14.0 (10.0–18.0)	15.0 (10.0–20.0)
HR	74.0 (69.0–80.0)	71.0 (68.0–78.0)	75.0 (70.0–80.0)
PW [mm]	8.0 (7.0–9.0)	8.0 (7.0–9.0)	7.5 (7.0–8.0)
IVS [mm]	8.0 (7.0–9.0)	8.0 (8.0–9.0)	8.0 (7.0–9.0)
LVEDD [mm]	44.0 (42.0–46.0)	45.0 (43.0–47.0)	42.5 (40.0–45.0)
Length [m]	1.68 (1.62–1.74)	1.74 (1.71–1.77)	1.62 (1.59–1.65)
Weight [kg]	75.0 (67.0–81.0)	79.0 (74.0–84.0)	68.0 (63.0–72.0)
BMI [kg/m <sup>2</sup> ]	26.10 (24.61–27.58)	26.12 (24.69–27.66)	26.08 (24.53–27.58)
BSA [m <sup>2</sup> ] <sup>#</sup>	1.84 ±0.16	1.95 ±0.11	1.74 ±0.12
LVEDV [mL]	87.68 (78.57–97.33)	92.44 (83.06–102.36)	80.82 (70.00–92.44)
LVEDV index [mL/m <sup>2</sup> ]	46.44 (42.40–51.45)	46.55 (42.88–51.04)	46.37 (41.94–51.92)
EF [%]	64.84 (62.14–68.11)	63.69 (61.04–66.30)	66.30 (63.26–69.41)
FS [%]	35.0 (33.33–37.5)	34.69 (32.60–36.36)	36.36 (34.09–38.46)
LV mass [g]	105.92 (89.97–132.92)	114.76 (99.92–138.32)	97.38 (82.49–119.17)
LV mass index [g/m <sup>2</sup> ]	57.55 (50.12–69.49)	59.33 (52.12–71.37)	55.33 (48.85–67.51)

BMI – body mass index; BSA – body surface area; EF – ejection fraction; FS – fractional shortening; HR – heart rate; IVS – interventricular septum; LV – left ventricle; LVEDD – left ventricular end-diastolic diameter; LVESD – left ventricular end-systolic diameter; LVEDV – left ventricular end-diastolic volume; LVESV – left ventricular end-systolic volume; PW – posterior wall; QTmax – QT maximum; QTc – QT corrected. <sup>#</sup> No other continuous values – except Tp–Te/QTc ratio and BSA [m<sup>2</sup>] – were normally distributed; the Kolmogorov–Smirnov test was used to evaluate these variables. A descriptive statistics test was used to evaluate Tp–Te/QTc ratio and BSA [m<sup>2</sup>].

**Table 2.** Ventricular repolarization parameters across age subgroups

Age subgroups (n)	Tp–Te [ms]	Tp–Te/QT ratio	Tp–Te/QTc ratio	Tp–Te(d) [ms]
10–19 years (116)	60.0 (58.0–63.0)	0.17 (0.16–0.18)	0.15 (0.14–0.16)	10.0 (5.0–10.0)
20–29 years (237)	63.0 (60.0–66.0)	0.18 (0.17–0.19)	0.16 (0.15–0.17)	10.0 (10.0–15.0)
30–39 years (322)	66.0 (63.0–68.0)	0.18 (0.17–0.18)	0.16 (0.15–0.17)	12.0 (10.0–16.0)
40–50 years (317)	67.0 (66.0–69.5)	0.18 (0.18–0.19)	0.17 (0.16–0.18)	15.0 (10.0–17.5)
50–59 years (311)	70.0 (67.0–70.0)	0.18 (0.18–0.19)	0.17 (0.16–0.18)	18.0 (10.0–20.0)
60–69 years (138)	70.0 (70.0–75.0)	0.19 (0.18–0.20)	0.17 (0.16–0.18)	20.0 (15.75–25.0)
70–79 years (44)	75.0 (70.0–80.0)	0.19 (0.19–0.20)	0.18 (0.17–0.18)	20.0 (20.0–29.0)

LVEDV, LVEDV index, LV mass, and LV mass index. Additionally, significant correlations were found between age and BMI ( $r = 0.416$ ;  $p < 0.0001$ ), BSA ( $r = 0.101$ ;  $p < 0.0001$ ), LVEDV index ( $r = 0.394$ ;  $p < 0.0001$ ), and LV mass index ( $r = 0.484$ ;  $p < 0.0001$ ).

## Discussion

The present study reports normal ECG TDR parameters by measuring the Tp–Te interval, Tp–Te(d) and the Tp–Te/QT ratio in a healthy population without any systemic/

cardiovascular disorders or risk factors for atherosclerosis (Tables 1 and 2). We demonstrated that there is a significant correlation between the TDR parameters and echocardiographic measurements (Table 3; Fig. 6). Notably, the TDR parameters increased with older age (Tables 2 and 3; Fig. 5).

Although the QT interval and QT dispersion measurements are important ECG predictors of ventricular arrhythmogenesis, some studies have questioned their prognostic importance.<sup>30</sup> The failure to adequately identify ECG parameters and to reach a consensus on the values identified – which is due to a variety of reasons – have spurred the search for a different assessment method for

**Table 3.** Pearson correlation analysis between ventricular repolarization parameters and echocardiographic parameters

Parameters	Tp–Te [ms]		Tp–Te/QT ratio		Tp–Te/QTc ratio		Tp–Te(d) [ms]	
	r	p-value	r	p-value	r	p-value	r	p-value
Age	0.583	<0.0001	0.297	<0.0001	0.350	<0.0001	0.476	<0.0001
PW [mm]	0.631	<0.0001	0.464	<0.0001	0.414	<0.0001	0.486	<0.0001
IVS [mm]	0.641	<0.0001	0.467	<0.0001	0.415	<0.0001	0.505	<0.0001
LVEDD [mm]	0.578	<0.0001	0.481	<0.0001	0.424	<0.0001	0.460	<0.0001
BMI [kg/m <sup>2</sup> ]	0.520	<0.0001	0.421	<0.0001	0.406	<0.0001	0.394	<0.0001
BSA [m <sup>2</sup> ]	0.204	<0.0001	0.191	<0.0001	0.213	<0.0001	0.136	<0.0001
LV mass [g]	0.708	<0.0001	0.548	<0.0001	0.484	<0.0001	0.560	<0.0001
LV mass index [g/m <sup>2</sup> ]	0.712	<0.0001	0.539	<0.0001	0.458	<0.0001	0.570	<0.0001
LVEDV [mL]	0.579	<0.0001	0.484	<0.0001	0.425	<0.0001	0.463	<0.0001
LVEDV index [mL/m <sup>2</sup> ]	0.550	<0.0001	0.450	<0.0001	0.366	<0.0001	0.453	<0.0001

BMI – body mass index; BSA – body surface area; IVS – interventricular septal thickness; LV mass – left ventricular mass; LVEDD – left ventricular end-diastolic diameter; LVEDV – left ventricular end-diastolic volume; PW – posterior wall thickness.

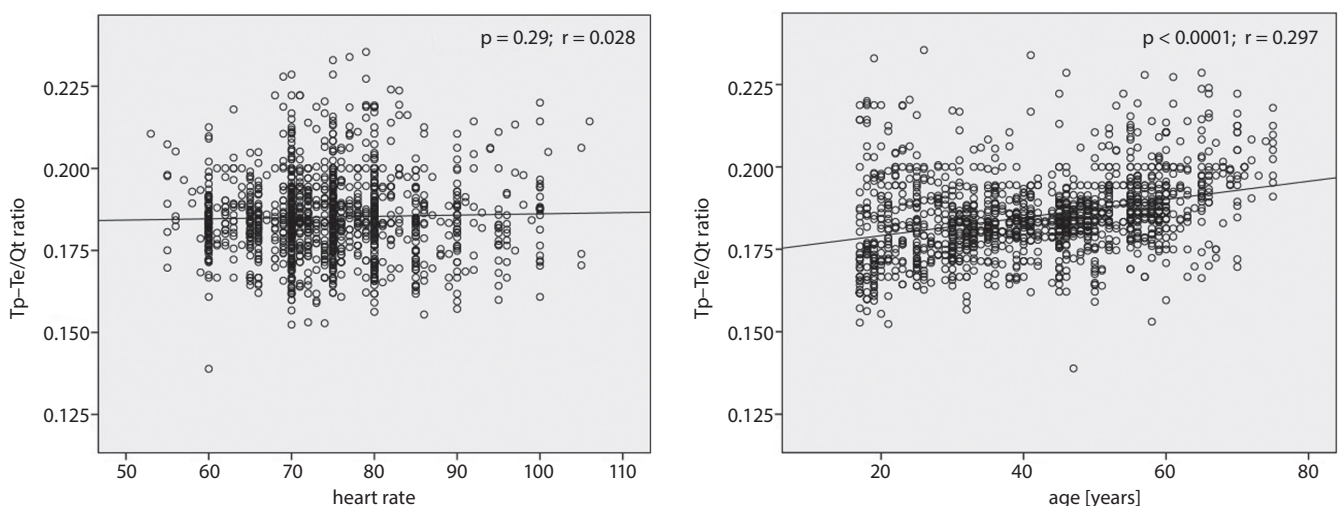
**Table 4.** Pearson correlation analysis between age and BMI, BSA, LVEDV index, and LV mass index

Parameters	BMI [kg/m <sup>2</sup> ]		BSA [m <sup>2</sup> ]		LVEDV index [mL/m <sup>2</sup> ]		LV mass index [g/m <sup>2</sup> ]	
	r	p-value	r	p-value	r	p-value	r	p-value
Age	0.416	<0.0001	0.101	<0.0001	0.394	<0.0001	0.484	<0.0001

the repolarization period.<sup>31</sup> The JT interval (the distance from the endpoint of the QRS structure to the endpoint of the T wave), the QT apex interval (the distance from the starting point of the QRS complex to the peak point of the T wave: QTa), and the T wave area (the total area below the J-point and the endpoint of the T wave) are examples of this search.<sup>32</sup> However, these novel repolarization parameters are no more accurate than conventional QT dispersion in assessing dispersion, and in some cases did not correlate with QT dispersion.<sup>32,33</sup>

In recent studies, the Tp–Te interval has been accepted as a TDR index.<sup>13,14</sup> However, variations in HR and body weight may affect the Tp–Te interval.<sup>15</sup> Ventricular myocardium is an electrically inhomogeneous construction

and is composed of 3 different cell types: epicardial, endocardial and M cells. The M cells (masonic midmyocardial Moe cells) are settled into the subendocardial lamina. These cells have a longer period of action potential than epicardial or endocardial cells when exposed to heart rate decelerating agents.<sup>15</sup> The period of action potential (PAP) is the longest in M cells. Among these 3 cell types, the M cells have the lowest, most slowly activating retarded potassium current (IKs) but the highest, late sodium current (INa). On the other hand, the density of the rapidly activating retarded potassium current (IKr) does not differ among the 3 layers. Thus, the discrepancy at the IKs/IKr ratio among the ventricular myocardial layers plays an important role in the transmural dispersion of TDR.<sup>33</sup>

**Fig. 5.** The correlations between age, heart rate and Tp–Te/QT ratio

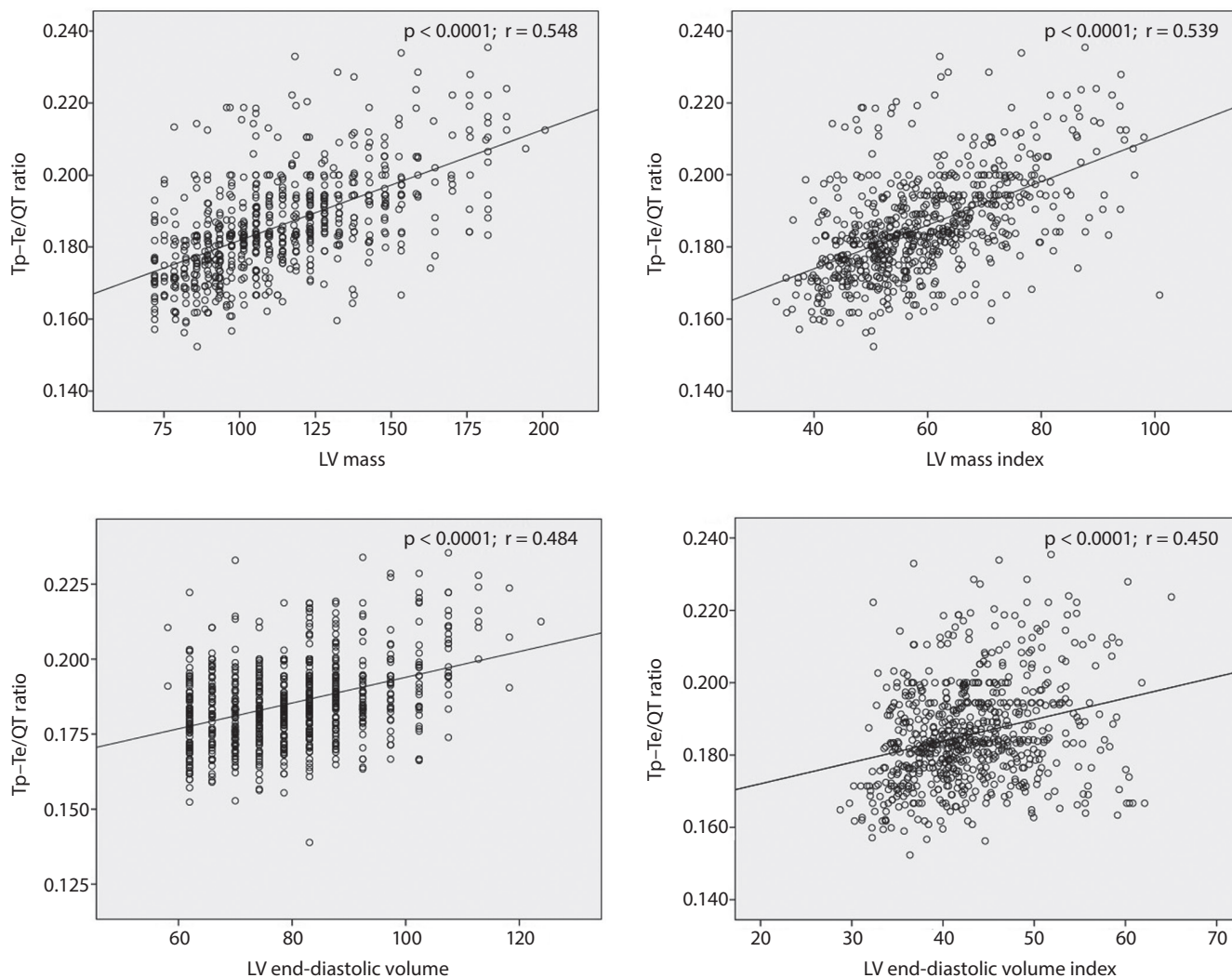


Fig. 6. The correlations between LV mass, LV mass index, LV volume, LV volume index, and Tp–Te/QT ratio

The epicardial cells complete their repolarization earlier than the other 2 cells. The highest point of the T wave (Tp) reflects the end of the epicardial PAP, and the final point of the T wave (Te) reflects the end of the midmyocardial PAP. Consequently, the Tp–Te duration is accepted as a representation of the TDR.<sup>17</sup> However, variations in HR might affect the Tp–Te duration.<sup>15</sup>

Recently, the Tp–Te/QT ratio has been accepted as a new, non-invasive ECG marker of ventricular repolarization inhomogeneity, and it has been suggested that it may be used as an accurate parameter of ventricular repolarization heterogeneity independent of changes in HR.<sup>15,16</sup> Gupta et al. also suggested that the Tp–Te/QT ratio is a more accurate indicator of ventricular arrhythmogenesis when compared with the QT, QTc and Tp–Te durations.<sup>15</sup> However, there are also conflicting reports on normal and abnormal values for these parameters.<sup>1,17–21</sup>

The present study demonstrated that the HR of healthy subjects varied from 53 bpm to 106 bpm. The Tp–Te duration diminished in parallel with an increase in HR, with the Tp–Te duration ranging from 50 ms to 86 ms

(66.0 (64.0–70.0) ms). Likewise, the Tp–Te/QTc ratio and Tp–Te(d) values diminished in parallel with increased HR. On the other hand, in spite of the alterations in HR, the Tp–Te/QT ratio remained stable with a median of 0.18 (0.17–0.19) (Fig. 5). The results suggest that the Tp–Te/QT ratio may be more appropriate than other parameters for assessing TDR.

Recent studies have demonstrated that risk factors for atherosclerosis, such as diabetes mellitus, hypertension and smoking – in addition to structural heart diseases and myocardial ischemia – give rise to an increase in ventricular repolarization parameters (TDR) and the heterogeneity of ventricular repolarization.<sup>1,16,17,19,23</sup> Furthermore, a number of studies have stated that LV enlargement and increased LV mass may be helpful indices for more ventricular arrhythmia risk stratification.<sup>34–36</sup> It has been reported that TDR parameters may increase with older age because of aging processes taking place in the myocardium, such as fibrosis.<sup>37</sup> Another explanation for the increased TDR with aging is distortion of the balance between sympathetic and parasympathetic tone in favor of sympathetic

**Table 5.** Pearson correlation analysis between BMI, BSA, LV mass, and LV mass index

Parameters	LV mass		LV mass index	
	r	p-value	r	p-value
BMI [kg/m <sup>2</sup> ]	0.447	<0.0001	0.265	<0.0001
BSA [m <sup>2</sup> ]	0.484	<0.0001	0.159	<0.0001

tone. In old age, this balance shifts substantially towards the sympathetic activity.<sup>38</sup> Increased sympathetic activity can cause several changes in myocardial membrane characteristics which cause early depolarizations and increased TDR.<sup>39–41</sup> Our study shows a relationship between age, BMI, BSA, and TDR parameters (Table 3). Although the mechanisms underlying such a relationship are not well-known, it is possible that an increase in sympathetic activity, BMI and BSA may lead to an increase in cardiac workload in these subjects, and this situation might be responsible for the increased LV mass and LV mass index (Tables 4 and 5).

Overlapping with previous research, the current study – which excludes myocardial ischemia and risk factors for atherosclerosis as well as systemic and structural heart disease – shows that BMI, BSA, age, and echocardiographic measurements have a direct effect on TDR parameters. The study demonstrated that the values of BMI, BSA, PW, IVS, LVEDD, BSA, LVEDV, LVEDV index, LV mass, and LV mass index among Turkish people increase with age; these findings significantly correlated with an elevated Tp–Te/QT ratio, suggesting an increased risk of ventricular arrhythmia (Tables 2–4; Fig. 6). More clearly, the LV mass and LV mass index values of Turkish people increase with age, and the Tp–Te/QT ratio increases along with these values (Tables 2–4). In other words, our data implies that aging and elevated BMI and BSA may cause increased ventricular repolarization heterogeneity via ventricular structural remodeling.

It is reasonable to suppose that the increase in myocardial mass, which leads to increased LV mass and LV mass index, may be caused by a further proportional increase in M cells, with the knowledge that M cells contribute more to repolarization time than epicardial and endocardial cells. However, an invasive method such as biopsy is required to enable a definitive evaluation of this link.

## Conclusions

The LV mass and LV mass index increase with age independently of the individual's health, and these parameters cause TDR values to increase. It is more rational to use the Tp–Te/QT ratio for TDR measurements because it is the least affected by HR. Future studies using the Tp–Te/QT ratio should evaluate the parameters of age, BMI, PW, IVS, LVEDD, BSA, LVEDV, LVEDV index, and LV mass and LV mass index in patient and control groups, and even if the individual appears healthy, it should be considered

in other situations (race, pregnancy, professions requiring intensive labor – such as portering and construction work – being a professional athlete, etc.) that may affect the individual's LV mass and LV mass index.

## ORCID iDs

Mücahid Yılmaz  <https://orcid.org/0000-0003-1458-8637>  
 Hidayet Kayaççiçek  <https://orcid.org/0000-0001-6493-5591>  
 Nevzat Gözel  <https://orcid.org/0000-0001-7326-6860>  
 Mehmet Nail Bilen  <https://orcid.org/0000-0003-1468-2930>  
 Ertuğrul Kurtoğlu  <https://orcid.org/0000-0001-5835-087X>  
 Özlem Seçen  <https://orcid.org/0000-0003-4657-8003>  
 Pınar Öner  <https://orcid.org/0000-0001-9592-5986>  
 Suat Demirkıran  <https://orcid.org/0000-0002-6769-8875>  
 Ökkeş Uku  <https://orcid.org/0000-0002-4392-7522>  
 Yusuf Çekici  <https://orcid.org/0000-0002-4585-3707>  
 Orkun Eroglu  <https://orcid.org/0000-0001-9392-5755>  
 Fikret Keleş  <https://orcid.org/0000-0003-1012-3875>

## References

- Karaagac K, Yontar OC, Tenekecioglu E, et al. Evaluation of Tp–Te interval and Tp–Te/QTc ratio in patients with coronary artery ectasia. *Int J Clin Exp Med.* 2014;7(9):2865–2870.
- Al-Zaiti SS, Fallavollita JA, Canty Jr JM, Carey MG. Electrocardiographic predictors of sudden and non-sudden cardiac death in patients with ischemic cardiomyopathy. *Heart Lung.* 2014;43(6):527–533.
- Schouten E, Dekker J, Meppelink P, Kok F, Vandenbroucke J, Pool J. QT interval prolongation predicts cardiovascular mortality in an apparently healthy population. *Circulation.* 1991;84(4):1516–1523.
- Di Iorio B. Relevance of qt dispersion in haemodialysis patients. *Nephrol Dial Transpl.* 2010;25(4):1357–1360.
- Malhis M, Al-Bitar S, Farhood S, Zaiat K. Changes in QT intervals in patients with end-stage renal disease before and after hemodialysis. *Saudi J Kidney Dis Transpl.* 2010;21(3):460–465.
- Genovesi S, Dossi C, Vigano MR, et al. Electrolyte concentration during haemodialysis and QT interval prolongation in uraemic patients. *Eurpace.* 2008;10(6):771–777.
- Ünal S, Yayla Ç, Açar B, et al. Tp–e interval and Tp–e/QT ratio in patients with human immunodeficiency virus. *J Infect Public Heal.* 2018;11(1): 35–38.
- Malik M, Batchvarov VN. Measurement, interpretation and clinical potential of QT dispersion. *J Am Coll Cardiol.* 2000;36(6):1749–1766.
- Punske BB, Lux RL, MacLeod RS, et al. Mechanisms of the spatial distribution of QT intervals on the epicardial and body surfaces. *J Cardiovasc Electrophysiol.* 1999;10(12):1605–1618.
- Surawicz B. Will QT dispersion play a role in clinical decision-making? *J Cardiovasc Electrophysiol.* 1996;7:777–784.
- Çelik T, Ilyisoy A, Çelik M, Işık E. The clinical significance of QT dispersion: How much reliable and beneficial? *Arch Turk Soc Cardiol.* 2007; 35(8):510–511.
- Fak AS, Tezcan H, Oktay A. QT dispersion: An interesting research field, or a useful diagnostic tool? *Arch Turk Soc Cardiol.* 2000;28:51–59.
- Kors JA, van Eck HJR, van Herpen G. The meaning of the Tp–Te interval and its diagnostic value. *J Electrocardiol.* 2008;41(6):575–580.
- Antzelevitch C, Sicouri S, Di Diego JM, et al. Does Tpeak–Tend provide an index of transmural dispersion of repolarization? *Heart Rhythm.* 2007;4(8):1114–1116.
- Gupta P, Patel C, Patel H, et al. Tp–e/QT ratio as an index of arrhythmogenesis. *J Electrocardiol.* 2008;41(6):567–574.
- Zhao X, Xie Z, Chu Y, et al. Association between Tp–e/QT ratio and prognosis in patients undergoing primary percutaneous coronary intervention for ST-segment elevation myocardial infarction. *Clin Cardiol.* 2012;35(9):559–564.
- Tokatli A, Kiliçaslan F, Alis M, Yiginer O, Uzun M. Prolonged Tp–e interval, Tp–e/QT ratio and Tp–e/QTc ratio in patients with type 2 diabetes mellitus. *Endocrinol Metab (Seoul).* 2016;31(1):105–112.
- Karaagac K, Emul A, Tenekecioglu E, et al. The effects of metabolic syndrome on Tp–Te interval and Tp–Te/QT ratio in patients with normal coronary arteries. *Eurasian J Med.* 2014;46(3):182–186.

19. Taşolar H, Ballı M, Bayramoğlu A, et al. Effect of smoking on Tp–e interval, Tp–e/QT and Tp–e/QTc ratios as indices of ventricular arrhythmogenesis. *Heart Lung Circ.* 2014;23(9):827–832.
20. İlgenli TF, Tokatlı A, Akpınar O, Kılıçaslan F. The effects of cigarette smoking on the Tp–e interval, Tp–e/QT ratio and Tp–e/QTc ratio. *Adv Clin Exp Med.* 2015;24(6):973–978.
21. Karaman K, Altunkaş F, Cetin M, et al. New markers for ventricular repolarization in coronary slow flow: Tp–e interval, Tp–e/QT ratio, and Tp–e/QTc ratio. *Ann Noninvasive Electrocardiol.* 2015;20(4):338–344.
22. Hevia JC, Antzelevitch C, Bárzaga FT, et al. Tpeak–Tend and Tpeak–Tend dispersion as risk factors for ventricular tachycardia/ventricular fibrillation in patients with the Brugada syndrome. *J Am Coll Cardiol.* 2006;47(9):1828–1834.
23. Yontar OC, Karaagac K, Tenekecioglu E, Tutuncu A, Demir M, Melek M. Assessment of ventricular repolarization inhomogeneity in patients with mitral valve prolapse: Value of T wave peak to end interval. *Int J Clin Exp Med.* 2014;7(8):2173–2178.
24. İcli A, Kayrak M, Akilli H, et al. Prognostic value of Tpeak–Tend interval in patients with acute pulmonary embolism. *BMC Cardiovasc Disord.* 2015;15:99.
25. Burns E. *ECG Basics: Waves, Intervals, Segments and Clinical Interpretation.* [https://lifeinthefastlane.com/ECG-Library.](https://lifeinthefastlane.com/ECG-Library/) Accessed May 20, 2018.
26. Lang RM, Bierig M, Devereux RB, et al. Recommendations for chamber quantification. *Eur J Echocardiogr.* 2006;7:79–108.
27. Lang RM, Bierig M, Devereux RB, et al. Recommendations for chamber quantification: A report from the American Society of Echocardiography’s Guidelines and Standards Committee and the Chamber Quantification Writing Group, developed in conjunction with the European Association of Echocardiography, a branch of the European Society of Cardiology. *J Am Soc Echocardiogr.* 2005;18(12):1440–1463.
28. Hudsmith LE, Petersen SE, Francis JM, Robson MD, Neubauer S. Normal human left and right ventricular and left atrial dimensions using steady state free precession magnetic resonance imaging. *J Cardiovasc Magn Reson.* 2005;7(5):775–782.
29. Bruce R, Blackmon J, Jones J, Strait G. Exercising testing in adult normal subjects and cardiac patients. *Ann Noninvasive Electrocardiol.* 2004;9(3):291–303.
30. Pueyo E, Martínez JP, Laguna P. Cardiac repolarization analysis using the surface electrocardiogram. *Philos Trans A Math Phys Eng Sci.* 2009;367(1887):213–233.
31. Kaya D, Guler C, Esen AM, Barutcu I, Dincel C. Sildenafil citrate does not alter ventricular repolarization properties: Novel evidence from dynamic QT analysis. *Ann Noninvasive Electrocardiol.* 2004;9(3):228–233.
32. Zabel M, Kligenheben T, Franz MR, Hohnloser SH. Assessment of QT dispersion for prediction of mortality or arrhythmic events after myocardial infarction: Results of a prospective, long-term follow-up study. *Circulation.* 1998;97(25):2543–2550.
33. Yan G-X, Lankipalli RS, Burke JF, Musco S, Kowey PR. Ventricular repolarization components on the electrocardiogram: Cellular basis and clinical significance. *J Am Coll Cardiol.* 2003;42(3):401–409.
34. Haider AW, Larson MG, Benjamin EJ, Levy D. Increased left ventricular mass and hypertrophy are associated with increased risk for sudden death. *J Am Coll Cardiol.* 1998;32(5):1454–1459.
35. Aleong RG, Mulvahill MJ, Halder I, et al. Left ventricular dilatation increases the risk of ventricular arrhythmias in patients with reduced systolic function. *J Am Heart Assoc.* 2015;4(8):e001566.
36. Narayanan K, Reinier K, Teodorescu C, et al. Left ventricular diameter and risk stratification for sudden cardiac death. *J Am Heart Assoc.* 2014;3(5):e001193.
37. Reardon M, Malik M. Qt interval change with age in an overtly healthy older population. *Clin Cardiol.* 1996;19(12):949–952.
38. Pfeifer MA, Weinberg CR, Cook D, Best JD, Reenan A, Halter JB. Differential changes of autonomic nervous system function with age in man. *Am J Med.* 1983;75(2):249–258.
39. Zipes DP. The long QT interval syndrome: A Rosetta Stone for sympathetic related ventricular tachyarrhythmias. *Circulation.* 1991;84(3):1414–1419.
40. Ben-David J, Zipes DP. Differential response to right and left ansae subclaviae stimulation of early afterdepolarizations and ventricular tachycardia induced by cesium in dogs. *Circulation.* 1988;78:1241–1250.



# Pharmacokinetics of xanthohumol in rats of both sexes after oral and intravenous administration of pure xanthohumol and prenylflavonoid extract

Beata Nowak<sup>1,A–D,F</sup>, Błażej Poźniak<sup>2,C–F</sup>, Jarosław Popłoński<sup>3,A,C–F</sup>, Łukasz Bobak<sup>3,C,E,F</sup>, Agnieszka Matuszewska<sup>1,B,E,F</sup>, Joanna Kwiatkowska<sup>1,B,F</sup>, Wojciech Dziewiszek<sup>1,B,E,F</sup>, Ewa Huszcza<sup>3,A,C,E,F</sup>, Adam Szela<sup>1,A,E,F</sup>

<sup>1</sup> Department of Pharmacology, Faculty of Medicine, Wrocław Medical University, Poland

<sup>2</sup> Department of Pharmacology and Toxicology, Faculty of Veterinary Medicine, Wrocław University of Environmental and Life Sciences, Poland

<sup>3</sup> Department of Chemistry, Faculty of Biotechnology and Food Science, Wrocław University of Environmental and Life Sciences, Poland

A – research concept and design; B – collection and/or assembly of data; C – data analysis and interpretation;

D – writing the article; E – critical revision of the article; F – final approval of the article

Advances in Clinical and Experimental Medicine, ISSN 1899–5276 (print), ISSN 2451–2680 (online)

Adv Clin Exp Med. 2020;29(9):1101–1109

## Address for correspondence

Beata Nowak

E-mail: beata.nowak@umed.wroc.pl

## Funding sources

National Science Centre, Poland,

Grant No. 2016/21/B/NZ7/02759.

## Conflict of interest

None declared

Received on April 28, 2020

Reviewed on May 20, 2020

Accepted on August 11, 2020

Published online on September 30, 2020

## Cite as

Nowak B, Poźniak B, Popłoński J. Pharmacokinetics of xanthohumol in rats of both sexes after oral and intravenous administration of pure xanthohumol and prenylflavonoid extract. *Adv Clin Exp Med.* 2020;29(9):1101–1109. doi:10.17219/acem/126293

## DOI

10.17219/acem/126293

## Copyright

© 2020 by Wrocław Medical University

This is an article distributed under the terms of the Creative Commons Attribution 3.0 Unported (CC BY 3.0) (<https://creativecommons.org/licenses/by/3.0/>)

## Abstract

**Background.** Female inflorescences of hops (*Humulus lupulus* L.) are widely used in the brewing industry. Hops have been also used for ages in folk medicine. Xanthohumol (XN) is a most abundant prenylated flavonoid present in hops.

**Objectives.** To determine pharmacokinetic parameters and bioavailability of pure XN and XN given in prenylflavonoid extract obtained from spent hops (HOP).

**Material and methods.** Fifty-six Wistar rats (28 females and 28 males) were administered with XN or HOP. Xanthohumol was administered either intravenously (iv.) (10 mg/kg) or orally (per os (p.o.)) (40, 100 and 200 mg/kg). Extract obtained from spent hops was administered p.o. and its doses were based on XN content (doses were equivalent to XN dose of 40, 100 and 200 mg/kg, respectively). After administration of XN or HOP serum, XN concentration was measured at different time points (0, 0.25, 0.5, 1, 2, 4, 6, 12, 24, 48, 72, and 96 h). Non-compartmental analysis was used to assess the pharmacokinetics (PK) of XN in rats.

**Results.** The XN PK in rats after intravenous administration is characterized by extensive distribution followed by delayed elimination from the body. Enterohepatic recirculation is likely to play a role in XN PK. Some fraction of the orally administered XN reaches central compartment rapidly; however, the overall absorption is very limited and probably saturable. The formulation-dependent factors also play an important role in the bioavailability of the drug. Although the C<sub>MAX</sub> concentration was higher in female rats receiving XN orally comparing to males, the other pharmacokinetic parameters were unaffected by the rats' sex.

**Conclusions.** The same doses of XN may be administered to male and female subjects, as its pharmacokinetics is not affected by sex.

**Key words:** bioavailability, pharmacokinetics, prenylflavonoid, rat, xanthohumol

## Introduction

Female inflorescences of hops (*Humulus lupulus* L.) are widely used in the brewing industry to preserve beer and to give beer aroma and flavor. Apart from being used in the brewing industry, hops have been used for ages in folk medicine. In traditional medicine, hops are used mainly to treat sleep disturbances. However, they are also used as stomachic, antibacterial and antifungal remedy.<sup>1</sup> They have also been known to be estrogenic,<sup>2</sup> and herbal remedies containing hops are used to alleviate menopausal symptoms.<sup>3</sup> Prenylated flavonoids belong to substances present in hops that contribute to their bioactivity, and xanthohumol (XN, Fig. 1) is the most abundant prenylated flavonoid present in hops.

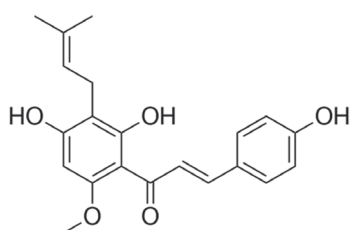


Fig. 1. Chemical structure of xanthohumol (XN)

Very few studies have been published on pharmacokinetics of XN and hop prenylflavonoids. On the one hand, reported studies investigated low doses of XN (1–17 mg/kg orally, 1.86 mg/kg intravenously (iv.)) and only male rats were used in these studies.<sup>4</sup> On the other hand, toxicological studies revealed that very high doses of XN are safe. The dose of 500 mg/kg induced no toxic effects and the dose of 1000 mg/kg was associated only with mild hepatotoxicity.<sup>5</sup> Taking these facts into account, we decided to investigate the pharmacokinetics of higher doses of XN and to investigate rats of both sexes. Additionally, we decided to compare pharmacokinetics of 2 formulations

of XN (pure XN and HOP) to evaluate whether compounds in extracts, mainly other prenylflavonoids, present in the extract affect the bioavailability of XN and its pharmacokinetics.

The aim of the present study was to compare the pharmacokinetic (PK) parameters of XN and prenylflavonoid extract in Wistar rats of both sexes, and to determine the influence of sex on the pharmacokinetics of XN. A single dose pharmacokinetic study was conducted at 3 oral (per os (p.o.)) dose levels and 1 iv. dose level in order to determine the bioavailability of XN and dependence of pharmacokinetic parameters on dose level, formulation (pure XN or HOP) and sex.

## Material and methods

### Plant materials and samples preparation of prenylflavonoid extract and xanthohumol

Xanthohumol and HOP used in animal studies were obtained from brewing industry waste – spent hops (Fig. 2). Spent hops were obtained from production of hop extracts (New Chemical Syntheses Institute, Puławy, Poland) by supercritical carbon dioxide extraction of hops *Humulus lupulus* cv. Magnum collected in 2015 in Lublin region (SE, Poland).

Prenylflavonoid extract was obtained as a result of semi-industrial and laboratory process. The first stage of production started at Wrocław Technology Park (Poland), where 92 kg of spent hops were added to 0.8 m<sup>3</sup> of acetone (POCH, Gliwice, Poland) in the batch reactor (2 m<sup>3</sup>) for 2 h with continuous stirring (120 rpm). The pulp formed was stirred for another 2 h at 30°C, left for sedimentation, and acetone fraction was pumped through a cotton bag filter (0.1 mm mesh) to vacuum-evaporatory module and the extract was concentrated

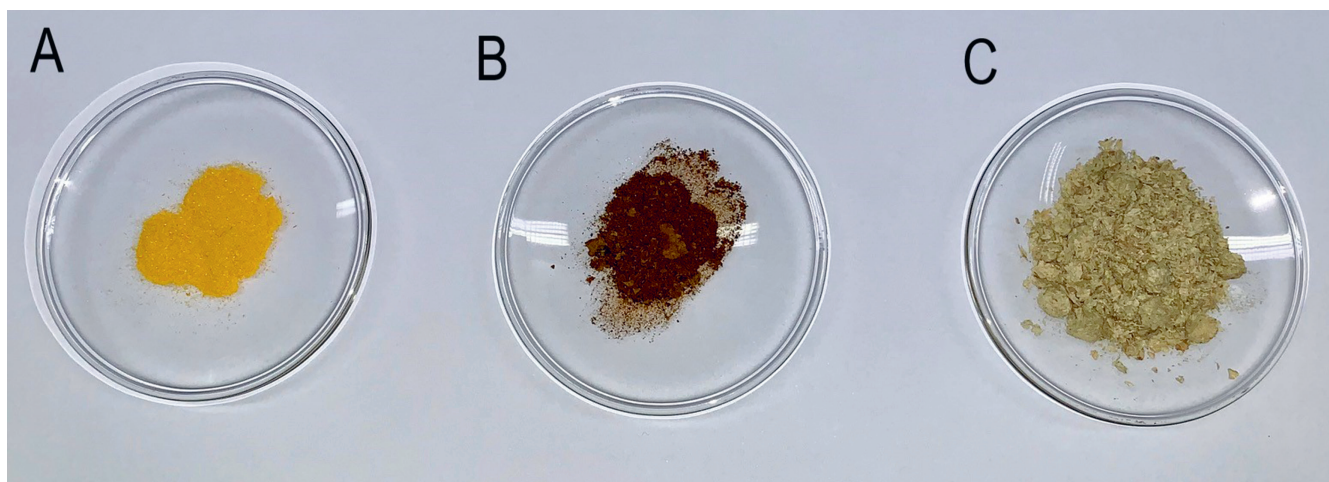


Fig. 2. Pure xanthohumol (A) prenylflavonoid extract (B) and spent hops (C)

under vacuum at 40°C to a volume of about 40 L, stored in a high-density polyethylene (HDPE) industrial barrel closed under nitrogen atmosphere at room temperature and used directly in further laboratory purification steps. Half a liter of the extract was concentrated with a rotary-evaporator to volume, at which the beginning of precipitation was observed, typically to about 80 mL; then 100 mL of ice cold 1M NaOH was added, followed by 400 mL of cold distilled water. The slurry obtained was centrifuged for 4 min at 3000 × g and the resulting supernatant was collected and acidified with ice-cold 1M HCl. A new precipitate was formed, collected, washed with cold distilled water, air dried and stored at –20°C. The precipitates (prenylflavonoid extract – HOP) consisting mainly XN (121 mg/g dry weight), isoxanthohumol (IXN), 41 mg/g dry weight) and polyphenol fraction were pooled, air dried, grinded and further used directly in animal studies or in the purification of XN.

Portions, 5–6 g, of precipitate were dissolved in 30 mL of MeOH (POCH) and purified on column chromatography with Sephadex LH 20 (GE Healthcare, Chicago, USA) and methanol as a mobile phase. Fractions were analyzed by TLC (Merck Silica Gel 60, F254, 0.2 mm, eluent: chloroform:methanol (9:1 v/v)) and fractions containing only XN were collected, evaporated and used after additional air drying in animal studies (>98% purity by HPLC/NMR). 6-prenylnaringenin (6PN), xanthohumol B (XN B) and xanthohumol D (XN D) standards were obtained as by-products during the purification of XN (results not shown). Xanthohumol C (XN C) was obtained by chemical oxidative cyclisation,<sup>6</sup> isoxanthohumol (IXN) by chemical isomerization of XN<sup>7</sup> and 8PN was obtained by chemical demethylation of XN.<sup>8</sup>

The XN content in XN batches and HOP was evaluated by HPLC on a Dionex Ultimate 3000 instrument (Thermo Fisher Scientific, Waltham, USA) with a diode array detector (detection at 360 nm wavelength) using the analytical HPLC column Agilent ZORBAX Eclipse XDB (Agilent, Santa Clara, USA) 5 µm (4.6 × 250 mm). Elution was carried out with a gradient of 40% to 100% of solvent B (1% formic acid in MeCN) in solvent A (aqueous 1% formic acid) in 15 min at the flow rate of 0.8 mL/min after the initial 2 min at 40% solvent B, then from 100% to 40% of solvent B over the course of 7 min and held for 2 min in 40% of solvent B. Isoxanthohumol content in HOP was evaluated with the same method, but detection was carried at 290 nm (Fig. 3). NMR spectra (1H-NMR) were recorded on a DRX Avance™ 600 (600 MHz) instrument (Bruker, Billerica, USA) in acetone-d<sub>6</sub> (Fig. 4).

## Animal study

The study was conducted on 56 12-week-old Wistar rats (28 males and 28 females, weighing 208.2 ± 17.3 g) that were housed under standard conditions of temperature

(21–23°C), humidity (60–70%), and a light-dark cycle (12:12 h). Animals were fed with a standard diet (LSM, Agropol, Motycz, Poland). Access to food and water was ad libitum and was monitored once daily.

Acclimated animals were randomized into 7 groups of 8 animals each (4 females and 4 males) receiving either XN or HOP: XN was administered either iv. (group XN-IV: 10 mg/kg), or p.o. (groups XN-L, XN-M and XN-H receiving 40, 100 and 200 mg/kg, respectively). Extract obtained from hops was administered p.o. and its doses were based on XN content (groups HOP-L, HOP-M and HOP-H received the extract at doses equivalent to XN dose of 40, 100 and 200 mg/kg, respectively).

For each oral dose level, appropriate amounts of XN powder or HOP were dissolved in dimethyl sulfoxide (DMSO) (Sigma-Aldrich, Darmstadt, Germany) (1 g of XN in 1 mL of DMSO) and then diluted in 0.9% saline solution. Animals received a single oral dose by gavage (40, 100 or 200 mg/kg in 2 mL solution/kg). The animals in the XN-IV group were given an iv. injection (10 mg/kg in 2 mL solution/kg) of XN dissolved in DMSO (1 g of XN in 1 mL of DMSO and diluted in 0.9% saline solution). Blood samples (0.3 mL) were obtained via catheter from the tail vein of each rat at the following time points: 0, 0.25, 0.5, 1, 2, 4, 6, 12, 24, 48, 72, and 96 h. After each blood draw, 0.3 mL of 0.9% saline solution was injected iv. and the catheter was flushed with heparinized saline (20 U/mL). Blood samples were placed in collection tubes coated with heparin and stored on ice immediately after collection. Samples were stored at –80°C until analysis for XN.

Study protocol was approved by the First Local Ethic Committee for Animal Experiments in Wrocław, Poland, and animal experiments were therefore performed in accordance with ARRIVE guidelines and were carried out in accordance with EU Directive 2010/63/EU for animal experiments.

## Sample preparation

Sample preparation procedure have been adapted from Legette et al.<sup>4</sup> with minor modifications. Aliquots of 50 µL of whole blood in duplicate were diluted with sodium acetate buffer (0.1M, pH 4.7), spiked with naringenin (NAR) (12.6 ng in 2-propanol) (Sigma-Aldrich,) as the internal standard, and treated with 600 U of *Helix pomatia* hydrolases dissolved in sodium acetate buffer (Sigma-Aldrich) for 3 h at 37°C in a total volume of 600 µL to convert conjugates (glucuronides and sulfates) into their free aglycone forms. After incubation, solutions were extracted thrice with diethyl ether (1 mL) and centrifuged for 1 min at 8500 g. The combined ether extracts were dried under a stream of nitrogen. The residues were dissolved in 0.1 mL of 0.1% formic acid solution in methanol, briefly vortexed, sonicated and analyzed directly by (LC-MS/MS).

Calibration curves were prepared by spiking blank rat whole blood with known concentrations of flavonoids

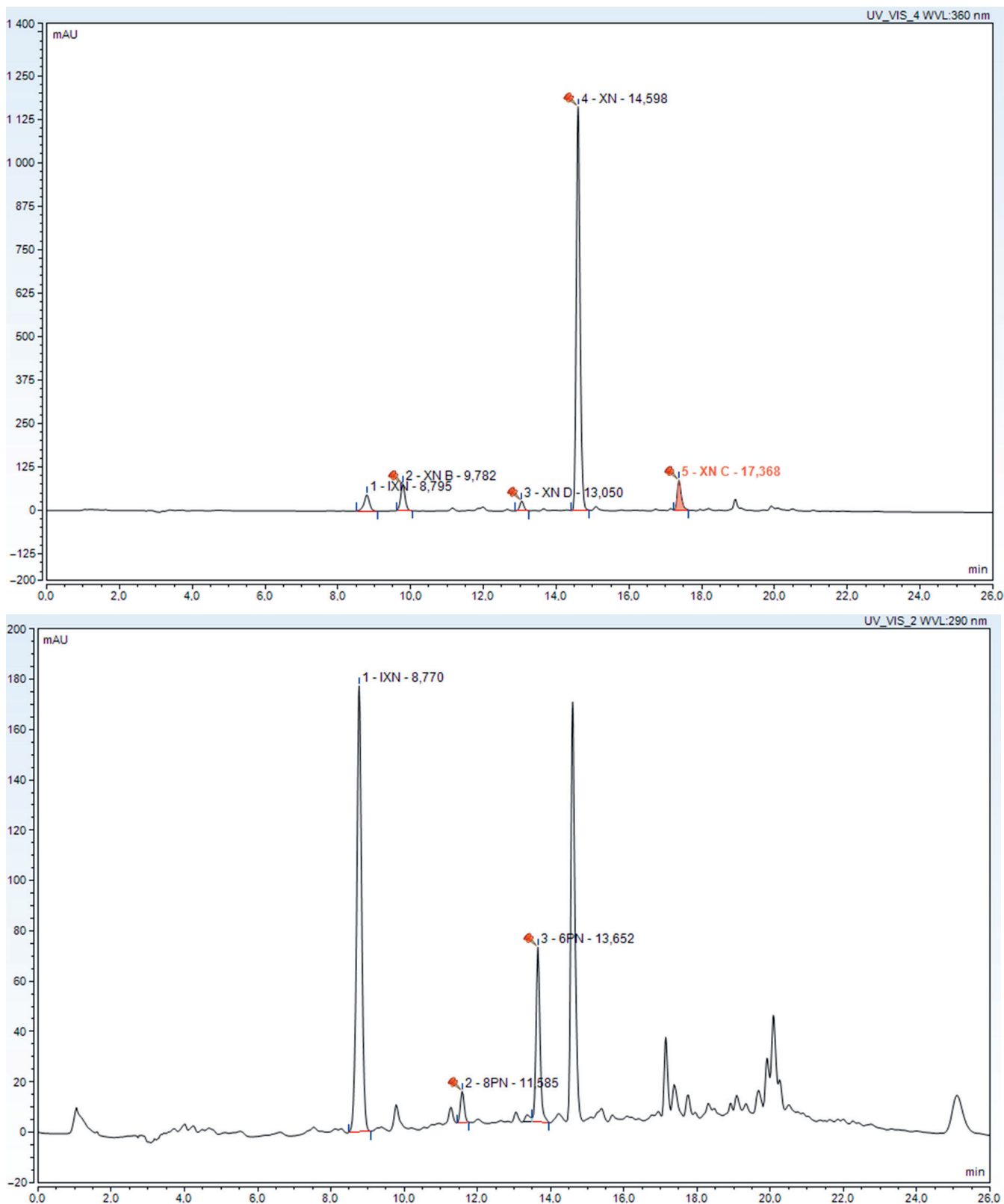


Fig. 3. HPLC chromatograms of HOP at 360 nm (left) and 290 nm (right)

and the internal standard, (NAR), using 16 concentration levels covering the entire concentration range for all analytes in the samples. The whole blood calibration samples were treated the same as the samples obtained from dosed animals. Limit of quantitation (LOQ)

represents the lowest concentration in a sample that can be determined with acceptable precision and accuracy ( $S/N > 10$ ), whereas limit of detection (LOD) represents the lowest concentration in a sample that can be detected ( $S/N > 3$ ).

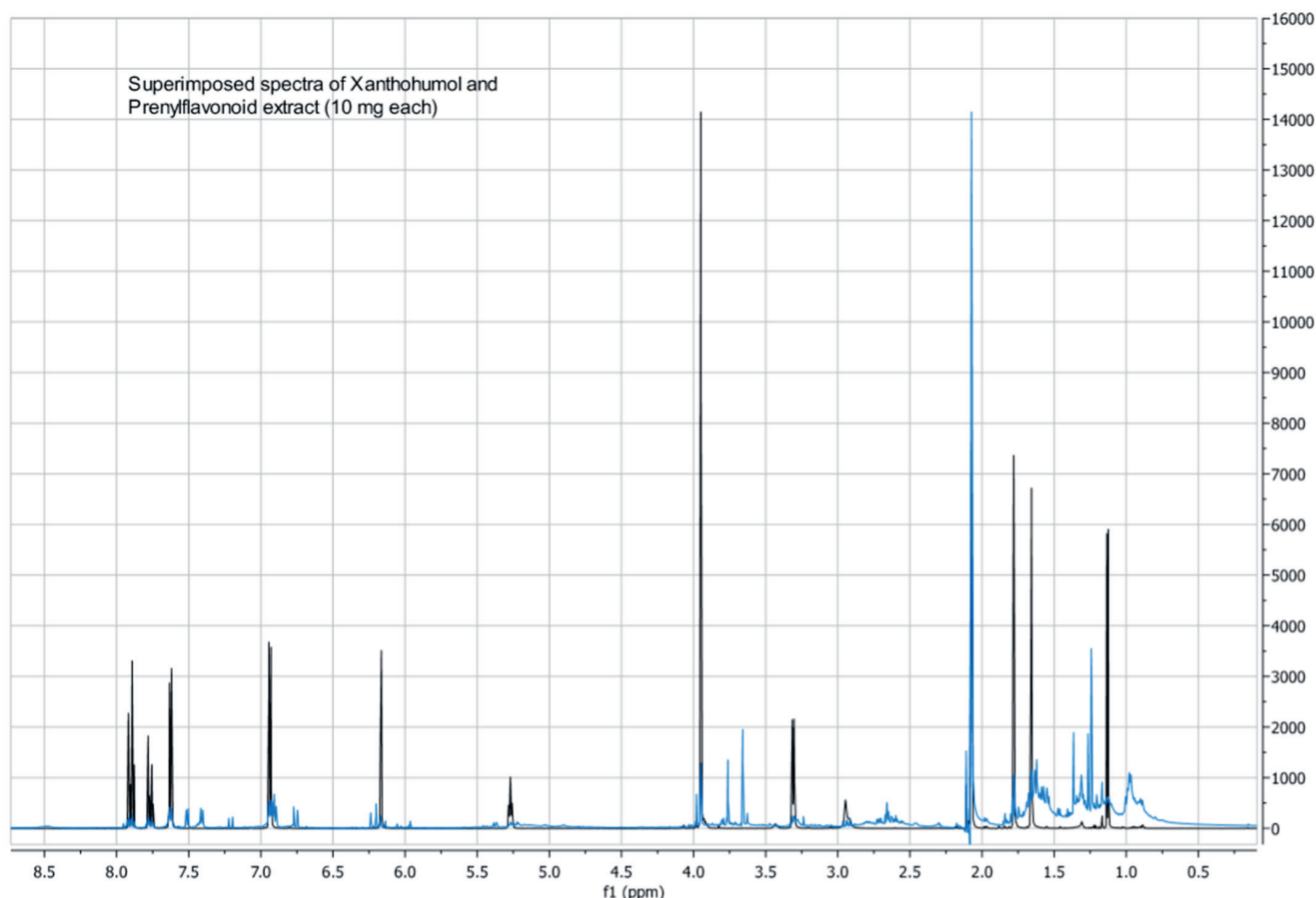


Fig. 4.  $^1\text{H}$  NMR spectrum of pure XN (grey) and HOP (blue)

## LC-MS/MS analysis

Liquid chromatography–mass spectrometry (LC-MS/MS) was performed on an Agilent 6400 triple quadrupole instrument (Agilent) operated at a source temperature of  $350^\circ\text{C}$  with a needle voltage of 4500 kV. Nitrogen was used as the source gas, curtain gas, and collision gas. Selected reaction monitoring (SRM) experiments were conducted at collision energies ranging from 25 to 40 eV. Concentrations were calculated using the internal standard calibration method.

The Agilent 1200 HPLC system (Agilent) was used in this study. Chromatographic separations of prenylflavonoids were achieved on a  $2.6\ \mu\text{m}$  Accucore C8 column  $150 \times 3\ \text{mm}$  (Thermo Fisher Scientific) eluted in a gradient from 25% to 60% solvent B (0.1% formic acid in ACN) in solvent A (aqueous 0.1% formic acid) over 8.5 min at a flow rate of 0.5 mL/min after an initial 2.0 min at 25% solvent B, then from 60% B to 100% B over 1.0 min. The column was washed with 100% solvent B for 2.0 min and re-equilibrated at 25% solvent B for 7 min prior to each injection. Precursor-product ion transitions for SRM were developed using standards. Selected reaction monitoring transitions used for quantitation included:  $[\text{M}]^-$  353-119 for XN and  $[\text{M}]^-$  271-119 for NAR.

## Pharmacokinetic analysis

Non-compartmental analysis was used to assess the pharmacokinetics (PK) of XN in rats (TP4.1 software; ThothPro, Gdańsk, Poland).

The following parameters were determined for iv. administration: the area under the concentration–time curve from time 0 to the last sampling ( $\text{AUC}_{0 \rightarrow t}$ ), the area under first moment curve from time 0 to the last sampling ( $\text{AUMC}_{0 \rightarrow t}$ ), mean residence time ( $\text{MRT}_{0 \rightarrow t}$ ), initial concentration ( $C_0$ ), relative body clearance ( $\text{Cl}_B$ ), relative apparent volume of distribution at steady state ( $\text{Vd}_{ss}$ ), elimination half-life ( $T_{1/2\text{el}}$ ) and biological half-life ( $T_{1/2}$ ). The areas were calculated by the trapezoidal rule. For the determination of  $T_{1/2\text{el}}$ , at least 3 last datapoints from the linear portion of the terminal slope were used. The  $T_{1/2}$  was calculated as follows:

$$T_{1/2} = \text{MRT}_{0 \rightarrow t} \times 0.693.^9$$

For the oral study,  $\text{AUC}_{0 \rightarrow t}$ ,  $\text{AUMC}_{0 \rightarrow t}$ ,  $\text{MRT}_{0 \rightarrow t}$ ,  $T_{1/2\text{el}}$ ,  $T_{1/2}$ , as well as the peak concentration ( $C_{\text{max}}$ ) and the time when it was observed ( $T_{\text{max}}$ ) were assessed. Mean absorption time (MAT) after oral administration was calculated as follows:  $\text{MAT} = \text{mean MRT}_{0 \rightarrow t} \text{ p.o.} - \text{mean MRT}_{0 \rightarrow t} \text{ iv.}$  The bioavailability (F) of orally administered XN was

calculated by comparing the AUCs of XN after p.o. and iv. administration according to the following formula:

$$F (\%) = \frac{\text{mean AUC}_{0 \rightarrow t} \text{ p.o.} \times \text{dose i.v.}}{\text{mean AUC}_{0 \rightarrow t} \text{ i.v.} \times \text{dose p.o.}} \times 100\%$$

Since numerous samples were found to contain very low and variable concentrations of XN, data below the limit of quantification (BLOQ) was not ignored but included calculations based on the method by Hornung and Reed.<sup>10</sup> All values appearing in the early part of the concentration-time curve were substituted by the value of LOQ/2 and treated as a real value. In the elimination phase, the first BLOQ value was substituted with LOQ/2 and the following BLOQ values were ignored.<sup>10,11</sup>

## Statistical analysis

The distribution of PK parameters was assessed by the Shapiro–Wilk test. Almost all parameters were characterized by normal distribution and were therefore compared with Student's t-test between groups. Only  $T_{\text{max}}$  lacked normal distribution and was compared using the Mann–Whitney U test. Statistical analysis was carried out by means of STATISTICA v. 13 (Tibco Software Inc., Palo Alto, USA) and Excel (Microsoft Corp., Redmond, USA).

## Results

Good linear relationship was obtained in the concentration range of 4.5–4500  $\mu\text{g/L}$  ( $y = 0.0005x + 0.0003$ ,  $R^2 = 0.9997$ )

of XN in whole blood. The LOQ and LOD for XN in the whole blood were 2.5  $\mu\text{g/L}$  and 0.4  $\mu\text{g/L}$ , respectively.

Figure 3A depicts the mean serum concentration-time profile of XN. The pharmacokinetic parameters are listed in Table 1. The elimination half-life of XN was 173.9 h and the half-life was 7.7 h.

The serum profile of XN after oral administration is shown in Fig. 3B for pure XN and in Fig. 3C for XN given in HOP. Pharmacokinetic parameters are listed in Table 1, showing the bioavailability of pure XN ranging from 0.96% to 1.16% and lower. After oral administration of pure XN (40, 100 and 200 mg/kg) and HOP in a dose equivalent for XN 200 mg/kg, XN was detectable up to 96 h, whereas after oral administration of HOP in doses equivalent for XN 40 and 100 mg/kg no XN was detected after 72 h. The  $\text{AUC}_{0 \rightarrow t}$  of XN was 7.7 times and 5.0 times higher for pure XN than for HOP for doses of 100 and 200 mg/kg, respectively. The  $C_{\text{MAX}}$  of XN was 2.3 times, 8.4 times and 11.7 times higher for pure XN than for HOP for doses of 40, 100 and 200 mg/kg, respectively.

Table 2 summarizes the influence of sex on XN pharmacokinetics.  $C_{\text{MAX}}$  was higher 1.7 times and 1.8 times in females than in males receiving XN in doses of 100 and 200 mg/kg, respectively.

## Discussion

The concentration-time curve and the PK parameters for the intravenous administration are shown in Fig. 3A and Tables 1 and 2, respectively. As can be appreciated from Fig. 3A, a relatively long distribution phase (lasting about

**Table 1.** Pharmacokinetic parameters (mean  $\pm$ SD) of xanthohumol after single intravenous or oral administration to rats ( $n = 8/\text{group}$ ). Groups IV, XN-L, XN-M, and XN-H received pure xanthohumol, whereas groups HOP-L, HOP-M and HOP-L were administered with prenylflavonoid extract that contained equivalent dose of xanthohumol

Parameter	Units	IV 10 mg/kg	Oral					
			40 mg/kg		100 mg/kg		200 mg/kg	
			XN – L	HOP – L	XN – M	HOP – M	XN – H	HOP – H
$\text{AUC}_{0 \rightarrow t}$	mg*h/L	13.60 $\pm$ 5.72	0.63 $\pm$ 0.34	–	1.31 $\pm$ 0.12	0.17 $\pm$ 0.06*	1.44 $\pm$ 0.49	0.29 $\pm$ 0.16*
$\text{AUMC}_{0 \rightarrow t}$	mg*h*h/L	93.95 $\pm$ 40.01	24.04 $\pm$ 14.94	–	42.83 $\pm$ 6.06	4.18 $\pm$ 2.56*	44.91 $\pm$ 12.04	8.56 $\pm$ 6.41*
$\text{MRT}_{0 \rightarrow t}$	h	7.95 $\pm$ 4.99	30.20 $\pm$ 16.23	–	33.01 $\pm$ 5.85	21.34 $\pm$ 10.02*	32.36 $\pm$ 6.35	24.98 $\pm$ 10.38
MAT	h	–	22.25	–	25.06	13.39	24.41	17.03
$\text{Cl}_{\text{B}(\text{rel})}$	L/h/kg	0.87 $\pm$ 0.33	–	–	–	–	–	–
$\text{Vd}_{\text{ss}(\text{rel})}$	L/kg	7.67 $\pm$ 6.78	–	–	–	–	–	–
$T_{1/2\text{el}}$	h	173.89 $\pm$ 131.09	127.49 $\pm$ 136.54	–	144.1 $\pm$ 131.5	–	–	–
$T_{1/2}$	h	7.67 $\pm$ 7.78	20.93 $\pm$ 11.25	–	22.88 $\pm$ 4.05	14.08 $\pm$ 7.54*	22.42 $\pm$ 4.40	17.31 $\pm$ 7.20
$C_{\text{MAX}}$	$\mu\text{g/L}$	9061 $\pm$ 4543	22.02 $\pm$ 2.18	9.46 $\pm$ 9.37*	90.64 $\pm$ 28.15	10.73 $\pm$ 4.47*	168.16 $\pm$ 59.38	14.38 $\pm$ 7.95*
$T_{\text{MAX}}$	h	–	1.31 $\pm$ 0.56	16.91 $\pm$ 21.99	1.19 $\pm$ 1.82	1.45 $\pm$ 1.42	0.88 $\pm$ 0.48	7.06 $\pm$ 9.84
F	%	–	1.16	–	0.96	0.13	0.53	0.11

IV – intravenous;  $\text{AUC}_{0 \rightarrow t}$  – area under the curve;  $\text{AUMC}_{0 \rightarrow t}$  – area under the first moment curve;  $\text{MRT}_{0 \rightarrow t}$  – mean residence time; MAT – mean absorption time;  $\text{Cl}_{\text{B}(\text{rel})}$  – relative body clearance;  $\text{Vd}_{\text{ss}(\text{rel})}$  – relative volume of distribution at steady state;  $T_{1/2\text{el}}$  – elimination half-life;  $T_{1/2}$  – half-life;  $C_{\text{MAX}}$  – peak plasma concentration;  $T_{\text{MAX}}$  – time to reach peak plasma concentration; F – absolute oral bioavailability.

\*  $p < 0.05$  as compared to the equivalent dose of pure xanthohumol.

**Table 2.** The influence of sex on pharmacokinetic parameters (mean  $\pm$ SD) of xanthohumol after single intravenous or oral administration of pure xanthohumol to rats of both sexes (n = 4/group)

Parameter	Units	IV		Oral					
		10 mg/kg		40 mg/kg		100 mg/kg		200 mg/kg	
		males	females	males	females	males	females	males	females
AUC <sub>0→t</sub>	mg*h/L	10.41 $\pm$ 2.96	16.79 $\pm$ 6.04	0.42 $\pm$ 0.37	0.84 $\pm$ 0.07	1.26 $\pm$ 0.12	1.36 $\pm$ 0.09	1.15 $\pm$ 0.25	1.73 $\pm$ 0.50
AUMC <sub>0→t</sub>	mg*h*h/L	78.64 $\pm$ 40.06	109.26 $\pm$ 33.59	15.76 $\pm$ 17.01	32.32 $\pm$ 4.50	46315 $\pm$ 35550	39.35 $\pm$ 6.06	42577 $\pm$ 11212	47.24 $\pm$ 12.38
MRT <sub>0→t</sub>	h	7.21 $\pm$ 1.85	8.70 $\pm$ 6.72	22.10 $\pm$ 19.55	38.30 $\pm$ 3.67	37.11 $\pm$ 4.54	28.91 $\pm$ 3.76	37.07 $\pm$ 5.04	27.65 $\pm$ 3.29*
MAT	h	–	–	14.89	29.60	29.90	20.21	29.85	18.95
Cl <sub>B(rel)</sub>	L/h/kg	1.03 $\pm$ 0.26	0.70 $\pm$ 0.31	–	–	–	–	–	–
Vd <sub>ss(rel)</sub>	L/kg	7.15 $\pm$ 1.72	8.18 $\pm$ 9.41	–	–	–	–	–	–
T <sub>1/2el</sub>	h	274.00 $\pm$ 114.91	73.76 $\pm$ 33.32	179.78 $\pm$ 176.49	75.21 $\pm$ 25.35	122.8 $\pm$ 87.12	172.5 $\pm$ 169.8	–	–
T <sub>1/2</sub>	h	4.99 $\pm$ 1.28	6.03 $\pm$ 4.66	15.31 $\pm$ 13.55	26.54 $\pm$ 2.54	25.72 $\pm$ 3.14	20.03 $\pm$ 2.61	25.69 $\pm$ 3.49	19.16 $\pm$ 2.28
C <sub>MAX</sub>	µg/L	11329 $\pm$ 4733	6793 $\pm$ 2930	21.50 $\pm$ 2.82	22.55 $\pm$ 1.01	66.61 $\pm$ 12.44	114.67 $\pm$ 16.58*	119.58 $\pm$ 18.96	216.74 $\pm$ 44.41*
T <sub>MAX</sub>	h	–	–	0.88 $\pm$ 0.22	1.75 $\pm$ 0.43	1.88 $\pm$ 2.38	0.50 $\pm$ 0.00	0.75 $\pm$ 0.25	1.00 $\pm$ 0.61
F	%	–	–	1.01	1.25	1.21	0.81	0.55	0.52

IV – intravenous; AUC<sub>0→t</sub> – area under the curve; AUMC<sub>0→t</sub> – area under the first moment curve; MRT<sub>0→t</sub> – mean residence time; MAT – mean absorption time; Cl<sub>B(rel)</sub> – relative body clearance; Vd<sub>ss(rel)</sub> – relative volume of distribution at steady state; T<sub>1/2el</sub> – elimination half-life; T<sub>1/2</sub> – half-life; C<sub>MAX</sub> – peak plasma concentration; T<sub>MAX</sub> – time to reach peak plasma concentration; F – absolute oral bioavailability.

\* p < 0.05 as compared to males receiving the same dose of xanthohumol.

10 h) is followed by an even longer and flat elimination. In some individuals (particularly males), concentrations in the elimination phase even exceed the concentrations at the end of the distribution phase. A similar rise in XN concentration after iv. administration of XN to rats has been reported by Legette et al.,<sup>4</sup> who have suggested enterohepatic recirculation as the underlying mechanism. Enterohepatic recirculation of hop prenylated phenols suggest also observation reported by Rad et al.<sup>12</sup> As can be seen in Table 2, no statistically significant differences between sexes have been found for iv. administration. Although there was a tendency of higher internal exposure (as expressed by AUC<sub>0→t</sub>) in females, high interindividual variability in this group and small number of animals preclude any firm conclusions. A relatively long MRT does not differ much between males and females. Volume of distribution is high and may suggest deep penetration into tissue(s). Although Cl<sub>B</sub> is slightly higher in males, the T<sub>1/2el</sub> estimates are also higher in this group suggesting somewhat slower elimination in males. The latter parameter, however, should be interpreted with caution as it may be biased by the aforementioned enterohepatic recirculation. The T<sub>1/2</sub>, which is less affected by the lack of linearity in the elimination phase, does not confirm any sex-related difference in XN elimination. The initial concentrations were somewhat higher in males but, again, high interindividual variability precludes firm conclusions.

Studies using the Caco-2 human intestinal epithelial model indicate that hop prenyled flavonoids are absorbed at a slow to moderate rate through the intestinal epithelium. XN accumulates in intestinal epithelial cells and then are gradually released to the general circulation,<sup>13</sup> while 8PN crosses the intestinal epithelium via passive

diffusion.<sup>14</sup> Tables 1 and 2 summarize the PK of XN administered orally at the dose of 40 mg/kg. Due to very low XN concentrations observed after administration of the HOP-L formulation, only the C<sub>MAX</sub> and the corresponding T<sub>MAX</sub> could be assessed. In the case of XN-L formulation, the C<sub>MAX</sub> was significantly higher as compared to HOP-L, and all PK phases could have been observed (Fig. 3B,C). Steep increase in blood XN followed by a pointed peak of C<sub>MAX</sub> may suggest zero-order absorption. Similar to the iv. administration, the distribution phase is followed by a flat and long elimination phase. No sex-dependent differences were observed in the PK parameters. A low AUC translated into low bioavailability of about 1%. Longer MRT values, as compared to iv. administration, resulted in very long MAT, particularly in females. Such a long MAT value could suggest a flip-flop phenomenon where the prolonged absorption is a limiting factor for the elimination.<sup>15</sup> However, this is not the case in the present study, as the absorption seems to be fast and there is no difference in the slope of the elimination phase between the intravenous and the oral studies (as seen in the T<sub>1/2el</sub>). Therefore, the current MAT estimations seem to be biased by the very low bioavailability of the oral formulations on the one hand, and slow elimination of the absorbed fraction of the drug on the other.

The administration of XN at the dose of 100 mg/kg in the formulation XN-M resulted in the proportional increase in the AUC without any visible effect on the absorption phase as seen in the lack of change in the MRT and MAT (Tables 1 and 2). This questions the possibility of zero-order absorption suggested by the shape of the curve in both XN-L and XN-M groups. The C<sub>max</sub>

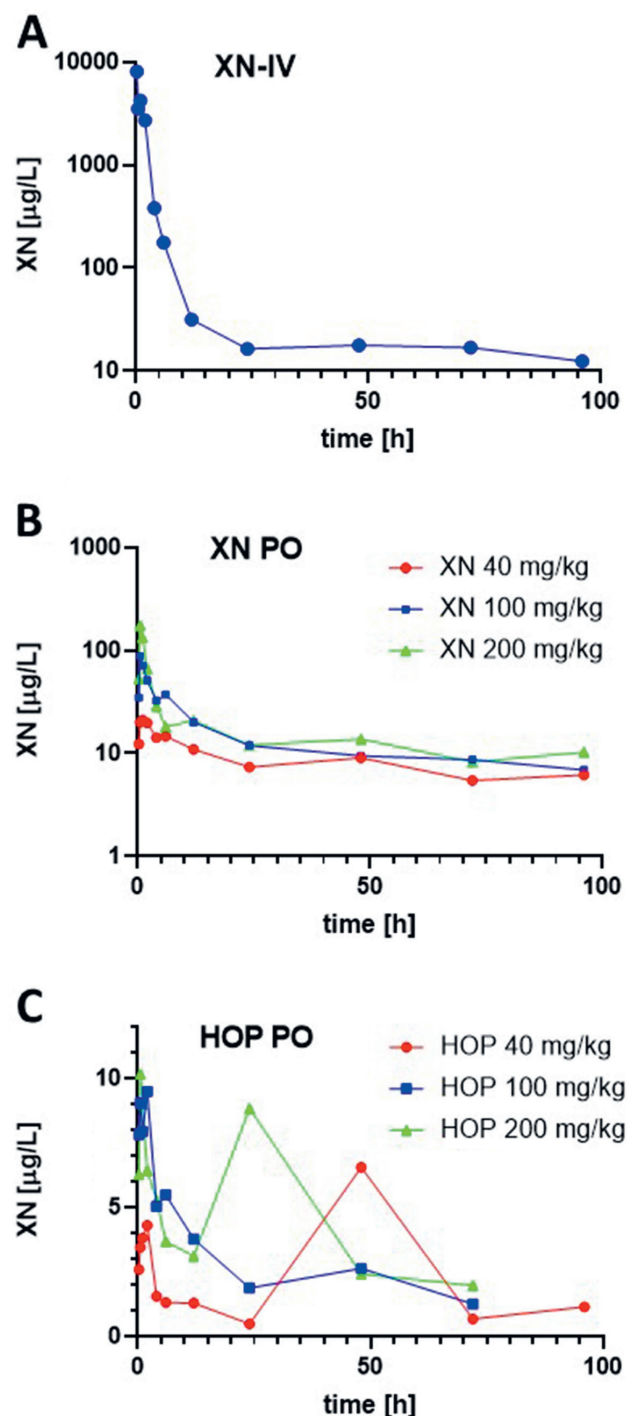


Fig. 5. Concentration-time profiles of xanthohumol in rat plasma following (A) intravenous injection (XN IV) of 10 mg/kg, (B) oral administration of pure xanthohumol (XN PO): 40 mg/kg, 100 mg/kg and 200 mg/kg, and (C) oral administration of prenylflavonoid extract (HOP PO): 40 mg XN/kg, 100 mg XN/kg and 200 mg XN/kg. Data is expressed as mean from 8 rats

was much higher in XN-M group, particularly in females, but the  $T_{\text{max}}$  was similarly short. Both half-lives were similar to the XN-L group, indicating no significant change in the elimination of the compound. In rats treated with the HOP-M formulation, the AUC was more than 7 times lower as compared to the rats administered with XN-M

(Table 1). Moreover, very low values (below LOQ) in 3 out of 4 females precluded PK analysis in these individuals. The MRT was significantly shorter and the mean  $C_{\text{MAX}}$  was about 9 times lower. The mean bioavailability of 0.13% should be considered extremely low. In the HOP-M group, it was not possible to calculate  $T_{1/2\text{el}}$  due to the lack of linearity in the elimination phase.

The saturation of XN absorption was much more visible in the PK of XN after the administration of the highest dose – 200 mg/kg (Tables 1 and 2). In the XN-H group, the mean AUC increased only very slightly as compared to the lower dose (XN-M), which translated into a drop in bioavailability (0.53%). Although the MRT, MAT and  $T_{1/2}$  were not changed, the lack of linearity in the elimination phase ( $T_{1/2\text{el}}$  impossible to calculate in 5 out of 8 individuals) may suggest limited/prolonged absorption.  $C_{\text{max}}$ , however, was proportionally higher as compared to the XN-M group. In the case of the HOP-L group, the saturated absorption is also seen in the less than proportional increase in the AUC and the drop in the bioavailability (as compared to HOP-M). The mean  $C_{\text{MAX}}$  is only slightly higher, and MAT,  $T_{\text{MAX}}$  as well as  $T_{1/2}$ , are prolonged. The concentration-time curve for this group lacks linear elimination and the presence of a secondary peak at 24 h further supports the presence of prolonged/disturbed absorption.

The lower bioavailability of HOP at every dosage level in comparison to similar dosage of pure XN is definitively associated with the complex composition of the prenylflavonoid extract. Despite the undertaken procedure of HOP preparation being highly selective for polyphenol fraction, the complete composition of the HOP cannot be determined. On the basis of the combined data from the HOP  $^1\text{H}$  NMR spectra (Fig. 4, especially the aromatic part 8.0–6.0 ppm) and HPLC analysis (Fig. 3), a rough estimation of total prenylflavonoid content in HOP would be about 30–35%, with XN and IXN being the most abundant. Therefore, it cannot be even speculated whether the complex matrix or other prenylflavonoids affects the bioavailability of XN from HOP.

## Conclusions

It is concluded that the XN PK in rats after intravenous administration is characterized by extensive distribution followed by delayed elimination from the body. Enterohepatic recirculation is likely to play a role in XN PK. Some fraction of the orally administered XN reaches the central compartment rapidly; however, the overall absorption is very limited and probably saturable. The formulation-dependent factors also play an important role in the bioavailability of the drug. Although the  $C_{\text{MAX}}$  concentration was higher in females receiving XN orally compared to males, the other pharmacokinetic parameters were unaffected by rats' sex. Therefore, the same doses of XN may be administered to males and females.

## ORCID iDs

Beata Nowak  <https://orcid.org/0000-0003-0014-6344>  
 Błażej Pożniak  <https://orcid.org/0000-0002-5813-1404>  
 Jarosław Popłoński  <https://orcid.org/0000-0002-7254-5937>  
 Łukasz Bobak  <https://orcid.org/0000-0002-4332-7252>  
 Agnieszka Matuszewska  <https://orcid.org/0000-0003-1082-0793>  
 Joanna Kwiatkowska  <https://orcid.org/0000-0002-2871-3366>  
 Wojciech Dziewiszek  <https://orcid.org/0000-0002-5788-5642>  
 Ewa Huszcza  <https://orcid.org/0000-0002-5950-3695>  
 Adam Szeląg  <https://orcid.org/0000-0001-8104-5267>

## References

- Zanoli P, Zavatti M. Pharmacognostic and pharmacological profile of *Humulus lupulus* L. *J Ethnopharmacol*. 2008;116:383–396. doi:10.1016/j.jep.2008.01.011
- Erkkola R, Vervarcke S, Vansteelandt S, Rompotti P, De Keukeleire D, Heyerick A. A randomized, double-blind, placebo-controlled, crossover pilot study on the use of a standardized hop extract to alleviate menopausal discomforts. *Phytomedicine*. 2010;17:389–396. doi:10.1016/j.phymed.2010.01.007
- Milligan SR, Kalita JC, Pocock V, et al. The endocrine activities of 8-prenylnaringenin and related hop (*Humulus lupulus* L.) flavonoids. *J Clin Endocrinol Metab*. 2000;85:4912–4915. doi:10.1210/jcem.85.12.7168
- Legette L, Ma L, Reed RL, et al. Pharmacokinetics of xanthohumol and metabolites in rats after oral and intravenous administration. *Mol Nutr Food Res*. 2012;56:466–474. doi:10.1002/mnfr.201100554
- Hussong R, Frank N, Knauff J, et al. A safety study of oral xanthohumol administration and its influence on fertility in Sprague Dawley rats. *Mol Nutr Food Res*. 2005;49:861–867. doi:10.1002/mnfr.200500089
- Popłoński J, Turlej E, Sordon S, et al. Synthesis and antiproliferative activity of minor hops prenylflavonoids and new insights on prenyl group cyclization. *Molecules*. 2018;23. doi:10.3390/molecules23040776
- Bartmańska A, Huszcza E, Tronina T. Transformation of isoxanthohumol by fungi. *J Mol Catal B Enzym*. 2009;61:221–224. doi:10.1016/j.molcatb.2009.07.008
- Anioł M, Szymańska K, Zołnierczyk A. An efficient synthesis of the phytoestrogen 8-prenylnaringenin from isoxanthohumol with magnesium iodide etherate. *Tetrahedron*. 2008;64:9544–9547. doi:10.1016/j.tet.2008.07.072
- Riviere JE. *Comparative Pharmacokinetics*. Oxford, UK: Wiley-Blackwell; 2011. doi:10.1002/9780470959916
- Hornung RW, Reed LD. Estimation of average concentration in the presence of nondetectable values. *Appl Occuo Env Hyg*. 1990;5:46–51.
- Ahn JE, Karlsson MO, Dunne A, Ludden TM. Likelihood based approaches to handling data below the quantification limit using NONMEM VI. *J Pharmacokinetic Pharmacodyn*. 2008;35:401–421. doi:10.1007/s10928-008-9094-4
- Rad M, Hümpel M, Schaefer O, et al. Pharmacokinetics and systemic endocrine effects of the phyto-oestrogen 8-prenylnaringenin after single oral doses to postmenopausal women. *Br J Clin Pharmacol*. 2006;62:288–296. doi:10.1111/j.1365-2125.2006.02656.x
- Pang Y, Nikolic D, Zhu D, et al. Binding of the hop (*Humulus lupulus* L.) chalcone xanthohumol to cytosolic proteins in Caco-2 intestinal epithelial cells. *Mol Nutr Food Res*. 2007;51:872–879. doi:10.1002/mnfr.200600252.
- Nikolic D, Li Y, Chadwick LR, Van Breemen RB. In vitro studies of intestinal permeability and hepatic and intestinal metabolism of 8-prenylnaringenin, a potent phytoestrogen from hops (*Humulus lupulus* L.). *Pharm Res*. 2006;23:864–872. doi:10.1007/s11095-006-9902-8
- Tanigawara Y, Yamaoka K, Nakagawa T, Uno T. Moment analysis for the separation of mean in vivo disintegration, dissolution, absorption, and disposition time of ampicillin products. *J Pharm Sci*. 1982;71:1129–1133. doi:10.1002/jps.2600711013



# The three-point bending test of fiber-reinforced composite root canal posts

Michał Biały<sup>1,A,B,D,F</sup>, Agnieszka Szust<sup>2,C,E,F</sup>, Piotr Napadtek<sup>1,B,E,F</sup>, Maciej Dobrzyński<sup>3,B,E,F</sup>, Włodzimierz Więckiewicz<sup>1,A,E,F</sup>

<sup>1</sup> Department of Dental Prosthetics, Wrocław Medical University, Poland

<sup>2</sup> Faculty of Mechanical Engineering, Wrocław University of Science and Technology, Poland

<sup>3</sup> Department of Conservative Dentistry and Pedodontics, Wrocław Medical University, Poland

A – research concept and design; B – collection and/or assembly of data; C – data analysis and interpretation;

D – writing the article; E – critical revision of the article; F – final approval of the article

Advances in Clinical and Experimental Medicine, ISSN 1899–5276 (print), ISSN 2451–2680 (online)

*Adv Clin Exp Med.* 2020;29(9):1111–1116

## Address for correspondence

Michał Biały

E-mail: [dentystamichalbialy@gmail.com](mailto:dentystamichalbialy@gmail.com)

## Funding sources

This research was financially supported by the Ministry of Health subvention according to the number of STM.B020.20.035 from the IT Simple system of Wrocław Medical University, Poland

## Conflict of interest

None declared

Received on March 28, 2020

Reviewed on May 25, 2020

Accepted on July 16, 2020

Published online on October 1, 2020

## Cite as

Biały M, Szust A, Napadtek P, Dobrzyński M, Więckiewicz W. The three-point bending test of fiber-reinforced composite root canal posts. *Adv Clin Exp Med.* 2020;29(9):1111–1116. doi:10.17219/acem/125426

## DOI

10.17219/acem/125426

## Copyright

© 2020 by Wrocław Medical University

This is an article distributed under the terms of the Creative Commons Attribution 3.0 Unported (CC BY 3.0) (<https://creativecommons.org/licenses/by/3.0/>)

## Abstract

**Background.** The primary reason for using a post is to retain the core with the objective to restore the missing coronal tooth structure. To achieve optimum results, the materials that are used to restore endodontically treated teeth should have physical and mechanical properties that are similar to that of dentin.

**Objectives.** To characterize the strength parameters of fiber-reinforced composite (FRC) posts with the application of a three-point test. The mean fracture load, flexural strength and flexural modulus were taken into consideration.

**Material and methods.** For the three-point strength tests, 5 kinds of fiberglass root-posts were used: GC Fiber Post (GC America, Alsip, USA), Mirafit White (Hager Werken, Duisburg, Germany), Innopost (InnoTech, Verona, Italy), Rebuilda Post (Voco, Cuxhaven, Germany), and EverStick Post (GC Europe, Leuven, Belgium). For each system, 15 FRC posts were tested. All posts had the same diameter, length and shape. The three-point test was carried out in accordance with ISO 10477:2004, using the Instron-5944 testing machine (Instron, Norwood, USA). The test was carried out until the sample was broken.

**Results.** The highest force values (67.6 N) were recorded for the GC posts, and the lowest force required to break the sample (29.6 N) was noted for the EverStick Posts. In the case of bending strength, the highest values were also recorded for GC posts (912.4 MPa). Low bending strengths were obtained for the Mirafit White posts (537.2 MPa); however, the EverStick Posts were the weakest (436.2 MPa). Rebuilda posts showed the highest modulus of elasticity – 31.1 GPa. The lowest values of the elastic modulus were registered for EverStick Posts – 12.5 GPa.

**Conclusions.** There were statistically significant differences in fracture loads, flexural strengths and flexural modulus of the FRC-post systems tested. Individually polymerized FRC material showed lower flexural properties than compared prefabricated FRC posts.

**Key words:** three-point bending test, flexural modulus, flexural strength, fiber-reinforced composite post, individually formed post

## Introduction

Posts provide retention for dental materials while the missing coronal tooth structure is being restored. They do not strengthen the tooth.<sup>1,2</sup> To achieve optimum results, the materials that are used for restoration of endodontically treated teeth should have physical and mechanical properties similar to dentin.<sup>3</sup> There is a difference of opinion whether a post should have an elastic modulus close to dentin<sup>4–6</sup> or whether it should be more rigid.<sup>7,8</sup> Posts can be classified based on the elastic modulus, with metallic posts (prefabricated or cast metal posts), ceramic posts and carbon fiber posts presenting high values, and glass fiber posts presenting low elastic modulus.<sup>9,10</sup> Prefabricated and cast metal posts are rigid in nature.<sup>11</sup> The rigidity may pose a risk for root fracture. One of the major reasons that motivated researchers to find alternative solutions to metal posts was to prevent root fracture, which was the main cause of failure with this type of restoration. The biomechanical properties of fiber-reinforced composite (FRC) posts have been reported to be similar to that of dentin.<sup>12–14</sup> Clinical prospective and retrospective studies on the use of fiber posts have reported encouraging results.<sup>15–19</sup>

The first FRC-posts were made of carbon/graphite fibers due to their good mechanical properties. However, they are black in color and thus lack cosmetic qualities. Instead posts made of glass or silica fibers are white or translucent and can be used in situations of higher cosmetic demand.<sup>12,20</sup>

Dental market offers prefabricated and individually formed glass fiber posts. However, prefabricated FRC posts have limitations in their properties, such as poor anatomical fit to the canal. They require preparation of the root canal to fit the shape of the post, which causes loss of dentin and makes the root more vulnerable to root fracture.<sup>21</sup> This emphasizes the importance of trying to preserve the original anatomy of the root canal and minimizing dentin loss throughout the endo-restorative treatment.<sup>22,23</sup> Large root preparation can be avoided by using individually formed FRC posts.<sup>12,24–26</sup> An individually formed FRC post can be polymerized in situ in the root canal, thus precisely following the shape of the canal.<sup>27</sup> The manufacturer's recommendation has been to light-polymerize in 2 phases; first, a short curing is carried out when the post material is placed in the root canal to copy the anatomical shape of the canal. After that the final curing is carried out after removing the post from the canal to ensure complete curing also at the apical parts of the post.

The polymer matrix of individually formed FRC post material consists of both linear and cross-linked phases, which is called semi-interpenetrating polymer network (IPN).<sup>21</sup> This matrix also allows the formation of secondary IPN bonding based on interdiffusion of the resin systems of post and luting cement. The IPN system improves adhesion to composite and increases flexural strength and fatigue strength through the reduction of crack initiation.

Polymer matrix of the FRC post used in the present study is composed of cross-linking monomer system of bisphenol-A-dimethacrylate (Bis-GMA) and linear polymers of polymethyl methacrylate (PMMA) which structurally form semi-interpenetrating polymer networks (semi-IPN).<sup>21</sup> Resiliency of semi-IPN based composites is higher and modulus of elasticity is lower compared to polymer made of crosslinking monomers only.<sup>28,29</sup>

The aim of this study is to:

1) characterize the strength parameters of FRC posts with the application of a three-point test. The mean fracture load, flexural strength and flexural modulus were taken into consideration.

2) compare the properties of prefabricated FRC posts with custom-made FRC posts in the form of a tape, which achieve full stiffness after the exposure to a polymerization lamp.

3) establish which FRC posts are the most suitable for clinical use.

## Material and methods

For this study, 5 different types of endodontic post were selected:

- group 1: GC Fiber Post (GC America, Alsip, USA);
- group 2: Mirafit White (Hager Werken, Duisburg, Germany);
- group 3: Innopost (InnoTech, Verona, Italy);
- group 4: Rebuilda Post (Voco, Cuxhaven, Germany); and
- group 5: EverStick (GC Europe, Leuven, Belgium).

Seventy-five endodontic posts, 15 for each group, were tested. All fiber posts were 1.2 mm in diameter, 20 mm in length and had a cylindrical shape with a tapered end. In order to reduce the influence of the conical end of the posts, a 10 mm parallel part of the post was used for the tests.

The EverStick fiber material containing silanized E-glass fibers in light-polymerizable dimethacrylate – polymethylmethacrylate matrix was made into a cylindrical shaped specimen with a diameter of 1.2 mm. EverStick Posts were treated according to the manufacturers' instructions. Tweezers were used to take the post out from the silicone. The length and suitability were checked using electronic caliper. The specimens were polymerized in a light curing lamp for 60 s. A light-polymerizing device (Elipar S10; 3M Espe, Maplewood, USA) with halogen lamp radiating blue light (wavelength 430–480 nm) and with an intensity of 1200 mW/cm<sup>2</sup> was used.

The three-point bending test according to the ISO 10477 standard (span 10.0 mm, crosshead speed 1.0 mm/min, cross-sectional diameter of loading tip 2 mm) was used to measure the flexural strength and modulus of FRC post specimens. All posts were tested with the material testing machine Instron-5944 (Instron, Norwood, USA). The test was carried out until the sample was broken

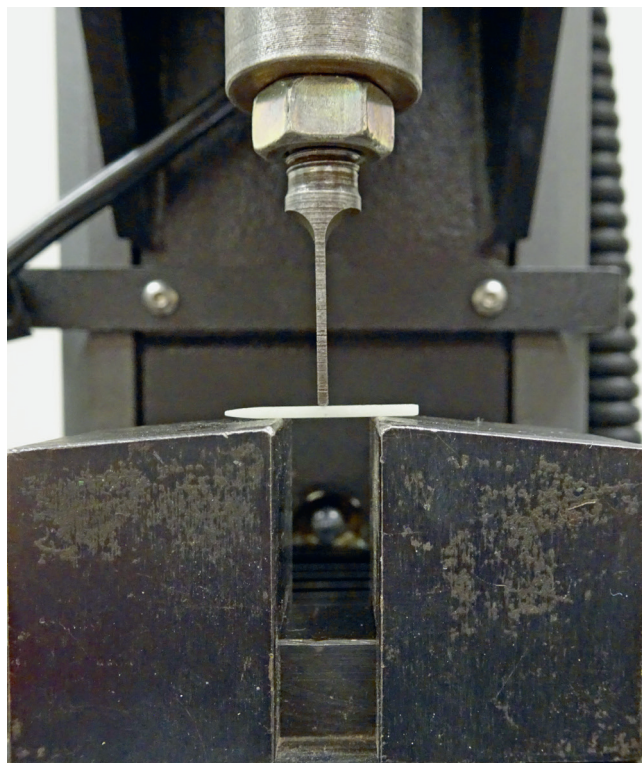


Fig. 1. The post during three-point bending test

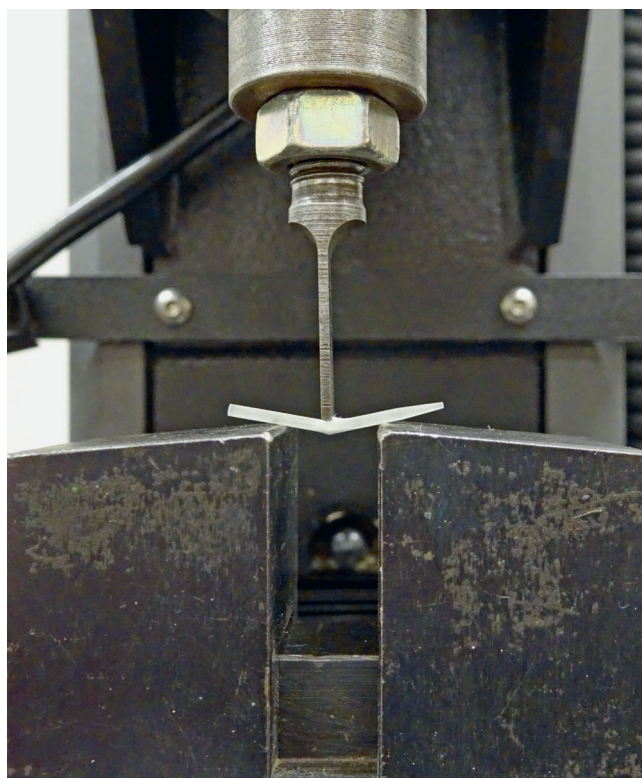


Fig. 2. The broken post after three-point bedning test

(Fig. 1,2). All the tests were carried out in temperature about 22°C. Fracture load of post was measured. Flexural strength ( $\sigma$ ) and flexural modulus (E) were calculated from the formula:

$$\sigma = 8F_{\max} L / \pi d^3 \text{ [MPa]}$$

$$E = 4F_{\max} L^3 / (D3\pi d^4) \text{ [GPa]},$$

where:  $F_{\max}$  is the maximum load point of the load-deflection curve [N], L is the distance between the support rollers (10.0 mm), d is the diameter of the specimens [mm], and D is deflection [mm] at  $F_{\max}$  [16] at a point in the straight-line portion of the trace.

The differences between specimens were evaluated using Kruskal–Wallis nonparametric analysis of variance (ANOVA) and the median test. The probability level was set at 0.05.

## Results

In the conducted three-point test, the values of maximum forces that caused damage to the FRC post were observed (Table 1). The ANOVA revealed significant differences ( $p = 0.05$ ) in fracture loads, flexural strengths and flexural modulus of the FRC-post systems tested. The highest force values (67.6 N) were recorded for the GC Fiber Posts and the lowest force required to break the sample (29.6 N) was noted for the EverStick Posts (Fig. 3). In the case of bending strength, the highest values were also recorded for GC Fiber Posts – 912.4 MPa (Fig. 4). Low bending strengths were obtained for the Mirafit White posts (537.2 MPa); however, the EverStick Posts were the weakest (436.2 MPa). The elastic modulus was also calculated. Rebuilda posts showed the highest modulus of elasticity – 31.1 GPa (Fig. 5). Slightly lower modulus was recorded for GC Fiber Posts – 30.9 GPa; however, the lowest values of the elastic modulus were registered for Mirafit White posts and EverStick Posts – 21.7 GPa and 12.5 GPa, respectively. The elastic module of EverStick Posts proved to be lower than the dentine elasticity modulus, which was  $17.5 \pm 3.8$  GPa.

Table 1. The fracture load and flexural properties

Group	Posts type	Fracture load [N]	Flexural strength [MPa]	Flexural modulus [GPa]
Group 1	GC Fiber Post	67.6 ±3.9	992.4 ±58.3	30.9 ±0.9
Group 2	Mirafit White	36.5 ±3.2	537.2 ±47.3	21.7 ±0.9
Group 3	Innopost	52.5 ±4.3	773.5 ±59.6	23.5 ±1.6
Group 4	Rebuilda Post	65.3 ±3.3	962.1 ±48.6	31.1 ±1.1
Group 5	EverStick Post	29.6 ±5.1	436.2 ±75.9	12.5 ±2.7

## Discussion

Many studies investigating the flexural properties of root canal posts have been published, reporting results that varied greatly.<sup>2,12,30–32</sup> The flexural modulus parameter

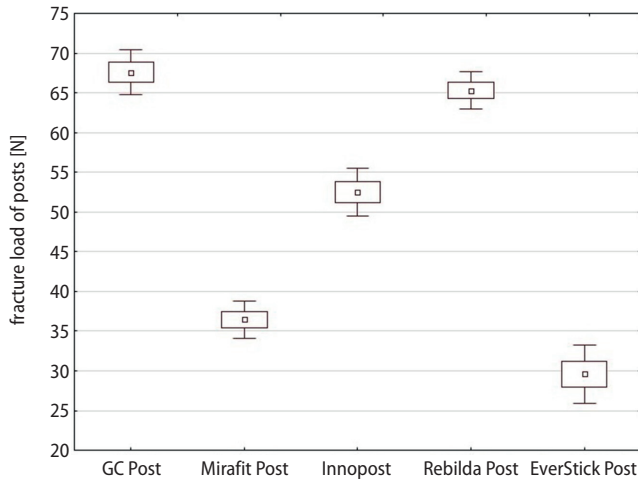


Fig. 3. The fracture load of posts

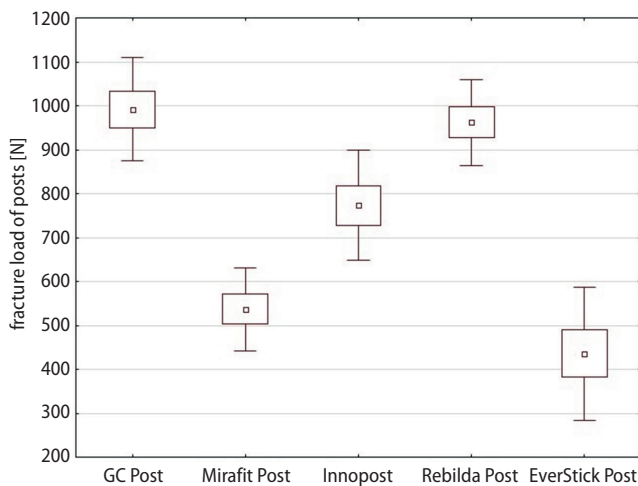


Fig. 4. The flexural strength of posts

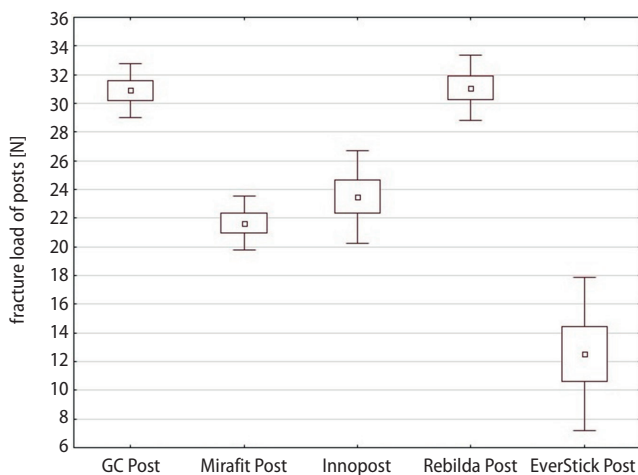


Fig. 5. The flexural modulus of posts

defines the flexibility of a sample and higher values indicate more stiffness, while lower values indicate more flexibility. The flexural modulus is calculated by taking into account the elastic behavior of a sample within a load range that will not cause plastic deformation. The flexural strength

parameter determines the resistance to fracture.<sup>2</sup> Higher values indicate that a sample is more resistant to fracture, whereas lower values indicate that it is less so. The flexural strength is determined by the highest load a sample can withstand and depends on the specimen configuration.

In this study, the posts were tested dry at room temperature and even though the authors agree with published reports that humidity can alter the mechanical properties of fiber posts,<sup>2,30,33,34</sup> it has been demonstrated that within the tooth, the behavior of posts is comparable to that of dry posts.<sup>14,32</sup> Lassila et al. revealed that thermocycling for FRC posts had a significant effect on the fracture load and flexural strength.<sup>12</sup> In general, thermocycling decreased the flexural modulus of the tested FRC posts by about 10%. Strength and fracture load decreased by about 18%. Thermocycling slightly decreased the bond strength at the fiber post–core interface.<sup>35</sup>

The EverStick Posts were polymerized in a light-curing lamp (Elipar) for 60 s. Cacciafesta et al. claimed that oven post-curing does not increase the flexural strength values of FRC EverStick Posts compared with conventional hand light-curing.<sup>36</sup>

In the case of prefabricated conventional FRC posts, the location of the post in the center of the root – in the neutral axis of tubular structure – is not optimal to provide effective reinforcing effect by the fibers of the post for the root–core–crown system.<sup>21</sup> In addition, by using the prefabricated FRC posts, the free space of the coronal root canal opening is filled only with weaker particulate filler composite resin cement. In the individually formed, also called custom-made, FRC posts, the fiber volume at the coronal part of the root canal is high and it fills the entire available root canal space. This increases the stiffness and strength of that part of the post and forms a strong support for the core. By considering the mechanics of tubular structure of a tooth and post system, the individually formed posts also provide fiber location closer to the outermost surface of the root, where the high functional stresses are located. Stress distribution in dentin is related to bone height level.<sup>37</sup> Singh et al. assessed that the stress in the dentin, post and the cement was much higher in the tooth with the alveolar bone height of 4 mm from cementoenamel junction (CEJ) compared to the tooth with bone support of 2 mm alveolar bone height from the CEJ.<sup>37</sup>

Lassila et al. claimed that EverStick in their studies presented the highest flexural strength values.<sup>12</sup> Their study investigated the flexural properties of different types of FRC posts (Snowpost, Carbopost, Parapost, C-post, Glassix, and Carbonite) and compared those values with a FRC material for dental applications (EverStick). A three-point bending test (span: 10 mm) was used to measure the flexural strength and modulus of FRC post specimens. The highest flexural strength was obtained with the control material (EverStick). They claimed that this unexpected finding could be explained by the optimization

of the polymer matrix and fiber properties to function as a composite material. More precisely, the difference in the polymer matrix of EverStick compared to the matrices of other tested FRCs is based on the existence of poly(methyl methacrylate) (PMMA) chains in the cross-linked polymer matrix. The PMMA chains with a molecular weight of 220 KD plasticize the cross-linked BisG-MA-based matrix of the EverStick FRC and reduce stress formation in the fiber–matrix interface during deflection. This may be assumed to contribute to the higher strength of EverStick FRC material.<sup>38</sup>

A different study examined the flexural strength of 2 different fiber post-resin cement systems and the results showed significant differences between the flexural strength of the prefabricated GC Fiber Posts and the individually formed EverStick Posts.<sup>39</sup> A four-point bend test was carried out till failure on all groups. The highest flexural strengths were found for the GC Fiber Posts without silane pretreatment and the second-highest flexural strengths were found for the GC Fiber Posts with silane pretreatment, both of which were higher than the flexural strengths of the EverStick Posts.

Cagidiaco et al. assessed whether the amount of residual coronal dentin and the placement of a prefabricated (DT Light Post) or a individually formed (EverStick Post) have a significant influence on the three-year survival of endodontically treated premolars.<sup>40</sup> Teeth restored with prefabricated DT Light Posts had a three-year survival rate higher (90.9%) than those restored with individually formed EverStick Posts (76.7%).

## Conclusions

The following conclusions can be drawn from the study:

1. There were statistically significant differences in fracture loads, flexural strengths and flexural modulus of the FRC-post systems tested.
2. Prefabricated FRC posts exhibit favorable mechanical properties in comparison to individually polymerized FRC. Therefore, their application may result in enhanced clinical performance of endodontically treated teeth.

### ORCID iDs

Michał Biały  <https://orcid.org/0000-0002-7999-046X>  
 Agnieszka Szust  <https://orcid.org/0000-0002-6448-6703>  
 Piotr Napadłek  <https://orcid.org/0000-0001-8464-2905>  
 Maciej Dobrzyński  <https://orcid.org/0000-0003-2368-1534>  
 Włodzimierz Więckiewicz  <https://orcid.org/0000-0002-8116-7229>

### References

1. Saupe WA, Gluskin AH, Radke Jr RA. A comparative study of fracture resistance between morphologic dowel and cores and a resin-reinforced dowel system in the intraradicular restoration of structurally compromised roots. *Quintessence Int.* 1996;27(7):483–491.
2. Plotino G, Grande NM, Bedini R, Pameijer CH, Somma F. Flexural properties of endodontic posts and human root dentin. *Dent Mater.* 2007; 23(9):1129–1135.
3. Fernandes AS, Shetty S, Coutinho I. Factors determining post selection: A literature review. *J Prosthet Dent.* 2003;90(6):556–562.
4. Stewardson DA, Shortall AS, Marquis PM, Lumley PJ. The flexural properties of endodontic post materials. *Dent Mater.* 2010;26(8): 730–736.
5. Ferrari M, Scotti R. *Fiber Posts. Characteristics and Clinical Applications.* Milan, Italy: Masson; 2002.
6. Prisco D, De Santis R, Mollica F, Ambrosio L, Rengo S, Nicolais L. Fiber post adhesion to resin luting cements in the restoration of endodontically treated teeth. *Oper Dent.* 2003;28(5):515–521.
7. Manning KE, Yu DC, Yu HC, Kwan EW. Factors to consider for predictable post and core build-ups of endodontically treated teeth. Part II. Clinical application of basic concepts. *J Can Dent Assoc.* 1995;61(8): 696–707.
8. Asmussen E, Peutzfeldt A, Sahafi A. Finite element analysis of stresses in endodontically treated, dowel-restored teeth. *J Prosthet Dent.* 2005;94(4):321–329.
9. Sarkis-Onofre R, Amaral Pinheiro H, Poletto-Neto V, Dalmolin Bergoli C, Cenci MS, Pereira-Cenci T. Randomized controlled trial comparing glass fiber posts and cast metal posts. *J Dent.* 2020;4:14.
10. Soares CJ, Valdivia AD, Silva GR, Santana FR, Menezes S. Longitudinal clinical evaluation of post systems: A literature review. *Braz Dent J.* 2012;23(2):135–140.
11. Ulgey M, Zan R, Hubbeozglu I, Gorler O, Uysalcan G, Cotur F. Effect of different laser types on bonding strength of CAD/CAM-customized zirconia post to root canal dentin: An experimental study. *Lasers Med Sci.* 2020;35(6):1385–1392.
12. Lassila LVJ, Tanner J, Le Bell AM, Narva K, Vallittu PK. Flexural properties of fiber reinforced root canal posts. *Dent Mater.* 2004;20(1):29–36.
13. Drummond JL, Bapna MS. Static and cyclic loading of fiber-reinforced dental resin. *Dent Mater.* 2003;19(3):226–231.
14. Mannocci F, Sherriff M, Watson TF. Three-point bending test of fiber posts. *J Endod.* 2001;27(12):758–761.
15. Dallari A, Rovatti L. Six years of in vitro/in vivo experience with Compositopost. *Compend Contin Educ Dent Suppl.* 1996;20:557–563.
16. Fredriksson M, Astback J, Pamenius M, Arvidson K. A retrospective study of 236 patients with teeth restored by carbon fiber-reinforced epoxy resin posts. *J Prosthet Dent.* 1998;80(2):151–157.
17. Ferrari M, Vichi A, Mannocci F, Mason PM. Retrospective study of the clinical performance of fiber posts. *Am J Dent.* 2000;13(Spec No): 9B–13B.
18. Ferrari M, Vichi A, Garcia-Godoy F. Clinical evaluation of fiber-reinforced epoxy resin posts and cast post and cores. *Am J Dent.* 2000; 13(Spec No):15B–18B.
19. Glazer B. Restoration of endodontically treated teeth with carbon fibre posts: A prospective study. *J Can Dent Assoc.* 2000;66(11):613–618.
20. Doshi P, Kanaparthi A, Kanaparthi R, Parikh DS. A comparative analysis of fracture resistance and mode of failure of endodontically treated teeth restored using different fiber posts: An in vitro study. *J Contemp Dent Pract.* 2019;20(10):1195–1199.
21. Makarewicz D, Le Bell-Rönnlöf AM, Lassila LVJ, Vallittu PK. Effect of cementation technique of individually formed fiber-reinforced composite post on bond strength and microleakage. *Open Dent J.* 2013;7:68–75.
22. Fräter M, Forster A, Jantyk Á, Braunitzer G, Nagy K, Grandini S. In vitro fracture resistance of premolar teeth restored with fibre-reinforced composite posts using a single or a multi-post technique. *Aust Endod J.* 2017;43(1):16–22.
23. Zicari F, Van Meerbeek B, Scotti R, Naert I. Effect of fibre post length and adhesive strategy on fracture resistance of endodontically treated teeth after fatigue loading. *J Dent.* 2012;40(4):312–321.
24. Peroz I, Blankenstein F, Lange K-P, Naumann M. Restoring endodontically treated teeth with posts and cores: A review. *Quintessence Int.* 2005;36(9):737–746.
25. Bitter K, Noetzel F, Neumann K, Kielbassa AM. Effect of silanization on bond strengths of fiber posts to various resin cements. *Quintessence Int.* 2007;38(2):121–128.
26. Le Bell-Rönnlöf A-M, Lassila LVJ, Kangasniemi I, Vallittu PK. Load-bearing capacity of human incisor restored with various fiber-reinforced composite posts. *Dent Mater.* 2011;27(6):e107–e115.
27. Le Bell A-M, Tanner J, Lassila LVJ, Kangasniemi I, Vallittu PK. Depth of light-initiated polymerization of glass fiber reinforced composite in a simulated root canal. *Int J Prosthodont.* 2003;16(4):403–408.

28. Bouillaguet S, Schutt A, Alander P. Hydrothermal and mechanical stresses degrade fiber-matrix interfacial bond strength in dental fiber-reinforced composites. *J Biomed Mater Res Part B Appl Biomater*. 2006;76(1):98–105.
29. Pastila P, Lassila LVJ, Jokinen M, Vuorinen J, Vallittu PK, Mäntylä T. Effect of short-term water storage on the elastic properties of some dental restorative materials: An ultrasound spectroscopy study. *Dent Mater*. 2007;23(7):878–884.
30. Torbjørner A, Karlsson S, Syverud M, Hensten-Pettersen A. Carbon fiber reinforced root canal posts: Mechanical and cytotoxic properties. *Eur J Oral Sci*. 1996;104(5–6):605–611.
31. Purton DG, Payne JA. Comparison of carbon fiber and stainless steel root canal posts. *Quintessence Int*. 1996;27(2):93–97.
32. Asmussen E, Peutzfeldt A, Heitmann T. Stiffness elastic limit, and strength of newer types of endodontic posts. *J Dent*. 1999;27(4):275–278.
33. Grant TS, Bradley WL. In situ observations in SEM of degradation of graphite/epoxy composite materials due to seawater immersion. *J Compos Mater*. 1995;29(7):852–867.
34. Lee MC, Peppas NA. Models of moisture transport and moisture-induced stresses in epoxy composites. *J Compos Mater*. 1993;27(12):1146–1171.
35. Hashemikamangar SS, Hasanitabatabaee M, Kalantari S, Gholampourdehaky M, Ranjbaromrani L, Ebrahimi H. Bond strength of fiber posts to composite core: Effect of surface treatment with Er,Cr:YSGG laser and thermocycling. *J Lasers Med Sci*. 2018;9(1):36–42.
36. Cacciafesta V, Sfondrini MF, Lena A, Scribante A, Vallittu PK, Lassila LV. Flexural strengths of fiber-reinforced composites polymerized with conventional light-curing and additional postcuring. *Am J Orthod Dentofacial Orthop*. 2007;132(4):524–527.
37. Singh SV, Gupta S, Sharma D, Pandit N, Nangom A, Satija H. Stress distribution of posts on the endodontically treated teeth with and without bone height augmentation: A three-dimensional finite element analysis. *J Conserv Dent*. 2015;18(3):196–199.
38. Vallittu PK. *The Second International Symposium on Fiber-Reinforced Plastics in Dentistry*. Turku, Finland: University of Turku. 2002:2–28.
39. Davis P, Melo LSD, Foxton RM, et al. Flexural strength of glass fibre-reinforced posts bonded to dual-cure composite resin cements. *Eur J Oral Sci*. 2010;118(2):197–201.
40. Cagidiaco MC, Garcia-Godoy F, Vichi A, Grandini S, Goracci C, Ferrari M. Placement of fiber-prefabricated or custom-made posts affects the 3-year survival of endodontically treated premolars. *Am J Dent*. 2008;21(3):179–184.

# Skin conductance measurement for the assessment of analgosedation adequacy in infants treated with mechanical ventilation: A multicenter pilot study

Wojciech Walas<sup>1,A–F</sup>, Zenon Halaba<sup>2,B–F</sup>, Agata Kubiacyk<sup>3,B,E,F</sup>, Andrzej Piotrowski<sup>4,C,E,F</sup>, Julita Latka-Grot<sup>5,B,C,E,F</sup>, Tomasz Szczapa<sup>3,C,E,F</sup>, Monika Romul<sup>4,B,E,F</sup>, Iwona Maroszyńska<sup>6,C,E,F</sup>, Ewelina Malinowska<sup>6,B,E,F</sup>, Magdalena Rutkowska<sup>7,B,E,F</sup>, Michał Skrzypek<sup>8,C,E,F</sup>, Robert Śmigiel<sup>9,B–F</sup>

<sup>1</sup> Pediatric and Neonatal Intensive Care Unit, University Hospital in Opole, Poland

<sup>2</sup> Department of Pediatrics, Institute of Medical Sciences, University of Opole, Poland

<sup>3</sup> Department of Neonatology, Neonatal Biophysical Monitoring and Cardiopulmonary Therapies Research Unit, Poznań University of Medical Sciences, Poland

<sup>4</sup> Department of Anesthesiology and Intensive Care, Children's Memorial Health Institute, Warszawa, Poland

<sup>5</sup> Neonatal Department, Children's Memorial Health Institute, Warszawa, Poland

<sup>6</sup> Department of Intensive Care and Congenital Malformations of Newborns and Infants, Polish Mother's Memorial Hospital Research Institute in Łódź, Poland

<sup>7</sup> Department of Neonatology, Institute of Mother and Child, Warszawa, Poland

<sup>8</sup> Department of Biostatistics, School of Public Health in Bytom, Medical University of Silesia, Poland

<sup>9</sup> Department of Pediatrics, Division of Propedeutic Pediatrics and Rare Disorders, Wrocław Medical University, Poland

A – research concept and design; B – collection and/or assembly of data; C – data analysis and interpretation;

D – writing the article; E – critical revision of the article; F – final approval of the article

Advances in Clinical and Experimental Medicine, ISSN 1899–5276 (print), ISSN 2451–2680 (online)

*Adv Clin Exp Med.* 2020;29(9):1117–1121

## Address for correspondence

Wojciech Walas

E-mail: wojciechwalas@wp.pl

## Funding sources

None declared

## Conflict of interest

None declared

Received on June 10, 2020

Reviewed on June 30, 2020

Accepted on August 11, 2020

Published online on September 16, 2020

## Cite as

Walas W, Halaba Z, Kubiacyk A, et al. Skin conductance measurement for the assessment of analgosedation adequacy in infants treated with mechanical ventilation: A multicenter pilot study. *Adv Clin Exp Med.* 2020;29(9): 1117–1121. doi:10.17219/acem/126286

## DOI

10.17219/acem/126286

## Copyright

© 2020 by Wrocław Medical University

This is an article distributed under the terms of the Creative Commons Attribution 3.0 Unported (CC BY 3.0) (<https://creativecommons.org/licenses/by/3.0/>)

## Abstract

**Background.** Patients treated in neonatal/pediatric intensive care units (N/PICUs) are frequently exposed to pain. To assess its severity, several behavioral and behavioral-physiological scales are used, but their usefulness is limited. It is therefore justified to search for additional methods to assess the adequacy of analgesia and sedation in these patients.

**Objectives.** To evaluate the usefulness of skin conductance (SC) measurement in the assessment of analgosedation quality in infants requiring mechanical ventilation treated in N/PICUs.

**Material and methods.** Thirty infants aged 6–208 days treated in 6 N/PICUs, mechanically ventilated and receiving analgosedation, were included for the study. Simultaneous COMFORT-B assessment and SC measurement using SCA (skin conductance algesimeter) monitor were performed. Due to technical problems, not all of the SC records could be interpreted, and finally 412 simultaneous assessments on the COMFORT-B scale and SC measurements in 29 patients were analyzed.

**Results.** We found a statistically significant correlation between the COMFORT-B scoring and the SC measurements. Additionally, SC was significantly lower when the behavioral score indicated deep sedation, in comparison to periods when it indicated moderate or insufficient analgosedation.

**Conclusions.** Skin conductance measurements are comparable with the COMFORT-B rating in mechanically ventilated infants receiving analgosedation. The SCA monitor may be of value in the assessment of analgosedation quality, and in particular may identify the situation where sedation is deep. Further research is needed regarding the suitability of this device in clinical practice.

**Key words:** pain, analgosedation, infant, skin conductance, COMFORT-B scale

## Introduction

As defined by the International Association for the Study of Pain, pain is an unpleasant sensory and emotional experience associated with actual or potential tissue damage, or described in terms of such damage.<sup>1</sup> It is understandable that patients treated in neonatal/pediatric intensive care units (N/PICUs) are exposed to pain. Newborns and infants may suffer both from illness, particularly after surgery, and from chronic use of the procedures causing discomfort, such as tracheal intubation, as well as experience additional procedural pain. This also applies to patients in analgosedation. Insufficient pain control is harmful not only from an ethical point of view, but also because of adverse development consequences.<sup>2–4</sup> On the other hand, the extensive use of sedation and analgesia may also cause side effects and disrupt neurological development.<sup>5–8</sup> For successful pain management, it is necessary to assess its occurrence and severity, which is difficult in newborns and infants due to the lack of verbal communication. In patients treated in N/PICU, behavioral and behavioral-physiological scales are used to assess pain. However, all these scales have disadvantages and limitations. Their use requires considerable staff involvement, is time consuming and the assessment is always more or less subjective. In addition, the assessment is intermittent and performed at intervals, and therefore there is a risk of overlooking pain episodes. For this reason, although pain should be considered a “fifth vital parameter”, the protection against pain is often unsatisfactory among N/PICU patients.<sup>9–13</sup> It is therefore understandable that additional objective pain assessment methods are constantly being sought. Of the various solutions, methods based on measurement electrical skin conductance (SC) are promising. Our goal was to assess the usefulness of Skin Conductance Algesimeter (SCA; MedStorm Innovation, Oslo, Norway) in the assessment of pain in mechanically ventilated infants receiving analgosedation by comparing the measurements with the scoring on the behavioral (COMFORT-B) scale.

This was a prospective observational study, which did not require any changes from the standard treatment of included patients. The acceptance of the local ethical committee was granted (approval No. 270 from October 11, 2018).

## Material and methods

### Patients

We enrolled 30 neonates and infants treated in N/PICUs. Inclusion criteria were as follows: gestational age at birth over 26 weeks and chronological age less than 1 year, mechanical ventilation through an endotracheal tube, and analgosedation (fentanyl/midazolam). Exclusion criteria included: bradycardia <80 bpm, tachycardia >250 bpm,

any cardiac rhythm other than sinus one, use of medication that have effects on sympathetic and parasympathetic activity (e.g., beta blockers) during a period of 7 days before the study, intraventricular hemorrhage of IV degree, severe perinatal asphyxia treated by therapeutic hypothermia, central nervous system congenital malformations, seizures in the 7 days preceding the study and neuromuscular diseases, and analgosedation other than fentanyl/midazolam. All parents/legal guardians were given an information form and gave their approval for the study.

### Study protocol

The fentanyl/midazolam analgosedation was carried out in accordance with the rules used by the participating departments and the study did not affect it. Patients were constantly monitored using a SCA monitor. They were also periodically evaluated using the COMFORT-B scale. The intervals between the COMFORT-B scoring were at least 1 h. Patients were not disturbed by any additional procedures during the 15-minute period before this assessment.

### Pain assessment

The COMFORT-B scale is dedicated for mechanically ventilated patients and is used to assess the degree of analgosedation.<sup>14</sup> The scale consists of 6 behavioral items: alertness, calmness, respiratory response, body movements, facial tension, and muscle tone. A scale from 1 point (the highest) to 5 points (the lowest) sedation level is assigned to each variable. The minimum and maximum of total scores is 6 and 30, respectively. Scores 6–10 indicate deep analgosedation, scores 11–23 indicate a moderately sedated patient and scores >23 indicate insufficient sedation. COMFORT-B assessment was performed by experienced neonatologists who did not have access to the measurements presented by the SCA monitor.

The SCA monitor works based on the analysis of SC changes in response to pain stimuli. Skin conductance activity reflects the sympathetic nervous system activity influenced by changes in emotions, releasing acetylcholine that acts on muscarine receptors and causes a subsequent burst of sweat and variations in ions secretion. The measurement is performed using 3 self-adhesive electrodes attached to palmar or plantar skin. A comprehensive description of the SC methodology has been published by Storm.<sup>15,16</sup> The SCA device displays several parameters, of which, according to the manufacturer's recommendations and the data from literature, peaks per second (PPS) parameter was chosen as the most suitable for assessing pain in preterm and term infants under analgosedation.<sup>17,18</sup> Recommended window of 15 s was used for analysis. A higher level of PPS corresponds to a stronger pain sensation.

## Statistical analysis

We analyzed the correlation of the COMFORT-B scoring and the PPS levels using Spearman’s correlation coefficient. We compared also the PPS levels using Mann–Whitney U test in the subgroups identified based on the COMFORT-B rating. We assumed the significance level  $p < 0.05$ . The SAS software v. 9.4 (SAS Institute Inc., Cary, USA) was used for statistical analysis.

## Results

Thirty patients were included, in whom an assessment using COMFORT-B scale was performed 442 times. The 30 SCA records (7% of all) were illegible for assessment due to artifacts (in 1 patient all records) and were excluded. In the final analysis, 412 simultaneous assessments on the COMFORT-B scale and PPS levels in 29 patients were analyzed. The details of patients are presented in Table 1. There was statistically significant correlation of the COMFORT-B scale and PPS levels with coefficient 0.279 ( $p < 0.0001$ ). The COMFORT-B rating  $\leq 10$  (deep analgesation) was measured in 324 cases (79%), 11–23 (moderate analgesation) in 86 cases (20.5%) and  $> 23$  (insufficient analgesation) in 2 cases (0.5%). Small number of events when COMFORT-B scores were  $> 23$  did not allow a comparison of the PPS levels in situations when the analgesation was moderate and when was insufficient. Therefore, we compared PPS levels between deep and moderate/insufficient subgroups. The PPS levels were significantly lower in the deep analgesation subgroup (median: 0.00) than in the moderate/insufficient analgesation subgroup (median: 0.04) ( $p < 0.001$ ). Nine data points in the deep analgesation subgroup (2.7%) and 6 in the moderate/insufficient analgesation subgroup (6.8%) have differed significantly from other observations and were considered outliers. The results are shown in Fig. 1.

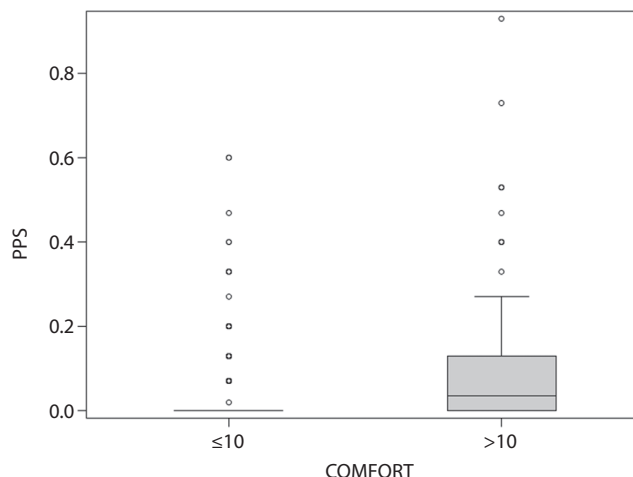


Fig. 1. SCA levels (PPS) depending on the assessment of analgesation using the COMFORT-B scale (deep compared to moderate/insufficient)

## Discussion

Our study included a specific group of patients: neonates and infants mechanically ventilated and receiving analgesation. We found a statistically significant correlation between the COMFORT-B score and PPS levels. From a clinical point of view, the quality of analgesation is of utmost importance. For this reason, we set thresholds based on a behavioral scale. We found that PPS levels are significantly lower in situations where the COMFORT-B rating indicates profound analgesation compared to situations where this assessment indicates that analgesation is moderate or insufficient. The identification of patients with deep analgesation seems to be important considering its adverse consequences.

Skin conductance measurements have been shown to be useful in assessing pain in patients of different age groups and in different clinical situations. Some of the research comprises neonates, infants and children, the vast majority concerning only the assessment of procedural pain. Storm, Scaramuzzo et al., Eriksson et al., Pereira-da-Silva et al., de Jesus et al., as well as Tristão et al. have shown that at-term neonates SC increases in response to pain stimuli.<sup>15,17–23</sup> Munsters et al. and Macko et al. have shown the same reaction in preterm neonates.<sup>24,25</sup> Zeiner et al., Hellerud et al., Lyngstad et al., and Salavitabar et al. noted that SC changes in response to various forms of handling, sensory stimulation, mother and newborn skin-to-skin contact and sound stimuli.<sup>26–29</sup> Only a few studies focus on assessing the usefulness of SCA in evaluating the severity of pain and the effectiveness of analgesation in infants and children in the postoperative period and/or treated in N/PICU. Gjerstad et al. obtained results similar to ours. They examined the correlation between SC, COMFORT score, heart rate, and arterial blood pressure during endotracheal suctioning in a group of 20 mechanically ventilated patients, including neonates. They noted that the PPS showed better

Table 1. Characteristics of the studied group

Overall characteristics (n = 29)	Mean $\pm$ SD (min–max*) median (1 <sup>st</sup> –3 <sup>rd</sup> quartile) (min–max**)
Gestational age [weeks]	34 $\pm$ 4.5 (25–40*)
Birthweight [g]	2408 $\pm$ 1036 (560–4200*)
Females/males	14 (48%)/15 (52%)
Characteristics at the time of the events (n = 412)	Mean $\pm$ SD (min–max*) median (1 <sup>st</sup> –3 <sup>rd</sup> quartile) (min–max**)
Age [days]	6 (4–23) (1–208**)
Postmenstrual age [weeks]	38 (35–41) (26–55**)
Weight [g]	3600 (2975–3800) (865–5800**)

\* normal distribution; \*\* non-normal distribution according to the Shapiro–Wilk test; SD – standard deviation.

correlation with the increase in the COMFORT score than heart rate and arterial blood pressure. They concluded that for monitoring of stress in artificially ventilated children, SCA seems to be an objective supplement to the behavioral scoring.<sup>30</sup> Hullet et al. assessed pain intensity in the postoperative period in 180 children aged 1–16 years using SC analysis and various 3 behavioral scales depending on the patient's age. They concluded that PPS may play an important role in the assessment of pediatric pain, especially when used as a predictor of moderate/severe pain.<sup>31</sup> The usefulness of SC monitoring in the assessment of pain in mechanically ventilated neonates was also studied by Karpe et al. They analyzed SC fluctuations during tracheal suctioning and heel stick in term and near-term neonates under analgesia. They noted a significant increase in SC levels in response to pain stimuli; however, they did not compare this reaction with other pain assessment methods. They concluded that changes of SC level demonstrate that, despite sedation and analgesia, neonates experience discomfort related to the therapeutic and diagnostic procedures.<sup>32</sup> On the contrary, results of research done by Solana et al. in 61 mechanically ventilated critically ill children aged from 1 month to 16 years and receiving analgesia showed that, although the PPS increased significantly during the painful procedures, it never reached the level considered diagnostic for pain or stress. The authors concluded that SC is no more sensitive or faster than clinical scales for the assessment of pain or stress in critical children undergoing painful procedures.<sup>33</sup> Van der Lee et al. performed a study in which they evaluated PPS in response to tracheal intubation in neonates receiving different types of premedication. They concluded that the variation in SC measurements between individual neonates limits the usefulness of PPS as stress monitor during intubation and the use of neuromuscular blockers for premedication precludes monitoring of PPS in neonates.<sup>34</sup> Also, Choo et al. based on research of 90 school-age children noted that PPS measurement is feasible in a perioperative setting but was not specific for postoperative pain intensity and was unable to identify analgesia requirements when compared with self-report measures.<sup>35</sup> The results of research performed by Dalal et al. in 34 infants aged 6–12 months in the postoperative period are less obvious. The authors assessed pain intensity on the NFCS scale and simultaneously measured various SC parameters. They found that SCA may be useful in assessing infant pain, but noticed that the peak amplitude of the SC values may be a better indicator of pain scores than the PPS.<sup>36</sup> Ledowski, on the basis of a review of the literature on instrumental pain monitoring, came to the conclusion that there is currently no evidence for a clinically relevant benefit arising from the perioperative utilization of SC monitoring.<sup>37</sup>

Our study has a significant limitation: too few COMFORT-B scores >23 prevented the assessment of the usefulness of the monitor in identifying situations when

analgesia is insufficient. Nevertheless, we believe that the ability to identify the deep analgesia using SCA is valuable from a clinical point of view, especially in the context of avoiding side effects of oversedation.

## Conclusions

Skin conductance measurements are comparable with the COMFORT-B rating in mechanically ventilated infants receiving analgesia. The SCA monitor may be of value in the assessment of analgesia quality, and in particular may identify the situation where sedation is deep. Further research is needed regarding the suitability of this device in clinical practice.

### ORCID iDs

Wojciech Walas  <https://orcid.org/0000-0001-7941-2718>  
 Zenon Halaba  <https://orcid.org/0000-0002-2905-0437>  
 Agata Kubiacyk  <https://orcid.org/0000-0002-2725-564X>  
 Andrzej Piotrowski  <https://orcid.org/0000-0002-1585-1815>  
 Julita Latka-Grot  <https://orcid.org/0000-0002-0442-4199>  
 Tomasz Szczapa  <https://orcid.org/0000-0002-5214-2719>  
 Monika Romul  <https://orcid.org/0000-0003-4728-1594>  
 Iwona Maroszyńska  <https://orcid.org/0000-0003-4061-4843>  
 Ewelina Malinowska  <https://orcid.org/0000-0001-8922-1819>  
 Magdalena Rutkowska  <https://orcid.org/0000-0002-4503-2829>  
 Michał Skrzypek  <https://orcid.org/0000-0003-3410-7407>  
 Robert Śmigiel  <https://orcid.org/0000-0003-2930-9549>

### References

1. International Association for the Study of Pain. <https://www.iasp-pain.org/Education/Content.aspx?ItemNumber=1698#Pain>. Accessed June 17, 2020.
2. Vinall J, Grunau RE. Impact of repeated procedural pain-related stress in infants born very preterm. *Pediatr Res*. 2014;75(5):584–587.
3. Ranger M, Grunau RE. Early repetitive pain in preterm infants in relation to the developing brain. *Pain Manag*. 2014;4(1):57–67.
4. Duerden EG, Grunau RE, Guo T, et al. Early procedural pain is associated with regionally-specific alterations in thalamic development in preterm neonates. *J Neurosci*. 2018;38(4):878–886.
5. Kesavan K. Neurodevelopmental implications of neonatal pain and morphine exposure. *Pediatr Ann*. 2015;44(11):e260–e264.
6. McPherson C, Haslam M, Pineda R, Rogers C, Neil JJ, Inder TE. Brain injury and development in preterm infants exposed to fentanyl. *Ann Pharmacother*. 2015;49(12):1291–1297. doi:10.1177/1060028015606732
7. Duerden EG, Guo T, Dodbiba L, et al. Midazolam dose correlates with abnormal hippocampal growth and neurodevelopmental outcome in preterm infants. *Ann Neurol*. 2016;79(4):548–559.
8. Schiller RM, Allegaert K, Hunfeld M, van den Bosch GE, van den Anker J, Tibboel D. Analgesics and sedatives in critically ill newborns and infants: The impact on long-term neurodevelopment. *J Clin Pharmacol*. 2018;58(Suppl 10):S140–S150. doi:10.1002/jcph.1139
9. Avila-Alvarez A, Carbajal R, Courtois E, Pertega-Diaz S, Anand KJ, Muñoz-García J; Grupo español del proyecto Europain. Clinical assessment of pain in Spanish neonatal intensive care units [in Spanish]. *An Pediatr (Barc)*. 2016;85(4):181–188.
10. Courtois E, Droutman S, Magny JF, et al. Epidemiology and neonatal pain management of heelsticks in intensive care units: EPIPAIN 2, a prospective observational study. *Int J Nurs Stud*. 2016;59:79–88.
11. Sposito NP, Rossato LM, Bueno M, Kimura AF, Costa T, Guedes DMB. Assessment and management of pain in newborns hospitalized in a neonatal intensive care unit: A cross-sectional study. *Rev Lat Am Enfermagem*. 2017;12;25:e2931. doi:10.1590/1518-8345.1665.2931
12. Lago P, Frigo AC, Baraldi E, et al. Sedation and analgesia practices at Italian neonatal intensive care units: Results from the EUROPAIN study. *Ital J Pediatr*. 2017;43:26.

13. Anand KJS, Eriksson M, Boyle EM, Avila-Alvarez A, Andersen RD, Sarafidis K; EUROPAIN Survey Working Group of the NeoOpioid Consortium. Assessment of continuous pain in newborns admitted to NICUs in 18 European countries. *Acta Paediatr.* 2017;106(8):1248–1259.
14. Ista E, van Dijk M, Tibboel D, de Hoog M. Assessment of sedation levels in pediatric intensive care patients can be improved by using the COMFORT “behavior” scale. *Pediatr Crit Care Med.* 2005;6(1):58–63.
15. Storm H. Skin conductance and the stress response from heel stick in preterm infants. *Arch Dis Child Fetal Neonatal Ed.* 2000;83(2):F143–F147.
16. Storm H. The development of a software program for analyzing skin conductance changes in preterm infants. *Clin Neurophysiol.* 2001;112(8):1562–1568.
17. Storm H. Changes in skin conductance as a tool to monitor nociceptive stimulation and pain. *Curr Opin Anaesthesiol.* 2008;21(6):796–804.
18. Storm H. Pain monitoring in anesthetized children: First assessment of skin conductance and analgesia-nociception index at different infusion rates of remifentanyl. Recommended preset values for the skin conductance equipment was not used. *Paediatr Anaesth.* 2013;23(8):761–763.
19. Scaramuzzo RT, Faraoni M, Polica E, Pagani V, Vaghi E, Boldrini A. Skin conductance variations compared to ABC scale for pain evaluation in newborns. *J Matern Fetal Neonatal Med.* 2013;26(14):1399–1403.
20. Eriksson M, Storm H, Fremming A, Schollin J. Skin conductance compared to a combined behavioural and physiological pain measure in newborn infants. *Acta Paediatr.* 2008;97(1):27–30.
21. Pereira-da-Silva L, Virella D, Monteiro I, et al. Skin conductance indices discriminate nociceptive responses to acute stimuli from different heel prick procedures in infants. *J Matern Fetal Neonatal Med.* 2012;25(6):796–801.
22. de Jesus JA, Campos D, Storm H, da Rocha AF, Tristão RM. Skin conductance and behavioral pain scales in newborn infants. *Psychol Neurosci.* 2015;8(2):203–210.
23. Tristão RM, Garcia NV, de Jesus JA, Tomaz C. COMFORT behaviour scale and skin conductance activity: What are they really measuring? *Acta Paediatr.* 2013;102(9):e402–e406.
24. Munsters J, Wallström L, Agren J, Norsted T, Sindelar R. Skin conductance measurements as pain assessment in newborn infants born at 22–27 weeks gestational age at different postnatal age. *Early Hum Dev.* 2012;88(1):21–26.
25. Macko J, Moravcikova D, Kantor L, Kotikova M, Humpolicek P. Skin conductance as a marker of pain in infants of different gestational age. *Biomed Pap Med Fac Univ Palacky Olomouc Czech Repub.* 2014;158(4):591–595.
26. Zeiner V, Storm H, Doheny KK. Preterm infants’ behaviors and skin conductance responses to nurse handling in the NICU. *J Matern Fetal Neonatal Med.* 2016;29(15):2531–2536.
27. Hellerud BC, Storm H. Skin conductance and behavior during sensory stimulation of preterm and term infants. *Early Hum Dev.* 2002;70(1–2):35–46.
28. Lyngstad LT, Tandberg BS, Storm H, Ekeberg BL, Moen A. Does skin-to-skin contact reduce stress during diaper change in preterm infants? *Early Hum Dev.* 2014;90(4):169–172.
29. Salavitarab A, Haidet KK, Adkins CS, Susman EJ, Palmer C, Storm H. Preterm infants’ sympathetic arousal and associated behavioral responses to sound stimuli in the neonatal intensive care unit. *Adv Neonatal Care.* 2010;10(3):158–166.
30. Gjerstad AC, Wagner K, Henrichsen T, Storm H. Skin conductance versus the modified COMFORT sedation score as a measure of discomfort in artificially ventilated children. *Pediatrics.* 2008;122(4):e848–e853.
31. Hullett B, Chambers N, Preuss J, et al. Monitoring electrical skin conductance: A tool for the assessment of postoperative pain in children? *Anesthesiology.* 2009;111(3):513–517.
32. Karpe J, Misiólek A, Daszkiewicz A, Misiólek H. Objective assessment of pain-related stress in mechanically ventilated newborns based on skin conductance fluctuations. *Anaesthesiol Intensive Ther.* 2013;45(3):134–137.
33. Solana MJ, Lopez-Herce J, Fernandez S, et al. Assessment of pain in critically ill children: Is cutaneous conductance a reliable tool? *J Crit Care.* 2015;30(3):481–485.
34. van der Lee R, Jebbink LJ, van Herpen TH, d’Haens EJ, Bierhuizen J, van Lingen RA. Feasibility of monitoring stress using skin conduction measurements during intubation of newborns. *Eur J Pediatr.* 2016;175(2):237–243.
35. Choo EK, Magruder W, Montgomery CJ, Lim J, Brant R, Ansermino JM. Skin conductance fluctuations correlate poorly with postoperative self-report pain measures in school-aged children. *Anesthesiology.* 2010;113(1):175–182.
36. Dalal PG, Doheny KK, Klick L, et al. Analysis of acute pain scores and skin conductance measurements in infants. *Early Hum Dev.* 2013;89(3):153–158.
37. Ledowski T. Objective monitoring of nociception: A review of current commercial solutions. *Br J Anaesth.* 2019;123(2):e312–e321.



# Advances in ultrasound-guided thermal ablation for symptomatic benign thyroid nodules

Zhigang Cheng<sup>B,D,E</sup>, Ping Liang<sup>A,C,F</sup>

Department of Interventional Ultrasound, Chinese People's Liberation Army General Hospital, Beijing, China

A – research concept and design; B – collection and/or assembly of data; C – data analysis and interpretation; D – writing the article; E – critical revision of the article; F – final approval of the article

Advances in Clinical and Experimental Medicine, ISSN 1899–5276 (print), ISSN 2451–2680 (online)

*Adv Clin Exp Med.* 2020;29(9):1123–1129

## Address for correspondence

Zhigang Cheng  
E-mail: 13691367317@163.com

## Funding sources

This study was supported with funding from the National Scientific Foundation Committee of China (grants No. 81871374 and No. 81627803).

## Conflict of interest

None declared

Received on June 16, 2017

Reviewed on April 10, 2018

Accepted on July 16, 2020

Published online on September 14, 2020

## Abstract

Benign thyroid nodules (BTNs), which account for 85–95% of all thyroid nodules (TNs), are a common clinical issue and have been increasingly detected over the last 2 decades due to the widespread use of ultrasound (US) imaging. The clinical treatment for BTNs is mainly focused on patients with nodular growth or clinical problems, either cosmetic or symptom-related. Percutaneous thermal ablation (TA) under US guidance has increasingly become a satisfactorily minimally invasive alternative to surgery for patients with symptomatic BTNs, especially for those in nonsurgical candidates, surgically high-risk individuals or patients refusing surgery. Based on the available English-language literature, the brief principles, procedures and clinical outcomes of 4 TA techniques, including laser ablation therapy (LAT), radiofrequency ablation (RFA), microwave ablation (MWA), and high-intensity focused ultrasound (HIFU) in the treatment of BTNs were retrospectively reviewed in this article. Good curative efficacy and clinical safety were noted in the published reports of the 4 TA techniques in the treatment of BTNs, with nodular volume reduction ratios of 46–93.5%, significant improvement in symptomatic and cosmetic problems, and euthyroid preservation for most patients. The conclusion is that all 4 TA techniques can be safe and effective treatment for patients with symptomatic BTNs; RFA seems to be the best because of the highest nodular volume reduction ratio (VRR) at follow-up. Furthermore, the image fusion navigation technique will play an important role through assisting in precise ablation for BTNs.

**Key words:** ultrasonography, thyroid nodule, ablation

## Cite as

Cheng Z, Liang P. Advances in ultrasound-guided thermal ablation for symptomatic benign thyroid nodules. *Adv Clin Exp Med.* 2020;29(9):1123–1129. doi:10.17219/acem/125433

## DOI

10.17219/acem/125433

## Copyright

© 2020 by Wrocław Medical University  
This is an article distributed under the terms of the Creative Commons Attribution 3.0 Unported (CC BY 3.0) (<https://creativecommons.org/licenses/by/3.0/>)

## Introduction

Thyroid nodules (TNs) are a common clinical issue, and their prevalence has been increasing over the last 2 decades<sup>1</sup> due to the widespread use of ultrasound (US) imaging. In the general population, more than 50% of TNs are detected with US examination, while only 3–7% are detected with palpation.<sup>2</sup> It is estimated that benign thyroid nodules (BTNs) account for 85–95% among all TNs.<sup>3</sup> Regular observation is recommended for most BTNs because they present no clinical problems and grow slowly.<sup>4</sup> Treatment is mainly focused on patients with progressive nodular growth or clinical problems, either cosmetic or symptom-related, associated with nodular volume. Partial thyroidectomy is a traditional and effective method for the treatment of BTNs with the advantages of significant symptomatic relief and definite pathological diagnosis, but the cervical scar and daily oral levothyroxine to maintain euthyroidism are common sources of dissatisfaction following surgery. On the one hand, the thyroid gland, which synthesizes and secretes thyroid hormones, plays a key role in human metabolism,<sup>5</sup> so it is critically important to preserve normal thyroid function. On the other hand, the thyroid is a small and superficial organ in the cervical region,<sup>6</sup> adjacent to several vital structures, such as the common carotid artery, internal jugular vein, vagus nerve, recurrent laryngeal nerve, superior laryngeal nerve, trachea, and esophagus, with high risks and possibilities of complications if surgical treatment is undertaken. This has led to an ongoing search for a minimally invasive procedure to maximize BTN patients' relief in terms of symptoms and cosmetics, and at the same time to minimize the occurrence of complications.

With over 10 years of development and improvement, 4 techniques of percutaneous US guided thermal ablation (TA) have become satisfactory minimally invasive alternatives to surgery for patients with symptomatic BTNs, especially for nonsurgical candidates, surgically high-risk individuals or those who refuse surgery: radiofrequency ablation (RFA), laser ablation therapy (LAT), microwave ablation (MWA), and high-intensity focused ultrasound (HIFU).<sup>7,8</sup> Besides significant improvement of the patients' clinical symptom-related and cosmetic problems related to BTNs,<sup>9–18</sup> other attractive advantages have been confirmed for TA treatment of BTNs, including low rates of both major and minor complications,<sup>19</sup> and good preservation of thyroid function.<sup>20,21</sup>

Therefore, based on the available English-language literature, the brief principles, procedures and clinical outcomes in the treatment of BTNs using 4 TA techniques were retrospectively reviewed, with the aim was of evaluating these 4 TA techniques in clinical applications, exploring feasible methods of further improvement, and providing an effective reference for clinical TA treatment of BTNs.

## Methods and results

### Laser ablation therapy

#### Brief principles

Infrared laser energy originates from the emission of photons connected to a laser source and is delivered into tissue by a specially designed tiny fiber. It can be converted into heat due to tissue absorption. The heat causes a temperature rise and eventually a lethal level is reached around the active tip within a target tissue.<sup>22</sup> Laser is an efficient and precise energy source for tissue heating, but only a small ablation zone is formed due to its limited penetration of the tissue.<sup>23</sup> Additionally, laser cannot penetrate carbonized and dehydrated tissue. The most popular laser source is a continuous-wave neodymium:yttrium aluminum garnet (Nd:YAG) laser medium operating at a wavelength of 1064 nm and an output power ranging between 2 W and 5 W.

#### Procedure

Under US guidance, a flexible silica optical fiber 0.3 mm in diameter is advanced into the TN through the sheath of a 21-gauge Chiba needle. A 5 mm bare fiber tip is exposed and contacts nodular tissue directly after the needle sheath is withdrawn. To ablate nodules in different volumes, 1–4 fibers can be arrayed manually in the target. Ablation starts in the deep part, 10 mm from the deep margin of the nodule. By the sheath and fiber pull-back of 10 mm every time, laser energy is repeatedly administered until a distance of 5 mm from the sheath tip to the superficial margin of the nodule is reached.

#### Clinical results

For efficacy, after LAT-induced histologically spindle-shaped, well-defined necrosis surrounding central vaporization and carbonization in a TN was confirmed by a pilot feasibility study in 2000,<sup>24</sup> an initially prospective non-randomized control study was reported in 2002.<sup>25</sup> The nodular volumes of BTNs in 15 patients in a control group presented no change at a median of 12 months of follow-up; the mean nodular volume of BTNs pathologically proven by fine needle aspiration (FNA) in 16 euthyroid patients ablated by US-guided percutaneous LAT significantly decreased, from  $10 \pm 7.9$  mL at baseline to  $5.4 \pm 5.1$  mL at 6 months of follow-up. The overall nodular volume reduction ratio (VRR) was 46% and pressure symptoms were significantly improved. The conclusion was drawn that US-guided LAT could become a useful nonsurgical alternative for treating a solitary solid cold BTN in patients who could not or would not undergo surgery. An encouraging multicenter prospective randomized trial of US-guided LAT for solid BTNs with long-term follow-up was published in 2014.<sup>26</sup> At 4 thyroid referral centers, 200 consecutive patients who met the inclusion criteria (euthyroid, no prior thyroid treatment and benign

cytological findings at least twice), were randomly assigned to 2 groups. One group underwent a single LAT session (101 cases); the rest (99 cases) had follow-up only. In the ablation group, the mean nodular volume significantly shrunk and VRR was  $57 \pm 25\%$  at 3 years of follow-up. The VRRs decreased more than 50% in 67.3% out of the cases. Local symptoms and cosmetic issues significantly improved after the treatment. In the follow-up group, the mean nodular volume was significantly increased by  $25 \pm 42\%$  at the three-year checkup and local symptoms became worse in 20.4% (20/98) of the cases. It was concluded that a single session of LAT offered an effective, safe and less expensive outpatient alternative to surgery for patients with clinical problems related to BTNs without influencing patients' thyroid function.

As far as safety is concerned, in a large-scale, three-year follow-up study of percutaneous LAT for cold BTNs,<sup>13</sup> major complications of a pseudocyst with fasciitis due to fluid leaks into the cervical muscle fascia occurred in 3 patients (2.5%), and were absorbed spontaneously in 3–6 months after an anti-inflammatory drug was prescribed. Two patients (1.6%) presented vocal cord paresis 12–24 h after the procedure. A six-week course of oral corticosteroids was administered, and indirect laryngoscopy showed recovery of vocal cord motility after 6–10 weeks. Out of 122 patients, only 24 (19.7%) complained of pain or significant discomfort during or following the procedure. Minor complications and side effects including mild pain (11.5%, 14/122), intense pain (8.2%, 10/122), intranodular or pericapsular bleeding (9.9%, 12/122), vasovagal reaction (4.1%, 5/122), cough (4.9%, 6/122), stridor (0.8%, 1/122), swelling (9.0%, 11/122), cutaneous burns (0.8%, 1/122), bruises (2.5%, 3/122), fever ( $37.5$ – $38.5^\circ\text{C}$ ; 4.1%, 5/122), pseudocystic transformation (4.9%, 6/122), transient hyperthyroidism (1.6%, 2/122), and late hypothyroidism (1.6%, 2/122) that presented in intraoperatively, immediately postoperatively, in the peri-procedural period, and during the follow-up were reported in detail. In 2012, a tracheal perforation – a rare but severe complication confirmed with tracheoscopy – occurred in a 73-year-old woman 50 days after a LAT procedure for multinodular goiter treatment; a total thyroidectomy plus tracheal repair were required.<sup>27</sup>

## Radiofrequency ablation

### Brief principles

During RFA in most biological tissue, a high-frequency electric current (200–1200 kHz) flows through ionic channels and causes frictional heat at the ion level, followed by a local temperature increase. The most efficient heating is produced by the high current within several millimeters of the electrode tip and results in tissue necrosis, and then heat conduction causes damage to the tissue further away from the electrode thermal damage.<sup>28</sup> The heating effect of RFA that causes thermal tissue necrosis is a combination

of frictional and conductive heat. Tissue carbonization when the temperature is higher than  $100^\circ\text{C}$  and the heat sink effect originating from tissue blood flow perfusion are the most important factors reducing the efficacy of RFA.

### Procedure

The moving shot technique under US-guided free-hand operation with local anesthesia, implementing a trans-isthmus approach and hydrodissection, is the recommended technique in BTN ablation using RFA.<sup>29</sup> First, the target nodule is divided into multiple conceptual ablation units, whose sizes might vary within the nodule. Then, following local anesthesia, the electrode is advanced into the targeted nodule from the direction of the thyroid isthmus. The electrode tip is then placed in the deepest portion of the nodule. Next, the active tip is fired and gradually pulled back unit by unit to ablate from a deep to a superficial area. Finally, the electrode is re-inserted in another direction in the nodule to start the next ablation unit by unit until the whole nodule is ablated. If the target nodule is adjacent to critical structures such as the trachea, esophagus, large vessels, and nerves, hydrodissection is a useful technique to separate the nodule from the structures.

### Clinical results

In terms of efficacy, the initial clinical report about RFA for BTNs was published in 2006, presenting the use of US-guided percutaneous RFA in treating 35 cold BTNs in 30 euthyroid patients.<sup>30</sup> One patient was lost to follow-up, but the mean nodular volume in 29 patients had a trend toward gradual shrinkage during a mean follow-up period of 6.4 months (range: 1.1–18.5 months). Among the 25 patients who complained of nodule-related symptoms, the symptoms improved in 22 patients (88%) after ablation, and it was concluded that RFA might be a non-surgical treatment for cold BTNs. In the 2010s, the efficacy of RFA in treating symptomatic BTNs has been increasingly confirmed by a number of non-randomized and randomized control trials. In 2013, a promising report with a mean follow-up period of  $49.4 \pm 13.6$  months presented the clinical outcomes of 111 patients, whose 126 BTNs underwent US-guided percutaneous RFA.<sup>10</sup> The mean VRR was  $93.5 \pm 11.7\%$  at the last follow-up, and the mean nodular volume significantly reduced from  $9.8 \pm 8.5$  mL before ablation to  $0.9 \pm 3.3$  mL after ablation. Compared to the original values, the mean nodular maximal diameter ( $3.3 \pm 1.0$  cm), vascularity classification ( $1.7 \pm 0.7$ ), cosmetic score ( $3.2 \pm 0.8$ ), and symptomatic score ( $4.3 \pm 1.6$ ) were significantly decreased after RFA to  $1.1 \pm 0.8$  cm,  $1.1 \pm 0.4$ ,  $1.3 \pm 0.6$ , and  $0.8 \pm 0.9$ , respectively. A reduction in the VRR of more than 50% was observed in 124 (98.4%) out of 126 nodules, and 28 target nodules (18.3%) had disappeared completely at follow-up. The authors found RFA to be a safe non-surgical method to effectively decrease nodular volumes and improve clinical problems related to BTNs, as confirmed by the long-term follow-up results.

Additionally, normal thyroid function was well-preserved in most patients following RFA,<sup>9,10</sup> except for cases that had undergone previous thyroid lobectomy<sup>20</sup> and bilateral BTNs.<sup>21</sup>

In terms of safety, a large multicenter study of complications related to RFA treatment of BTNs was published in 2012.<sup>19</sup> Among 1459 patients with 1543 ablated nodules, the incidence rate of complications and side effects were 3.15% (46/1459) and 3.3% (48/1459), respectively. Only 20 patients (1.4%) underwent major complications, including voice changes in 15 cases (1.02%), nodular rupture in 2 cases (0.14%), nodular rupture with abscess formation in 1 case (0.07%), hypothyroidism in 1 (0.07%), and brachial plexus injury in 1 (0.07%). Minor complications were reported in 28 patients (1.92%), including hematoma (1.02%), vomiting (0.62%) and skin burn (0.27%). Side effects of pain (2.6%), vasovagal reaction (0.34%) and coughing (0.21%) were presented by 48 patients (3.15%).

## Microwave ablation

### Brief principles

The frequencies of electromagnetic wave commonly used for medical MWA range from 915 MHz to 2450 MHz. Dielectric hysteresis, known as rotating dipoles, is the physical principle of heat generation in a microwave field.<sup>31</sup> Molecules with an intrinsic dipole moment, such as water, are forced to realign under the alternating electromagnetic field. The increase in kinetic energy produced by polar molecular rotation results in local tissue temperatures rising high enough to cause irreversible coagulative tissue necrosis. The high central temperature of 150°C or more easily penetrates biological tissue, including dehydrated or charred tissue. Microwave ablation was less affected by the heat sink effect than RFA,<sup>32</sup> and might be suitable for treating nodules with rich blood flow or to block the blood supply of large vessels adjacent to the ablated lesion.<sup>33</sup>

### Procedure

As in RFA, the moving shot technique under US-guided free-hand operation with local anesthesia is the usual MWA technique for ablation of BTNs. Fixed-antenna ablation could be used to ablate an area with rich blood flow in the target nodule, or to block large vessels around the nodule prior to undertaking the moving shot technique.<sup>33</sup> An easy operating approach is decided according to the nodular location in the thyroid and the peripheral structures around the nodule; trans-isthmus approach is the generally preferred choice. If necessary, hydrodissection is used to separate the target nodule from surrounding critical structures. Usually, 5–10 s of microwave fire is enough for a conceptual ablation unit, and then the antenna is pulled back about 10 mm to ablate the next unit. Internally cooled-shaft needle antenna can be helpful in effectively decreasing overheating of the needle, to prevent skin burns and efficiently increase the energy transferred

to the tissue.<sup>34</sup> While the energy is firing, the antenna tip cannot be placed beyond the target nodular margin.

### Clinical results

In terms of efficacy, after the development of an internally cooled-shaft antenna with a 16 gauge diameter, 10 cm in length and 3 mm active tip, the pilot clinical application of 2450 MHz MWA for BTNs was reported in 2012.<sup>15</sup> The researchers concluded that MWA was a feasible technique for BTNs, based on the results of 11 solid or mixed BTNs in 11 human patients treated using MWA under US guidance following an *ex vivo* feasibility study on swine liver tissue. After that, a large-scale clinical study of 222 patient with 477 BTNs but only short-term follow-up was published, using the same microwave system and antenna as in the pilot study.<sup>16</sup> Data at the six-month follow-up was obtained in 254 out of 477 nodules with a mean nodular VRR of 65 ±65%. Nodular VRRs over 50% and complete the disappearance rates were 82.3% (209/254) and 30.7% (78/254), respectively. The conclusion was drawn that MWA seemed to be a safe and effective technique for the treatment of BTNs. A clinical study for BTN ablation was documented using a microwave system at a frequency of 902–928 MHz in 2015.<sup>35</sup> Three kinds of antennas, with diameters from 14 G to 16 G, were used and the power output was 24–36 W. The mean volume of 18 nodules in 14 patients shrank from 19.8 ±21.3 mL at the baseline to 8.9 ±8.9 mL 3 months after ablation, and the mean VRR was 55.4 ±17.9%. It was concluded that MWA can be considered an effective and low-risk new approach to treating BTNs.

In terms of safety, the largest clinical study to date reported that mild sensations of heat during the procedure were complained of by most patients, but it was easy to tolerate and cessation was not necessary.<sup>16</sup> The most serious short-term complication was voice change, which presented in 8 patients (3.6%) out of 222, and improved in 3 months. Using the microwave system at frequencies of 902–928 MHz resulted in no major complications such as nerve injuries, severe infections, secondary hemorrhage, or nodular rupture.

## High-intensity focused ultrasound

### Brief principles

The basic principles of HIFU for tumoral ablation are the typical clinical application of thermal effects between US waves and biological tissue.<sup>36</sup> During the HIFU procedure, some low-intensity US beams produced by a curved or phase-arrayed piezoelectric probe with a central frequency of 1–7 MHz are concentrated on a focused zone in the target tissue in the body. The procedure is totally noninvasive because no needle puncture into the skin is necessary.<sup>37</sup> When an acoustic wave is propagated in tissue, part of the acoustic energy is absorbed and transformed into thermal energy. In the focused zone, due to the high

density of acoustic energy, the temperature rises over 60°C in several seconds and can result in lethal damage to local tissue. At the same time, tissue beyond the focused zone remains intact due to the low density of acoustic energy. A focused acoustic zone can cause a small ellipsoidal necrosis unit in the target tissue.

### Procedure

In accordance with pre-treatment planning, HIFU therapy is performed unit by unit to result in an ablated lesion in the target tumor. A pause between every 2 sonication pulses was necessary to prevent tissue overheating and gas bubble formation, which might cause reflections and distortions of incident waves, unexpected increases in ablation or even unpredictable injuries beyond the target tumor. The patient undergoes conscious sedation in the HIFU procedure to ablate BTNs. The HIFU is a time-consuming therapy; from 1 h to several hours is needed to ablate the target tumor.<sup>37</sup> To monitor the focused US energy reaching the target tissue, HIFU therapy is usually guided using US or magnetic resonance imaging (MRI).

### Clinical results

As far as efficacy is concerned, only a few clinical reports about HIFU treatment for BTNs have been published. The initial clinical application of HIFU ablation was documented in 2010, to treat a 26-year-old male patient with hyperthyroidism.<sup>38</sup> A 9 × 8 mm solid isoechoic nodule, which was a clearly hot on a <sup>123</sup>I thyroid scan, with rich blood flow, was located in the right isthmus lobe. The ablated nodule became cystic 2 weeks after treatment with 15 min of HIFU ablation at 4 kJ. The patient's thyroid function recovered to normal range in 3 months. After 18 months of follow-up, the ablated lesion shrank and presented a 1.4 × 1.6 mm hypoechoic scar with no blood flow. Thyroid function remained in the normal range and iodine uptake was recovered on thyroid scintigraphy. The authors of this pilot clinical study concluded that HIFU seemed to be a safe and effective treatment for AFTNs, with excellent clinical, biologic, ultrasonographic, and scintigraphic results. In 2015, a prospective clinical study reported the results of HIFU ablation of 20 BTNs in 20 euthyroid patients.<sup>17</sup> The average duration of the procedures was 86.8 min. The mean nodular volume decreased significantly from 4.96 ± 2.79 mL at baseline to 3.05 ± 1.96 mL 3 months after ablation. The results of a six-month follow-up were obtained in 16 out of 20 patients, whose mean nodular and maximal VRR was 48.7 ± 24.3% and 92.9%, respectively. The cosmetics improved significantly, with the mean cosmetic score decreasing from 2.6 ± 1.0 to 1.9 ± 0.9. Vascularity in the nodules was reduced significantly. It was the conclusion that US-guided HIFU ablation is safe and effective treatment for BTNs, and that the clinical outcomes could be affected by US echoic features and vascularity.

In terms of safety, the clinical outcomes of a feasibility study showed no major complications, but 3 patients (12%)

underwent insufficient HIFU ablation because of pain or the appearance of skin blisters during the procedure.<sup>39</sup> The results of the 2015 prospective study outlined above indicated that all 20 patients tolerated HIFU ablation well, with a mean pain score during procedures of 2.8 ± 2.6 on a visual analog scale ranging from 0 to 7.5.<sup>17</sup> No additional analgesics were administered after ablation. Subcutaneous edema was observed in 1 patient; it gradually disappeared after 1 week. Mild skin redness presented in 1 case after ablation and became a small rash area with red papules after 1 week, and disappeared by the one-month follow-up. No major complications such as dysphonia or thermal injury of the trachea or esophagus occurred.

## Discussion

The clinical applications of RFA and LAT, which have been employed for a decade, with hundreds of published documents, are considered a minimally invasive alternative to surgery for patients with symptomatic BTNs, especially for nonsurgical candidates due to high surgical risk, comorbidities or refusal of surgery. Comparing the clinical outcomes of RFA and LAT for BTNs, the procedures are similar in terms of safety, but the efficacy of RFA has been found to be superior to LAT,<sup>5,40,41</sup> although no randomized controlled trials with large-scale cohorts and long-term follow-up have been published. Under local anesthesia, the moving shot technique with a trans-isthmus approach monitored using real-time US imaging has been recommended as a standard procedure in RFA for BTNs and could be helpful to improve the curative efficacy of other methods. Unfortunately, the moving shot technique is difficult to adapt to the LAT procedure. This might be a crucial reason limiting its clinical efficacy in low nodular VRR compared to RFA.<sup>40</sup>

The moving shot technique could easily and conveniently be applied in MWA for BTNs, so MWA might technically achieve similar clinical outcomes to RFA. However, only a small number of clinical results of MWA for BTNs have been published in recent years, due to the complexity of the design and development of microwave antennae. In principle, MWA is more effective in ablating nodules with rich blood flow. However, it is undeniable that dehydrated or charred tissue caused by higher central temperatures during MWA is difficult to absorb and non-beneficial to shrinking the nodular volume. Obviously charred thyroid tissue was present on a gross thyroidectomy specimen after MWA treatment with a power output of 30–50 W.<sup>16</sup> Microwave ablation with low power outputs (20–30 W) is therefore recommended in BTN ablation in order to minimize tissue charring. The results of a recent large-scale prospective multicenter comparative study between MWA and RFA concluded that both MWA and RFA are safe and effective techniques for selected patients

with symptomatic BTNs, and the VRR achieved in the RFA group was greater than in the MWA group at 6 months and later.<sup>42</sup>

Theoretically, HIFU should be a non-invasive method to ablate BTNs because skin penetration is not required<sup>43</sup>; there is a short approach to the target nodule without bone and gas to influence acoustic propagation; and unit-by-unit ablation in spatially proper order according to the treatment planning is similar to the moving shot technique. However, its disadvantages also originate mainly from its non-invasive nature: Acoustic beams reach the target nodule after propagating through several non-target tissues including skin, subcutaneous adipose and muscles. It might be possible to damage non-target tissue due to excessive energy deposition, and results after HIFU ablation have observed that the range of necrosis was beyond the target nodule.<sup>18</sup> Therefore, the most primary challenges in the clinical application of HIFU ablation are to deliver enough acoustic energy to the target nodule, and meanwhile to avoid or minimize injuries to important surrounding structures.

So far, surgery has been the most common therapy for BTNs. Except for nodules with large volume (over 35 mL) or behind the sternum and autonomously functioning thyroid nodule (AFTN), a comparative clinical study concluded that RFA is an effective alternative to surgery for treating BTNs in patients with local cosmetic and symptomatic problems.<sup>44</sup> A large-scale comparative study between RFA and surgery in treating BTNs was published in 2015.<sup>45</sup> Four hundred patients with BTNs were enrolled and separated into 2 groups: RFA and surgery, with 200 patients in each group. The results indicated that nodular volume in the RFA group shrank significantly at the one-year follow-up, with a mean nodular VRR of  $84.8 \pm 17.1\%$  (range: 61.3–100%). The RFA group had a significantly lower residual rate, lower complication rate, lower hypothyroidism with medication rate, and shorter mean hospitalization after treatment than the surgery group did: These rates in the surgery group compared to the RFA group were 11.9% vs 2.9%, 6% vs 1%, 71.5% vs 0%, and  $6.6 \pm 1.6$  days vs  $2.1 \pm 0.9$  days, respectively. The conclusion was that RFA was as effective as surgery for treating BTNs and should be considered a first-line therapy because of the advantages of a low complication rate, good preservation of thyroid function and shortening of mean hospitalization time. Nevertheless, it would be indispensable to carry out further prospective multicenter and large-scale randomized controlled trials between TA and surgery for BTNs before a non-surgical therapy can be recommended as an effective alternative to surgery.

Thermal ablation treatment for BTNs has shown several obvious advantages in terms of safety, such as low rates of complications and side effects, being an outpatient procedure under local anesthesia; however, because of the occasional occurrences of several major complications, it is essentially necessary to recommend that

the procedure should be performed in special clinics and by experienced teams, ensuring good clinical outcomes and minimal complications. In addition, ablation treatment guided by virtual navigation techniques or image fusion navigation<sup>46,47</sup> could provide beneficial support, and be helpful in decreasing most of the complications caused by US guidance alone,<sup>48</sup> shortening the learning curve and minimizing the influence of microbubble formation obscuring the view of the needle tip during ablation.<sup>46</sup> Fortunately, image fusion navigation has become standard software in modern US imaging systems for the precise and safe clinical application of TA techniques.<sup>49</sup>

The last issue that must be mentioned is that the benignity of TNs ablated by a nonsurgical treatment such as TA have to be proven using fine needle aspiration (FNA), the sensitivity and specificity of which are not 100%. In other words, there is a possibility, albeit very low, that a malignant TN could theoretically be ablated. Therefore, regular follow-up to promptly detect and manage the recurrence of any potential malignant nodules is strongly recommended for patients with TNs treated with a non-surgical TA technique.

## Conclusions

As non-surgical treatments, all 4 TA techniques can be safe and effective treatment for patients with symptomatic BTNs. The RFA seems to be the best one, because of the highest nodular VRR at follow-up. Furthermore, image fusion navigation techniques promise to provide significant assistance in the precise ablation of BTNs.

## References

1. Russ G, Leboulleux S, Leenhardt L, Hegedüs L. Thyroid incidentalomas: Epidemiology, risk stratification with ultrasound and workup. *Eur Thyroid J*. 2014;3(3):154–163.
2. Gharib H, Papini E, Paschke R, et al; AACE/AME/ETA Task Force on Thyroid Nodules. American Association of Clinical Endocrinologists, Associazione Medici Endocrinologi, and European Thyroid Association medical guidelines for clinical practice for the diagnosis and management of thyroid nodules: Executive summary of recommendations. *J Endocrinol Invest*. 2010;33(5 Suppl):51–56.
3. Ha EJ, Baek JH. Advances in nonsurgical treatment of benign thyroid nodules. *Future Oncol*. 2014;10(8):1399–1405.
4. Durante C, Costante G, Lucisano G, et al. The natural history of benign thyroid nodules. *JAMA*. 2015;313(9):926–935.
5. Muller R, Liu YY, Brent GA. Thyroid hormone regulation of metabolism. *Physiol Rev*. 2014;94(2):355–382.
6. Choi SH, Kim EK, Kim SJ, Kwak JY. Thyroid ultrasonography: Pitfalls and techniques. *Korean J Radiol*. 2014;15(2):267–276.
7. Gharib H, Hegedüs L, Pacella CM, Baek JH, Papini E. Clinical review: Nonsurgical, image-guided, minimally invasive therapy for thyroid nodules. *J Clin Endocrinol Metab*. 2013;98(10):3949–3957.
8. Papini E, Pacella CM, Hegedüs L. Diagnosis of endocrine disease. Thyroid ultrasound (US) and US-assisted procedures: From the shadows into an array of applications. *Eur J Endocrinol*. 2014;170(4):R133–R146.
9. Jeong WK, Baek JH, Rhim H, et al. Radiofrequency ablation of benign thyroid nodules: Safety and imaging follow-up in 236 patients. *Eur Radiol*. 2008;18(6):1244–1250.
10. Lim HK, Lee JH, Ha EJ, Sung JY, Kim JK, Baek JH. Radiofrequency ablation of benign non-functioning thyroid nodules: 4-year follow-up results for 111 patients. *Eur Radiol*. 2013;23(4):1044–1049.

11. Deandrea M, Limone P, Basso E, et al. US-guided percutaneous radiofrequency thermal ablation for the treatment of solid benign hyperfunctioning or compressive thyroid nodules. *Ultrasound Med Biol*. 2008;34(5):784–791.
12. Papini E, Guglielmi R, Bizzarri G, Pacella CM. Ultrasound-guided laser thermal ablation for treatment of benign thyroid nodules. *Endocr Pract*. 2004;10(3):276–283.
13. Valcavi R, Riganti F, Bertani A, Formisano D, Pacella CM. Percutaneous laser ablation of cold benign thyroid nodules: A 3-year follow-up study in 122 patients. *Thyroid*. 2010;20(11):1253–1261.
14. Døssing H, Bennedbaek FN, Hegedüs L. Long-term outcome following interstitial laser photocoagulation of benign cold thyroid nodules. *Eur J Endocrinol*. 2011;165(1):123–128.
15. Feng B, Liang P, Cheng Z, et al. Ultrasound-guided percutaneous microwave ablation of benign thyroid nodules: Experimental and clinical studies. *Eur J Endocrinol*. 2012;166(6):1031–1037.
16. Yue W, Wang S, Wang B, et al. Ultrasound guided percutaneous microwave ablation of benign thyroid nodules: Safety and imaging follow-up in 222 patients. *Eur J Radiol*. 2013;82(1):e11–e16.
17. Kovatcheva RD, Vlahov JD, Stoinov JI, Zaletel K. Benign solid thyroid nodules. US-guided high-intensity focused ultrasound ablation: Initial clinical outcomes. *Radiology*. 2015;276(2):597–605.
18. Korkusuz H, Fehre N, Sennert M, Happel C, Grünwald F. Volume reduction of benign thyroid nodules 3 months after a single treatment with high-intensity focused ultrasound (HIFU). *J Ther Ultrasound*. 2015;3:4.
19. Baek JH, Lee JH, Sung JY, et al. Complications encountered in the treatment of benign thyroid nodules with US-guided radiofrequency ablation: A multicenter study. *Radiology*. 2012;262(1):335–342.
20. Ha EJ, Baek JH, Lee JH, et al. Radiofrequency ablation of benign thyroid nodules does not affect thyroid function in patients with previous lobectomy. *Thyroid*. 2013;23(3):289–293.
21. Ji Hong M, Baek JH, Choi YJ, et al. Radiofrequency ablation is a thyroid function-preserving treatment for patients with bilateral benign thyroid nodules. *J Vasc Interv Radiol*. 2015;26(1):55–61.
22. Masters A, Steger AC, Lees WR, Walmsley KM, Bown SG. Interstitial laser hyperthermia: A new approach for treating liver metastases. *Br J Cancer*. 1992;66(3):518–522.
23. Skinner MG, Iizuka MN, Kolios MC, Sherar MD. A theoretical comparison of energy sources: Microwave, ultrasound and laser for interstitial thermal therapy. *Phys Med Biol*. 1998;43(12):3535–3547.
24. Pacella CM, Bizzarri G, Guglielmi R, et al. Thyroid tissue. US-guided percutaneous interstitial laser ablation: A feasibility study. *Radiology*. 2000;217(3):673–677.
25. Døssing H, Bennedbaek FN, Karstrup S, Hegedüs L. Benign solitary solid cold thyroid nodules. US-guided interstitial laser photocoagulation: Initial experience. *Radiology*. 2002;225(1):53–57.
26. Papini E, Rago T, Gambelunghe G, et al. Long-term efficacy of ultrasound-guided laser ablation for benign solid thyroid nodules: Results of a three-year multicenter prospective randomized trial. *J Clin Endocrinol Metab*. 2014;99(10):3653–3659.
27. Di Rienzo G, Surrente C, Lopez C, Quercia R. Tracheal laceration after laser ablation of nodular goitre. *Interact Cardiovasc Thorac Surg*. 2012;14(1):115–116.
28. Haemmerich D, Pilcher TA. Convective cooling affects cardiac catheter cryoablation and radiofrequency ablation in opposite directions. *Conf Proc IEEE Eng Med Biol Soc*. 2007;2007:1499–1502.
29. Na DG, Lee JH, Jung SL, et al. Radiofrequency ablation of benign thyroid nodules and recurrent thyroid cancers: Consensus statement and recommendations. *Korean J Radiol*. 2012;13(2):117–125.
30. Kim YS, Rhim H, Tae K, Park DW, Kim ST. Radiofrequency ablation of benign cold thyroid nodules: Initial clinical experience. *Thyroid*. 2006;16(4):361–367.
31. Ahmed M, Brace CL, Lee FT Jr, Goldberg SN. Principles of and advances in percutaneous ablation. *Radiology*. 2011;258(2):351–369.
32. Brace CL. Microwave ablation technology: What every user should know. *Curr Probl Diagn Radiol*. 2009;38(2):61–67.
33. Liang P, Wang Y. Microwave ablation of hepatocellular carcinoma. *Oncology*. 2007;72(Suppl 1):124–131.
34. Wang Y, Sun Y, Feng L, Gao Y, Ni X, Liang P. Internally cooled antenna for microwave ablation: Results in ex vivo and in vivo porcine livers. *Eur J Radiol*. 2008;67(2):357–361.
35. Korkusuz H, Nimsdorf F, Happel C, Ackermann H, Grünwald F. Percutaneous microwave ablation of benign thyroid nodules: Functional imaging in comparison to nodular volume reduction at a 3-month follow-up. *Nuklearmedizin*. 2015;54(1):13–19.
36. Malietz G, Monzon L, Hand J, et al. High-intensity focused ultrasound: Advances in technology and experimental trials support enhanced utility of focused ultrasound surgery in oncology. *Br J Radiol*. 2013;86(1024):20130044.
37. Jenne JW, Preusser T, Günther M. High-intensity focused ultrasound: Principles, therapy guidance, simulations and applications. *Z Med Phys*. 2012;22(4):311–322.
38. Esnault O, Rouxel A, Le Nestour E, Gheron G, Leenhardt L. Minimally invasive ablation of a toxic thyroid nodule by high-intensity focused ultrasound. *AJNR Am J Neuroradiol*. 2010;31(10):1967–1968.
39. Esnault O, Franc B, Ménégau F, et al. High-intensity focused ultrasound ablation of thyroid nodules: First human feasibility study. *Thyroid*. 2011;21(9):965–973.
40. Ha EJ, Baek JH, Kim KW, et al. Comparative efficacy of radiofrequency and laser ablation for the treatment of benign thyroid nodules: Systematic review including traditional pooling and Bayesian network meta-analysis. *J Clin Endocrinol Metab*. 2015;100(5):1903–1911.
41. Baek JH, Lee JH, Valcavi R, Pacella CM, Rhim H, Na DG. Thermal ablation for benign thyroid nodules: Radiofrequency and laser. *Korean J Radiol*. 2011;12(5):525–540.
42. Cheng Z, Che Y, Yu S, et al. US-guided percutaneous radiofrequency versus microwave ablation for benign thyroid nodules: A prospective multicenter study. *Sci Rep*. 2017;7(1):9554.
43. Esnault O, Franc B, Monteil JP, Chapelon JY. High-intensity focused ultrasound for localized thyroid-tissue ablation: Preliminary experimental animal study. *Thyroid*. 2004;14(12):1072–1076.
44. Bernardi S, Dobrinja C, Fabris B, et al. Radiofrequency ablation compared to surgery for the treatment of benign thyroid nodules. *Int J Endocrinol*. 2014;2014:934595.
45. Che Y, Jin S, Shi C, et al. Treatment of benign thyroid nodules: Comparison of surgery with radiofrequency ablation. *AJNR Am J Neuroradiol*. 2015;36(7):1321–1325.
46. Turtulici G, Orlandi D, Corazza A, et al. Percutaneous radiofrequency ablation of benign thyroid nodules assisted by a virtual needle tracking system. *Ultrasound Med Biol*. 2014;40(7):1447–1452.
47. Mauri G, Solbiati L. Virtual navigation and fusion imaging in percutaneous ablations in the neck. *Ultrasound Med Biol*. 2015;41(3):898.
48. Orlandi D, Turtulici G. Reply regarding virtual navigation and fusion imaging in percutaneous ablations in the neck. *Ultrasound Med Biol*. 2015;41(3):899.
49. Maybody M, Stevenson C, Solomon SB. Overview of navigation systems in image-guided interventions. *Tech Vasc Interv Radiol*. 2013;16(3):136–143.

